Dresden Center for Computational Materials Science, TU Dresden

Leibniz-Institut für Polymerforschung Dresden e.V.

Fachrichtung Chemie und Lebensmittelchemie

Fakultät Mathematik und Naturwissenschaften

Technische Universität Dresden

A Bottom-up Computational Approach to Semiconducting Block Copolymers: From Monomer Design to Charge Transport Properties

DISSERTATION

zur Erlangung des akademisches Grades

Doctor rerum naturalium

(Dr. rer. nat.)

vorgelegt

von

M. Sc. Deyan Raychev

geboren am 01.09.1989 in Varna, Bulgarien

1. Gutachter: Prof. Dr. Gotthard Seifert

2. Gutachter: Prof. Dr. Jens-Uwe Sommer

Dresden, 2019

Acknowledgements

Content

List of Abbreviations

A_+	Acceptor (Electron Deficient Unit)
BTZ	Benzothiadiazole
B	Bohr (Radius)
BR	Branched (Side Chains)
C_∞	Characteristic Ratio
CT	Charge Transport
d	Distance
d_h	Center-to-Center Distance
$d_{\pi-\pi}$	π-π Distance
$d_{lamella}$	Lamella Distance
D_-	Donor (Electron Rich Unit)
D	Debye
DFT	Density Functional Theory
DPP	Diketopyrrolopyrrole
ESP	Electrostatic Potential
e^-	Electron
E	Energy
E_{bind}	Binding Energy
E_{con}	E conformer (at different sides with respect to a plane)
E_g	Band Gap Energy
eq(s).	Equation(s)
ET	Electron Transfer
FF	Force Field
Fl	Flank (*Fu* or *Th*)
Fu	Furan
h	Plank Constant
$\hbar$	Reduced Plank Constant
h^+	Hole
HOMO	Highest Occupied Molecular Orbital
HT	Hole Transfer
$\hat{H}$	Hamiltonian
K	Kinetic (Energy)
k_B	Boltzmann Constant
K_{CT}	Charge Rate Constant
l_K	Kuhn Segment
LN	Linear (Side Chains)
LUMO	Lowest Unoccupied Molecular Orbital
l_0	Monomer Size
m	Mass
MD	Molecular Dynamics
NPT	Isobaric-Isothermal (Ensemble)
NVT	Canonical (Ensemble)
n_0	Ground State Electron Density
NS	Non-Shifted (Non-Interdigitating Configuration of the Side Chains)

p.	Page (Number)
P	Pressure
PBC	Periodic Boundary Conditions
PCFF	Polymer Consistent Force Field
PCM	Polarizable Continuum Model
q	(Partial) Charge
R_e	End-to-End Distance
r	Cartesian Coordinates
r_{XX}	Distance (between Two Atoms)
RMSD	Root-Mean-Square Deviation
SH	Shifted (Interdigitating Configuration of the Side Chains)
TD	Time-Dependent
Th	Thiophene
T	Temperature
t	Time
U	Potential (Energy)
UV-VIS	Ultraviolet-Visible
$V^{ET/HT}$	Electronic Coupling (Charge Transfer Integrals for Hole/Electron Transfer)
V^{ESP}	Electrostatic Potential
vdW	van der Waals
$X_{(atom)}$	Heteroatom
Z_{con}	Z conformer (at same sides with respect to a plane)
α_A	Model Angle
σ	Spin Variable
ε	Dielectric Permittivity (Constant)
λ_{max}	Wavelength (Maximum)
λ_i	Internal Reorganization Energy
λ_o	Outer Reorganization Energy
λ_{tot}	Total Reorganization Energy
$\mu^{-/+}$	Charge Carrier (Electron/Hole) Mobility
μ_d	Dipole Moment
ρ	Density
ϕ	Single Particle Wave Function
φ	Valence Angle
θ	Torsion Angle
χ	Improper Torsion Angle
Ψ	Many-Body Wave Function
Φ_0	Slater Determinant

List of Publications

I. Articles:

1. O. Guskova, <u>D. V. Raychev</u> & M. V. Makarova, Modern Trends in Computer Simulations of Materials for Organic Electronics, *Herald of Tver State University*, Ser.: Chemistry, 2016, 1, 23-32 (in Russian).

2. <u>D. Raychev</u>, O. Guskova, G. Seifert & J.-U. Sommer, Conformational and Electronic Properties of Small Benzothiadiazole-Cored Oligomers Substituted with Aryl Flanking Units: Thiophene versus Furan, *Comp. Matter. Sci.*, 2017, 126, 287-298.

3. <u>D. Raychev</u> & O. Guskova, Charge Carrier Mobility in One-Dimensional Aligned π-Stack of Conjugated Small Molecules with Benzothiadiazole Central Unit, *Phys. Chem. Chem. Phys.*, 2017, 19, 8330-8339.

4. <u>D. Raychev</u>, G. Seifert, J.-U. Sommer & O. Guskova, A Comparative Analysis of Symmetric Diketopyrrolopyrrole-Cored Small Conjugated Molecules with Aromatic Flanks: From Geometry to Charge Transport, *J. Comp. Chem.*, 2018, 39, 2526-2538.

5. <u>D. Raychev</u>, R. D. M. López, A. Kiriy, G. Seifert, J.-U. Sommer & O. Guskova, Copolymers of Diketopyrrolopyrrole and Benzothiadiazole: Design and Function from Simulations with Experimental Support, *Macromolecules*, 2019, 52, 904-914.

II. Conference Papers:

6. <u>D. Raychev</u>, O. Guskova & J.-U. Sommer, Conformational Preferences of Conjugated Benzothiadiazole-Cored Oligomers: The Impact of Through-Space Interactions, DPG-Frühjahrstagung, 6-11.03.2016, Regensburg, Germany, p. 159.

7. <u>D. Raychev</u>, O. Guskova, G. Seifert & J.-U. Sommer, Microscopic Charge Transport in Small π-Conjugated Benzothiadiazole Derivatives from First Principles, The 1st Zing Conference on Organic Semiconductors Conference, 22-25.09.2016, Dubrovnik, Croatia, p. 90-91.

8. <u>D. Raychev</u>, O. Guskova, G. Seifert & J.-U. Sommer, A Comparative Study of Benzothiadiazole-Cored Acceptor Units for All-Conjugated Block Copolymers, Computational Molecular Science, 19-22.03.2017, Warwick, UK.

9. <u>D. Raychev</u>, Y. Karpov, A. Kiriy, J. Grenzer, J.-U. Sommer & O. Guskova, Solid State Structure and Charge Transfer Properties of D-A-D Conjugated Blocks: A Joint Experimental-Theoretical Approach, DPG-Frühjahrstagung, 19-24.03.2017, Dresden, Germany, p. 151.

10. <u>D. Raychev</u>, O. Guskova, G. Seifert & J.-U. Sommer, A Step-by-step Theoretical Study of Monomers for All-conjugated Block-Copolymers, 13th International Conference on Organic Electronics - 2017 (ICOE - 2017), 4-8.06.2017, St. Petersburg, Russia, p. 153.

11. <u>D. Raychev</u>, O. Guskova, G. Seifert & J.-U. Sommer, Charge Transport Properties and Mechanical Behaviour of Conjugated Block Copolymers - Effect of the Heteroatom in the π-Bridges and Side Chains, 14th European Conference on Molecular Electronics 29.08-02.09.2017, Dresden, Germany, p. 34.

12. O. Guskova, <u>D. Raychev</u>, Y. Karpov, A. Kiriy, J. Grenzer, G. Seifert & J.-U. Sommer, Synthesis and Characteristics of Crystalline Phases of Small-Molecule Semiconductors and *In Silico* Estimation of Their Charge Transport Properties, CPP5 Annual General Meeting Material Modelling: Simulation Meets Experiment, 11-13.09.2017, Glasgow, U.K., p. 17.

13. <u>D. Raychev</u>, G. Seifert, J.-U. Sommer & O. Guskova, Charge Transport of Thiophene Containing D/A Small Molecules and Monomer in π-π Isolated Stacks, DPG-Frühjahrstagung, 11-16.03.2018, Berlin, Germany, p. 161.

14. R. D. M. López, <u>D. Raychev</u>, A. Kiriy, O. Guskova & J.-U. Sommer, Conjugated Polymers with Alternating Benzothiadiazole-diketopyrrolopyrrole Units for OTFTs: Synthesis and DFT/MD Simulations, DPG-Frühjahrstagung, 11-16.03.2018, Berlin, Germany, p. 148.

15. O. Guskova, <u>D. Raychev</u>, G. Seifert & J.-U. Sommer, Charge Transport in Organic Crystals of Small Benzothiadiazole-Containing Molecules Probed by Molecular Simulations, 14th International Conference on Organic Electronics, 18-22.06.2018, Bordeaux, France, p. 135.

16. <u>D. Raychev</u>, G. Seifert, J.-U. Sommer & O. Guskova, Combined MD/QM Approach for Investigation of Charge Transport Properties and Molecular Organization of Conjugated Block Copolymers: The Effect of the Side Chains and the Heteroatom Substitution in the Flanks, 14th International Conference on Organic Electronics, 18-22.06.2018, Bordeaux, France, p. 179.

III. Reports:

17. O. Guskova, <u>D. Raychev</u>, M. Makarova & J.-U. Sommer, Charge Transport in Stacked Pairs and Crystalline Phases of Small Conjugated Molecules for Organic Electronics, *IPF Dresden Jahresbericht*, 2016, p. 74-75.

1. Preface

The electronics based on organic compounds (usually polymers) is very attractive for the scientists and industry due to low cost of the organic materials, their lightweight, easy large-area processing from solution at low temperature and mechanical flexibility. Organic electronics is considered as a new generation of technologies with a wide range of (opto)electronic applications including organic light-emitting diodes (OLEDs), organic photovoltaic cells (OPVs) and organic field-effect transistors (OFETs). These materials could additionally provide a free clean renewable energy source, high power conversion, low energy consumption of the devices and combining all these properties with wear resistance, environment friendliness, bio- renewability and degradability, they would completely substitute the traditional inorganic (mainly silicon based) semiconductors. Moreover, the synthetic chemistry provides a wide variety of possible molecules, which are applicable in the organic electronics as well as they can be easily modified in order to manipulate and tune their properties. One of the most negative characteristics of the semiconducting polymers (and small molecules) is their instability especially to thermal and air exposure and this is also one of the hindrances for their wide use into the market and their further successful development. Additional disadvantage of the conjugated polymers is on the one side, the theoretical prediction of their properties and defining which are the tunable parameters responsible for making the devices with high efficiency and controlled crystal packing ordering, and on the other side, the poor reproducibility of their synthesis. Many experimental and theoretical efforts are done in order to improve the performance of the devices at ambient conditions as well as to shed light on the relation between the chemical structure and their intrinsic properties but the governing factors, which define the properties of these materials are still under debate and this remains a great challenge for the researchers. One way to gain insight into the characteristics of polymeric materials is to begin exploring the polymers from small units, which they consist of and then step-by-step to construct and characterize all the compounds up to macromolecules. In this work, the semiconducting block copolymers, as promising candidates for application in organic transistors, are investigated starting from their small donor and acceptor blocks up to monomers and macromolecules, using computational methods working on different time and length scales. At each step the results are compared with available experimental data.

2. Introduction into Conjugated Polymers

This chapter explains general terms and ideas for the construction, manipulation, some of the crucial factors and rules of molecular design, which influences on the properties of the conjugated polymers, and how the charge transport (CT) properties can be predicted in computer simulations. This chapter ends presenting the aim and the objectives of this work.

2.1. Characteristics of Semiconducting Polymers

Conjugated polymers represent the compounds with alternating simple and multiple chemical bonds or atoms with lone electron pairs (such as nitrogen, oxygen, sulphur etc.) which form π-conjugated systems. This conjugation grants the molecules with π-delocalized orbitals shown schematically in Figure 3 (p. 12). This conjugation narrows the band gap (E_g) of the materials and they possess semiconducting properties.

A semiconductor could be defined as an insulator with narrow E_g (forbidden band) which is capable to conduct electricity (unlike insulator). Alternatively, it can be defined by resistivity which lies in the range between $10^{-5} \div 10^{6}$ $\Omega \cdot$cm. Moreover, some supplemental characteristics of the essential physical properties of the semiconductors should be added such as the resistivity decreases with rise of the temperature (at least for a certain temperature range, unlike metals), they are sensitive to visible light but transparent in the infrared region and they often give rise to rectifying or non-ohmic contacts. Inorganic semiconductors are constructed by periodic structures with covalent bounded atoms or molecules, whereas the organic semiconductors are composed by conjugated systems (small molecules or polymers) which are hold together by much weaker van der Waals (*vdW*) interactions. This leads to a fundamental difference between the CT mechanism where the former one has delocalized electron (e^-) density, whereas the later one has more localized charge carriers, which are related to band-to-band and hopping mechanisms, respectively. Additionally, this leads to a difference in their electronic structures where the inorganic semiconductors have periodic bands, whereas the organic molecules have discrete electron states (molecular orbitals) - Figure 1.
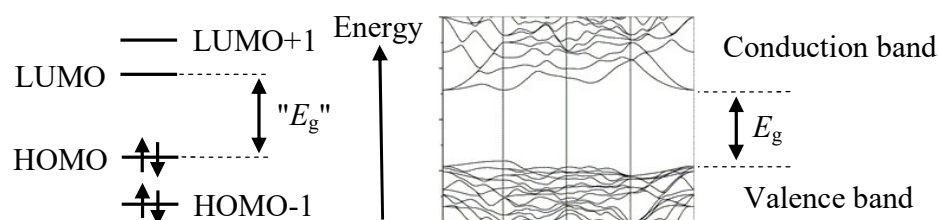

Figure 1. Schematic representation of electronic structure of organic (left) and inorganic (right) semiconductors.

One efficient way in order to obtain semiconducting polymers, introduced by Havinga et al. [1], is to attach an electron rich donor (D_-) unit to an electron deficient acceptor (A_+) unit making D_--A_+ alternating conjugated compounds achieving band gap (E_g) of 0.5 eV for a polymer. The spatial overlap of the highest occupied molecular orbital (HOMO) of D_- molecule and the lowest unoccupied molecular orbital (LUMO) of A_+ molecule in polymers is often related to a decrease of the exciton binding energies (weakly bounded electron-hole pairs) and promotes the ultrafast intramolecular charge transport.
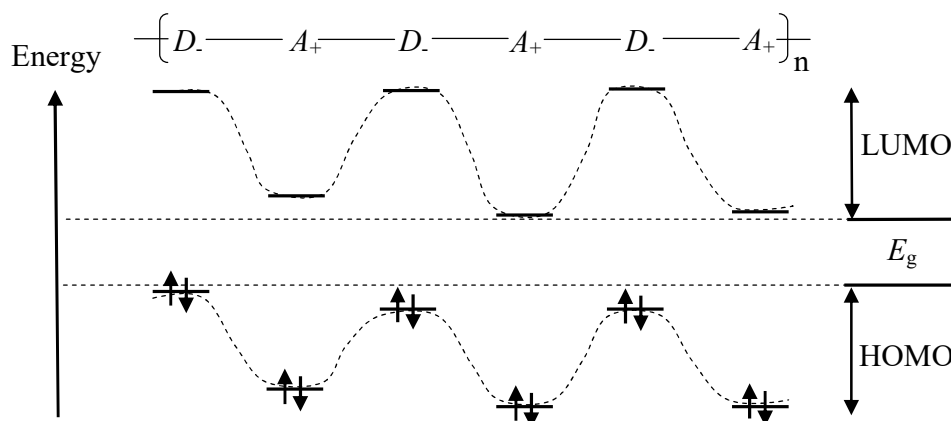

Figure 2. Schematic representation of e^- density gradient in D_--A_+ conjugated polymers.

This D_--A_+ ("push-pull") design strategy (attaching electron donating and electron withdrawing units) also provides e^- density gradient (curved bands) due to electronegativity difference of the units along the backbone and creates a lower energy band gap, which promotes better charge transport (Figure 2), as well as a large degree of freedom to manipulate the optical and electrical properties [2, 3, 4, 5, 6, 7, 8], including not only different combinations of D_- and A_+ molecules or adding additional units (D_- or A_+) into the backbone of polymers but also varying the ratio between D_-:A_+ moieties in the macromolecules [9, 10, 11]. If this specific ratio is selected properly, it can improve the performance of the polymers and change the macromolecular arrangement [10, 11, 12, 13]. A supplemental proof of the importance of unit alternation is that in the case of a random D_--A_+ arranged copolymers, it is found that the charge carrier mobilities are lower as compared to their alternating counterparts [12, 13].

The charge carrier mobility (μ), which is an experimentally measurable quantity, is related to the drift velocity of the charge carrier (v_d, cm/s) per unit of applied electric field (E_F, V/cm) and determines the performance and efficiency of the devices:

$$\mu = \frac{v_d}{E_F}$$

(1)

The D_--A_+ approach additionally ensures better π-stacking structures of cofacially packed polymer backbones due to better spatial molecular orbital overlap. Moreover, this approach also implies possibilities of different spatial orientation, i.e. packing motif - segregated or mixed stacks (Fig. 7, p. 19) which correspond to the extreme cases [14, 15].

Also this strategy could facilitate the intermolecular interactions due to dipoles [16] and strong interchain communications in polymer solid-state films resulting in high charge carrier mobilities [2, 17, 18, 19, 20]. Typical examples for D_- and A_+ units are shown in Figure 4 (p. 15).

One very important and complicated factor of the organic semiconductors is the crystallinity and the thin-film structure of these materials, similar to the inorganic analogues. The morphology of conjugated polymers can vary from amorphous or semicrystalline to highly crystalline [21] and it is the main factor for high performance of the devices.

A lot of efforts in the molecular design were done in order to improve the degree of crystallinity of polymeric semiconductors to promote efficient CT [2, 3, 4, 22, 23, 24, 25]. The most of high-performance polymers form highly crystalline solids with a strongly long-range-ordered structure that can transport charge carriers effectively [26, 27, 28, 29, 30, 31, 32, 33]. Moreover, such highly crystalline polymers tend to provide an optimal phase separation structure in bulk-heterojunction films, which can enhance both exciton dissociation efficiency and charge carrier mobility [34, 35]. There are a lot of ways with respect to the structural design which can be applied in order to stimulate more ordered structure of the polymers and they will be discussed later, for instance, modification of D_- and A_+ units or spacers with heteroatom (X_{atom}) enhancing the electrostatic or dispersion interchain interactions. The micro-structure is not always the main factor for successful development of high performance conjugated polymers and it could compete, for instance, with backbone planarization which is the next consideration.

Another factor which influences the properties of semiconducting polymers is the planarity of the backbone, which has significant impact on the improvement of the crystallinity. Combining planar D_- and A_+ units ensures more rigid and planar molecules, which can make the π-electron delocalization more effective, as well as promotes the formation of crystalline domains in the active layer [36] and also provides a narrow optical E_g due to orbital interactions [37] (as aforementioned), which leads to widening and red-shifting of the absorption of the solar spectrum [38, 39, 40, 41]. Another example can be given, when specifically selected hydrogen atoms (for instance, the end groups of a chain) are substituted by fluorine in phenylene oligomers leads to a loss of planarity and to altered electrooptical properties such as lower conductivities due to steric intramolecular interactions [42]. Additionally, some D_--A_+ alternating polymers showed high mobilities even though they have less ordered packing structures [20, 43, 44, 45, 46] and this contradiction is ascribed to the promotion of planarization and strengthening π-π intermolecular interactions, which compensates the effect of the reduced ordering [47, 48]. Moreover, the planar conformation induced from e^- delocalization between neighbouring monomers leads to a rod like behaviour and liquid crystallinity of the polymers [49, 50]. The planarity can be improved by introducing a X_{atom} into the backbone due to supplemental non-covalent interactions or with modification of the side chains. The improvement of the planarity of polymers additionally affects the conjugation length and the stacking of polymer chains [13, 51].

The so called conjugation length plays an important role in the conductivity of the polymers. The conjugation length is the effective π-orbital delocalization between adjacent conjugated units and correlates with the CT properties of conjugated polymers. Decreasing the conjugation length leads to decrease of the mobilities [52] due to increased disorder in polymers.

More conventional definition of the conjugation length is the length of a defect-free oligomer which has approximately the same values of the ionization potential, electron affinity and optical E_g like the corresponding polymer [53]. The conjugation length promotes coplanar conformation allowing better overlap of the π-conjugated systems along the backbone [54], forming lamellar structure of π-orbital stacked backbones separated by regions of alkyl side chains [55]. The conjugation length is typically broken by a steric hindrance especially from the side chain interactions or distortion of the backbone planarity [56]. The conjugation length also can be increased by higher molecular weight mainly due to increased planarity causing stronger interchain interaction and lowers the E_g [57]. The conjugation length can be estimated experimentally [58, 59, 60] or theoretically [58]. Nevertheless, long conjugation length accompanied with planar geometry and rigid structure in organic electronics often leads to poor solubility or even insolubility in common solvents. Schematic representation of the conjugation length is shown in Figure 3.
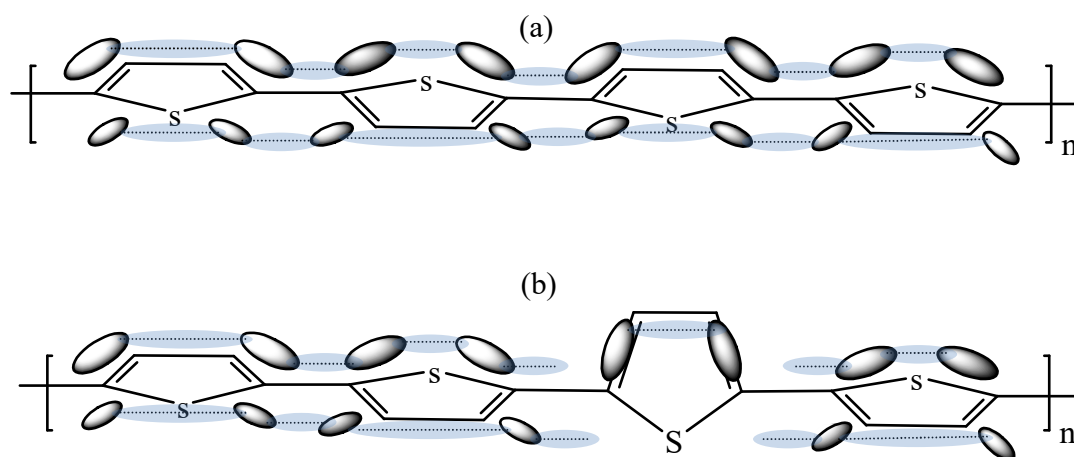

Figure 3. Schematic representation of the conjugation length in polythiophene when the molecule is completely planar (a) and when the conjugation length is interrupted due to geometry distortion (b).

One more aspect which allows manipulating the properties of the conjugated polymers are the side chains. Generally, the side chains are considered as an insulating part and they do not contribute to the CT properties directly. They are vital for the organic devices not only because of increasing the solubility of the polymers in common organic solvents but they also play a role in the self-assembly, which is related to the packing mode and morphology, and further to the mobilities. There are different types of side chains depending on the chemical composition, for instance, alkoxy, thioalkyl, fluoroalkyl, triethyleneglycol but the most common side chains are alkyl chains. Depending on their structure they can be linear or branched but the branched side chains are much more favourable for synthesis due to increased solubility of the polymers. At the same time branched side chains lead to reduced crystallinity [61] but this can be overcome, for instance, with controlled vapour annealing [62] in order to restore the crystallinity of the samples.

Generally, when alkyl side chains are attached to the conjugated backbone they may introduce two competing effects: a steric hindrance and intermolecular dispersive attraction. The modifications of side chains such as chain lengths [25, 63, 64, 65], branching positions [63, 64, 66, 67, 68, 69, 70], odd-even effects [71, 72] and chirality (of carbon atoms in the side chains) [73] have great impact on the semiconducting polymers and further influence the charge carrier mobility. The steric hindrance can be minimized by moving the branching point away from the backbone, which leads to a decrease of the π-π distance [63, 64, 66, 67, 68], which is transformed into increased mobility [66, 68]. However closer π-π distance does not always improve the CT properties and the film quality [63, 67]. The adjustment of the branching position can also lead to stacking of the polymer chains, which mainly tunes the planarity, and hence the effective conjugation length and further improves the photovoltaic efficiency [74, 75, 76, 77, 78, 79, 80]. Also, it is shown that different side chain branching positions result in different polymer crystallinities and the solid-state packing conformations thus leading to different hole (h^+) mobilities [3] and a shorter π-π distance leads to higher mobility using branching side chains [73].

It is found that the most of semiconducting polymers made of a conjugated backbone bearing alkyl side chains have a "layered" structure made of an alternation of π-stacked backbones and layers of more or less ordered side chains [81, 82]. Longer side chains usually lead to higher charge carrier mobility, nevertheless, it is observed that increasing the side chain length from C_6H_{10} to C_8H_{12}, a decrease of the charge mobility is measured due to low crystalline ordering [63]. Also, it was reported that linear alkyl side group with even numbers of carbon atoms results in one order of magnitude higher hopping mobility due to shorter (π-π) spacing between adjacent backbones [72].

The side chain attractive dispersion forces systematically increase with increasing alkyl chain length and they are the main source of increase in the total cohesive energy [51] thus polymers exhibit decreased π-π stacking distance, which results in a higher mobility [42]. Different chemical composition of the side chains can lead to different crystal structure parameters and supramolecular organization [83]. Additionally, the chain conformation of conjugated polymers can be studied experimentally, for instance, using dilute solution light scattering [84] and small-angle neutron scattering [58]. Moreover, it is demonstrated that asymmetric side chains (two different side chains of the same polymer) lead to increase of the CT properties due to better packing, forming bimodal (both face-on and edge-on) orientation as well as asymmetric chains influence on the mechanical properties [85]. The choice of appropriate alkyl chains has become an important factor for the design of high performance organic electronics because it could influence on the other properties such as crystallinity, planarity etc.

Additional modification which can be applied in order to affect the properties of the conjugated polymers is the X_{atom} substitution. This is a very broad field of possible realizations not only because of the variety of synthetic chemistry but also because when some atoms of the molecules are added or exchanged, new molecules are formed with different properties and benefits. This is a simple and an effective way to tune the electronic, inter- and intramolecular interactions in polymers and small molecules, mainly due to non-covalent interactions, which are dominant forces in organic molecular crystals.

Non-covalent interactions play an important role in polymers and oligomers because of their multiple growth along the polymer backbones [86]. The simplest way for incorporating a heteroatom is a hydrogen substitution or synthesis of heterocycles. Introducing a X_{atom} substitution has a great impact on the electronic properties, especially on the energy of frontier orbitals and UV-VIS absorption spectra [87]. The X_{atom} substitution affects also the crystal packing, the band structures as well as the conductivity of the samples [88]. Changing the X_{atom} has a strong impact on the potentials of internal rotation and interconversion of conformers, which is related further to the molecular and mechanical properties of the materials [89, 90]. On the other hand, the X_{atom} mainly induces non-covalent (through-space) interactions, which affects primary the planarity of the backbones. Substituting the X_{atom} can also lead to improved air stability and to balanced the e^- and h^+ mobilities [91].

The most popular X_{atom} substitution is the substitution of a hydrogen with fluorine, which influences strongly the electronic and CT properties as well as strengthens the non-covalent interactions of polymers without negative steric effects [92, 93]. One example for such non-covalent interaction (for instance, in fluorinated benzothiadiazole based polymers) is F···S planarization interactions between the nearest neighbour (flank) which have been seen to affect the crystal lattice parameters [94], to increase the barrier and energy difference of torsion rotation [95] and to change the crystallinity of polymers [96]. Another example of through-space intermolecular interaction (in case of polythiophenes) is the S···S multiple short interactions increasing the effective cross-conjugation (forming networks) of orbital overlap, which leads to enhanced CT properties [97, 98]. One more example of the importance of the non-covalent interactions is the self-organization of molecules into single-crystal microribbons via an attractive intermolecular S···S non-covalent interaction [99] or similar S···O interaction (in thienoisoindigo based polymer), which leads to ultra-high hole mobility of 14.4 cm^2/V·s [100]. Moreover, a non-covalent interaction causes the charge penetration, which can occur in stacked monomers. This charge penetration appears when the π-electron clouds of two stacked monomers overlap at relatively small intermolecular distances, which leads to reduced screening of the nuclei. This interaction between stacked molecules is found to be significant in organic crystals [101, 102].

One special case of the through space interactions is the hydrogen bonding (H-bonding). Many investigations are done in order to clarify the interactions due to H-bonding [103, 104, 105]. It is possible to modify the morphology, crystal structure and molecular organization in systems with H-bonding interactions, which is more pronounced for small molecules due to spatial preferences in the crystal structure [106] as compared to polymeric materials. Besides, there is also so called non-conventional H-bonding such as CH···O and CH···N, which has great impact as potential "locking" forces in small molecules and polymers [89]. Additionally, H-bonding can affect the structure and the molecular packing of the molecules [83].

The next factor which has a strong influence on the properties of conjugated polymers are the so-called spacers (flanking units). The D_- and A_+ units can be connected directly to each other or through spacers. It has been shown that when spacers are included between the blocks some of the properties can be changed significantly.

In the most simple case spacers can be -C=C-,-C≡C- bonds as the simplest molecular fragments. These common spacers primary affect the planarity, conjugation length and the rigidity of the polymers and further the electronic and CT properties. For instance, inserting vinylene linker between the units leads to backbone planarization and to extension of the π-conjugation length and further to higher charge carrier mobility [43, 107, 108]. Another example is when units are connected through cyanovinylene spacer. Here the corresponding devices showed maximum e^- mobility and also exhibited the lowest h^+ mobility, which can be used for tuning the polarity of devices [109]. A simple change of double with triple bond between thiophene rings in thienoisoindigo polymer can alter the electronic properties of materials such as increasing the mobilities and decreasing the E_g [110]. Furthermore, the spacers (for instance vinylene) provide reduction of the steric interactions, which partially increases the polymer solubility [111]. More complicated spacers like aromatic rings, for example, thiophene as a small D_- fragment or pyrrole as a small A_+ unit, are very promising π-conjugated units. This approach also allows one to control the electronic properties of polymers because of e^--donating or e^--withdrawing nature of the spacers. Examples of types of spacers are shown in Figure 4.

All the similarities of these linkers are that they are π-conjugated (sometimes one can utilize a methylene fragment in order to prevent further conjugation) but using small molecules as linkers provides much more extension of the π-conjugation (better orbital overlap leads to better performance of the devices). For instance, increasing the number of spacers in benzothiadiazole polymer leads to increased mobility due to changes in the micro-structure of thin films [112].
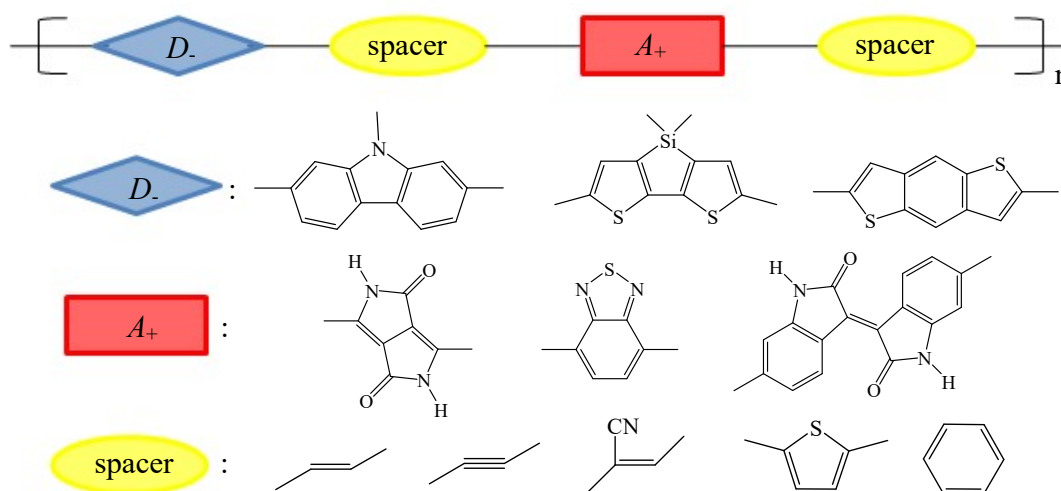
Figure 4. Schematic representation of conjugated D_--A_+ alternating block copolymer linked with spacers (flanking units). Examples for spacers, D_- and A_+ units are also shown.

From experimental viewpoint very important factors during the synthesis of conjugated polymers are the polydispersity, the molecular weight distribution, the terminal chemical groups, which can vary in each synthesis. Increasing the molecular weight leads to higher charge carrier mobilities and improvement of the device performance, which ultimately relates to the

supramolecular order and morphology [20, 113]. Additionally, high molecular weight is desirable for application in bulk heterojunction solar cells, which enhances the efficiency by improved inter-polymer interaction to enhance the current [114, 115, 116].

Along with the molecular weight, the increased solubility due to incorporation of side chains plays a crucial role in the performance of polymers [112] as it was already mentioned. The impurities influence on the CT in semiconducting polymers, acting as charge-carrier traps or exciton quenching sites [117, 118]. The chain end groups have also impact on the device parameters by acting as chemical traps which are quenching the photogenerated excitons, disrupting the chain packing or accelerating degradation [119, 120, 121]. Additional manipulations on the polymers could be done, for instance, by a simple change of the orientation of the repeat units along the backbone that affects the bulk film order and electronic behaviour [122, 123], which is ascribed to higher regioregularity, due to improvement of the interchain packing [124]. The effect of the surrounding medium is observed forming well-ordered aggregation in several common organic solvents and that aggregation strongly affects the solution and the bulk optical properties [125], which can be used for optimization of the regioregularity and crystallinity [126]. Moreover, by careful selection of solvent mixtures (taking into account vapour pressure, solubility and the solvent amount) the performance of organic solar cells can be enhanced by influence on the morphology [127].

Additionally, there are some methods of treatments of the polymers which are very effective for inducing a high crystallinity such as solvent vapour annealing [128, 129], zone casting [130, 131], epitaxy [132, 133, 134, 135], high-temperature rubbing [136, 137, 138, 139, 140] or with presence of additives (such as 1,8-diiodooctane) in the processing, which induces layered structures [141, 142, 143, 144, 145], or adding extra two polar solvents playing the role of additives [146]. Other factors such as changes in the underlying substrate [147] and the thermal management history of the samples also influence on film characteristics and can ultimately define the final optoelectronic performance, for instance, charge carrier mobility decreases when the dielectric constant of insulating layer is increased [148]. Moreover, the hopping mobility is very sensitive to the packing in the first few layers adjacent to the dielectric interface (substrate), which adds another consideration to supramolecular control [149].

Effect of the pressure on the properties of conjugated polymers is described theoretically [150], where the planarity of a polymer can be tuned by applying pressure. Experimentally, the effect of pressure on the charge transport properties of a single crystal is also observed, where with increasing the pressure the mobility is improved due to reduction of the intermolecular distance [151].

Additionally, there are some factors which remain absolutely unexplained such as (i) how the size and orientation of the repeat unit can be used to control the organization or (ii) the influence of processing conditions in determining the final bulk properties cannot be understood as well as (iii) the impact of crystal grain boundaries.

General difficulties emerged that polymers are mixtures of statistical structurally related macromolecules (mainly due to polydispersity and irregular unit arrangement) that differ in number, arrangement and distribution of the repeat units per polymer chain, which leads to the

fact that the polymeric properties can vary in a wide range. One is a reason for the poor reproducibility of polymer synthesis and the difficulty of prediction of their properties. Thus improving the chemical synthesis and the purification processes has ultimate impact on the properties of the polymers [122, 152, 153, 154,155] especially in order to achieve high molecular weight, which leads to better device performance accompanied with changes in thin-film morphology and more isotropic films as it was already mentioned [156].

The complexity of the polymeric properties can be summarized for the attempt to combine solution processability, high charge carrier mobility, wide range optical absorption profiles and large absorption coefficients, appropriate energy band structure and environmental stability. Their electronic properties reflect the interplay between polaronic relaxation, energetic and positional disorder. Strong electron-phonon coupling in polymer solids results in polaron formation, and consequently, the charge transport processes are affected by polaronic relaxation. On the other hand, variation in the local conformation as well as the presence of defects along the polymer chains can cause large energetic disorder and broadening of the electronic density of states.

From theoretical point of view a lot of efforts are done in order to clarify and predict the properties of semiconducting polymers and usually they support the experimental studies. As a rule, the calculations are done on small isolated molecules [86, 157, 158, 159, 160] or using periodic boundary conditions (PBC) on small crystals [86, 161, 162] in order to avoid extremely expensive calculations of real polymeric materials. These simplified calculations provide knowledge about the ground state geometry, possible distortion of the planarity as well as the electronic properties.

The charge transport properties depend on the mutual orientation of the molecules in crystals so they depend on the crystal structure and the intermolecular distances. If the crystal structure of the current compound under investigation is experimentally resolved, it is very easy to compute the CT properties in all the possible pathways (described as stacks of dimers) [163]. The problems arise when the crystal structure is unknown, which is a usual case for polymers, and so a lot of possible structures should be studied and all the different crystal cells reproduce different charge carrier mobilities. Moreover, the prediction of the crystal structure is a very complicated computational task and there are only few cases where the crystal structure is successfully predicted, usually starting from well-known structure of derivatives of the current compounds [164].

One alternative of the crystal structure calculations is to study dimer systems for calculation of the CT properties or binding energies (E_{bind}), which is useful to scan all the possible spatial positions of dimer forming 2D quasi-surface (shifting one of the molecules both horizontally and vertically) [165, 166, 167]. One advantage of this method is that it gives the order of maximum (and minimum) value of the mobility or the dimer configuration with minimum energies. On the other hand, it is difficult to say which of these values will be obtained experimentally. Another disadvantage of this method is that it takes into account only cofacial or perpendicular stacked orientation and it is not suitable for herringbone orientation (Fig. 5, p. 18) since a 3D scan has to be performed around one of the molecules under certain angle (different from 90 or 180°) as well as the dimer molecules are kept at the same distance during the scan.

Typical characteristics obtained from theoretical studies, with respect to the electronic properties, are frontier orbitals (HOMO and LUMO), E_g (and band structures), UV-VIS absorption bands, torsion potential calculations and the quantities required in order to calculate the hopping mobilities (reorganization energies, charge transfer integrals and charge rate constants) which will be discussed in the next section. The non-covalent interactions, including H-bonding [86, 89, 168] and excitation energies [169] are also in focus of computations.
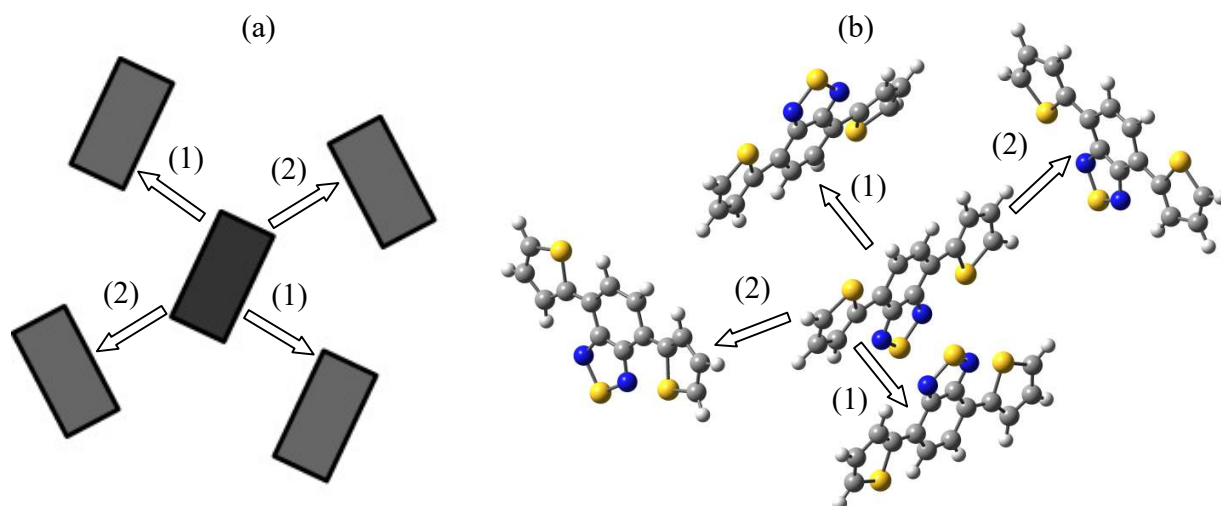

Figure 5. Schematic (a) and molecular (b) representation of the cofacial (1) and herringbone (2) stacks arrangement.

There are only a few cases when oligomers are studied using Quantum Mechanical (QM) approach with periodic boundary conditions [170, 171], whereas the major part of studies has been done for small molecular fragments.

Usually, theoretical investigations do not consider long side chains explicitly. One reason is that the computational effort is increased significantly and after attachment of side chains the backbone geometry of the monomers is commonly distorted. The second reason is that the side chains do not affect the electronic properties of isolated molecules and do not influence on charge transport properties directly. At the same time some crystal structure calculations showed that the side chains could have a great influence of the electronic properties. For instance, the electronic couplings of small-molecule organic semiconductors have isotropic behaviour (with respect to their molecular orientation) with longer side chains and those with shorter alkyl side chains become highly anisotropic, which affect the mobilities subsequently [51], or different side chain length can lead to different crystal structure and further to different electronic properties in benzothiadiazole based polymer [172]. Additionally, the hopping mobilities depend on the length of side chains and also on the type of orientation (herringbone or cofacial) [173]. It is found that the electronic properties (charge transfer integrals and E_g) depend on the torsion angle [174]. The third reason for avoiding the side chains in single molecule calculations is that there are numerous possible ways how to orient the side chains in isolated molecules or in 3D periodic structures.

The number of possible side chain orientations could be reduced if configurations with steric hindrances or unfavourable structures are avoided, involving highly coiled alkyl chains or minimal interactions between the side chains but this attachment still remains a challenge.

According to the experimental studies, linear (hexyl) side chains can adopt primary two types of configurations: shifted (interdigitated) side chains, which are presented in thin films (usually obtained by spin-coating), and non-shifted (non-interdigitated) side chains obtained by growth from extremely slow cooling of melt [175, 178], which are referred to kinetic and thermodynamic structures, respectively (Figure 6).

One more tool to study semiconducting materials is by the means of Molecular Dynamics (MD), which is not so widely applied in semiconducting small molecules [176, 177], oligomers [83, 169] or polymers as compared to QM calculations. One reason is that classical MD cannot provide the electronic properties of the molecules under investigation but there could be found some combined MD/QM approaches, which allow obtaining of the CT properties as additional calculations [83, 178]. Classical MD primary allows one to gain an insight into the packing mode of molecules and the self-organization, for example, two extreme cases of mutual orientation of the D_- and A_+ units in the polymers, mixed or segregated stacks (Fig. 7), can be observed as aforementioned. Additionally, classical MD can provide (statistical) average values obtained from the trajectory of the simulations and the effect of the temperature is taken into account, which are the main advantages as compared to QM.
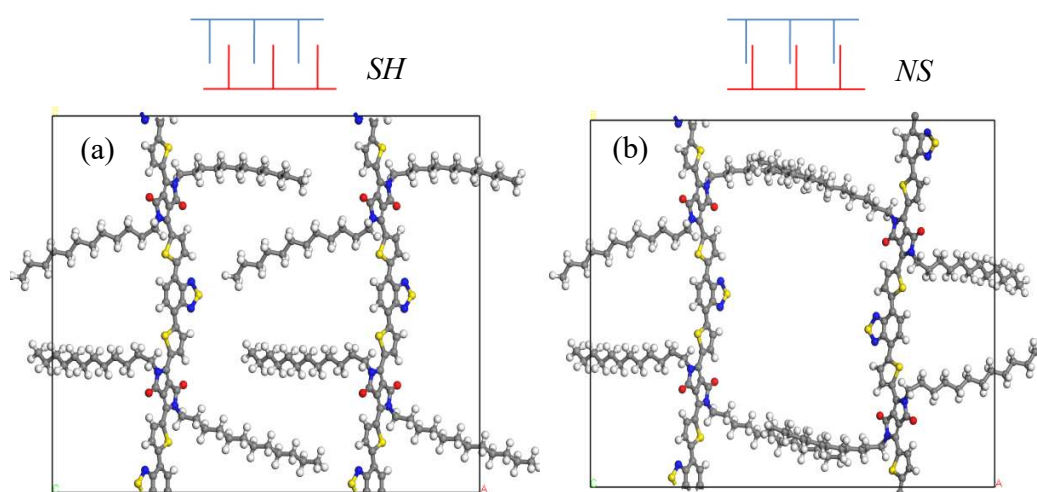

Figure 6. Representation of shifted (a, *SH*, interdigitating) and non-shifted (b, *NS*, non-interdigitating side chains.
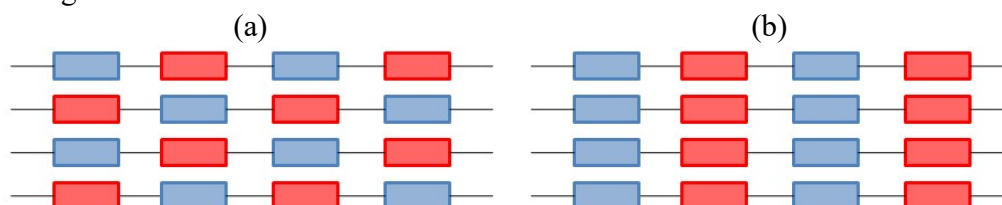

Figure 7. Schematic representation of mixed (a) and segregated (b) stacks.

However, using periodic boundary conditions (PBC) within MD for polymers is a challenge since the system becomes ideal and defects are not taken into account such as isolated molecules, polydispersity or irregular units when the periodicity is along the backbone.

Some theoretical characteristics of the conjugated polymers are absolutely lacking or very rare such as excited state optimizations or mechanical properties and detailed and systematic investigations of their properties are not available or they are very specific.

According to the conductive properties, there are two kinds of conductance: n- and p- type depending on the charge transport of e^- or h^+, respectively. After n-type conductance was discovered in organic electronics, which is intrinsic property of the organic semiconductors [179], this field of the science has undergone new advances. It is very interesting, for the advanced technologies, when the materials exhibit simultaneously n- and p-type conductance, i.e. ambipolarity, which is not only a fundamental property of the materials but this character allows investigation, for instance, of surface phenomena where on the surface states of topological insulators conductivity with well defined n- and p- regions can be observed [180, 181]. The devices which exhibit ambipolarity have many advantages such as very low power consumption, compensating effects in device tolerances (varying the device performance) [182], low power dissipation [183], high noise margin [184], greater operation stability [185], the ability to change the type of the conductance under suitable biasing conditions and device configurations [179, 186, 187, 188]. There are some approaches which demonstrate how ambipolar materials can be obtained: using two stacked layers of discrete e^-- and h^+-transporting organic semiconducting materials [189], using two-component layer comprising a blend of unipolar e^-- and h^+-transporting organic semiconductors [190] and using a single-component layer with symmetric or asymmetric electrodes [191]. In order to achieve high performance air-stable ambipolar polymers, three criteria should be taken into consideration: low-lying LUMO ($\leq$ -4.0 eV) for air-stable electron injection, appropriate deep HOMO ensuring small gap (E_g) ($\leq$ 1.8 eV) and oxidative stability and structural planarity of the polymer backbone for tight solid-state packing and therefore efficient charge delocalization [192].

Even though, the polymers are complicated molecules themselves, they are not so different from the classical inorganic semiconductors according to the charge transport limitation factors. There are some crucial differences between organic and classical inorganic semiconductors such as thermal conductivity [193, 194] and heat energy dissipation, which are much less for conjugated molecules as compared to the Si based devices, but generally they depend on the same factors mentioned above (chemical composition, impurities, molecular structure etc.) with respected to their conductivity. The most critical difference is the crystal structure, which is even more difficult to be resolved for polymeric materials especially when the side chains are included. Conjugated molecules and polymers [195] usually possess more than one (two or more) polymorph forms, which can differ in a few kJ/mol energy, which makes the picture complicated since it is well-known from the inorganic semiconductors that different crystal structures exhibit different charge transport properties. And this problem can be extended very easy to occurrence of more than one mesophase such as liquid crystalline or plastic one (for instance, C_{60} does not have orientation order at room temperature [196]).

Organic crystal structures usually provide devices anisotropic CT within two directions and only in few cases three dimensional mobility is achieved [197, 198].

The temperature has a great influence on the organic electronics materials. For example, the maximum mobility of a device was found in the range from 30 to 200K [199, 200] or quasi-constant mobility was observed in high temperature range 400÷450K [201]. Also, it should be kept in mind that these devices are constructed by several layers of materials with different thermal expansion coefficients and the temperature dependence becomes already a complicated factor.

One very important feature of the performance of the devices is that it depends on the fabrication methods of their architectures, working principles, current-voltage characteristics as well as of the measurable instrument and the working operation which cannot be excluded when the mobilities should be compared or discussed experimentally. One example can be given that the charge carrier mobility varies by a factor of 20 has been recorded when the gate voltage sweep rate is changing [202], so the mobilities depend on the experimental measurement conditions.

There are three general ways of how the hopping mobilities can be improved: first, developing crystal structures with shorter intermolecular distances, second, the surface modifications for single crystals in order to reach trap-free transport which remains unexplored field and third, with improvement of metal-semiconductor contacts [203].

From an overview of the reported mobilities of the conjugated polymers or organic small
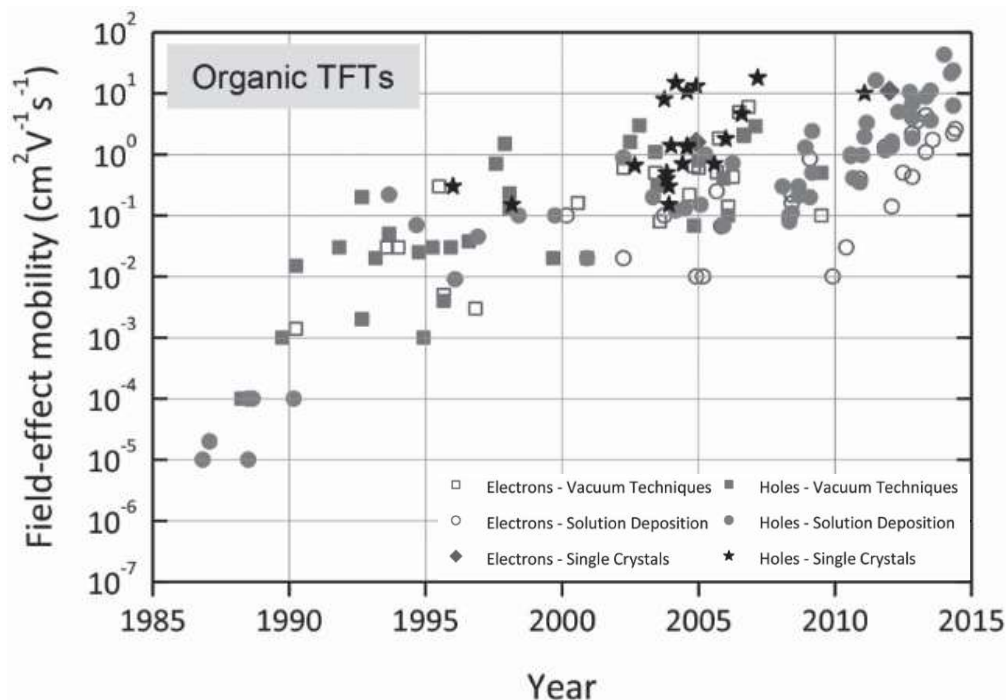

Figure 8. Reported field-effect charge carrier mobilities (in cm^2/V·s) as a function of the publication date adapted from Ref. [204].

molecules (Fig. 8, p. 21) follows that during the last 30 years investigations the charge carrier mobility is increased by seven orders of magnitude (from 10^{-5} up to 10^{2} cm^2/V·s) which shows remarkable progress in this field.

From Figure 8 (p. 21) it looks like that there is an upcoming plateau and the maximum obtained mobility would be of the order of 10^{3} cm^2/V·s and the highest reported mobility so far is 170 cm^2/V·s [205]. If the maximum reached mobilities for conjugated molecules are compared with that of inorganic semiconductors, so far they correspond to the values of disordered classical inorganic semiconductors. Nevertheless, organic materials are still very interesting for science and industrial applications. There are some additional reasons (except of those mentioned above) why organic semiconductors are so intensively studied in recent years: a wide variety of possible molecules, multi-functionality (for example they can emit or absorb light) and they exceeded the mobility of amorphous silicon.

Summarizing all the factors, one can conclude that promising organic semiconductors should have coplanar backbone, low conformational disorder, short π-π distances in a stack, strong intermolecular interactions, high and narrow molecular weight distribution, ordered crystal structure, increased solubility, low lying LUMO, low band gap, pronounced interchain interdigitation, stability upon ambient conditions, soft conditions of performance (operation stability), should be easy and available for synthesis, simple for fabrication etc. When computational methods are applied many of these parameters are simplified or omitted and the mobility depends only on the chemical composition and the structure of the materials. In the next section is described how can be predicted the charge transport properties using theoretical methods.

2.2. Charge Transport Modelling

Two widely used theories describing charge transport in organic materials are the band gap theory (coherent electron transport) and the hopping model (incoherent electron transport) [206, 207, 208]. The first one is ascribed to ordered organic materials at low temperature and there are some experimental confirmations of this model [200]. It assumes that the charge carriers are delocalized all over the system although this mechanism is observed also at room temperature [209]. The second one is attributed as CT in high temperature limit and considers the charge carriers as localized ones due to strong coupling to thermally excited intra- and intermolecular vibrations (electron-phonon coupling). Besides, if weak intermolecular electronic coupling occurs the hopping regime becomes dominant and in this case the charge transport is described as intermolecular hopping.

The charge carrier mobility characterizes the ability of a semiconductor to transport charges and it determines the device performance as it was discussed in the previous chapter. According to the two above mentioned mechanisms the hopping mobility can be approximated as a sum of two contributions:

$$\mu = \mu_{tun} + \mu_{hop} \qquad (2)$$

where μ_{tun} is the contribution for the band-like regime (electron tunneling) and μ_{hop} is the term for hopping like regime. Standard mathematical expression for the charge carrier mobility (μ) is given by Einstein-Smoluchowski equation and if the CT is considered as one dimensional, similarly to the diffusion processes:

$$\mu = \frac{eD_c}{k_B T} = \frac{1}{2} \frac{ed^2 K_{CT}}{k_B T} \qquad (3)$$

where e is the elementary charge, D_c is the diffusion coefficient, d is the (travel) distance, K_{CT} is the charge rate constant, k_B is the Boltzmann constant and T is the temperature.

In order to compute the mobility, the charge rate constant (K_{CT}) has to be evaluated. The charge (electron) transport is usually assumed as a "chemical reaction" between two neighbouring molecules at appropriate distance. Classically, the calculation of the charge rate constant involves estimating the probability of reaching a many-dimensional intersection region of a transition state on a potential energy curve. Moreover, it should be taken into account a suitable weighted frequency for crossing this intersection region and a transition probability going from one state to another one. Since the electron transfer is much faster as compared to nuclei motion the Franck-Condon principle (during electron transition nuclei do not change their coordinates) can be applied. Additionally, the charge transport between two molecules (bimolecular reaction) assumes that the molecules do not share atomic groups since only electron is transferred during the reaction as it is described like weak electronic coupling. First-order charge rate constant for electron transfer at fixed distance is given by [210, 211]:

$$K_{CT} = \frac{2\pi}{\hbar} V^2 F_{FC} \qquad (4)$$

where $\hbar$ is reduced Plank constant, V is the electronic coupling (charge transfer integrals) and F_{FC} is the Franck-Condon factor. F_{FC} is a sum of products of overlap integrals of the vibrational and solvational wave functions of the reactants with those of the products weighted by Boltzmann factors. Typically, quantum-mechanical theories treat the nuclear motion like (i) all coordinates at fixed distance as a collection of independent oscillators or like (ii) assuming harmonic (or Morse) oscillators for the reactants and the rest (the solvent) is treated classically using the free energy of solvent reorganization. When the first (i) choice is made eq. (4) takes the form:

$$K_{CT} = \frac{2\pi}{\hbar} V^2 \sum_{v_r, v_p} (F_{FC})_v \, p(v_r) \qquad (5)$$

where $(F_{FC})_v$ is the Franck-Condon (vibrational) factor for any given set of vibrational quantum numbers v_r of the reactants' and v_p of the products' (including the solvent oscillators) and $p(v_r)$ is the equilibrium (Boltzmann) probability of finding the system in the vibrational state v_r.

When all of the vibrational frequencies v_i in $(F_{FC})_v$ are small ($h v_i / 2 k_B T \leq 1$), eq. (5, p. 23) becomes a standard Arrhenius type equation:

$$K_{CT} = \frac{V^2}{\hbar} \sqrt{\frac{\pi}{\lambda_{tot} k_B T}} e^{-(\Delta E^{0*} + \lambda_{tot})^2 / 4 \lambda_{tot} k_B T} \tag{6}$$

where ΔE^{0*} is the enthalpy of the reaction and λ_{tot} is the total reorganization energy.

When the second assumption (ii) is made in the high temperature limit, the charge rate constant is transformed into the equation of semiclassical Marcus theory:

$$K_{CT} = \frac{V^2}{\hbar} \sqrt{\frac{\pi}{\lambda_{tot} k_B T}} e^{-(\Delta G^0 + \lambda_{tot})^2 / 4 \lambda_{tot} k_B T} \tag{7}$$

where ΔG^0 is the free energy of the reaction. The difference between eq. (6) and eq. (7) is only that eq. (7) contains ΔG^0 instead of ΔE^{0*}. However, if eq. (7) is accompanied with the most simple case when the reactants and the products are identical, and there are no broken or new formed chemical bonds, so called self-exchanged reactions ($\Delta G^0 = 0$, eq. 57, p. 42), it results:

$$K_{CT} = \frac{V^2}{\hbar} \sqrt{\frac{\pi}{\lambda_{tot} k_B T}} e^{-\lambda_{tot} / 4 k_B T} \tag{8}$$

This is the most frequently applied equation for estimation of the charge rate constants in organic materials at room temperature since it is easy for implementation. The same expression (eq. 8) can be obtained from the more general polaron model where electron-polaron interactions are taken into account (Holstein theory). In the polaron model if it is considered the limiting case when the phonon energy is much less as compared to the thermal energy ($\hbar \omega_0 \ll k_B T$) and assuming that the polaron energy is equal to $E_{pol} = \lambda_{tot} / 2$ it will be obtained again the expression of the semiclassical Marcus equation (for self-exchanged reactions). The polaron model can be used to estimated both hopping and tunneling mechanisms (eq. 2, p. 23) since semiclassical Marcus theory is suitable to evaluate only for hopping mechanism.

Since chemical and physical defects are usually presented in organic materials (for instance, presence of an amorphous regions in the crystal structure) the charges are more and more localized and the CT regime becomes hopping-like mechanism (which is expected for organics). There are two main models for description of disordered structures. One is the above mentioned Marcus theory. Another model, the Miller-Abrahams' formalism, originally has been developed to describe doped inorganic semiconductors and the charge rate constant from hopping mechanism from site i to site j is given by:

$$K_{CT} = \omega e^{-2\gamma R_{ij}} \begin{cases} e^{-\frac{\varepsilon_j - \varepsilon_i}{k_B T}} & \varepsilon_j > \varepsilon_i \\ 1 & \varepsilon_j < \varepsilon_i \end{cases} \tag{9}$$

where ω is the hopping frequency, R_{ij} is the separation between site i and j, γ is an overlap factor, ε_i and ε_j are the site energies.

Both Marcus and Miller-Abraham theories can be derived as two limiting cases by the means of time-dependent perturbation theory in case of weak electronic coupling.

Theories describing inorganic and organic semiconductors are different because they differ in the scale of the mobility, for instance, AlGaAs/GaAs heterostructures grown by molecular beam epitaxy afford incredible mobility on the order of about $3.5 \cdot 10^7$ cm^2/V·s [212]. A united theory for both types of semiconductors which covers the whole range of temperature (both mechanisms) still does not exist. However, calculating CT properties in organic molecular crystal is a challenging task, since electron and nuclei (phonon/vibrations) motions are coupled together.

In this work eq. (3, p. 23) and eq. (8, p. 24) are utilized for calculation of the mobility and the charge rate constant, respectively, because they predict correct values for organic devices at room temperature according to the experimental measurements and they are easy for implementation: they depend only on two parameters λ_{tot} and V.

λ_{tot} is the total reorganization energy which measures the strength of the local electron-phonon coupling [207, 213] and it should be minimized in order to achieve high mobilities with respect to eq. (8, p. 24). It consists of two contributions, one is due to the fast changes in molecular geometry (λ_i, inner contribution) and the other one is due to the slow variations in polarization of surrounding medium (λ_o, outer shell contribution):

$$\lambda_{tot} = \lambda_i + \lambda_o \qquad (10)$$

Generally, λ_{tot} is a individual molecular properties and it can be calculated for each molecule. The inner shell contribution (λ_i) can be estimated by so called four-point formalism as a difference of geometry relaxation energies upon going from neutral (0) to charged state ($\pm$) geometry [206]:

$$\lambda_i = (E_\#^\pm + E_\#^\pm) - (E^\pm + E^0) \qquad (11)$$

where $E^\pm$ and E^0 are the ground (equilibrium) state energies of charged and neutral state, respectively, $E_\#^\pm$ and $E_\#^0$ are the energies of charged states at optimized neutral-state geometry, and vice versa. The outer shell contribution is usually adjustable parameter and also it can be omitted for conjugated molecules [206] as well as it can be computed by frequency-resolved cavity model (FRCM) [214, 215]:

$$\lambda_o^{FRCM} = (\Delta q)^2 \left(\frac{1}{2r_1} + \frac{1}{2r_2} - \frac{1}{R} \right) \left(\frac{1}{\varepsilon_{op}} - \frac{1}{\varepsilon_{st}} \right) \qquad (12)$$

where q is the transferred charge, r_1 and r_2 are the effective radii of solvated molecules, $R=r_1+r_2$ is the intermolecular distance, ε_{op} and ε_{st} are the optical (square of the refractive index) and static

dielectric constants of the solvent, respectively. Another way for calculation of the outer shell contribution is to take into account the solvent effect [216]: first to evaluate the total reorganization energy (with surrounding medium) and afterwards to subtract the obtained value from the value calculated without solvent interactions (λ_i):

$$\lambda_o = \lambda_{tot}^{Solvent} - \lambda_i \tag{13}$$

The second parameter (V) required for computation of the charge rate constant (and further the mobilities) is the electronic coupling (charge transfer integrals). It describes the transition between two electronic states when a charge is transferred between adjacent molecules in an interacting dimer. It is determined by the electronic nature of the molecules or fragments involved and it depends on the mutual orientation of the molecules, especially of the distance between them or more correctly it depends on the degree of the wave function overlap which in turn depends on the bonding/anti-bonding pattern between adjacent molecules [217]. The electronic coupling is defined by the matrix element:

$$V = \left\langle \Psi_\alpha \left| H \right| \Psi_\beta \right\rangle \tag{14}$$

where H is the electronic Hamiltonian of the system, Ψ_α and Ψ_β are the wave functions of the initial and final charge-localized state, respectively. There are various procedures of how V can be estimated [218, 219]. One simplified approach is the energy splitting in dimer (ESID) method which provides an approximation evaluated from the Kohn-Sham (KS) orbital energies of dimer system (two molecules):

$$\left| V^{ET} \right| \approx \frac{\left| E_{LUMO}^{KS} - E_{LUMO+1}^{KS} \right|}{2} \tag{15}$$

$$\left| V^{HT} \right| \approx \frac{\left| E_{HOMO}^{KS} - E_{HOMO-1}^{KS} \right|}{2} \tag{16}$$

where V^{ET} and V^{HT} are the electron coupling for e^- and h^+ transfer, respectively, *LUMO, LUMO+1, HOMO* and *HOMO+1* are the corresponding orbital energies. This approach is the most frequently utilized for evaluation of the electronic coupling [166]. The next section describes the aim and objectives of this theoretical investigation.

2.3.　　Aim and Objectives

The goal of this study is to investigate semiconducting D_-/A_+ copolymers by the means of a multiscale computational approach starting from the constitutive small units via rational monomer design to the charge transport properties of copolymers.

As A_+ units, diketopyrrolopyrrole (*DPP*) and benzothiadiazole (*BTZ*) molecules are selected, linked either with furan (*Fu*) or thiophene (*Th*) spacers as D_- in one polymer chain (Figure 9). In order to reach the above mentioned goal the following steps have been undertaken: (1) starting from isolated small molecules *Fu-BTZ-Fu*, *Th-BTZ-Th*, *Fu-DPP-Fu*, *Th-DPP-Th* and *Th-DPP-Th*, and their corresponding monomers *Fu-BTZ-Fu-DPP-Fu*, *Th-BTZ-Th-DPP-Th*, the conformational, energetic and the optical properties are characterized using Density Functional Theory (DFT) calculations. Here, the effect of the spacer (flank, *Fl*) linking two units is evaluated. (2) The next stage of the study is based on calculations of parallel and anti-parallel interacting dimers of the above mentioned molecules on DFT level. Here the effect of the mutual orientation of the molecules in dimers (two molecules in a stack) are described in the binding energies and the electronic couplings depending on the spacer, π-π distance in the stacks and later to the transversal and longitudinal shifts of the molecular backbone. Additionally, n-mers (n=2÷5) of *Fl-(BTZ-Fl-DPP-Fl)*$_n$ are studied within DFT in order to reproduce better electronic properties as compared with available experimental data. (3) The third part of this work is related to the classical Molecular Dynamics simulations of the crystalline phases of the constructive parts (*Th-BTZ-Th*) and polymeric crystals (*-Fu-BTZ-Fu-DPP-*)$_6$, (*-Th-BTZ-Th-DPP-*)$_6$ subjected to periodic boundary conditions (PBC). Here the effect of the thermal disorder is simulated implicitly. Additionally, the type of the side chains (here, linear or branched) is taken into account for polymers (Figure 9). (4) Finally, the predicted charge transport properties are compared with available experimental data.

The chosen molecules are very common in experimental investigations and they are very effective in fabrication of organic electronic devices.
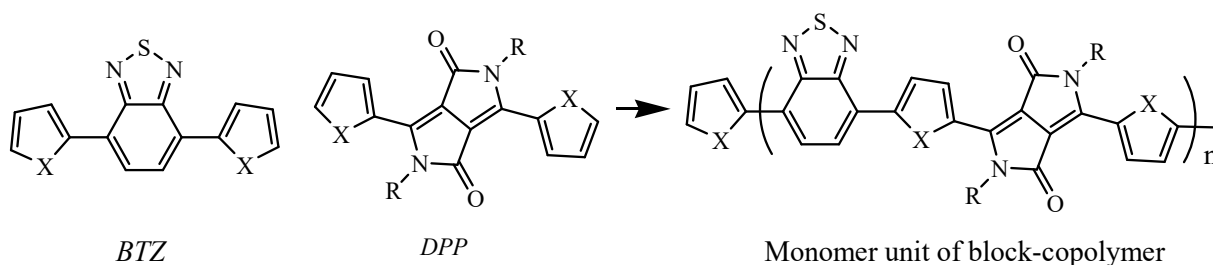

BTZ   *DPP*   Monomer unit of block-copolymer

Figure 9. Schematic representation of the molecules under study (X=O or S, *Fu* or *Th*, respectively), R=-H, -CH$_3$, -C$_{12}$H$_{25}$ or -C$_2$H$_3$(-C$_8$H$_{17}$)-C$_{10}$H$_{21}$, n=1÷5 or 6.

BTZ molecule unit has been widely utilized in organic electronics especially in organic photovoltaics [220, 221] and it can be considered as a building block for both n- and p-type materials [110, 192]. *BTZ* is one of the most promising A_+ unit in D_--A_+ polymers owing to its strong electron affinity [92, 93, 222, 223] and it can be easily modified by introducing electronegative substituents such as fluorine or nitrile (-CN) groups. Single junction devices based on *BTZ* containing polymers have achieved power conversion efficiency of over 10% [26]. Some of *BTZ* polymers exhibit high charge carrier mobilities [20] as well as ambipolarity and air stability [192].

DPP unit has become like a benchmark in organic electronics and a lot of *DPP* containing polymers are studied and many high performance ambipolar conjugated polymers are based on this unit [43, 224, 225] and some of them possess high thermal stability (5% loss over 360 °C) [226]. *DPP* has a strongly polarized core, which increases dramatically the intermolecular interactions in polymers. *DPP* requires a number of long or bulky alkyl side chains to ensure solubility, however, the side chains often interfere with an effective π-π overlap, leading to low crystallinity. An additional benefits of *DPP* is that it is relatively easy and inexpensive for synthesis and there are a lot of possibilities for its decoration.

Combining *DPP* and *BTZ* in D-A+ polymers results in high performance ambipolarity and reproducible characteristics [44, 227, 228, 229, 230, 231].

First of all, molecules containing fused-ring systems (such as *BTZ* and *DPP*) intend to maximize the π-overlap by restricting the intramolecular rotation in the oligomer and possibly due to inducing face-to-face π-stacking, facilitating charge transport through intermolecular hopping. On the other hand, the fused aromatic rings can make the polymer backbone more rigid and coplanar, therefore enhancing effective π-conjugation, lowering E_g and extending absorption [232].

Nevertheless, increasing the planarity could decrease the solubility, which leads to low molecular weight, but in some cases the CT properties remain unaffected [233]. Usually, molecules with coplanar and rigid structure have smaller $λ_{tot}$, which is beneficial for achieving high charge-carrier mobility according to eq. (8, p. 24) as it was mentioned.

Usually, D-/A+ units are linked with spacers and one more advantage (in addition to the mentioned ones in the introductions) of the aromatic spacers (such as *Fu* and *Th*) is that they will reduce the steric hindrance between adjacent *BTZ* and *DPP* units and thereby the planarity will be improved (and further the charge transport properties) as well as the side chain interactions will be facilitated. Regardless, the solubility could be significantly reduced when more flanks like *Th* are introduced in a polymer [234].

Polythiophenes and fused thiophenes are perhaps the most prevalent class of conjugated organic semiconductors [186, 235, 236, 237] and nowadays *Th* remains as flaking units or D- block in organic semiconductors [86, 91, 109, 110, 112, 126, 192]. One reason for the wide use of *Th* based compounds is the high polarizability of sulphur atoms and their ability to engage in strong S···S and S···π intermolecular interactions, which contributes to the good charge carrier mobility of oligothiophenes and their derivatives [238, 239] as it was already discussed. Additionally, oligothiophenes have greater stability than other π-conjugated oligomers. But there are also some drawbacks of sulphur containing molecules such as relatively low solubility, inefficient luminescence because of the quenching "heavy atom" effect and low rigidity of *Th-Th* bond, which allows twisted conformations.

The analogues of polythiophenes are polyfurans. *Fu* based materials are not so intensively studied as compared to *Th* compounds. One reason is that upon replacing sulphur with oxygen atom, the aromaticity is reduced and the oxidation potential is lowered. On the other hand, *Fu* molecules are considered as promising candidate for sustainable organic electronics because they

are biodegradable and can be produced from renewable resources [240, 241]. One major advantage of *Fu* containing molecules is that they are much more soluble as compared to *Th* ones. Additionally, *Fu* based derivatives can be synthesized in non-chlorinated solution processing [242].

If one compares the properties of *Th* and *Fu* oligomers, *Fu* ones are much more rigid, they have greater E_g [171], better charge delocalization and strong fluorescence [243, 244] as compared to *Th* molecules. According to their CT properties it is shown that *Fu* and *Th* containing polymer analogues have comparable, high and balanced mobilities [225, 227, 228, 229, 230, 245]. There are only several studies where *Fu* containing molecules are investigated theoretically [171, 176, 243, 244, 246, 247, 248, 249].

Despite of all experimental and theoretical efforts in this field it is still debated which are the tuning parameters for achieving high performance devices and there are mainly specific investigations of conjugated organic electronic molecules where the main aims are to obtain high hopping mobilities or high power conversion.

This work answers several questions regarded to how to obtain high (and balanced) performance organic electronics with systematic and detailed research of the chosen objects (Fig. 9, p. 27):

- ✓ Which are the parameters defining high and balanced mobilities for organic molecules?
- ✓ How does the charge carrier mobility depend on molecular orientation?
- ✓ What is the influence of heteroatom on molecular properties?
- ✓ How do the side chains influence on the crystal structure in polymers?
- ✓ How do the charge transport properties depend on crystal structure?
- ✓ Which are the dominant interactions in polymeric materials?
- ✓ How do the mechanical properties depend on heteroatom and side chains?

The scientific novelty of this work is in the step-by-step investigation and comparison of the properties on each level combing classical and quantum methods. Moreover, different methods for calculation of the charge transport properties are compared. This work can point out how the chemical structure can be manipulated in order to achieve desirable (for example, ambipolar) properties and it will be useful for design of high performance materials applied in organic electronics. In the next chapter the computational tools are explained, which are utilized in order to obtain the goal of this study.

3.   Computational Methods and Models

This chapter gives a brief introduction of the theoretical methods and models which are employed in order to achieve the goal of this work.

3.1.   Oligomer Molecular Approach

Since the theoretical description of polymers is computationally expensive and usually, it is even impossible to simulate infinitely long chains, the so called oligomer molecular approach can simplify the calculations. The idea of this approximation is to investigate small molecules or oligomers, which the polymers are constructed from, and further to relate the properties of small molecules to the polymeric materials. This approach is very useful when it considers only static molecular arrangements because the semiconducting polymers are usually stacked in networks and their motion (for instance, due to diffusion) is hindered as compared to organic electronics based on small molecules. On the other hand, this method does not take into account some of details, for example, such as side chains and interactions due to the closest neighbours. One of the most applicable ways to apply this oligomer molecular approach is to study systems systematically increasing the number of molecules (the system size) involved in the calculations and further to apply an extrapolation method in order to predict the properties of polymers (infinite number of units). Applying such an approach, usually the electronic properties of the conductive polymers are evaluated such as E_g or electronic coupling (V) and further the charge transport properties [157, 160, 250]. But also it could be used to calculate the mechanical properties (rigidity of the chains, Kuhn segment) of polymers [251].

The oligomer approach also allows obtaining another key parameter like the reorganization energy (λ_{tot}) and it is shown that for polymers the reorganization energy tends to zero [252], which is favourable for higher mobilities according to the semiclassical Marcus theory (eq. 8, p. 24). It is very useful to study molecular organizations and assemblies in periodic systems of oligomers, which provides information about the preferable orientations and the packing modes. Moreover, this approach is very easy for implementation and shows good results for polymers, if the polymers are not amorphous. Nevertheless, it should be kept in mind that the most specific and fundamental properties of the organic materials and generally for polymers are obtained when it is considered the whole macromolecules such as electron delocalization and conductivity, mechanical flexibility, crystal structure, stacking mode, relaxation effects, glass transition, which cannot be investigated only with monomer (or oligomer) units. In order to reproduce good results all the details must be included, which is usually done with periodic boundary conditions. The next sections explain the computational tools which are used in order to study organic electronics materials from small molecules up to block copolymers.

3.2. Density Functional Theory

Density Functional Theory (DFT) is a quantum mechanical method based on Hohenberg-Kohn theorem - every stationary many-particle system in its ground state can be characterized fully (uniquely) by the ground state electron density. DFT does not rely on the wave function (Ψ) itself but only on the electron density (n_0), which depends on three spatial coordinates. If N interacting particles are considered the standard Hamiltonian ($\hat{H}$) for stationary system has the following form:

$$\hat{H} = \hat{T} + \hat{V}_{ext} + \hat{W} \tag{17}$$

where $\hat{T}$ is the operator of kinetic energy, $\hat{V}_{ext}$ is the interaction of particles with an external source operator, which is characterized by time-independent potential v_{ext} (due to nuclei), and $\hat{W}$ is the particle-particle interaction. Many-body eigenstates $|\Psi_k\rangle$ corresponding to the $\hat{H}$ are obtained by the stationary Schrödinger equation:

$$\hat{H}|\Psi_k\rangle = E_k|\Psi_k\rangle \tag{18}$$

The ground state electron density is introduced by:

$$n_0(r) = \langle \Psi_0 | \hat{n}(r) | \Psi_0 \rangle = N \sum_{\sigma_1...\sigma_N} \int d^3r_2...d^3r_N \left| r\sigma_1 r_2\sigma...r_N\sigma_N | \Psi_0 \rangle \right|^2 \tag{19}$$

where $\hat{n}(r)$ is a spin density operator, r is spatial coordinate and σ is a spin variable.

The Hohenberg-Kohn theorem leads to three fundamental statements: (1) the ground state is a unique function of the ground state electron density, (2) any ground state observables are density functionals and (3) the ground state energy can be obtained only with the ground state density (variational principle).

In order to introduce the Kohn-Sham equations (DFT method), it should be considered a system with non-interacting particles (electrons) with a multiplicative effective (external) potential v_s. The corresponding N-particle ground state $|\Phi_0\rangle$ where $|\Phi_0\rangle$ is a Slater determinant (where the subscript "s" means non-interacting):

$$\hat{H}_s|\Phi_0\rangle = E_{s,0}|\Phi_0\rangle \tag{20}$$

$$\langle r_1\sigma_1...r_N\sigma_N | \Phi_0 \rangle \equiv \Phi_0(r_1\sigma_1...r_N\sigma_N) = \frac{1}{\sqrt{N!}} \det \begin{pmatrix} \phi_1(r_1\sigma_1) & \cdots & \phi_N(r_1\sigma_1) \\ \vdots & \ddots & \vdots \\ \phi_1(r_N\sigma_N) & \cdots & \phi_N(r_N\sigma_N) \end{pmatrix} \tag{21}$$

which is constructed from the energetically lowest solutions (ϕ_i) of single particle Schrödinger equation:

$$\left\{ -\frac{\hbar^2 \nabla^2}{2m} + v_s(r) \right\} \phi_i(r\sigma) = \varepsilon_i \phi_i(r\sigma) \qquad (22)$$

The last step is to introduce the potential v_s, which can be subdivided into the individual contributions:

$$v_s(r) = v_{ext}(r) + v_H[n_0](r) + v_{xc}[n_0](r) \qquad (23)$$

where $v_H[n_0]$ and $v_{xc}[n_0]$ are the potentials for Hartree (direct Coulomb) and exchange-correlation, respectively. Finally, inserting eq. (23) into eq. (22) the Kohn-Sham equations for single particle interacting system are obtained:

$$\left\{ -\frac{\hbar^2 \nabla^2}{2m} + v_{ext}(r) + v_H[n_0](r) + v_{xc}[n_0](r) \right\} \phi_i(r\sigma) = \varepsilon_i \phi_i(r\sigma) \qquad (24)$$

The total energy can be decomposed as:

$$E[n_0] = T_s[n_0] + E_H[n_0] + E_{ext}[n_0] + E_{xc}[n_0] \qquad (25)$$

where $T_s[n_0]$ is the kinetic energy, $E_H[n_0]$ is classical (Hartree) interaction energy between N particles with density n_0 (including their self-interaction), $E_{ext}[n_0]$ describes the couplings between the particles and the external potential and $E_{xc}[n_0]$ is called exchange-correlation energy.

The functionals $T_s[n_0]$, $E_H[n_0]$ and $E_{ext}[n_0]$ are universal and this is valid also for $E_{xc}[n_0]$. It should be emphasized that DFT exchange-correlation energy is not identical with the conventional exchange-correlation energy, which is usually employed in standard many-body theory and in quantum chemistry (the difference between the energy of system with interacting particles and its classical counterpart without taking into account the electron correlation).

However, system of interacting particles is described by another system with non-interacting particles in an effective external potential (due to the nuclei), it appears the problem that it is required the exact $E_{xc}[n_0]$ in order to map the electron density, and a universal exchange-correlation functional is still not found. The exact representation of $E_{xc}[n_0]$ provides an ideal starting point, which can be improved later in order to reach the exact solution. In this sense DFT is called first-principle approach. Also, there are many approximations which provide expressions for the exchange-correlation functional (different DFT functionals).

In this work mainly two so-called DFT hybrid functionals are employed. Within this approximation the exact exchange functional is an admixture with other (gradient) type functionals. As a consequence the exchange-correlation energy is split into two terms, one for exchange and one for correlation energy, which are usually treated as parameterized linear combinations:

B3LYP functional [253] - Becke (B), three-parameter (3), Lee-Yang-Parr (LYP) has the following form of the exchange energy:

$$E_{xc}^{B3LYP} = E_x^{LDA} + E_c^{:LDA} + a_0(E_x^{HF} - E_x^{LDA}) + a_x(E_x^{GGA} - E_x^{LDA}) + a_c(E_c^{GGA} - E_c^{LDA}) \qquad (26)$$

where the parameters a_0, a_x and a_c have values 0.20, 0.72 and 0.81 respectively, the subscript indexes "x" and "c" are for exchange and correlation (energy), respectively. The superscripts correspond to the following functionals: Local-Density Approximation (LDA), Hartree-Fock (HF) and Generalized-Gradient-(Density)-Approximation (GGA). B3LYP has the same parameters as B3PW91 functional but instead of correlation functional term PW91 it has LYP. B3LYP has been widely and successfully employed in studies of conjugated polymers delivering the most accurate ground state geometries [161, 254, 255, 256].

M06-2X [257] - Minnesota (M) 06 two time exchange (2X). This is global hybrid functional based on meta-GGA approximation with 54% Hatree-Fock exchange. It has high accuracy for thermochemistry, kinetics and the π-π non-covalent interactions which are important, for instance, for determination of the binding energies (E_{bind}) in stacked dimers.

Additionally, in order to describe a N-electron system (wave function) it is required N-single-electron orbitals and each single-electron orbital should be defined by a set of functions. In order to simplify the efforts the number of the functions is reduced to a set of pre-defined functions (basis set) which is capable to describe different types of electrons (for instance, functions for 1s, 2s, 2p etc. electrons). Moreover, a basis set can provide functions for specific interactions (polarization function, diffusion function etc.) and also different type of functions (Gaussian functions, Slater type functions, plane waves etc.).

In this study 6-31G* basis set (Pople's split-valence double zeta) is applied with B3LYP. This basis set provides six (6) primitive Gaussian functions (G) for the inner shell and four primitive Gaussian functions split into two (31) for the valence shell and there is an additional polarization function (*) on the heavy (without hydrogen) atoms. Dunning correlation-consistent polarized (cc-p) valence triple-zeta (VTZ) basis set is utilized with M06-2X, which includes large set of polarization functions for the corresponding shells (d, f, g etc.). It provides 16 functions for the H-atoms, 30 functions for the atoms up to Ne and 34 functions for the atoms from Na to Ar.

In order to access excited states time-dependent (TD)-DFT is additionally applied. TD-DFT shows that there is a unique mapping between the time-dependent external potential of a system and its time-dependent e^- density at given initial wave function (known as Runge-Gross theorem). Many-body wave function $|\Psi(t)\rangle$ corresponds to the time-dependent Schrödinger equation at initial state $|\Psi(t_0)\rangle = |\Psi(0)\rangle$ can be written as:

$$i\hbar\frac{\partial}{\partial t}|\Psi(t)\rangle = \hat{H}(t)|\Psi(t)\rangle \qquad (27)$$

where $\hat{H}(t)$ is standard time-dependent Hamiltonian (eq. 17, p. 31). If a Slater determinant with time-dependent many-body state $|\Phi(t)\rangle$ (constructed from N single-particle time-dependent orbitals $\phi_i(r\sigma t)$) satisfies a given initial condition (t_0), a unique solution of a TD-non-interacting system is guaranteed. If one can find a non-interacting TD potential $v_s(rt)$, which reproduces an identical density with interacting system, TD-DFT is capable to simulate interacting systems.

The time-dependent Kohn-Sham equations for single-particle take the form:

$$\left\{-\frac{\hbar^2\nabla^2}{2m} + v_{ext}(rt) + v_H(rt) + v_{xc}(rt)\right\}\phi_i(r\sigma t) = i\hbar\frac{\partial}{\partial t}\phi_i(r\sigma t) \tag{28}$$

However, DFT method provides static description of the system since it is assumed that the nuclei are immobilized as the electrons move much faster than the nuclei. This is known as Born-Oppenheimer approximation, which allows separation of the wave function into two contribution - one for the nuclei coordinates (R) and one for the electronic coordinates (r):

$$\Psi(R,r) = \Psi_n(R)\Psi_e(R,r) \tag{29}$$

where $\Psi_n(R)$ is the wave function, which depends only on the nuclei coordinates, and $\Psi_e(R,r)$ is the wave function, which depends on the electronic coordinates and only parametrically of the nuclei coordinates.

Therefore, in this work quantum chemical calculations are performed on oligomers and further they are combined with classical Molecular Dynamics (MD) where the motion of the atoms is included explicitly and additionally it allows simulation of systems with many particles. Moreover, due to high computational efforts DFT is not suitable for simulation of large systems consisting of many molecules or macromolecules especially when the basis set is large enough. In the next section MD is described in order to gain insight into the details of interactions and molecular organization in polymeric materials.

3.3.   Molecular Dynamics

Molecular Dynamics (MD) is based on solving classical equation of motion for a system of N particles via a potential U given in eq. (36, p. 35) as U_{tot}. These equations can be written in various ways but perhaps the most fundamental form is the Lagrangian equation of motion:

$$\frac{d}{dt}\left(\frac{\partial L}{\partial \dot{q}_k}\right) - \left(\frac{\partial L}{\partial q_k}\right) = 0 \tag{30}$$

where t is time, q_k are generalized coordinates ($\dot{q}_k$ is the first time derivative of q_k) and the Lagrangian function $L(q,\dot{q})$ is defined in terms of kinetic and potential energy:

$$L = K - U \tag{31}$$

If a system of atoms is considered and if one chooses appropriate forms for the kinetic (eq. 32, p. 35) and the potential (eq. 33, p. 35) energy, it can be obtained the second Newton's law (eq. 34, p. 35):

$$K = \sum_{i=1}^{N} \sum_{\alpha} p_{i\alpha}^2 / 2m_i \tag{32}$$

$$U = \sum_i u_1(r_i) + \sum_i \sum_{j>i} u_2(r_i, r_j) + \sum_i \sum_{j>i} \sum_{k>j>i} u_3(r_i, r_j, r_k) + \ldots \tag{33}$$

$$m_i \ddot{r}_i = f_i \tag{34}$$

where p_i is the momentum, m_i is the mass, u_i are pair potentials, $\ddot{r}_i$ are second time derivatives cartesian coordinates (acceleration), f_i is the force, i, j, k run over all particles (N) and α runs over all the components (x, y, z).

It has to be computed all the force (f_i) between the particles, i.e. the Newton's equation of motion (eq. 34) requires integration. There are many procedures in order to integrate eq. (34) and the quality of MD simulation depends on the method of integration. One way to do this integration is so-called Verlet algorithm, which has the following form:

$$r(t + \Delta t) \approx 2r(t) - r(t - \Delta t) + \frac{f(t)}{m} \Delta t^2 \tag{35}$$

where Δt and Δr are the time (equal to time step in MD simulations) and the coordinate difference between two steps, respectively.

Verlet algorithm estimates the new coordinate positions with an error of order of Δt^4 and does not use the velocity to compute the new positions. It computes the new positions from the previous ones and only for the first two steps an initialization is needed.

If the particles in the system are considered not like single beads but molecules consisting of connected atoms, the inter- and intra-atomic interactions have to be computed, i.e. the total potential energy in MD system (eq. 36).

The total potential energy can be estimated using so-called force-field (FF). Usually, FF is described by parameterized potentials where the atoms are considered as rigid (undeformable) spheres and the total potential energy can be subdivided into individual contributions of the interactions: bond stretching, torsion rotation, etc. There are many force fields available in order to simulate the behaviour of a certain system. In this work the Polymer Consistent Force Field (PCFF) is employed, which is the second-generation FF. It is developed for a wide range of organic compounds and intended for application in polymers and organic materials.

The total potential energy of FF can be expressed as:

$$U_{tot} = U_{bonded} + U_{cross} + U_{nonbonded} \tag{36}$$

where U_{bonded} and $U_{nonbonded}$ correspond to intra- and inter-molecular interaction, respectively, U_{cross} corresponds to the coupling between the individual contributions of U_{bonded}, if all the terms are written down it will be obtained:

$$U_{bonded} = U_{bond} + U_{angle} + U_{tor} + U_{impr} \tag{37}$$

$$U_{cross} = U_{stretch-stretch} + U_{stretch-bend-stretch} + U_{bend-bend} + U_{tor-stretch} + U_{tor-bend-bend} + U_{bend-tor-bend} \qquad (38)$$

$$U_{nonbonded} = U_{LJ} + U_{electr} \qquad (39)$$

where U_{bond} is bond stretch, U_{angle} is angle bend, U_{tor} is torsion, U_{impr} is inversion (or out of plane), U_{LJ} is Lennard-Jones (or van der Waals) and U_{electr} is electrostatic.

In PCFF, the torsion rotation (U_{tor}) term has the following form:

$$U_{tor} = \frac{1}{2} \sum_{\theta} \sum_{i=1}^{3} V_i [1 + \cos(i(\theta - \theta_0))] \qquad (40)$$

where θ and θ_0 are the actual and equilibrium torsion angles, respectively, V_1, V_2 and V_3 are parameters and i is a phase factor.

Angle-bend (U_{angle}) has the term:

$$U_{angle} = \sum_{\varphi} \left[k_2 (\varphi - \varphi_0)^2 + k_3 (\varphi - \varphi_0)^3 + k_4 (\varphi - \varphi_0)^4 \right] \qquad (41)$$

where φ and φ_0 are the actual and equilibrium valance angles, respectively, and k_2, k_3 and k_4 are parameters.

Bond-stretch (U_{bond}) term:

$$U_{bond} = \sum_{b} \left[k_2 (b - b_0)^2 + k_3 (b - b_0)^3 + k_4 (b - b_0)^4 \right] \qquad (42)$$

where b and b_0 are the actual and equilibrium bond lengths, respectively, k_2, k_3 and k_4 are parameters.

Improper (U_{impr}) or out of plane term reads:

$$U_{impr} = \sum_{\chi} k_{\chi} \chi^2 \qquad (43)$$

where and χ is the improper torsion angle and k_{χ} is a parameter.

Lennard-Jones (U_{LJ}) or vdW term:

$$U_{LJ} = \varepsilon_0 \left[2 \left(\frac{\sigma_0}{r} \right)^9 - 3 \left(\frac{\sigma_0}{r} \right)^6 \right] \qquad (44)$$

where ε_0 is the depth of the potential well, σ_0 is the minimum distance between two particles when the interaction energy is zero and r is the distances between the particles.

Electrostatic (U_{electr}) interaction term are taken into account with Ewald summation method. The basic idea of Ewald is to split the interaction into two terms, one for short-range (U_{sr}) and one for long-range (U_{lr}) interactions:

$$U_{electr} = U^{Ewald} = U_{sr} + U_{lr} \tag{45}$$

Usually, the short-range interactions are calculated in the real space by classical Coulomb potential (eq. 46) and the long-range interactions are evaluated in reciprocal space by standard Ewald summation (eqs. 47 and 48):

$$U_{sr} = \sum_{i>j} \frac{Cq_i q_j}{\varepsilon r} \tag{46}$$

$$U_{lr} = \frac{1}{2V_0} \sum_{k \neq 0} \frac{4\pi}{k^2} |\rho_0(k)|^2 e^{-k^2/4\alpha} \tag{47}$$

$$\rho_0(k) = \sum_{i=1}^{N} q_i e^{ik \cdot r_i} \tag{48}$$

where C is energy-conversion constant, q_i and q_j are the charges of two atoms, ε is the dielectric constant of the medium, i is the imaginary unit, V_0 is the volume, ρ_0 is the electrostatic potential, k are the lattice vectors in reciprocal space and α is a parameter responsible for the width of a Gaussian function. This technique provides a rapid convergence of long-range interactions in reciprocal space for application in periodic systems.

All the other terms have standard expressions which are usually power series.

In order to compute the statistical average quantities of a system with N particles a (partition) function (Q) is required. In this wok two partition functions (ensembles) are employed:

NPT or isobaric-isothermal ensemble is utilized where the constant quantities are the number of particles, pressure and temperature:

$$Q(N,P,T) = \frac{P_0}{k_B T \Lambda^{3N} N!} \int d(\ln V_0) V_0^{N+1} e^{-\frac{P_0 V_0}{k_B T}} \int ds^N e^{-\frac{U(s^N;L)}{k_B T}} \tag{49}$$

where Λ is the thermal de Broglie wavelength (eq. 50), P_0 is the momentum of a particle, s is a time scaling coordinate.

$$\Lambda = \sqrt{\frac{h^2}{2\pi m k_B T}} \tag{50}$$

where m is the mass of the particle and h is the Plank constant.

NVT or canonical ensemble is used where the corresponding quantities (the number of particles, volume and temperature) are constant:

$$Q(N,V,T) \equiv \frac{1}{\Lambda^{3N} N!} \int dr^N e^{-\frac{U(r^N)}{k_B T}} \tag{51}$$

The major advantage of the classical MD approach for simulation of organic semiconductors is the possibility to mimic the experimental conditions, takes into account the environment and allow averaging the quantities over the time scale.

3.4.   Computational Details

First, DFT is applied in order to obtain the ground-state molecular geometries of all conformers of the small *BTZ* and *DPP* molecules. All molecules are optimized without any symmetry constraints. After geometry optimization, a frequency analysis is performed in order to check whether these structures correspond to a local minimum on the potential energy surfaces. D_-A_+ monomers are constructed from the most stable conformers of the small individual units.

Torsion potentials are obtained in the relaxed rotor approximation by computing partially optimized energies at each constrained value of the torsion angle θ, i.e. all internal degrees of freedom are allowed for relaxation during the rotation expect of the four atoms describing the torsion angle θ, which remains fixed. The value of θ varied from 0° to 180° by 10° step, i.e. by scaling the torsion angle along potential energy surface.

The electrostatic potentials (ESP) are calculated using Merz-Singh-Kollman procedure [258] and mapped onto a surface with an isovalue of electron density of 0.02 a.u. This defines a molecular surface in 3D space around the atoms, which characterizes a continuous molecular shape in terms of electron density. The electrostatic potential is represented as the interaction energy between the electrical charge generated from the molecule electrons and a positive point charge as a probe located at position r:

$$V^{ESP}(r) = \sum_{A=1}^{N} \frac{Z_A}{\left|R_A - r\right|} - \int \frac{\rho_e(r')d^3r'}{\left|r'-r\right|} \tag{52}$$

where Z_A is the charge of the nucleus A, which is a point charge located at R_A. The term $\rho_e(r)$ is the electron density function. The sign of the electrostatic potential is correlated to the partial charges on the atoms/atomic groups, i.e. the value at the minimum of $V^{ESP}(r)$ quantifies the electron-rich character of that region, and vice versa.

Two atomic population analyses are utilized in this study: Mulliken population analysis which separates the electron density into the individual atomic contributions using the basis set functions:

$$q_A = Z_A - \sum_{B=1}^{N} \left(\sum_{l\in k} c_{Bl}^2 + \sum_{l,s\in k, l\neq s} c_{Bl}c_{Bs}S_{ls} + \sum_{l\in k, s\notin k} c_{Bl}c_{Bs}S_{ls} \right) \tag{53}$$

where q_A are the partial charges, B is a molecule orbital, which runs over the total number of electrons (N), l and s are the indexes of atomic orbitals, c are the coefficians of molecular orbital basis functions, S is the overlap matrix and k runs over all the atoms.

The second atomic population analysis is ESP analysis where the charges are fitted to a electrostatic potential surface calculated by eq. (52, p. 38), which is usually reproduced by a grid of points surrounding the *vdW* surface of the molecule. The partial charges are determined minimazing eq. (52, p. 38) and eq. (54):

$$V^{ESP}(r) = \sum_{A=1}^{N} \frac{q_A}{|R_A - r|} \tag{54}$$

The atomic population analyses allow estimating the partial charges of each atom in the molecules and for instance, further they can be transferred into MD simulations.

Solvent effects are simulated by embedding the molecules in a polarizable continuum model (PCM) [259] as a continuum phase with dielectric constant of toluene (ε=2.379) and chloroform (ε=4.9), which are chosen for consistency with the experimental studies [260, 261].

The optical properties of the molecules at the optimized geometries for the most stable conformers and monomers are characterized by investigating the vertical singlet-singlet electronic transition energies calculated with time-dependent Density Functional Theory (TD-DFT) method of the same level of the theory including solvent effects of toluene and chloroform since the experimental UV-VIS spectra are measured with these solvents. In this work excited state energies are computed for the lowest twenty excited states. The UV-VIS absorption spectra are simulated employing Gaussian functions with the GaussView5 default parameters for half-width to build a continuous spectrum from a collection of transition peaks corresponding to TD-DFT transition energies and oscillator strengths.

The charge transport properties and binding energies (E_{bind}) are calculated for the most stable conformers (and monomers) in the case of π-π stacks: the ground state geometry is duplicated in two different starting configurations for interacting dimer - parallel (face-to-face) and anti-parallel (one of the molecules is rotated over 180° over its center of mass) orientations (Fig. 10, p. 40) and further single point calculation is performed in order to obtain the energy of the system. For each orientation, two different stacking modes are investigated: (1) dimers with a perfect registry, i.e. segregated stacking motif when both the central unit (*BTZ* or *DPP*) and flanks (*Fu* or *Th*) of one molecule are a top of the same blocks of neighbouring molecule, (2) dimers forming slipped cofacial orientations with longitudinal (*l*) and transverse (*k*) shifts, i.e. mixed stacking motif. Each molecule is shifted with a certain step (0.1 or 0.2 Å) along the corresponding direction (*d*, *k* or *l*) shown in Figure 11 (p. 40).

When the functions of the basis sets are centered on the nuclei (like in this work) and the basis set is incomplete (small amount of functions), an absolute error in the energy occurs since the geometries could be different. The quality of the basis set is not the same at all geometries, owing to the fact the electron density around one nucleus may be described by functions centered by another nucleus. This appears in stack of dimers where the basis functions from one molecule can contribute to the basis functions of the other molecule and vice versa. This is called basis set super position error (BSSE). In this work BSSE is taken into account via counterpoise method only for calculation of E_{dim} (in dimers), which estimates the difference between monomer

energies with the regular basis set and the energies calculated with the full set functions for the whole system. Later binding energies (E_{bind}) are evaluated via the equation:

$$E_{bind} = E_{dim} - 2E_{mon} \qquad (55)$$

where E_{dim} is the energy of a dimer system (single point) and E_{mon} is the energy of a monomer unit (ground state). The counterpoise energy (E_{CP}) is estimated via the equation:

$$E_{CP} = E^{AA}(AA) - 2E^{AA}(A) \qquad (56)$$

where the superscript indexes "AA" indicates the basis sets of the systems AA (dimer) and A (single molecule). BSSE is estimated subtracting eq. (55) and eq. (56).
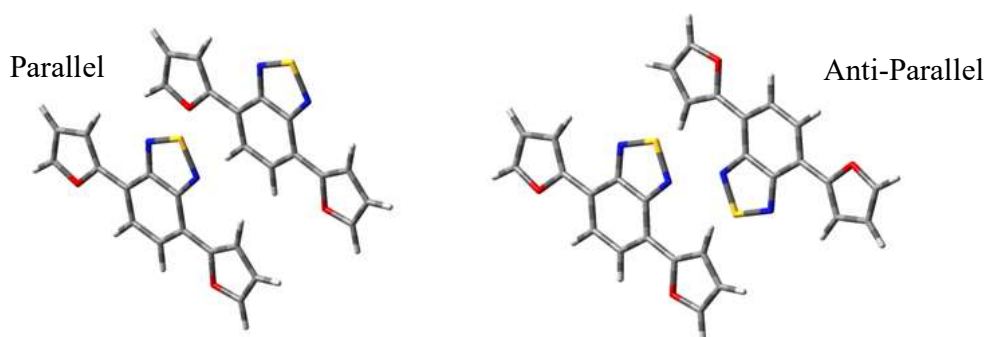

Figure 10. Representation of parallel (left) and anti-parallel (right) stacked dimers.
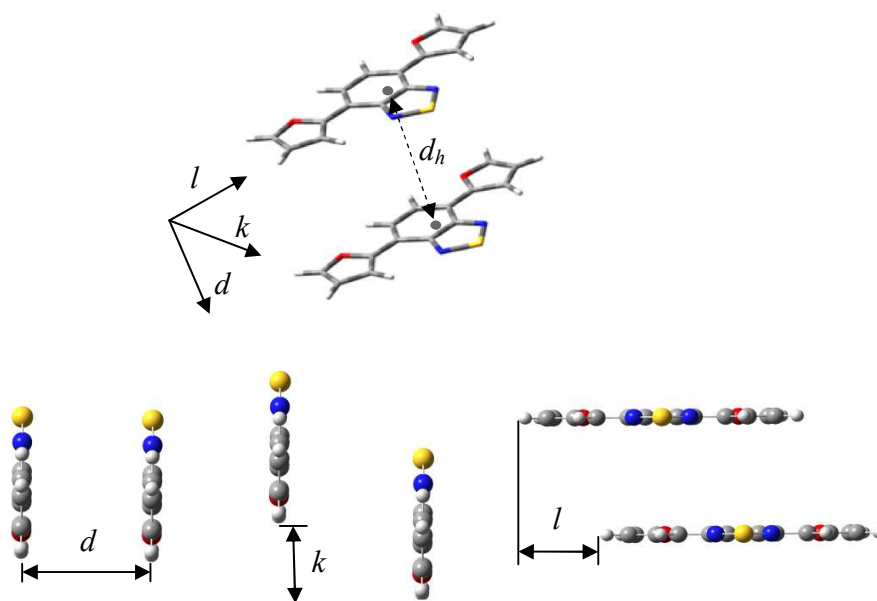

Figure 11. Representation of the stacking modes in dimers and the shift over certain axes (d, k and l). The distance between center of mass to center of mass in one dimer (d_h) is also shown.

40

Since DFT is not capable to simulate large amount of atoms and also it takes into account only static properties of the system under investigation, later DFT is combined with classical MD.

Experimentally resolved crystal structure of *Th-BTZ-Th* is simulated using MD in NVT ensemble (t=10 ns) with periodic boundary conditions (PBC) in all the directions. PBC allows simulation of infinite number of particles or unit cells. If a particle leaves the unit cell from one side, it automatically appears from the other side. PBC consist of infinite number of unit cells where only one of them is the original unit cell and all the others are copies. It is useful to simulate polymers (infinite system) and periodic crystal structures as well as it avoids surface phenomena.

The elementary unit cell of *Th-BTZ-Th* is replicated three times in all the directions in order to reproduce a larger super cell. From the crystal structure of *Th-BTZ-Th* molecule stacks of dimers corresponding to each possible pathway (dimer orientation) for charge transport are extracted in order to perform single point DFT calculation required for estimation of the electronic properties. This approach allows obtaining average values of the CT properties corresponding to every possible direction for each dimer stack. At every 100000 step a frame is taken and each (CT) property is averaged over 100 frames.

In MD simulations ESP charges are implemented, adopted from DFT calculations of optimized small molecules (as well as for monomers and dimers, n=1 or 2).

Polymers in certain simulation boxes are constructed from $D_/A_+$ monomers (with backbone created from six monomers, n=6) using PBC in all the directions and simulated without a solvent within MD. Since the atoms connected to the backbone are included in the periodicity the number of the monomers (n), which the polymer is constructed from, in the backbone goes to infinity (infinitely long chains are reproduced). Four π-π stacks of backbones are taken into account and further these stacks are multiplied four times in the direction of the alkyl side chains in order to form a polymeric material (totally 16 backbones per super cell, Fig. 37, p. 94). The attached side chains have stretched initial conformations. In the beginning, all the super cells are extended in order to avoid steric conflicts of the side chains. The starting π-π distance of the backbones is in range of 3.6÷4.0 Å where for linear side chains the range is shorter (3.6÷3.7 Å).

Two starting positions of the side chains are modelled with respect to the shift of backbone: when the side chains are shifted (*SH*, interdigitating) and when they are non-shifted (*NS*, non-interdigitating) (Fig. 6, p. 19). In order to reproduce *SH* side chains the backbones are initially shifted by 9 Å where the *BTZ* unit coincides with *DPP*.

For each MD simulation of polymers, first short NPT run (t=1 ns) is performed with isotropic pressure ($P_{x=y=z}$=1 atm.) and T=300 K in order to check the planarity of the backbone and to obtain a proper density of the system. After the NPT run, the system is annealed from 300K to 600K and cooled down to 300K with two subsequent NVT runs (with a rate of 3K per·$1·10^{-10}$ s) and finally a productive NVT run (T=300K) is performed for the analysis. Each NVT run has simulation time of 10 ns, totally 31 ns for each polymer. From the MD trajectory of the NVT productive run (the last 10 ns of a simulation) at every 100000 frame a snapshot is taken for analysis in order to estimate average properties of the polymers (each property is averaged over 100 frames).

The partial charges for each polymer are adopted from DFT calculation (ESP charges) where the backbone charges are applied from optimized dimer (n=2) molecules and the charges on the side chains are taken from optimized monomers with side chains and later the excess of the charge (maximum ±0.5e^-) is redistributed over the whole molecule. For estimation of the CT properties stacks of dimers (*Fl-BTZ-Fl-DPP-Fl*, *Fl*(*Flank*)=*Fu* or *Th*) are extracted from the most planar regions of the samples and further all molecules are saturated with H-atoms since in MD they are included in the infinitely long polymer chains, and the side chains are reduced to methyl (-CH_3) groups. Finally, single point DFT calculations are performed in order to reproduce the CT properties for each polymer. Since the backbone of the polymers are stacked there is only one possible direction (pathway) for charge transport.

For all MD simulations a modified PCFF force field is applied with Nosé-Hoover thermo- and barostat with Verlet integration algorithm with time step of $1 \cdot 10^{-15}$ s. The changes in the FF are shown in Table 1. Ewald summation method with accuracy of 10^{-6} is applied for the electrostatic energy. The Lennard-Jones interactions are modelled as atom-based and calculated applying cut-off radius of 18.5 Å - a 9-6 Lennard-Jones potential with sixth power mixing rule.

All CT properties are taken into account only for self-exchanged reactions when the charge transport is carried out between two identical molecules (*M*), $\Delta G^0 = 0$:

$$M^{-/+} + M^0 \rightleftharpoons M^0 + M^{-/+} \tag{57}$$

Type:	Definition:	Values:			
Bond:		b_0 [Å]	k_2 [kcal/mol·Å^2]	k_3 [÷]	k_4 [÷]
	np-sp	1.6384	719.2471	0.0	0.0
Angle:		φ_0 [°]	k_2 [kcal/mol·rad^2]	k_3 [÷]	k_4 [÷]
	cp-op-cp	107.330	130.6992	-18.4789	0.0
	cp-cp-op	105.530	96.2006	-44.9267	0.0
	c5-c5-c5	106.780	61.0226	-34.9931	0.0
	c5-c5-op	108.900	61.0226	-34.9931	0.0
	cp-c5-c5	134.320	220.0226	0.0	0.0
	cp-cp-c5[a]	134.320	220.0226	0.0	0.0
	cp-c5-op[a]	134.320	220.0226	0.0	0.0
	cp-c5-c5	118.900	61.0226	-34.9931	0.0
	cp-cp-op	118.900	61.0226	-34.9931	0.0
	c5-np-sp	106.880	220.9746	0.0	0.0
	np-sp-np	99.670	220.1730	0.0	0.0
Improper:		χ [°]	k_χ [kcal/mol·rad^2]		
	cp-c5-c5-np[b]	0.0	0.3		
	cp-c5-c5-op[b]	0.0	10.0		
	cp-cs-c5-sp[b]	0.0	0.3		

Table 1. Introduced changes in PCFF force field. [a]Parameters modified only for *Fu* derivatives. [b]Improper parameters are taken from Ref. [262].

In order to obtain the hopping mobilities (eq. 3, p. 23) it is required the distance (d) between the molecules. d is taken as π-π stacking distances ($d_{\pi\text{-}\pi}$) for monomers (as well as for extracted dimers from polymers) and as a distance between centroids (d_h) for isolated stacks of small molecules (one dimensional shift) as well as in dimers taken from the crystal structure in case of *Th-BTZ-Th* small molecule (Fig. 11, p. 40).

In order to evaluate the mechanical properties of the polymers, Kuhn segment (l_K) is calculated of small molecules. l_K represents an equivalent chain length of a polymer, which is reduced to effective number of chains due to universal properties of the polymers (independence of the local chemical structure). The length of one effective segment is called Kuhn segment and it is estimated by the hindered rotation model:

$$l_K = C_\infty l_0 / \cos \frac{\pi - \alpha_A}{2} \tag{58}$$

where C_∞ is the characteristic ratio, l_0 is the monomer size and α_A is the valence angle of the "model" chain. α_A is taken as the angle between center of mass of the three constitutive units of a small molecule (*Flank*, *BTZ* or *DPP* and *Flank*, average for each derivatives) - Figure 17 (p. 55).

The hindered rotation model assumes that all the bonds have the same bond length, all the bond angles are constants and all the torsion angles hindered by a potential $U(\theta_i)$ are not correlated. The characteristic ratio (C_∞) is the average sum of all bond vectors when the number of monomers (n) tends to infinity and it has the following expression:

$$C_\infty = \left(\frac{1 + \cos(\pi - \alpha_A)}{1 - \cos(\pi - \alpha_A)} \right) \left(\frac{1 + \langle \cos \theta \rangle}{1 - \langle \cos \theta \rangle} \right) \tag{59}$$

where $\langle \cos \theta \rangle$ is the average value of the cosine of the torsion angle θ with probability, which is proportional to the Boltzmann factor $e^{-U(\theta_i)/kT}$. In the hindered rotation model, the mean-square end-to-end distance (R_e) has the following expression:

$$\langle R_e^2 \rangle = C_\infty l_0^2 n \tag{60}$$

where n is the number of the monomers.

In order to check the quality of the theoretical methods, with respect to the structure of the molecules, experimentally resolved crystal structures and theoretically obtained structures are compared with root-mean-square deviation (RMSD) between the covalent bonds. RMSD between the difference of two data sets is evaluated where one set is the covalent bonds from the experiment and the other set is the covalent bonds obtained from the theory (DFT):

$$RMSD = \sqrt{\frac{\sum_{i=1}^{j}(x_{1,i} - x_{2,i})^2}{j}} \tag{61}$$

where j is the number of the values (covalent bonds) in each data set, $x_{1,i}$ and $x_{2,i}$ are the two sets of data (experimental and theoretical bond lengths, respectively).

The utilized software packages for MD simulations are BIOVIA Material Studio (for small molecules and preparation of polymers) and LAMMPS (for polymeric materials). For all the DFT calculations Gaussian09 software is used.

In the next chapter are presented the results of small molecules.

4. Donor-Acceptor Small Units

This chapter describes the results of DFT calculations of isolated constitutive units in its environment, modelled by Polarizable Continuum Model (PCM).

4.1. Conformational Properties

First, the conformational preferences of small molecules flanked with *Fu* or *Th* spacers are considered depending on conformational state (Fig. 12 and Fig. 13, p. 46).
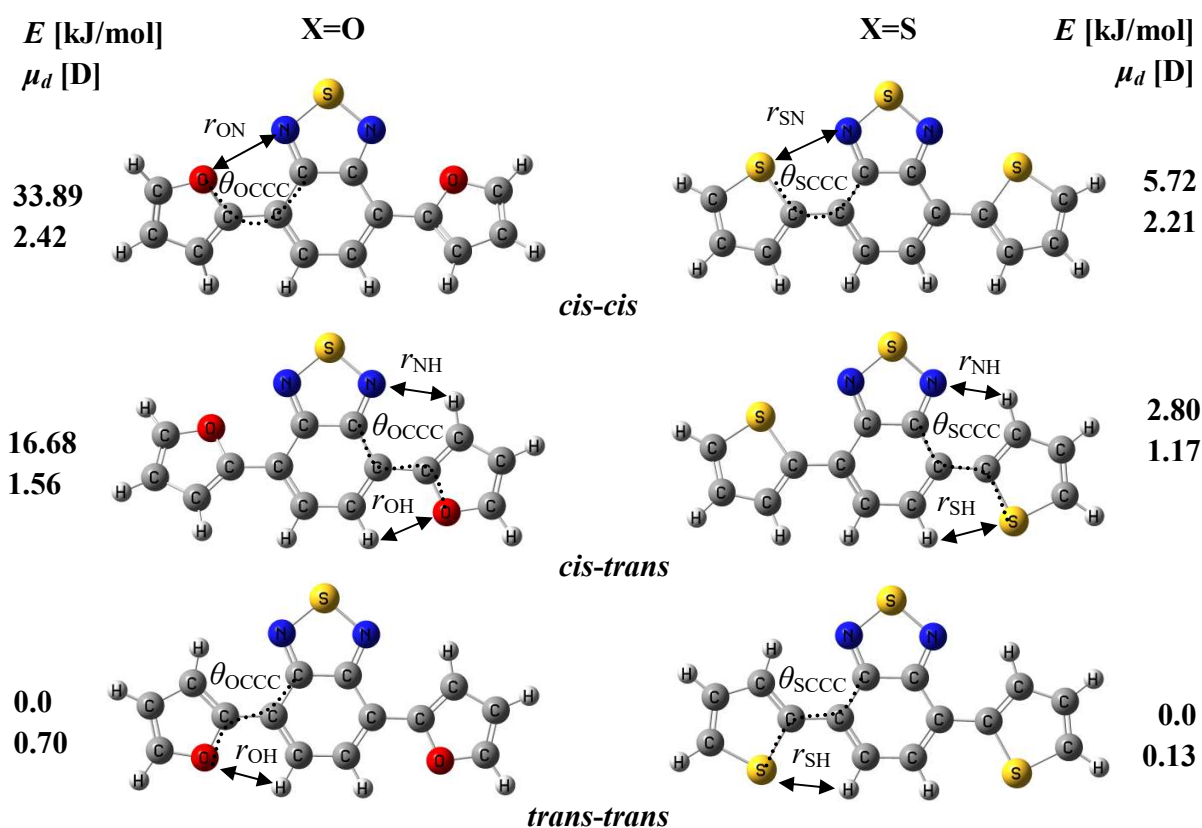

E [kJ/mol]
μ_d [D]

X=O

X=S

E [kJ/mol]
μ_d [D]

r_{ON} θ_{OCCC}

33.89
2.42

r_{SN} θ_{SCCC}

5.72
2.21

cis-cis

r_{NH} θ_{OCCC} r_{OH}

16.68
1.56

r_{NH} θ_{SCCC} r_{SH}

2.80
1.17

cis-trans

θ_{OCCC} r_{OH}

0.0
0.70

θ_{SCCC} r_{SH}

0.0
0.13

trans-trans

Figure 12. Optimized geometries of the conformers of *Fu-BTZ-Fu* (left column) and *Th-BTZ-Th* (right column); the relative energy difference between *trans-trams* state and respective conformer is given in kJ/mol. The dipole moments (in D) are also shown (B3LYP/6-31G*, ε=0).

In this work, one conformer of *BTZ* molecules is called *cis-cis* when both heteroatoms of the flanks, i.e. oxygen from furan or sulphur from thiophene, are pointing out in the direction of 1,2,5- thiadiazole.

For *trans-trans* conformational state, the heteroatoms are oriented to benzene ring of *BTZ*. Finally, the *cis-trans* conformer has two flanks with different orientations.

For *DPP* compounds this definition of the conformers is not available because of symmetry reasons of its core but it will be used the same nomenclature with respect to the relative energy difference shown in Figure 13 or it can be used the following assumption: if a line passes through the diagonal of *DPP* molecule (through the two nitrogen atoms) and in the remaining half of the molecule (together with one *Fl*) if the X_{atom} of the *Fl* is pointing the oxygen atom from *DPP* (X···O contact) this will be called *cis-* conformation and if the heteroatom in the flank is pointing the opposite direction to the hydrogen atom of N-H group (X···H-N contact) this will be named *trans-* conformation.
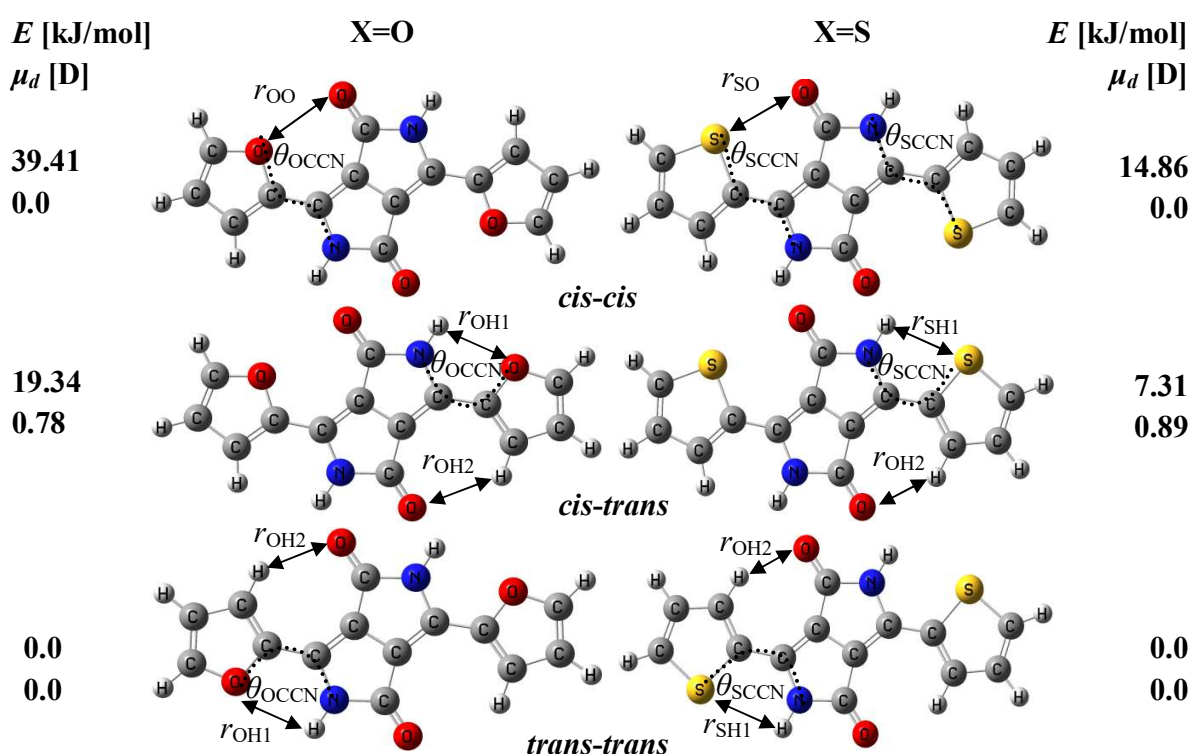

Figure 13. Optimized geometries of the conformers of *Fu-DPP-Fu* (left column) and *Th-DPP-Th* (right column); the relative energy difference between *trans-trams* state and respective conformers is given in kJ/mol. The dipole moments (in D) are also shown (B3LYP/6-31G*, $\varepsilon=0$).

In both cases the most stable conformers are *trans-trans* ones and they are considered as a reference system, i.e. its relative energy difference E is zero. The rotation of one *Fl* of *BTZ* derivatives about θ_{XCCC} angle (Fig. 12, p. 45) is accompanied by the energy penalty of $E=16.68$ and 2.80 kJ/mol for *Fu-BTZ-Fu* and *Th-BTZ-Th*, respectively; the rotation of the second flank doubles these values. For the *DDP* molecules the rotation of one *Fl* about the equivalent angle θ_{XCCN} is slightly higher when X_{atom} is oxygen and it is two times higher when X_{atom} is sulphur as

compared to the energies of *BTZ* molecules, E=19.34 and 7.31 kJ/mol for *Fu-DPP-Fu* and *Th-DPP-Th* (Fig. 13, p. 46), respectively. Again the rotation of the second flank doubles these values similar to *BTZ* derivatives.

For both molecules when X_{atom}=O the greater energy difference between the conformers can be explained by the existence of H-bonding, which stabilizes the *trans-trans* conformers. With rotation of a *Fl* from *cis-* to *trans-* conformation the number of the H-bonding is increased and the energy difference rapidly reduced. This energy difference is significantly lower in the case when X_{atom} is sulphur because of different interactions (S⋯H). The number of H-bonds is the same (four) when X_{atom}=O in both *DPP* and *BTZ* derivatives but in *BTZ* there are two types of N⋯H and O⋯H, whereas in *DPP* there are four types of O⋯H, which means that in *DPP* the H-bonding is stronger and the energy penalty for *Fu-DPP-Fu* is slightly higher (ca. 3 kJ/mol). In case of sulphur containing molecules these S⋯H interactions are not conventional H-bonds and they are unfavourable, which explains the lower energy difference between conformers, which was mentioned above. An additional proof is that when the X_{atom} is sulphur *DPP* compounds still have H-bonding due to O⋯H-N interactions unlike *Th-BTZ-Th* molecules where in the later one the H-bonding is N⋯H (weaker), which explains the two times higher energy difference between the corresponding conformers. Additionally, these flank/core intramolecular interactions will give rise to a large stiffening effect for the corresponding polymers, which is discussed later.

The *cis-cis* conformations of the molecules with *Fu* flanks appear to be highly unfavourable, which is in line with theoretical predictions by Kayi for *Fu-BTZ-Fu* [158]. On the other side, for both molecules with *Th* flanks *cis-* and *trans-* orientations can be realized since both conformers are relatively stable. Indeed, Nielsen et al. [94] in H-NMR studies indicated that thiophene *Fl* of *BTZ* can rotate freely even at low temperature allowing *cis-trans* interconversion [94]. Considering the X-ray crystal structures of *Th-BTZ-Th*, it was concluded that approximately 71% of the molecules are in *cis-trans* conformation, and the remaining molecules adopt *cis-cis* one [94], on the other hand, only *cis-trans* conformation is found for the same compound by other authors [263]. The *cis-trans* conformation of *Th-BTZ-Th* has been observed in crystalline structures of a parent compound by Dhar et al. [264]. Moreover, the torsion angles defining the orientation of the flanking units and the *BTZ* core deviate from the experimentally observed values (Table 2, p. 48).

For example, the *cis-* oriented thiophene *Fl* of *cis-trans Th-BTZ-Th* conformer in crystalline samples is characterized by the value of dihedral angle of 2.03° [94] and of 5° [264], i.e. the deviation from planarity is smaller than the predicted value here of 13.4° for the molecule in gas phase where the planarity is distorted. It can be explained by the tight packing in the crystalline solid-state where the presence of ordered adjacent molecules held together via intermolecular interactions including π-π stacking generates more coplanar structures. The *trans-* oriented *Th* flank of *cis-trans Th-BTZ-Th* is almost coplanar to the central *BTZ* unit, as follows from the calculations and from the available experimental data [94, 264]. In this work in order to compare the experimental [94] and calculated structures RMSD (root-mean-square deviation) between covalent bonds (eq. 61, p. 43) is utilized.

For *cis-trans* conformer of *Th-BTZ-Th* RMSD is estimated to be 0.0241 Å, which follows that B3LYP/6-31G* gives rather accurate bond lengths [265] and this is one of the criteria choosing this functional and basis set for theoretical investigations.

All *DPP* conformers with *Fu* and *Th* flanks possess perfectly planar structures as well as the *trans-trans* conformers of both *BTZ* molecules with *Fu* and *Th* flanks, as follows from Table 2 and 3. Similar conclusions have been drawn by Pina et al. [266], Lima et al. [267] and Grisorio et al. [268] for the torsion angles along the conjugated backbones of *Th-BTZ-Th* molecules, and by Kayi [158] in computational study of *Fu-BTZ-Fu* oligomers. The *cis-cis* conformers of *Fu-BTZ-Fu* and *Th-BTZ-Th* deviate from the planar geometry with dihedral angles 22.0 and 12.2°, respectively. The latter one corroborates well with the value predicted for *Th-BTZ-Th* by Özen et al. (12.3°) [86].

B3LYP/6-31G*	*Fu-BTZ-Fu* (X=O)			*Th-BTZ-Th* (X=S)		
$\varepsilon=0$	*cis-cis*	*cis-trans*	*trans-trans*	*cis-cis*	*cis-trans*	*trans-trans*
r_{XN} [Å]	2.82	2.82	-	2.93	2.93	-
r_{NH}/r_{XH} [Å]	-	2.49/2.43	2.50/2.43	-	2.33/2.66	2.32/2.66
$\theta_{XCCC}/\theta_{XCCC}$ [°]	22.0	21.8/179.8	180.0	12.2	13.4/179.7	180.0
Exp.[Å] r_{SN}/r_{SH}	-	-	-	-	2.88/2.64[94]	-
Exp. [Å] r_{SN}	-	-	-	-	2.83[263]	-
Exp. [°] θ_{XCCC}	-	-	-	-	5/171[263]	-

Table 2. Intramolecular non-conventional hydrogen bond N···H, O···H, S···H, X···N interactions and interring torsion angles of all *BTZ* conformers (for definitions see Fig. 12, p. 45).

Unfortunately, *Fu-BTZ-Fu* structure is not available experimentally and *Fu-DPP-Fu* as well as *Th-DPP-Th* small compounds are resolved only with side chains attached to *DPP* or in octanoic acid ($C_7H_{15}COOH$) as a solvent on graphite surface [106]. The closest structures, which were found to *Fu-DPP-Fu* is with hexyl (-C_6H_{13}) or tetradecane (-$C_{14}H_{29}$) [269] chains, with branched side chains (-C_2H_3-(C_4H_9)-C_6H_{13}) [270] or polymer with additional *Fu* unit [271]. For *Th-DPP-Th* is found a structure with only one hexyl (-C_6H_{13}) side chain [272], with two hexyl (-C_6H_{13}) chains [273] or with two methyl groups [274].The theoretical support of the experiment of *Th-DPP-Th* (with one hexyl side chain) [272] also shows planar geometry with torsion angle θ_{SCCN} less than 1°, which is in agreement with the results shown here (0.0°) as well as the authors

B3LYP/6-31G*	*Fu-DPP-Fu* (X=O)			*Th-DPP-Th* (X=S)		
$\varepsilon=0$	*cis-cis*	*cis-trans*	*trans-trans*	*cis-cis*	*cis-trans*	*trans-trans*
r_{XO} [Å]	3.14	3.17	-	3.17	3.18	-
r_{XH1}/r_{OH2} [°]	-	2.61	2.61/2.52	-	2.88/2.30	2.88/2.30
$\theta_{XCCN}/\theta_{XCCN}$ [°]	180.0	180.0/0.0	0.0/0.0	180.0	180.0/0.0	0.0/0.0
Exp. [Å] r_{OH2}	-	-	2.41[269]	-	-	2.27[272]/2.29[274]
Exp. [°] θ_{SCCN}	-	-	0.9[269]	-	-	1.9[274]

Table 3. Intramolecular non-conventional hydrogen bond O···H, S···H, X···O interactions and interring torsion angles of all *DPP* conformers (for definitions see Fig. 13, p. 46).

propose herringbone orientation in the crystal (Fig. 5, p. 18). The intermolecular distance CH···O (r_{OH2}) in *Th-DPP-Th* here is predicted very well with respect to the experimental values of 2.30 Å and 2.27 Å, in theory and experiment, respectively, which proves again the fact that B3LYP/6-31G* precisely predicts the geometric characteristics.

In the case when *Th-DPP-Th* is substituted with methyl groups [274] and also with two hexyl chains [273] the crystal structures show *trans-trans* conformation represented by the most stable conformer estimated here by the theory and the torsion angle between *Th* and *DPP* indicates planarity (1.9°), whereas DFT (both B3LYP/6-31G* and M06-2X/cc-pVTZ) predicts close value of 0.0° in gas phase as compared to the experiment. RMSD between covalent bonds is obtained to be 0.0116 Å, which is one more proof for the effectiveness of B3LYP/6-31G*. According to *Fu-DPP-Fu* crystal structure (with hexyl chains) [269], one is represented again with the most stable (*trans-trans*) conformer found here (like *Th-DPP-Th*). The predicted CH···O distance (r_{OH2}) of 2.52 Å in *Fu-DPP-Fu* coincides with the experimental evaluated one (2.41 Å) as well as the torsion angle of 0.9 and 0.0° in experiment and theory, respectively. RMSD is estimated to be 0.0077 Å, which again proves B3LYP/6-31G* for successful description of organic molecules.

Comparing the ground-state geometries with the second main functional employed here it can be concluded that M06-2X/cc-pVTZ yields larger deviation of the torsion angles for *BTZ* derivatives (up to plus 10°) as compared to B3LYP/6-31G* for *cis-* and *cis-trans* orientations. Additionally, M06-2X/cc-pVTZ does not predict absolutely planar structure for *trans-trans* conformers of *Th-BTZ-Th* where one of the θ_{SCCC} torsion angles is distorted (162.3°), whereas *DPP* derivatives are not affected and they remain planar.

For *BTZ* compounds the dipole moments are reducing with rotation of the flanks from *cis-* to *trans-* conformation and in *trans-trans* state the dipole moments are vanished (Fig. 12, p. 45). *DPP* derivatives only have dipole moment in case of *cis-trans* conformations where the symmetry is partially broken (Fig. 13, p. 46).

Increasing the dielectric permittivity from zero (vacuum) to 4.9 (chloroform, the most polar solvent considered in this study) causes only small changes in torsion angles: the planarity of backbones of both *Fu* and *Th* based *BTZ* compounds has been improved by 1-2° in *cis-cis* and *cis-trans* conformers, and the impact of solvent is more pronounced for furan-containing derivatives. *DPP* compounds remain unaffected from the solvent.

In the case of the *DPP* molecules, if the H atoms in N-H groups are substituted with methyl groups (which is typically realized in experiments) the picture remains the same and there are only slight differences is the relative energy difference: with 2 kJ/mol the energy difference is increased for molecules containing sulphur in the *Fl* and with 2 kJ/mol the energy difference is reduced for molecules containing oxygen in the *Fl*, respectively, as well as a slight distortion of the planarity occurs only for *cis-cis* and *cis-trans* conformers (up to 10°).

The steric repulsive interactions might be sufficient to evoke non-planar structures of conjugated polymers hampering cofacial interactions. These repulsive forces originate from the steric conflicts in the *BTZ* derivatives from the two hydrogen atoms, which belong to benzene part of *BTZ* and flanks, or the benzene part of *BTZ* and alkyl substituents of flanks [264].

On the other side in the *DPP* compounds these repulsion forces are vanished and there are only attractive interactions originating from the backbone structure. These attractive interactions can impose strong restrictions to local conformations and therefore called "conformational locks", which in turn direct the planarity and rigidity of the chains. In some sense the conformational locks act in a similar way as, for instance, additional chemical bonds between the aromatic units of the backbone but they have non-covalent nature.

Coulomb forces [86, 94, 275, 276] and D_--A_+ orbital interactions have been discussed to be the origin of the conformational locks [39, 90]. These potential non-bonding interactions have gained special attention becoming one of the major parts of design rules used for the precise control of the local molecular structures in conjugated systems [89, 277].

In order to clarify the non-covalent interactions the electrostatic potentials (ESP) are calculated and mapped onto molecular surfaces. These maps describe the charge distributions with the negative (red) and the positive (blue) electrostatic potential at the selected value of the electron density (Fig. 14 and Fig. 15, p. 51).
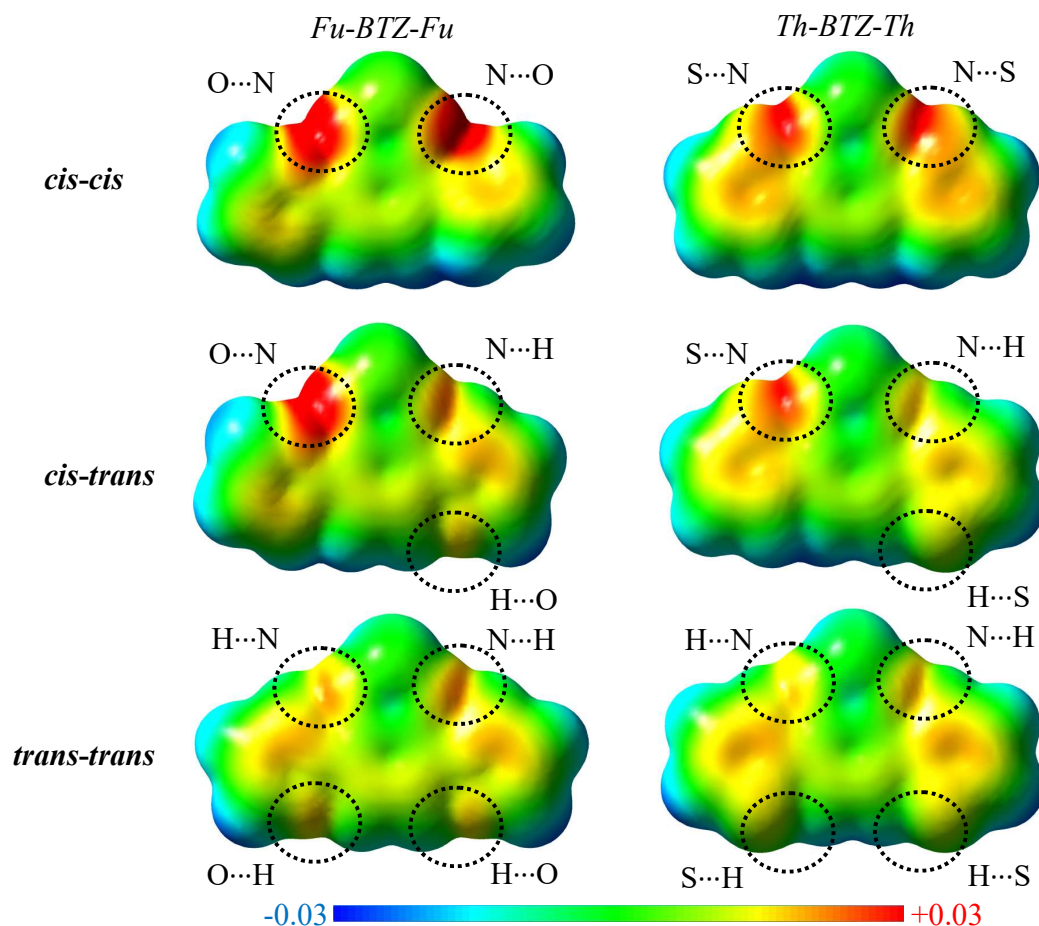

Figure 14. ESP maps of all the conformers of *Fu-BTZ-Fu* (left column) and *Th-BTZ-Th* (right column) in e^- units. The special interactions are shown between the atoms (B3LYP/6-31G*, ε=0).

As follows from Figure 14 (p. 50) for the *BTZ* compounds, the molecules having a *cis*-oriented *Fl* demonstrate a strong localization of a negative charge arising from the spatial proximity of the oxygen of *Fu* flank and the nitrogen atoms of 1,2,5-thiadiazole in *Fu-BTZ-Fu*. Similarly, this interaction is observed from the sulphur atom of *Th* flank and the nitrogen atoms of 1,2,5-thiadiazole in *Th-BTZ-Th* (red ESP regions, *cis*- orientation). This localization is less pronounced in case of the thiophene derivative, which explains the different value of torsion angle between the units (Table 2, p. 48). The torsion angle is reduced twice (12.2° versus 22.0°) as compared to *Fu-BTZ-Fu cis-cis* (as well as *cis-trans*) conformer because the negative charge is not so strongly localized and the charge is partially redistributed into the five-membered ring (*Th*). In other words, the negative ESP region (X···N interaction) is smeared over the flank (yellow ESP regions, *cis*- orientation) when a *Fl* is rotated. In the case of *trans-trans* orientation of the *BTZ* molecules the whole negative charge is equally redistributed into the whole molecules and this is a reason why these conformers are the most stable ones (because of reduced electrostatic interactions, which is equal to delocalized electron density).
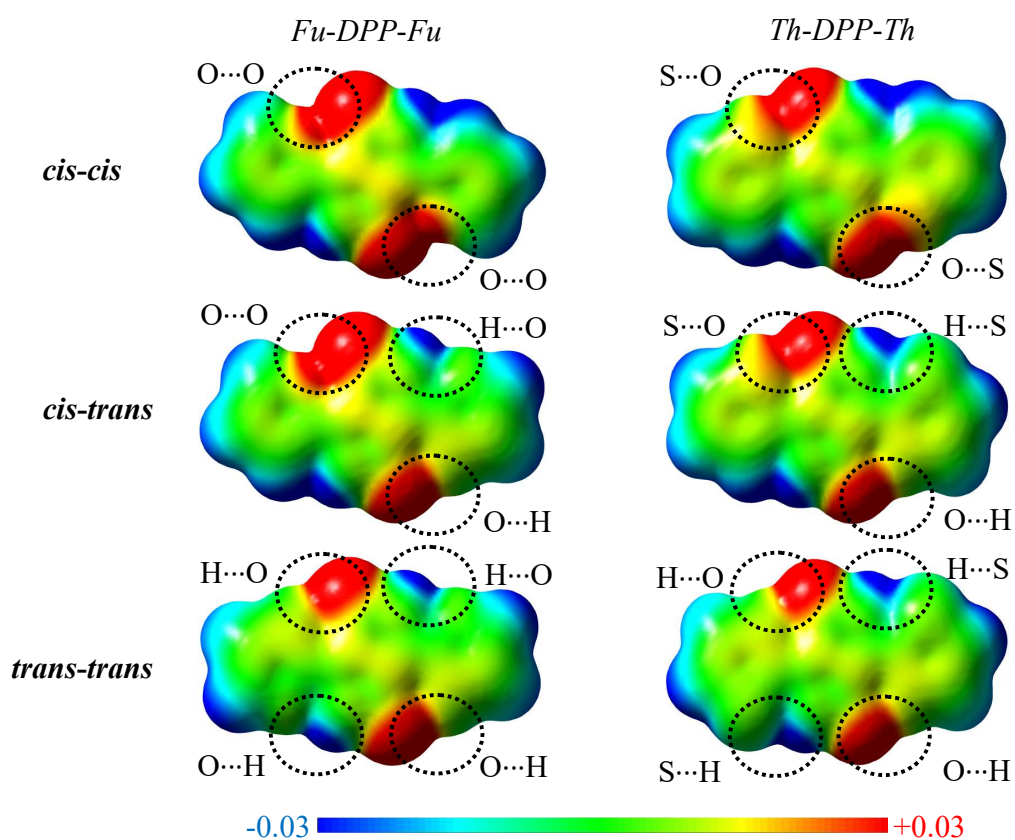

Figure 15. ESP maps of all the conformers of *Fu-DPP-Fu* (left column) and *Th-DPP-Th* (right column) in e^- units. The special interactions are shown between the atoms (B3LYP/6-31G*, $\varepsilon=0$).

In case of *DPP* molecules (Fig. 15, p. 51) again in *cis-cis* conformation there is a strong negative charge localization but the difference between *Fu* and *Th* (O and S) is not so well pronounced and there is only a minor difference where in the *Th* flank the charge is slightly more delocalized. This contradiction from *BTZ* molecules can be explained with the planarity of *DPP* molecules and with the larger distance between the corresponding atoms (Table 3, p. 48): the oxygen atoms are far away (with ca. 0.3 Å further than X···N in *BTZ*) in *cis-* and *cis-trans* conformers and the steric interactions are reduced, which leads to planar geometry and reduced electrostatic interactions (more delocalized e^- density). After rotation of a *Fl* the negative charge is delocalized in the molecules and the most stable conformers are these ones without X···O interactions similar to the *BTZ* molecules.

Here a second conclusion is reached (in addition to the increased H-bonds) that the molecules prefer charge delocalization (reduced electrostatic interactions) in ground states.

In all the conformers of both molecules the positive charge is spread over the periphery of the molecules and it is slightly affected during rotation of a flank unit. Similar ESP maps of *cis-cis* and *trans-trans* conformers of the *DPP* molecules are obtained by C. Fu et. al. [106].

The distortion of the planarity of *cis-cis* (and *cis-trans*) conformers in *BTZ* can be explained also with the partial charges of the atoms (Table 4). The highest energy *cis-cis* conformer of *Fu-BTZ-Fu*, both atoms of O···N non-covalent interaction are negatively charged ones. Since equally charged species repel each other, the *cis-cis* conformer of *Fu-BTZ-Fu* is characterized by a pronounced non-planar structure. By contrast, the partial charges on both sulphur atoms of thiophene rings are positive, their interaction with negatively charged nitrogen atoms of 1,2,5-thiadiazole is attractive and sequentially the torsion angle is reduced twice.
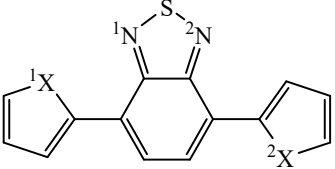
B3LYP/6-31G*	*Fu-BTZ-Fu* (X=O)			
$\varepsilon=0$	*cis-cis*	*cis-trans*	*trans-trans*	
X=O	-0.424	-0.426/-0.457 (^{1}X/^{2}X)	-0.457	
^{1}N/^{2}N	--0.556	-0.552/-0.588	-0.585	
	Th-BTZ-Th (X=S)			
X=S	0.310	0.310/ 0.251(^{1}X/^{2}X)	0.252	
^{1}N/^{2}N	-0.578	-0.575/-0.585	-0.582	
	Fu-DPP-Fu (X=O)			
X=O	-0.426	-0.428/-0.466	-0.467	
^{1}O/^{2}O	-0.498	-0.493/-0.528	-0.514	
^{1}N/^{2}N	-0.435	-0.409/-0.433	-0.408	
	Th-DPP-Th (X=S)			
X=S	0.346	0.345/ 0.259	0.258	
^{1}O/^{2}O	-0.502	-0.499/-0.514	-0.521	
^{1}N/^{2}N	-0.423	-0.421/-0.420	-0.418	

Table 4. Mulliken population (in e^-) of the X_{atom} of both flanks and central core. The right panel provides the definition of the X_{atom} for *cis-trans* conformers, which are unequally charged. Nitrogen atoms of *DPP* are a sum of partial charges of N plus H atoms on the N-H bond.

These interactions are not observed in *DPP* derivatives since the molecules are absolutely planar and the atoms are at longer distance (no steric conflicts) as it was mentioned above.

Further to investigate the conformational properties and to define the barriers to internal rotations, the torsion potentials between the central core units (*BTZ* or *DPP*) and heterocyclic flanks are calculated. Figure 16 shows these curves for the rotation of one *Fl*. For *BTZ* derivatives the potential energy curves have two maxima located at 0° and 90°, which correspond to the *cis-* (the local maximum) and to the propeller-like orientation of the *Fl* (the global maximum), respectively, and two minima at ~20° (*Fu-BTZ-Fu*) or ~12° (*Th-BTZ-Th*) for *cis-gauche* (the local minimum) and 180° for *trans*-orientations (the global minimum), respectively.
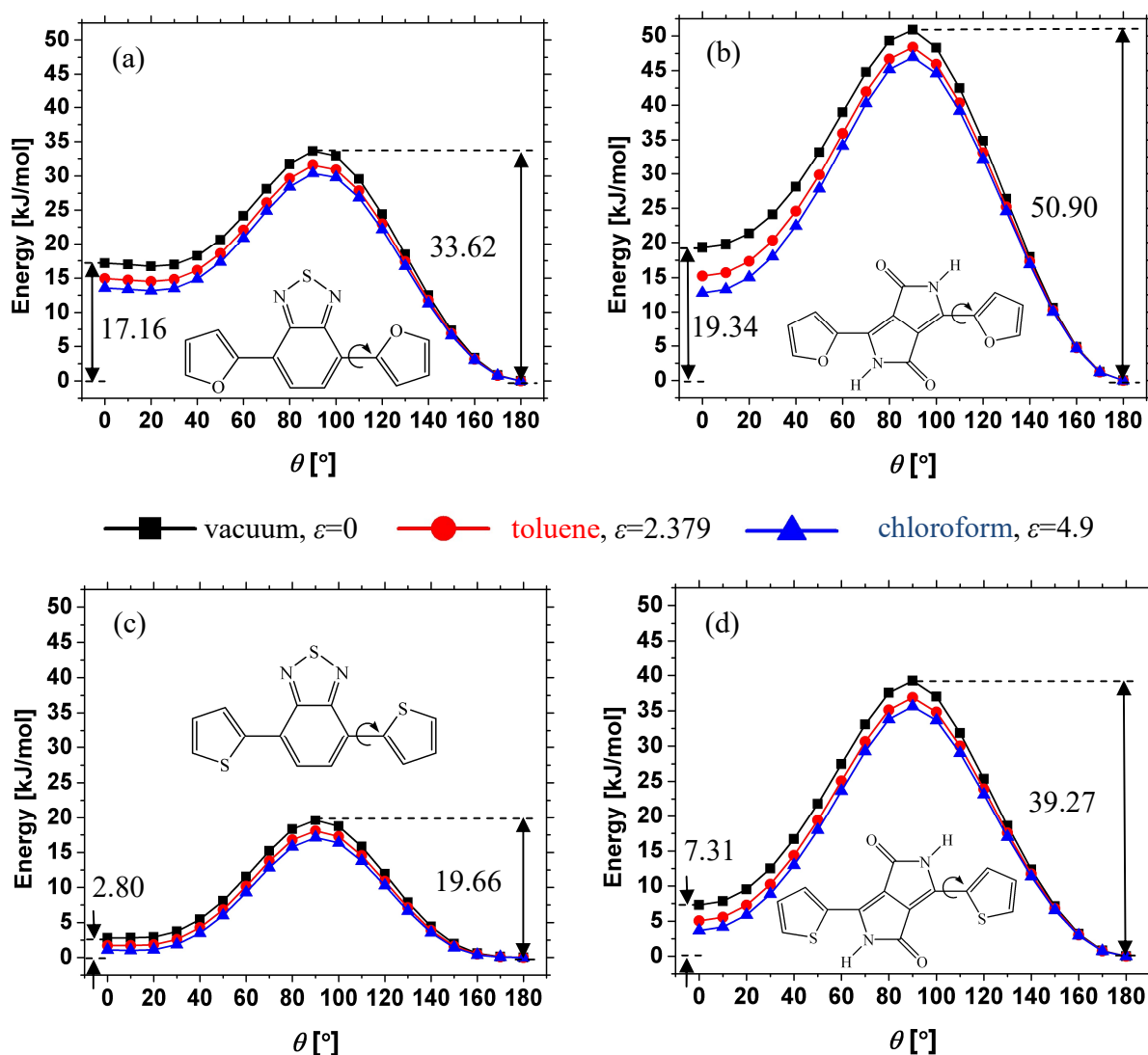

Figure 16. Torsion potentials *U(θ)* (in kJ/mol) of *cis-trans* conformers of *Fu* (a, b) and *Th* (c, d) derivatives (B3LYP/6-31G*, *ε*=0). The rotation flank is marked with an arrow.

There is only one maximum at 90° and two minima at 0° and 180° for the *DPP* compounds, corresponding to the local (*cis-*) and global minimum (*trans-*), respectively. *DPP* molecules do not possess second maximum in the torsion potentials due to planarity. If the second *Fl* is rotated the same charts are reproduced for all the molecules because of symmetry.

It is worth noting that the *Th* derivatives show two energy minima that differ only by 2.80 and 7.31 kJ/mol for *BTZ* and *DPP*, respectively. The energy for *BTZ* is similar to k_BT at room temperature (1 $k_BT \approx 2.497$ kJ/mol), therefore both orientations can be realized [94, 264] and this two times energy difference was explained by the different types of H-bonds.

Fu molecules have much higher energy difference, which suggests for the unfavourable existence of *cis-* conformers for both acceptor units. It is notable that *Fu* flank in both derivatives has two times higher barrier than *Th* one. This is in agreement with the higher stiffness of the *Fu* molecules as compared to *Th* ones [171]. In all the cases *Fu* compounds have higher values for the barriers and the energy differences as compared to *Th* ones, which can be explained with the different type of H-bonding mentioned above. This proves the effect of four locking interactions (H-bonding for *trans-trans* conformers) preventing the rotations of the flanks.

The dielectric medium slightly affects both the height of barrier at 90° and the energetics of *cis-* conformer, which is another proof of the hypothesis about the electrostatic nature of the all non-covalent interactions. If the H atoms in *DPP* derivatives are exchanged with methyl groups the barriers are slightly reduced (by 7.5 and 9 kJ/mol, for *Fu* and *Th* derivatives, respectively) and there is a minor effect into the energy differences (minus and plus 2 kJ/mol, for *Fu* and *Th* molecules, respectively), which is an additional proof for the importance of H-bonding. Moreover, torsion potentials obtained by M06-2X/cc-pVTZ showed only minor reduction in the barrier heights by 3 kJ/mol as well as more pronounced minimum points of the charts. C. Fu et. al. predicted similar torsion potentials for both *DPP* molecules [106].

In summary, the difference in barrier heights of furan- and thiophene- containing species at 90° makes it entirely possible to conclude that planarization/chain stiffening is dictated by intramolecular interactions, which are discussed above.

As follows from the previous discussion, *Th* compounds can rotate around *θ* with a relatively small difference in energy between the *trans-* and the *cis-* orientations of the flanks (Fig. 16, p. 53). By contrast, rotations are highly suppressed by conformational locks of the *trans-trans Fu* molecules. Thereby, for the polymer chains consisting of –[*BTZ/DPP-Th*]ₙ– units, one can expect shorter persistence and conjugation lengths, as compared to –[*BTZ/DPP-Fu*]ₙ– chains.

In order to describe the conformational properties of these macromolecules, the hindered rotation model simplified to rotational isomeric states model is applied. Here three states of each monomer unit are considered: the first state corresponds to the energy minimum and two other states are at the local minima. In this model, the mean-square end-to-end distance (R_e) is evaluated by eq. (60, p. 43) and the characteristic ration (C_∞) is estimated by eq. (59, p. 43). The valence angle of the "model" chain (α_A) is taken as the angle between center of mass of the corresponding units (Fig. 17, p. 55). The estimated angles are 147.7° and 180° for *BTZ* and *DPP* molecules, respectively.
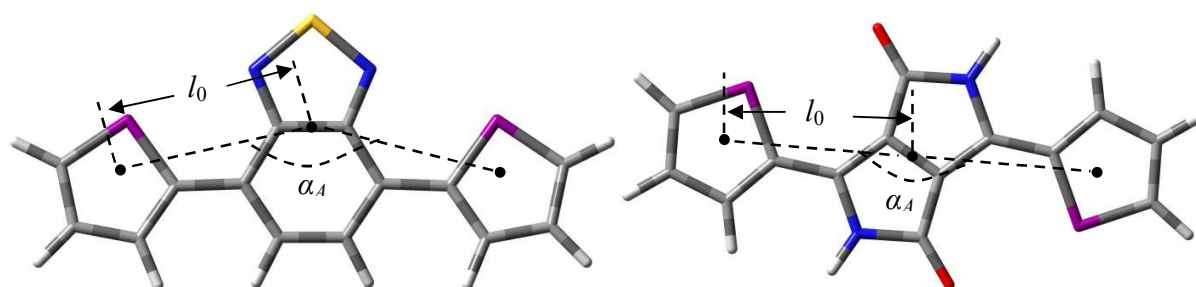
Figure 17. Representation of the "model" chain angle (α_A) between the center of mass of the units utilized in hindered rotation model. The monomer lengths (l_0) are also shown.

The monomer lengths (l_0) are obtained to be 0.432 and 0.424 nm for *BTZ* and *DPP* compounds, respectively. Both the "model" angles and the monomer lengths are taken as an average of each derivatives (averaged over *Fu* and *Th* molecules for each A_+ unit).

The model predicts that the fraction of the *trans-* state chain of the *Th* derivatives is 0.6070 and 0.9053, and the Kuhn segment estimated by eq. (58, p. 43) is l_K=8.5 and 48.9 nm, for *BTZ* and *DPP*, respectively, i.e. it includes 12 and 70 repeating units for the corresponding compounds. The two times energy difference the *Th* conformers of the *BTZ* and *DPP* molecules (as well as the angle) has a great impact into the macromolecules.

Chain	Property	State 1 (*trans*)	State 2 (*cis-gauche+*)	State 3 (*cis-gauche-*)
–[BTZ-Fu]$_n$–	U [kJ/mol]	0.0	16.680	16.680
	Fraction	0.9976	0.0012	0.0012
	$\langle\cos\theta\rangle$	0.99542		
	C_∞	5196.39		
	l_K [nm]	2338.17		
–[BTZ-Th]$_n$–	U [kJ/mol]	0.0	2.8000	2.800
	Fraction	0.6070	0.1965	0.1965
	$\langle\cos\theta\rangle$	0.22395		
	C_∞	18.82		
	l_K [nm]	8.47		
–[DPP-Fu]$_n$–	U [kJ/mol]	0.0	19.340	19.340
	Fraction	0.9992	0.0004	0.0004
	$\langle\cos\theta\rangle$	0.9984		
	C_∞	14649.74		
	l_K [nm]	6204.76		
–[DPP-Th]$_n$–	U [kJ/mol]	0.0	7.310	7.310
	Fraction	0.9053	0.0474	0.0474
	$\langle\cos\theta\rangle$	0.8127		
	C_∞	115.49		
	l_K [nm]	48.91		

Table 5. Calculation of the Kuhn segment (l_K) of –[BTZ–Fu]$_n$–, –[BTZ–Th]$_n$–, –[DPP–Fu]$_n$– and –[DPP–Th]$_n$– based polymers using hindered rotation model at 298 K.

In case of $-[BTZ\text{-}Th]_n-$ the mechanism of the polymer chain flexibility is realized as a rotational-isomeric one, and this rather flexible polymer can be characterized as a chain having an isotropic rigidity, whereas $-[DPP\text{-}Th]_n-$ the flexibility is significantly hindered.

By contrast, for *Fu* based chains the fraction of the *trans-* conformer is 0.9976 and 0.9992, for *BTZ* and *DPP*, respectively, which means that two other states are very scarcely populated. Consequently, the hindered rotation model would predict values of both C_∞ and Kuhn segment, which appear to be several orders of magnitude higher than *Th* chains: C_∞=5196, l_K=2.3 μm and C_∞=14650, l_K=6.2 μm, for $-[BTZ\text{-}Fu]_n-$ and $-[DPP\text{-}Fu]_n-$, respectively. Here the energy difference between *BTZ* and *DPP* compounds with different *Fl* increases three times the Kuhn segment. This result points out a very high stiffness of *Fu* containing chains.

Because of the high energy difference of the macromolecule where the rotation of the rings is strongly suppressed, the finite chain flexibility can arise via accumulation of the small thermal vibrations of atoms around their equilibrium positions (persistent flexibility mechanism) or due to the bending of the chain, which requires much more energy. Indeed, the *Fu* chains can be considered as two-dimensional ribbon-like polymers with highly anisotropic rigidity [278]. However, unlike true ribbon-like chains do, $-[BTZ\text{-}Fu]_n-$ and $-[DPP\text{-}Fu]_n-$ backbones have two inter-tied strands of non valence character and they are characterized by a curved shape of the 2D ribbon. One possible self-organization formation of a long–chain could be a cylinder-like structure (Figure 18) shown for $-[BTZ\text{-}Fu]_n-$. In Table 5 (p. 55) are summarized all the calculations.
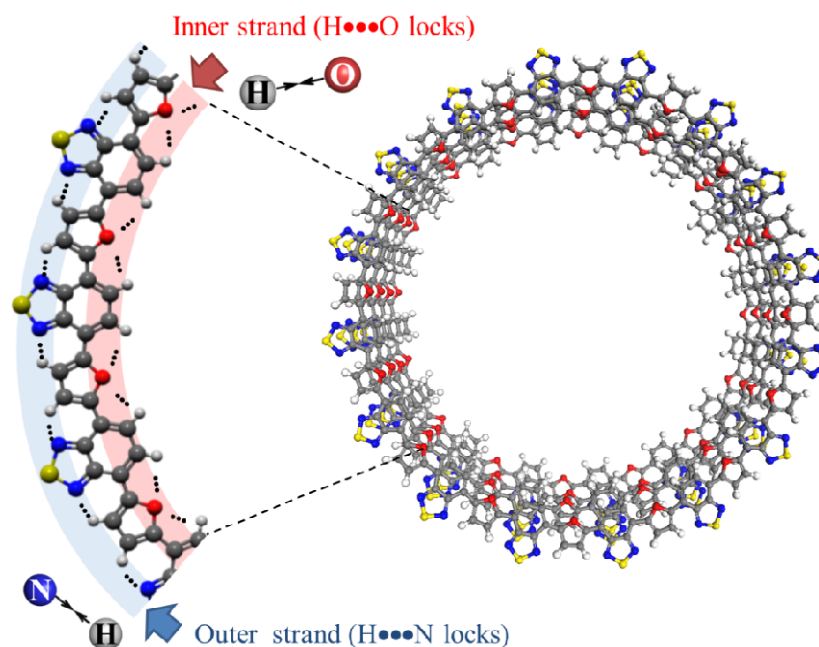

Figure 18. Chain curvature of the all-*trans* $-[BTZ–Fu]_n-$ ribbon-like polymer with two inter-tied strands (inner and outer strands as sequences of H···O and H···N locks, respectively, left panel). These hydrogen bonds extend over the whole structure (cylinder-like aggregate is shown on the right panel).

It should be stressed here that theoretical predictions of the hindered rotation model are performed for molecules calculated in vacuum. Better results can be obtained if molecular dynamics simulations of longer chains with explicit-solvent are performed.

For further calculations only the most stable conformers (*trans-trans*) are utilized and there are only a few exceptions with other conformers where the results are compared with experimental data.

4.2.   Electronic and Optical Properties

For small molecules the "band gaps" are considered as the energy differences between frontier HOMO and LUMO orbital energies. The "band gap" values and the orbital energies of all *trans-trans* conformers are summarized in Table 6.

B3LYP/6-31G*, $\varepsilon=0$	*Fu-BTZ-Fu*	*Th-BTZ-Th*	*Fu-DPP-Fu*	*Th-DPP-Th*
HOMO [eV]	-5.18	-5.35	-5.03	-5.13
LUMO [eV]	-2.48	-2.61	-2.55	-2.62
"E_g" [eV]	2.69	2.73	2.58	2.51
"E_g" [Exp., eV]	2.10[260]/2.28[264]	2.43[263]/2.45[280]	2.14[270]	2.16[270]/2.20[272]

Table 6. Summary of the orbital energies of the small *BTZ* and *DPP* molecules. "E_g" are shown as well.

As it can be seen from Table 6, *DPP* derivatives have slightly lower "band gap" values than *BTZ* compounds, with 0.1 and 0.2 eV lower, for *Fu* and *Th* flanks, respectively. Additionally, the "band gap" energies for the corresponding molecules (*DPP* and *BTZ*) are very close and they differ with less than 0.1 eV. The difference between the molecules with different flanks in negligible with respect to the "band gap" values and it can be concluded that the heteroatom does not influence on the "E_g". It is also notable that for *BTZ* derivatives, *Th* flanks have always deeper HOMO and LUMO as compared to *Fu* flanks, by contrast this dependence is inverse for *DPP* compounds.

According to the *BTZ* derivatives, the results of the "E_g" values are 2.69 and 2.73 eV for *Fu* and *Th* flanks, respectively, and these calculations correspond to previously obtained values predicted by Kayi for *Fu-BTZ-Fu* (2.70 eV) [158], and for *Th-BTZ-Th* by Özen et al. (2.72 eV) [86] and by Ogunyemi et al. (2.46 eV) [279]. Remarkably, the values of the electronic "band gaps" corroborate the experimental data from (i) cyclic voltammetry of 2.10 eV [260] for *Fu-BTZ-Fu* and another one of 2.28 eV [264], (ii) optical measurement of 2.43 eV [263] for *Th-BTZ-Th*, and photophysical data 2.45 eV [280] for *Th-BTZ-Th*.

Measured "E_g" of *DPP* molecules with branched side chains showed very close values of 2.14 and 2.16 eV [270], for *Fu* and *Th* flanks, respectively, and these values are still close to the predicted ones here of 2.58 and 2.51 eV, for *Fu* and *Th* flanks, respectively.

One confirms the minor effect of the X_{atom} into the electronic properties. J. Dhar et. al. showed similar value of the predicted "E_g" of 2.48 eV for *Th-DPP-Th* using DFT [272], which is very well obtained to the prediction one here (2.51 eV). Additionally, these theoretically predicted values are also close to the experimentally measured "E_g" of 2.16 eV (optical) [270] and 2.20 eV (electrochemical) [272] "band gaps".

The theoretical agreement with the experiment with respect to the "band gap" energies is the main motivation for using of B3LYP/6-31G* in order to estimate the charge transport properties since they are evaluated from the orbital energies of dimer systems (eqs. 15 and 16, p. 26). Moreover, B3LYP/6-31G* showed the best results of "E_g calculations from series of different functionals and basis sets.
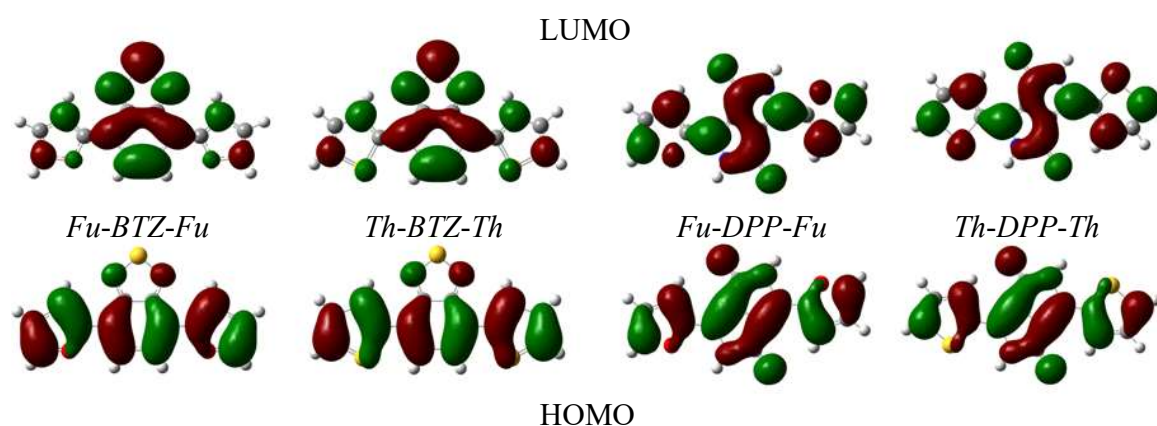

Figure 19. Frontier orbitals (LUMO top and HOMO bottom) of the molecules under investigation (B3LYP/6-31G*, ε=0). Here the lobes of MOs are represented by the isodensity surfaces with a contour of ±0.02 a.u. with positive (green) and negative (red) phases of the wave function. MOs show similar and complete delocalization.

The spatial distribution of the frontier molecular orbitals are shown in Figure 19. In all the cases the electron density is delocalized along the whole molecules as it is expected due to their conjugated nature. Planar ground state geometries of the *trans-trans* conformers is indicative of an extended conjugation. Similar patterns of HOMO and LUMO distributions are predicted by Kayi [158] for *Fu-BTZ-Fu*. Moreover, the orbital shapes predicted by Ponnappa et. al. [270] and J. Dhar et. al. [272] for *DPP* molecules are very similar to the corresponding shapes obtained here.

This character of the electron density is also corroborated by the analysis of the molecular orbitals topologies, which show that the most likely position of pair of electrons in HOMO orbital is distributed along the backbone of the oligomers, whereas the electron density of LUMO is partially localized on the A_+ (*BTZ* and *DPP*) moieties.

This delocalization confirms the existence of a significant charge transfer character in the HOMO-LUMO transition [266]. Additionally, there is no difference in the shape of the electron density of HOMO and LUMO orbitals between the derivatives of corresponding *BTZ* and *DPP* molecules.
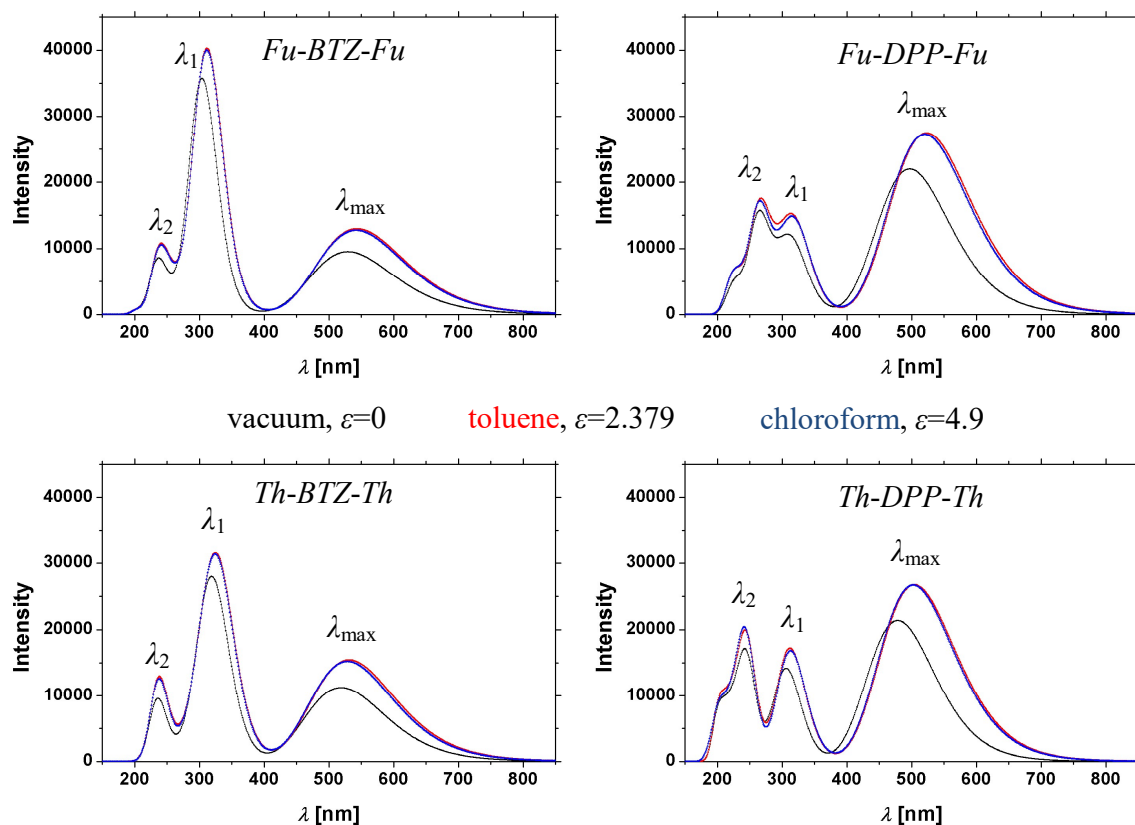
Figure 20. UV-VIS spectra obtained from TD-DFT/B3LYP/6-31G*.

TD-DFT	vacuum ε=0, toluene ε=2.379, chloroform ε=4.9			Experiment:
	λ_{max} [nm]	λ_1 [nm]	λ_2 [nm]	$\lambda_{max}/\lambda_1/\lambda_2$ [nm]
Fu-BTZ-Fu	530, 544, 542	306, 314, 314	235, 237, 237	450/300/-[260]
Th-BTZ-Th	519, 531, 529	321, 326, 325	233, 239, 239	445/316/-[264]
Fu-DPP-Fu	479, 505, 503	307, 312, 313	244, 245, 244	†538/353/279[270]
Th-DPP-Th	497, 523, 520	315, 320, 321	265, 266, 265	540/-/-[272]

Table 7. Summary of the wavelengths of UV-VIS spectra of all small molecules shown in Figure 20 (TD-DFT/B3LYP/6-31G*). †In this case the solvent is dichloromethane (ε=8.93).

Further, the UV-VIS spectra of the *trans-trans* conformers are investigated (Figure 20). The absorption spectra exhibit a dual-band character, which is attributed to the charge transfer between electron-rich flanks and the electron-deficient *BTZ* and *DPP* cores (a low energy band at longer wavelength λ_{max}) and to higher-energy $\pi \rightarrow \pi^*$ transitions (denoted as λ_1 and λ_2).

It should be emphasized that all absorption bands are associated to $\pi \rightarrow \pi^*$ transitions because of the conjugated nature of the compounds. Here the low-energy transitions λ_{max} are HOMO$\rightarrow$LUMO independently of the molecules. This explains the same intensity of absorption band at λ_{max} for the corresponding *BTZ* and *DPP* derivatives. Since the major contributions are from HOMO$\rightarrow$LUMO, this band can be identified as charge-transfer transition.

By contrast, a higher energy band λ_1 has HOMO→LUMO+1 transition for both *BTZ* molecules where for *Th-BTZ-Th* is a mixed excitation with HOMO-3→LUMO, whereas for both *DPP* derivatives (*Fu-DPP-Fu* and *Th-DPP-Th*) is a mixed transition of HOMO-3→LUMO and HOMO→LUMO+2. The highest energy band λ_2 is a mixed transition: HOMO→LUMO+4 and HOMO-1→LUMO+1 for *Fu-BTZ-Fu*, and for *Th-BTZ-Th* is HOMO-2→LUMO+2 and HOMO-4→LUMO. For *DPP* derivatives λ_2 is HOMO→LUMO+2, HOMO-3→LUMO and HOMO-4→LUMO+1 mixed excitation, whereas for *Fu-DPP-Fu* is accompanied additionally with HOMO-6→LUMO. The transitions of *BTZ* molecules are very similar independently on the heteroatom, which is true also for *DPP* derivatives, and it can be concluded that the X_{atom} has a minor effect on the excitations.

Generally, all the molecules have the same transitions in very close range (λ_{max} in 500÷540 nm, λ_1 in 310÷330 nm and λ_2 in 240÷270 nm), which could be related to the same nature of the flanks (five membered aromatic rings). It is notable that the higher transitions (λ_1 and λ_2) are separated in *BTZ* compounds and they trend to merge in *DPP* molecules where in *Th-DPP-Th* they form almost one band together. All the transitions are summarized in Table 7 (p. 59). From this table follows that the polarity of solvents red-shifts (bathochromic) the position of absorption bands as compared to the calculations in vacuum. Comparing the calculated absorption maxima in chloroform at λ_1 and λ_{max} with experimentally measured values for *BTZ* derivatives (Table 7, p. 59) λ_1 is better predicted (300/316 and 314/325 nm for *Fu/Th* molecules, in experiment and theory, respectively), than λ_{max} (450/445 and 544/529 nm for *Fu/Th* molecules, in experiment and theory, respectively). This deviation is probably due to limitations of the models used here: the calculations are done for isolated molecules, i.e. the molecular aggregation and solvation effects cannot fully be covered by the PCM model.

For *DPP* molecules, the experimental values for *Fu* flank are 538, 353 and 279 nm [270] for λ_{max}, λ_1 and λ_2, respectively, and 540 nm [272] for λ_{max}, for *Th* flank, which are much closer to the theoretical predictions of 503, 313, 244 nm (λ_{max}, λ_1 and λ_2, respectively,) for *Fu* flank and 520 nm (λ_{max}) for *Th* flank, respectively.

The slightly larger deviation (up to 40 nm) of absorption bands for *Fu-DPP-Fu* can be explained with different solvent of the measured spectrum (dichloromethane and chloroform, in experiment and theory, respectively). It should be emphasized that a split of λ_{max} of *DPP* molecules exist in the experiments as well as the experiments show additional small splitting of the other two bands λ_1 and λ_2, which are not captured by TD-DFT

4.3. Binding Energies

For further investigation of the non-covalent interactions the binding energies (E_{bind}) of isolated stacks are evaluated from the difference between the energy of a dimer and the energies of two monomers (eq. 55, p. 40).

Two cases are taken into account: when the dimers are oriented parallel or anti-parallel (Fig. 10, p. 40) as well as one of the molecules is shifted in all the spatial directions (Fig. 11, p. 40).

First, E_{bind} dependence of the distance between the molecules (d) is investigated (Fig. 21, p. 62). In case of face-to-face (parallel) orientation all the compounds have equilibrium distance at 3.7 Å (with small deviation of *Fu-DPP-Fu* at 3.6 Å) and not all of the distances are accessible since segregated cofacial arrangements usually exhibit large repulsive interactions [166, 238]. This shows that there is a strong repulsion due to steric and orbital interactions when the molecules are parallel oriented at short distance.

The equilibrium distances are not well pronounced for parallel oriented molecules where the charts have shallow and not deep minima as compared to the case of anti-parallel orientation (*BTZ* molecules) where in the later one the minima are better pronounced. It seems that parallel oriented molecules would form disordered crystals where the distance between the molecules can vary due to thermal fluctuations and this could be also a reason why the crystal structures of *DPP* derivatives, which are investigated here, are not resolved experimentally (without side chains). Nevertheless, these "equilibrium" minimum distances are utilized further in order to compute the same dependencies over the other axes and later the CT properties.

In anti-parallel orientation (*BTZ* molecules) the equilibrium distances are shorter than parallel orientation and there is a dependence of the X_{atom}: *Fu* stacks are at closer distance (3.3 Å) than *Th* stacks (3.5 Å) because sulphur atom of *Th* ring has larger radius than the oxygen of *Fu* flank. In the anti-parallel case the repulsion forces are reduced and more distances (at closer range) are accessible as compared to parallel orientation.

Comparing parallel and anti-parallel orientation, in case of anti-parallel orientation E_{bind} values are lower (deeper minima) with 20÷30 kJ/mol as compared to parallel oriented molecules. Consequently, it could be expected that in crystal structure the molecules will occupy anti-parallel orientation due to stronger attractive (or reduced repulsive) forces and more compact (more densely packed) crystal structure with shorter intermolecular distances. Indeed, this is in agreement with experiments for *Th-BTZ-Th* molecule and π-π (d) distances of 3.41÷3.44 Å [94] and 3.5 Å [263] for anti-parallel *cis-trans* conformer are measured. It could be expected that *Fu-BTZ-Fu* should also realize anti-parallel orientation in the crystal structure. It should be emphasized that the calculations are obtained for *trans-trans* (the most stable) conformers, whereas the preferable conformation in experiments is *cis-trans* one of *Th-BTZ-Th* compound.

In the case of *Th-DPP-Th* substituted only with one hexyl side chain the measured π-π distance is 3.71 Å [272], which very well coincides with theoretical value obtained here (3.7 Å). The same $d_{π-π}$ (3.70 Å) is also obtained for a derivative with different (triethyleneglycol) side chains [274] of the same compound. Interesting, when two hexyl chains are attached to *Th-DPP-Th* this π-π distance is reduced to 3.5 Å according to the experiments [273, 274], which could be related to the strong interchain interactions.

The experimental crystal structure of *Fu-DPP-Fu* with hexyl (as well as with -$C_{14}H_{29}$) side chains the π-π distance is measured to be 3.32 Å [269], which is much shorter as predicted by DFT here (3.6 Å) as well as it is also shorter than the same compound with *Th* flanks (3.50 Å) [273, 274].
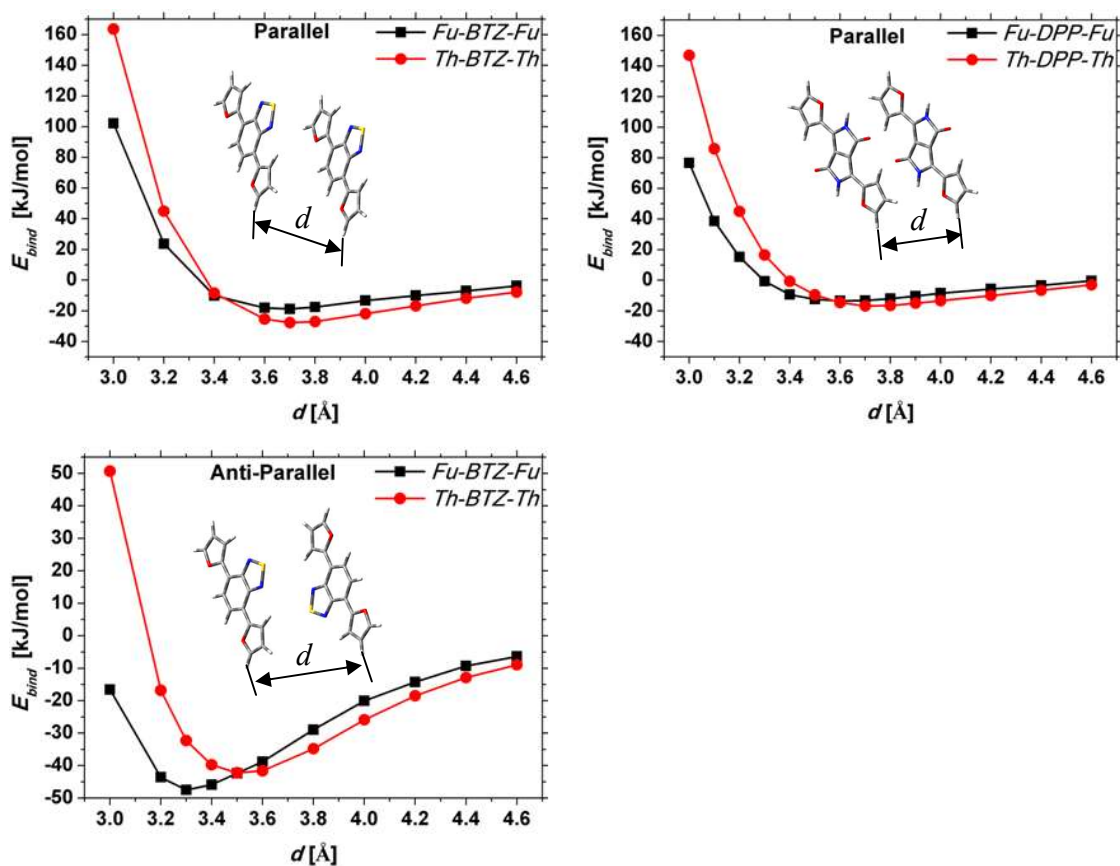
Figure 21. Binding energies (in kJ/mol) of *trans-trans* conformers of *BTZ* (left) and *DPP* (right) derivatives in perfect segregated stacks as a function of distance between them (*d*) in case of parallel (top) and anti-parallel (bottom) orientation - M06-2X/cc-pVTZ, ε=0.

These contradictions could be due to the packing of the side chains. However, DFT predicts slightly shorter $d_{\pi\text{-}\pi}$ for *Fu-DPP-Fu* (with 0.1 Å shorter) than *Th-DPP-Th*. Moreover, DFT shows binding energy close to zero at 3.3 Å for *Fu* based compounds (Fig. 21).

DPP derivatives due to symmetry reasons (symmetry group C_{2h}) do not have anti-parallel orientation (over the inversion center) and this affects the CT properties, which is discussed in the next section. Also, it could be expected that *DPP* molecules will be shifted over the other axes in order to compensate the repulsive forces caused by segregated stacks (or to find a better configuration with stronger attraction), which is shown in the next paragraph.

If the hydrogen atoms in N-H groups are substituted with methyl groups both *DPP* derivatives have the same equilibrium $d_{\pi\text{-}\pi}$ at 3.8 Å due to steric repulsion from the methyl groups $CH_3\cdots CH_3$ and according to the experiment this distance is 3.27 Å for *Th-DPP-Th* with methyl groups [274]. In this case DFT does not predict correct value but the reason could be that X-ray scattering is not capable to define precisely the positions of H atoms (in C-H bonds).

Similar "equilibrium" *d* values of 3.7 and 3.8 Å are obtained by K. Thorley and C. Risko [281] for benzodithiophene molecules with the same symmetry (C_{2h} group) as *DPP* molecules studied here as well as for asymmetric molecules (C_{2v} group), which shows the independence of

the molecules when high symmetry (or no explicit anti-parallel orientation) is presented due to strong orbital interactions.

Further E_{bind} are computed for molecular stacks when one of the molecules is shifted over the other two axes (k and l) with constant d values obtained from the minimum distances over d displacements (Fig. 21, p. 62). Figure 22 shows that all the energies are below zero, which means that all of these molecular shifts can be realized in the crystal structures. There are very well pronounced minimum points even in parallel oriented (BTZ) molecules and it can be concluded that these are equilibrium distances. Even though Fu based parallel compounds (shifts over l axis) some of these equilibrium distances trend to become shallow and the clear minimum points slightly disappear. It is also notable that BTZ molecule in anti-parallel orientation E_{bind} are lower than parallel one, which is additional proof for the preference of the anti-parallel orientation in crystal structure.
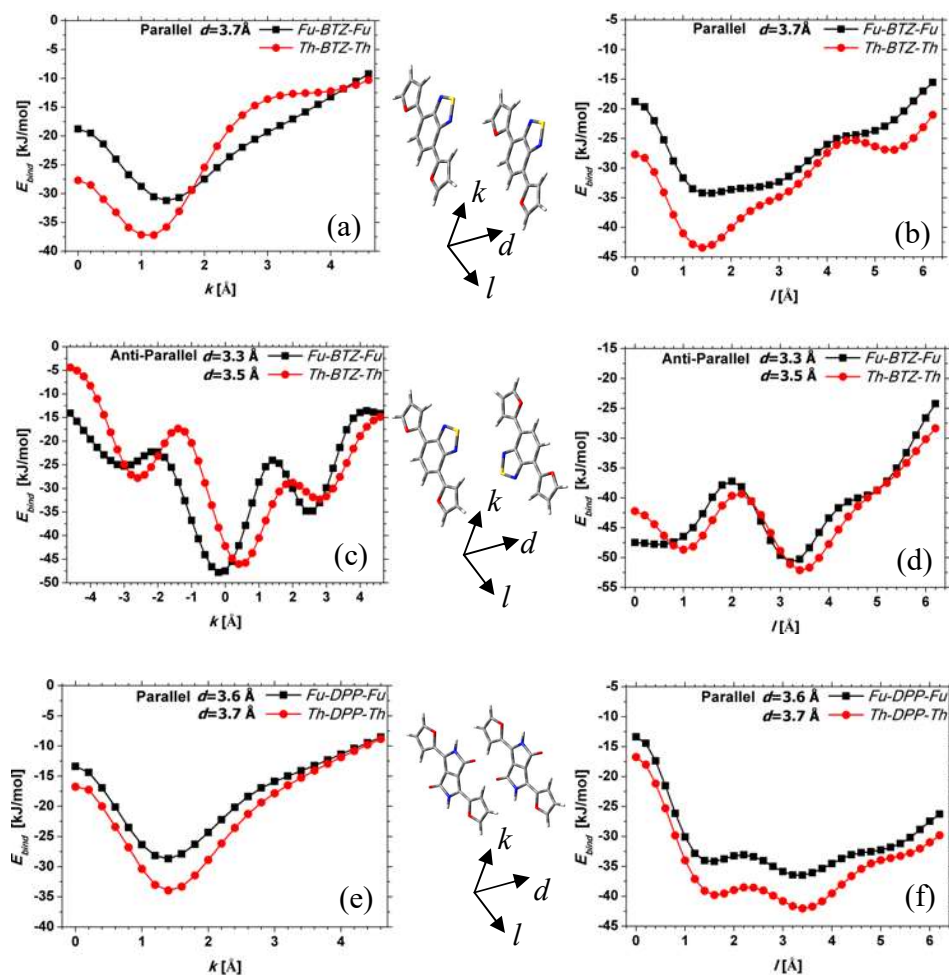

Figure 22. Binding energies (in kJ/mol) of *trans-trans* conformers of BTZ in parallel (a, b) and anti-parallel (c and d) orientation, and DPP (e and f) parallel derivatives in slipped cofacial stacks as a function of transverse (k - left) and longitudinal (l - right) shifts. The distances between molecules (d) are taken from Figure 21 (p. 62) - M06-2X/cc-pVTZ, $\varepsilon=0$.

Additionally, *BTZ* molecules which differ in the X_{atom} have very similar global (and other) minimum point positions in all the directions as well as they have similar dependencies and the difference could be addressed to the slightly different valence angle (geometry) between the cores and the flanks. Parallel oriented *BTZ* molecules have equilibrium distances at k=1.4 and 1.6 Å, and at l=1.6 and 1.4 Å, for *Fu* and *Th* molecules, respectively. In anti-parallel orientation *BTZ* molecules have minimum distances at k=-0.2 and 0.4 Å, and for l=3.2 and 3.4 Å, for *Fu* and *Th* molecules, respectively, which are also close.

It could be expected that in the crystal structure the molecules would prefer shifted position (and anti-parallel orientation) due to increased attractive interactions since in anti-parallel orientation the minimum points (Fig. 22, p. 62) are deep enough. Indeed, in *Th-BTZ-Th* crystal structure the pair of molecules (in anti-parallel orientation) is shifted at k=-0.6 Å and l= 3.8 Å (shown as a white point in Fig. 26, p. 71), which is close to the one dimensional predictions from E_{bind} (k=0.4 Å and l=3.4 Å), and better results could be obtained if the whole potential surface is scanned (two dimensional dependence), which is done for monomer units of the polymers discussed in the next chapter, or if the same E_{bind} calculations are performed for the conformer, which corresponds in the experimental crystal structure (*cis-trans*). It could be expected that *Fu-BTZ-Fu* molecule would have similar structure due to similar E_{bind} dependencies.

For *DPP* derivatives the equilibrium distances coincide perfectly independently of the X_{atom} in the flanks at k=1.4 Å and l=3.4 Å and according to the experiment of *Th-DPP-Th* with methyl groups the crystal structure coincide perfectly with the theoretical prediction where shifts over k=1.53 Å and l=3.27 Å are measured [274]. These correct predictions explain why the CT properties of this molecule are computed correctly (because the experimental structure is very close to the stacks obtained by DFT) discussed in the next section. Interesting, *Th-DPP-Th* with hexyl (as well as with other types) side chains has different displacement: k=0.13 Å and l=4.13 Å [274], which might be addressed to the interdigitation of the side chains. It could be suggested that *Fu-DPP-Fu* molecule should exhibit similar or the same crystal structure.

Indeed, in the crystal structure of *Fu-DPP-Fu* with hexyl side chains the measured displacements are k=1.12 Å and l=3.60 Å [269] and the theory shows k=1.4 and l=3.4 Å. The crystal structures of *Fu-DPP-Fu* (with hexyl chains) and *Th-DPP-Th* (with methyl groups) have very similar molecular orientations (cofacial stacks) according to the experiment, which differ only with 0.2÷0.3 Å over the corresponding axes. This small deviations is expected due to the smaller size of the oxygen atom than the sulphur one in the *Fl* (and the small difference in the valence angle, which was mentioned) and the stacks of molecules are shifted in both axes in order to compensate repulsive forces in parallel orientation as it was discussed above.

Moreover, parallel oriented *Fl-BTZ-Fl* and *Fl-DPP-Fl* have also similar charts (especially over k shift) which suggests that the E_{bind} depends of the orbital overlapping between the stacks and the difference could be explained with the slightly different ground state geometries.

Further the minimum distances obtained from E_{bind} graphics (Fig. 21, p. 62 and Fig. 22, p. 63) are utilized for estimation of the CT properties (the electronic couplings and the charge carrier mobilities).

4.4.　　Charge Transport in Isolated Stacks

In order to compute the CT properties, first the total reorganization (λ_{tot}) energies and the electronic coupling (V) have to be calculated. Two contributions to λ_{tot} must be evaluated: for the inner (eq. 11, p. 25) and for the outer shell (eq. 12, p. 25 and eq. 13, p. 26). First, the reorganization energies of *BTZ* molecules are considered (Table 8).

B3LYP/6-31G* $\varepsilon=0$		*Fu-BTZ-Fu*			*Th-BTZ-Th*		
		$\varepsilon=0$	$\varepsilon=2.379$	$\varepsilon=4.9$	$\varepsilon=0$	$\varepsilon=2.379$	$\varepsilon=4.9$
λ_{i} [eV]	λ^-	0.224	0.225	0.228	0.218	0.220	0.219
	λ^+	0.276	0.277	0.277	0.299	0.296	0.294
λ_{o} [eV]	λ^-	-	0.003	0.034	-	0.003	0.032
	λ^+	-	0.003	0.037	-	0.003	0.034
λ_o^{PCM} [eV]	λ^-	-	0.001	0.004	-	0.002	0.001
	λ^+	-	0.001	0.001	-	0.003	0.005

Table 8. Reorganization energies for the inner (λ_{i}) and outer (λ_{o}) shells of *BTZ* molecules.

From Table 8 it is seen that the inner shell terms (λ_{i}) are substantially larger than the outer shell (λ_{o}) values obtained with two methods. Since λ_{o} has a small contribution to the relaxation energy (less than 2%) it can be neglected. It should be mentioned that molecule volume of neutral and charged states are computed as the volume inside a contour of 0.001 e^-/B^3 density in order to estimate the radii of the molecules. Further, the outer shell reorganization energies are omitted and for the rest of the investigations only λ_{i} ($\varepsilon=0$) are estimated, and for *DPP* molecules λ_{i} are shown in Table 9.

	Fu-DPP-Fu	*Th-DPP-Th*
λ_i^- [eV]	0.171	0.177
λ_i^+ [eV]	0.311	0.322

Table 9. Inner reorganization energies of *DPP* molecules (B3LYP/6-31G*, $\varepsilon=0$).

If λ_{i} values of *BTZ* and *DPP* (Table 8 and Table 9, respectively) are compared it can be concluded that all the values are in range of 0.17÷0.32 eV and the boundary of the lowest and the highest values is covered by *DPP* molecules, whereas *BTZ* derivatives have tighter range in the middle (0.22÷0.29 eV). It is noticeable that λ_i^- are always smaller than λ_i^+ for all the molecules due to loss of conjugation in positive charged state and this is translated further to the CT properties - the hole transfer is less favourable and these molecules always show dominant electron mobility. Additionally, the values corresponding to each unit (*BTZ* or *DPP*) for different types of reorganization energies (positive or negative) have the same values independently of the flanks due to the fact that they have similar planar geometries (the X_{atom} does not influence on the λ_{i}). Moreover, because *DPP* molecules show the boundary values of λ_{i} and it could be expected that if one combines these two molecules into single one (*DPP-BTZ*) *DPP* values would

dominate, which is true only for λ_i^-, whereas for λ_i^+ these values are closer to *BTZ* molecules and the monomers (*Fl-DPP-Fl-BTZ-Fl*) have intermediate λ_i^- and lower λ_i^+ values as compared to *DPP* and *BTZ* small molecules, respectively, and this is demonstrated later (Table 19, p. 88). In any case, these (*trans-trans*) molecules have small reorganization energies and they are suitable for application as charge-transporting layers.

R. Jin and K. Wang [282] obtained similar values for the reorganization energies of similar *DPP* compounds with side chains and additional thiophene rings: with *Fu* flanks 0.153 and 0.301 eV, for λ_i^- and λ_i^+, respectively, and with *Th* flanks 0.160 and 0.293 eV, for λ_i^- and λ_i^+, respectively.
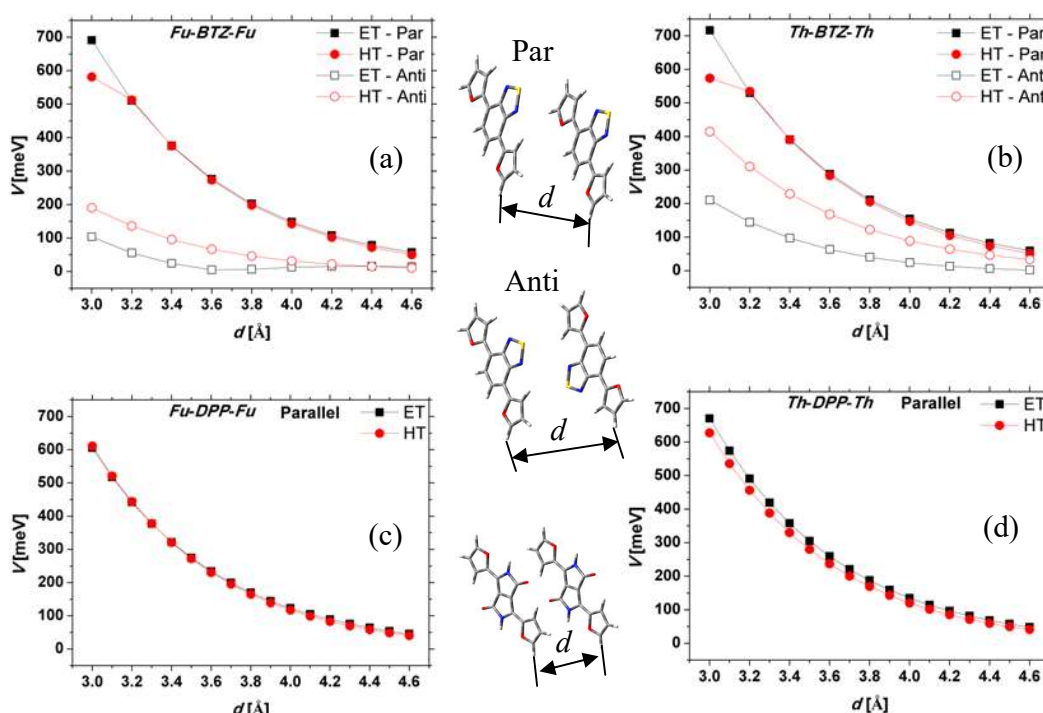

Figure 23. Electronic couplings (in meV) for electron (ET - squares) and hole (HT - circles) transfers of *trans-trans* conformers of *BTZ* (a and b) in parallel (filled symbols, Par) and anti-parallel (empty symbols, Anti) orientation, and *DPP* (c and d) parallel oriented derivatives as a function of the distance between the molecules (*d*) - B3LYP/6-31G*, ε=0.

The next (and the last) parameter governing the CT properties is the electronic coupling (*V*). The *V* values are computed with ESID method (eqs. 15 and 16, p. 26), which utilized the orbital energies in stack of dimers. First, it is performed an approach which considers the energetically accessible geometries of two molecules in (isolated) dimer. In this case, the overlap integrals for a range of potential packing motifs are calculated as a function of all the possible directions in one dimensional (and two dimensional for comparison with experimental data) approximation similar to the E_{bind} for both electron (ET) and hole (HT) transfers. First, the dependence of *V* as a function of the distance between the molecules (*d*) is considered (Fig. 23) for all small molecules in segregated stacking motif in parallel and anti-parallel orientation.

From Figure 23 (p. 66) it can be seen that V drops exponentially with an increase of the intermolecular distance (d) and at closer distance they have maximum values. It can be concluded that if the molecules can be brought at closer distance they will possess higher hopping mobilities since the charge carrier mobility ($\mu^{-/+}$) is proportional to the distance to according eq. 3 (p. 23) and the charge rate constant is proportional to V (on power two) according to eq. 8 (p. 24). This is proved experimentally when pressure is applied into the sample [151] as it was mentioned in the introduction. It is interesting that in parallel orientation e^{-} and h^{+} couplings coincide for all the molecules (*BTZ* and *DPP* derivatives) independently of the *Fl* and they have very close values (which will lead to balanced mobilities). Whereas for anti-parallel orientation (*BTZ* molecules) the V values are much lower than parallel orientation since only a part of the molecule, namely "flank-benzene ring-flank" is involved in the interaction and h^{+} coupling dominates, which means that generally these molecules will posses different CT properties and in particular they will exhibit larger h^{+} mobilities than e^{-} mobilities.

A second conclusion can be suggested (in addition to the closer distance) that if high symmetric molecules (*DPP*) or if the molecules can form parallel orientated stacks in the crystal structure they will possess balanced and high couplings/mobilities (as compared to anti-parallel stacks), which explains the wide application of *DPP* blocks in organic electronics. Additionally, many small molecules utilized as dopants in organic electronics have the same (and sometimes even higher) symmetry [283]. Moreover, small molecules with the same symmetry such as tetrathiafulvalene and 7,7,8,8-tetracyanoquinodimethane used as blends with polymers induce more ordered CT pathways [284], which leads to increased hopping mobilities. As it was already mentioned, *Th-BTZ-Th* molecule has anti-parallel orientation in the crystal structure due to increased interaction (E_{bind}) energies and indeed, it exhibits one order of magnitude lower μ^{+} mobility (Table 11, p. 73) as compared, for instance, with *Th-DPP-Th* molecule (Table 12, p. 75) according to the experiments. Additionally, if anti-parallel orientated *Fu* and *Th* derivative of *BTZ* are compared, *Th-BTZ-Th* dimer has much greater V values even in anti-parallel orientation, which explains the wide incorporation of *Th* molecules into the semiconducting polymers.

K. Thorley and C. Risko [281] obtained similar charts for the V dependencies of the d, like obtained in the parallel case here, for benzodithiophene molecules, which posses the same symmetry as *DPP* and also for asymmetric molecules. This proves the fact that when the anti-parallel orientation do not exist explicitly the interaction between dimers will be stronger and this will lead to better performance of the devices.

In anti-parallel orientation, the hole exchange governed by the overlap of monomeric HOMO orbitals proceeds with larger values of coupling. Thiophene for furan substitution affects mainly the anti-parallel stacked molecules, leading to a decrease in both HOMO and LUMO splitting. The high values of electronic couplings in parallel orientation could be also explained with so called strong orbital interaction where the electron density is overlapping between the space of two molecules in dimer (forming bridge like shapes) shown for *Fu-BTZ-Fu* dimer in Figure 24 (p. 68).

Moreover, V values are computed as a function of one geometric variable k and l (Fig. 25, p. 69) when one of the molecules of the dimer is shifted over the short (k) or long (l) axis.

The distances between dimers (d) are taken as constants from Figure 21 (p. 62). Both k and l dependencies of V of the molecules under study show in general a non-monotonic behaviour. The oscillations are primary related to the bonding/anti-bonding patterns of molecular HOMO/LUMO orbitals involved in hole and electron exchange, which is observed also in experiment [285].
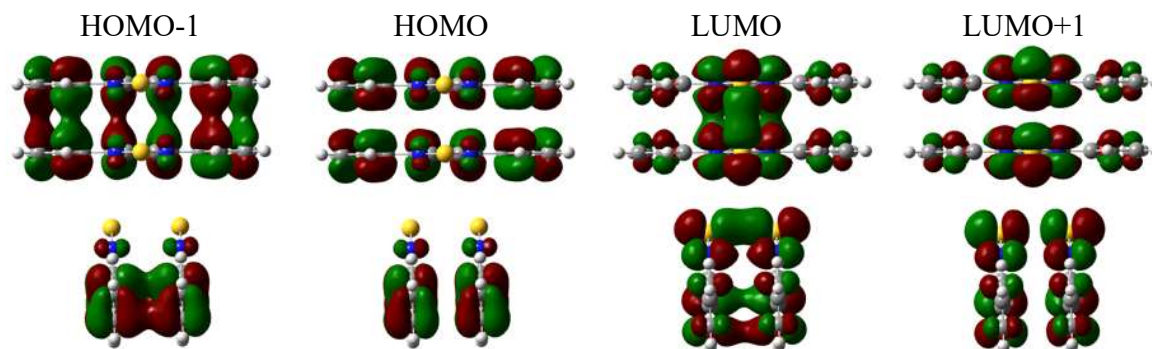

Figure 24. The top and side views of HOMO-1, HOMO, LUMO and LUMO+1 molecular orbitals (MO) of *Fu-BTZ-Fu* parallel dimer at d=3.4, k=0, l=0 Å (B3LYP/6-31G*, ε=0). Here the lobes of MOs are shown as isodensity surfaces with a contour of ±0.02 a.u. with positive (green) and negative (red) phases of the wave function.

All LUMO orbitals have lobes which are parallel to the long molecular axes, and the lobes of HOMO are oriented perpendicularly [286, 287, 288] (Fig. 19, p. 58). LUMO orbitals are localized on the central units (*BTZ* and *DPP*). In HOMO level, the distribution shows an alternation of the positive and the negative phases every half ring for the flanks and for the central part of the units. Both *BTZ* and *DPP* molecules have similar behaviour of the oscillations over the corresponding axes because they have similar shape of the orbitals (and similar *Fl*) and the dependence of the *Fl* is mainly due to the height of the peaks (maybe due to different d).

Moreover, most of the peaks have extrema at approximately the same positions of the shifts independently on the compounds. This is explained with similar overlap (superposition) of molecular fragments with certain units (overlapping of the flanks with the central cores). In addition, these peaks are usually slightly shifted because *Fu* and *Th* have slight difference in the size of the five-membered rings (as well as the angle between the units), which was discussed. So if the molecules are placed at exact positions related to the points with maximum couplings their CT properties can be enhanced.

Generally, for parallel orientation all the molecules show maximum values at the starting (k=l=0) face-to-face positions and all the other values are lower. Here one can conclude that when *Fu* and *Th* derivatives are compared the values of V^{ET} and V^{HT} are nearly balanced where this is more pronounced for *DPP* molecules. There is only one exception over l axis of *BTZ* molecules where V^{HT} is larger for *Th* flank (Fig. 25 - b, p. 69) and V^{ET} have phase shifted behaviour at long distance. It could be concluded that *Th* will be better flank for *BTZ* molecules only for h^+ transfer (V^{HT}) and the effect of the heteroatom in the flank is not so strongly pronounced in parallel orientation.
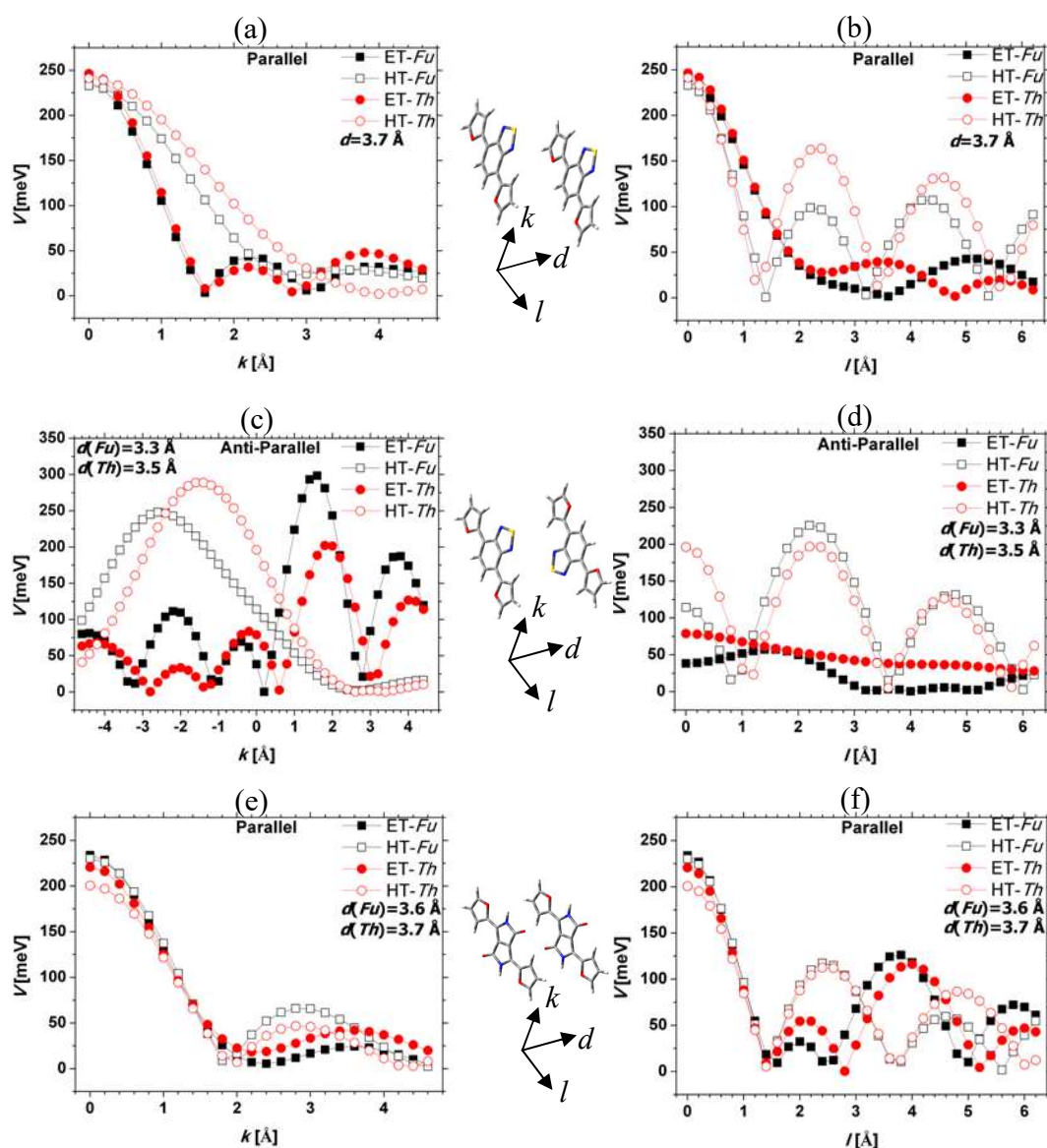
Figure 25. Electronic couplings (in meV) for electron (ET - filled symbols) and hole (HT - empty symbols) transfer of *trans-trans* conformers of *BTZ* (a, b, c and d) in parallel (a and b) and anti-parallel (c and d) orientation and *DPP* (e and f) parallel oriented derivatives with *Fu* (squares) and *Th* (circles) flanks as a function of *k* (left) and *l* (right) shifts (B3LYP/6-31G*, ε=0). The *d* values are taken as a constant from Figure 21 (p. 62) for each pair of molecules.

Similar $V(k)$ dependencies like obtained here for parallel orientation case were calculated by K. Thorley and C. Risko [281] for benzodithiophene molecules, which possesses the same symmetry as *DPP* as well as for asymmetric molecules. This shows that symmetric molecules which do not have explicit anti-parallel orientation exhibit similar electronic couplings (CT) due to the similar overlap and distribution of the electron density of the frontier orbitals.

In anti-parallel *BTZ* molecules the values of V^{ET} and V^{HT} do not coincide except of only one case of V^{HT} over *l* shift (Fig. 25 - d). The peaks are usually shifted because of broken symmetry and the molecular fragments do not overlap equally.

It is worth noting that some of the peaks have the same or even higher values of the electronic couplings than the maximum point ($k=l=0$) in parallel orientation, which is a contradiction according to Figure 23 (p. 66) where parallel orientation have always higher values. This occurred because of d depends on the orientation and in the case of anti-parallel oriented stacks this distance is shorter (with 0.4 and 0.2 Å, for *Fu* and *Th* flanks, respectively) - $d_{parallel} > d_{anti-parallel}$. Consequently, the molecules could exhibit similar or greater charge carrier mobilities even in anti-parallel orientation if they can be placed at special positions as compared to parallel orientation. These special configurations correspond to the cases when thiadiazole parts of *BTZ* are overlapping (S atoms are in the middle of benzene rings) at $k=1.6$ Å and $k=1.8$ Å, for *Fu* and *Th*, respectively, when the flanks of each molecule are in superposition (in case of *Fu* there is O⋯O interaction) at $k=-2.8$ Å and $k=-1.4$ Å, for *Fu* and *Th* respectively, and in the case where the molecular fragments do not overlap and only individual atoms are placed one above (fully occupied free space) at $l=2.2$ Å and $l=2.0$ Å, for *Fu* and *Th*, respectively. All of these interactions lead to maximum V values.

The disadvantage of anti-parallel alignment is that when one of the couplings (ET or HT) has maximum value the other one usually has minimum or low value, which is a hindrance in order to obtain balanced charge carrier mobilities or it could be used to maximize only one type mobility (e^- or h^+).

In *BTZ* anti-parallel molecules, *Fu* flank generally dominates over *Th* one because *Fu* molecules are at closer d in dimer, which is obtained from the binding energies (Fig. 21, p. 62). There is only one exception of V^{ET} over l shift where *Th* dominates over *Fu* flank. In anti-parallel orientation the X_{atom} has great influence of the V values mainly due to different d in the dimer units.

If E_{bind} and V are compared (Fig. 22, p. 63 and Fig. 25, p. 69) some of the extremum points coincide very well (especially over k shift in anti-parallel orientation), which suggests that these quantities are closely related and the minimum points in E_{bind} can be used in order to estimate later the CT properties. Several points from Figure 25 (p. 69) are summarized in Table 10 where V have maxima and they are compared for parallel and anti-parallel orientation.

	Coordinates: *Fu*/*Th* [Å]	V [meV]	-*BTZ*-		-*DPP*-	
			Fu	*Th*	*Fu*	*Th*
Parallel	$k=l=0$	V^{ET}	236.7	246.4	233.8	220.8
		V^{HT}	232.9	241.2	230.2	200.6
Anti-Parallel	$k=-2.8$/$k=-1.4$ $l=0$	V^{ET}	65.4	6.9	-	-
		V^{HT}	244.9	289.0	-	-
	$k=1.6$/$k=1.8$ $l=0$	V^{ET}	298.4	202.2	-	-
		V^{HT}	22.7	26.3	-	-
	$l=2.2$/$l=2.0$ $k=0$	V^{ET}	42.9	53.5	-	-
		V^{HT}	225.6	184.5	-	-

Table 10. Summary of the electron (V^{ET}) and hole (V^{HT}) couplings (in meV) of *BTZ* and *DPP* molecules with *Fu* and *Th* flanks in the main (highest) maximum points from Figure 25 (p. 69) - B3LYP/6-31G*, $\varepsilon=0$.

Calculating the same couplings in Figure 23 (p. 66) and Figure 25 (p. 69) with M06-2X/cc-pVTZ shows only slightly increased values maybe due to π-π non-covalent interactions.

In order to get better insight into the CT properties in experimental crystal structure of *Th-BTZ-Th*, two-dimensional scan of the electronic couplings is performed, which are presented in Figure 26 of anti-parallel dimer of *cis-trans* conformer. As follows from the data, *V* ranges from very small values to 350 meV, depending on the stacking dimer geometry and substantial changes in the hopping mobilities can be expected in *Th-BTZ-Th* crystals. One can conclude that the regions characterizing the largest and lowest electronic interactions coincide with the values obtained from one dimensional charts (Fig. 25 c and d, p. 69). Here the peaks are more pronounced and there are regions of high and low *V* values.

The coordinates of the experimental crystal structure are shown as a white point. It is noteworthy that this arrangement of the molecules provides the structure reduced repulsion caused by the heteroatoms. The dipole-dipole interaction is attractive since the molecular dipoles of 1.17 D in anti-parallel dimer point out in opposite directions; and finally, one of the electron-rich thiophene flanks builds mixed stack with the electron-deficient *BTZ* core of the other molecule in dimer, favouring D_--A_+ interactions.
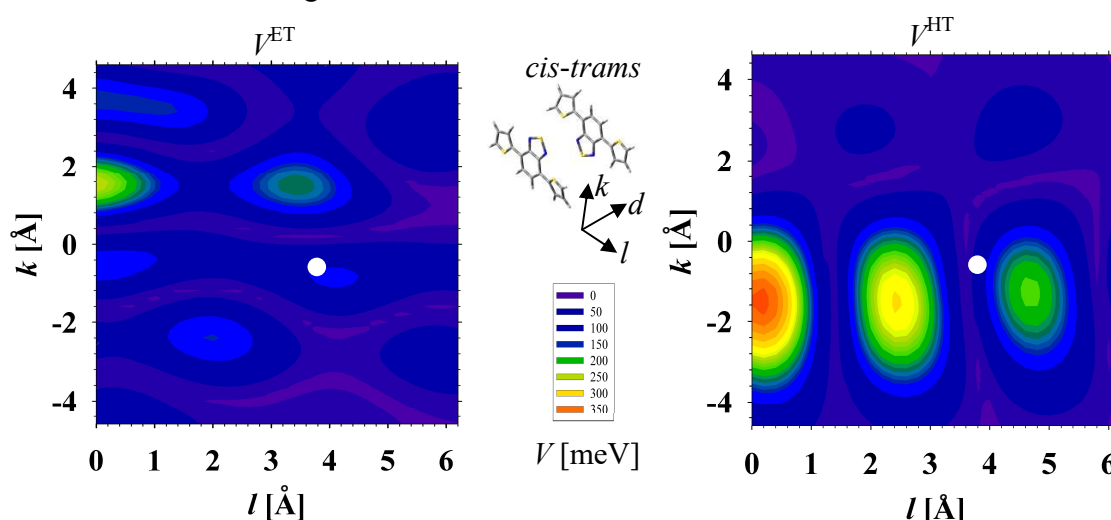

Figure 26. 2D diagrams of electronic couplings *V* (in meV) versus *k* and *l* shifts for ET (left) and HT (right) in anti-parallel dimers of *cis-trans Th-BTZ-Th* calculated at *d*=3.4 Å (B3LYP/6-31G*, ε=0). The dimer with *d*, *k* and *l* coordinates corresponding to the experimental crystal structure [94] is shown as a white dot (*d*=3.4 Å, d_h=5.15 Å, *k*=-0.6 Å, *l*=3.8 Å).

The electronic coupling values for electron and hole exchange are 109 meV and 70 meV, respectively, for cofacial stack of molecules in their ground state geometry and for dimer taken from the XRD crystal structure are 34 meV and 8 meV (for V^{ET} and V^{HT}, respectively). For both cases, the efficiency of electron exchange is higher than hole exchange. The lower values of *V* for the second dimer can be explained by (i) different geometry of the molecules in tightly packed crystals as compared to ground state geometry of *cis-trans* conformer in gas phase (ii) a slight

rotation of molecules in stacks, and (iii) lengthening the intermolecular spacing from 3.4 Å (calculation) to 3.44 Å (experiment).

For anti-parallel *trans-trans* conformers of *BTZ* derivatives are obtained similar charts.

For parallel orientation the only difference is that there is a only one maximum for V^{HT}, which is expected from Figure 25 (a and b, p. 69) and the maximum values of the electronic coupling is higher than anti-parallel orientation. The difference between *Fu* and *Th* flanks in *BTZ* molecules is that *V* values of *Th* are slightly higher than *Fu* ones at the same *d*.
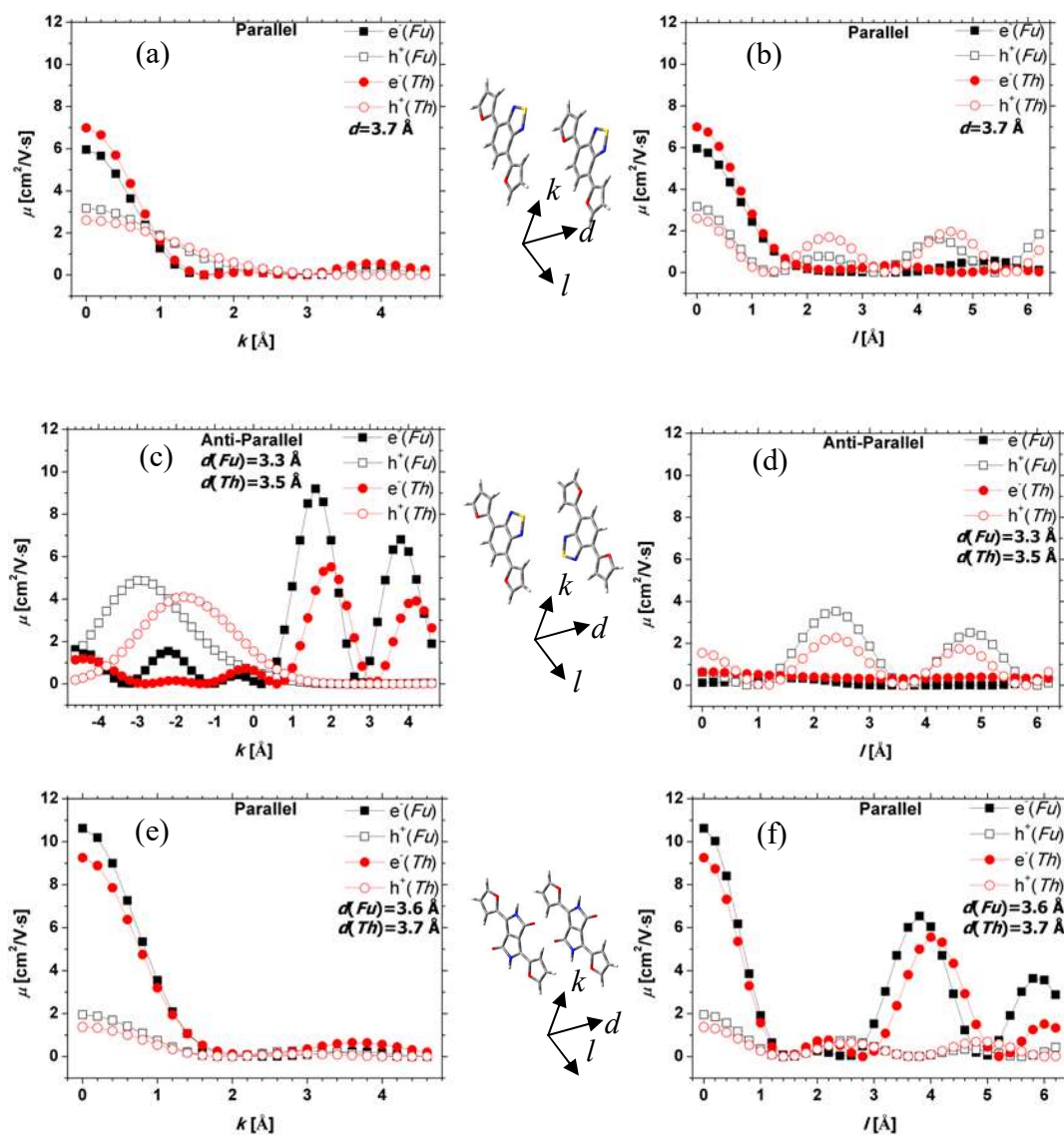

Figure 27. Hopping mobilities (in cm^2/V·s) of electrons (e^- - filled symbols) and holes (h^+ - empty symbols) of *trans-trans* conformers of *BTZ* (a, b, c and d) in parallel (a and b) and anti-parallel (c and d) orientation, and *DPP* (e and f) parallel oriented derivatives with *Fu* (squares) and *Th* (circles) flanks as a function of *k* (left) and *l* (right) shifts (B3LYP/6-31G*, $\varepsilon=0$). The *d* values are taken as a constant from Figure 21 (p. 62) for each pair of molecules.

Finally, the hopping mobilities are computed with Einstein-Smoluchowski equation (eq. 3, p. 23) in one dimensional approximation at T=298K for both e^- and h^+ mobilities where only the electronic coupling and the distance between the molecules (and λ_i) are required (Fig. 27, p. 72). One molecule of the dimer stacks is shifted in one direction over two axes (k and l) for both compounds (similar to Fig. 25, p. 69) and the distance between dimers is taken as center-to-center distance (Fig. 11, p. 40). Comparing Figure 27 (p. 72) and Figure 25 (p. 69), i.e. hopping mobilities and couplings, respectively, the same oscillations are observed for the charge carrier mobilities as it is expected due to the mutual dependence of these two quantities. The mobilities are very sensitive to small intermolecular displacement over one of the axes. Generally, in parallel orientation the mobilities are higher than anti-parallel one (*BTZ* molecules) with exception of two maxima mentioned above for *V* values where the overlap of anti-parallel oriented molecules can reach higher values due to shorter *d*.

The greatest difference between the figures describing the electronic coupling (Fig. 25, p. 69) and the hopping mobilities (Fig. 27, p. 72) is that for *V* values of e^- and h^+ couplings coincide in the most of the cases, whereas the electron mobilities are much larger than hole mobilities with only one exception for anti-parallel *BTZ* molecules over *l* shift (and the half of the values over *k* shift), which exception is also observable for *V* values.

	Coordinates: Fu/Th [Å]	μ [cm²/V·s]	-BTZ-		E_{bind} [kJ/mol]
			Fu	Th	Fu/Th
Parallel	k=l=0	μ^-	5.957	6.992	-18.80/-27.70
		μ^+	3.164	2.600	
	k=1.4/k=1.2 l=0	μ^-	0.098	0.700	-31.21/-37.21
		μ^+	1.116	1.567	
	l=1.6/l=1.4 k=0	μ^-	0.588	1.015	-34.26/-43.45
		μ^+	0.106	0.058	
Anti-Parallel	k=l=0	μ^-	0.125	0.640	-47.49/-42.23
		μ^+	0.606	1.540	
	k=-3.0/k=-2.6 l=0	μ^-	0.243	0.029	-25.32/-27.82
		μ^+	4.874	3.221	
	k=2.4/k=2.8 l=0	μ^-	1.888	0.835	-34.81/-32.32
		μ^+	$7 \cdot 10^{-4}$	$2 \cdot 10^{-4}$	
	k=-0.2/k=0.4 l=0	μ^-	0.326	0.145	-47.82/-46.04
		μ^+	0.741	0.926	
	l=0.6/l=1.0 k=0	μ^-	0.169	0.510	-47.81/-48.69
		μ^+	0.151	0.041	
	l=3.2/l=3.4 k=0	μ^-	$6 \cdot 10^{-4}$	0.310	-50.77/-52.11
		μ^+	1.027	0.116	
Exp. [263]	k=-, l=- k=-0.6, l=3.8	μ^-	-	-	-
		μ^+	-	0.038	

Table 11. Summary of the electron (μ^-) and hole (μ^+) hopping mobilities (in cm²/V·s) of *BTZ* molecules (with *Fu* or *Th* flanks) for non-shifted dimers ($k=l=0$) and in the minimum points of E_{bind} (Fig. 22, p. 63). The *d* values are taken from Figure 21 (p. 62) - B3LYP/6-31G*, ε=0.

This dominant e^- mobility for parallel orientation occurred due to the difference in the other parameter (λ_i) where the reorganization energies for negative charged states are lower than positive charged ones (as it was already mentioned that these molecules do not prefer positive charged states) and in anti-parallel orientation (*BTZ* molecules) over *l* shift the hole mobilities become dominant (with except of two peaks over *k* shift) due to difference in the electronic coupling.

Thus the parallel orientation alignment where the couplings are equal is not enough and also the reorganization energies should be equalized ($\lambda_i^- = \lambda_i^+$) or as an alternative way if can be chosen a position of dimer stacks (the crossing points) where this effect is compensated.

According to the experiment of *Th-BTZ-Th*, h^+ mobility of 0.038 cm^2/V·s is measured [263] and the prediction of mobility varies from 0.0002÷5.5 cm^2/V·s for shifts over *k* and *l* in anti-parallel orientation (as it is according to the experiment) as well as the prediction of the corresponding crystal structure (the white point in Fig. 26, p. 71) has values of 2.252 and 0.365 cm^2/V·s, for μ^- and μ^+, respectively, which is with two and one orders of magnitude higher than the experiment 0.038 cm^2/V·s (for μ^+) [263]. This high deviation could be due to presence of defects or due to overestimation of the electronic coupling from the theory.

In order to clarify better the CT properties of *BTZ* molecules some values of mobilities are shown in Table 11 (p. 73), which correspond to non-shifted dimers ($k=l=0$) and special dimer orientations with minimum energies, which are taken from E_{bind} (Fig. 22, p. 63). Table 11 (p. 73) shows that for parallel orientation both *Fu* and *Th* derivatives of *BTZ* have the same order of mobilities independently of the X_{atom} in the *Fl* (with one exception over *l* shift for μ^+ and one more over *k* shift for μ^-) and usually μ^- is greater than μ^+ except over *k* shift. Non-shifted dimers ($k=l=0$) have always dominant mobilities. It is worth to notice that in the deepest minimum of E_{bind} the μ^+ is higher and the μ^- is lower as compared to the second one, which is true also for *Fu-BTZ-Fu* molecule. Interesting, the global minimum of *Th-BTZ-Th* ($l=1.4$, $k=0$ Å) predicts very well the μ^+ of 0.058 and 0.038 cm^2/V·s [263] in theory and experiment, respectively, although the crystal structure is anti-parallel according to the experiments [94, 263].

In anti-parallel orientation, *BTZ* molecules in the most of the cases *Fu* molecules dominates *Th* ones due to shorter π-π (*d*) distance and better orbital overlap, which leads to the fact that X_{atom} in the flank has impact into the CT properties in anti-parallel orientation. Non-shifted dimers are no longer dominant for all the mobilities and $k=0$ ($l=0$) Å is a minimum point for *Fu* compound. The highest μ^+ correspond to the point with the lowest E_{bind} energy. Additionally, the second minimum of *Th-BTZ-Th* ($l=1.0$, $k=0$ Å) $\mu^+=0.041$ cm^2/V·s corresponds very well to the experimental obtained value (0.038 cm^2/V·s) [263]. Moreover, this point is close to the experimental measurement at least in *k* shift ($k=-0.6$ Å and $l=3.8$ Å). It can be concluded that with dimer with minimum energy in E_{bind} (the second or the global minimum) predicts goods charge carrier mobilities as compared to the experiment since the predicted molecular stacks are close to the experimentally obtained crystal structure with respect to their mutual orientation.

The predicted values of the crystal structure (the white point in Fig. 26, p. 71) deviate from the experimentally obtained ones, which can be explained with the fact that the mobilities

depend strongly on small molecular displacements as it was already mentioned but, for instance, *BTZ*-quarterthiophene polymer [289], the computed value here of μ^+ (0.365 cm^2/V·s) coincides fairly well with experimentally obtained one of 0.20 cm^2/V·s, which leads to the conclusion that in polymers the molecular displacement are restricted (mainly due to stacked chains) and the preferable charge transport direction is along the π-π stacks.

For *DPP* derivatives (Table 12) the case is similar as for *BTZ* parallel oriented molecules. Non-shifted dimers have dominant charge transport properties but in the deepest minimum of E_{bind} both μ^- and μ^+ are higher than the second one and the effect of the X_{atom} trends to disappear, and *DPP* compounds with different *Fl* have comparable mobilities (without μ^- value at $l=1.6$, $k=0$ Å). Moreover, the μ^- is always higher than μ^+ without exceptions this time.

	Coordinates: *Fu*/*Th* [Å]	μ [cm^2/V·s]	-*DPP*-		E_{bind} [kJ/mol]
			Fu	*Th*	*Fu*/*Th*
Parallel	$k=l=0$	μ^-	10.621	9.257	-13.38/-16.75
		μ^+	1.943	1.378	
	$k=1.4$/$k=1.4$ $l=0$	μ^-	1.069	1.065	-28.69/-33.95
		μ^+	0.211	0.170	
	$l=1.6$/$l=1.6$ $k=0$	μ^-	0.021	0.105	-34.20/-39.80
		μ^+	0.048	0.040	
	$l=3.4$/$l=3.4$ $k=0$	μ^-	4.702	2.365	-36.48/-42.03
		μ^+	0.104	0.105	
Exp.	$k=1.12$, $l=3.60$[269]	μ^-	-	-	-
	$k=1.53$, $l=3.27$[274]	μ^+	-	0.3[272]	

Table 12. Summary of the electron (μ^-) and hole (μ^+) hopping mobilities (in cm^2/V·s) of *DPP* (with *Fu* or *Th*) molecules for non-shifted dimers ($k=l=0$) and in the minima of E_{bind} (Fig. 22, p. 63). The *d* values are taken from Fig. 21 (p. 62) - B3LYP/6-31G*, $\varepsilon=0$.

For *Th-DPP-Th*, the μ^+ is again good predicted as compared to experiment (0.3 cm^2/V·s with one hexyl side chain) [272] with a value in the same order of magnitude and this time at two minimum points of E_{bind} where again one of the points corresponds to the highest E_{bind} ($k=1.4$ Å, $l=0$ Å, $\mu^+=0.170$ cm^2/V·s) and the other one corresponds to a global minimum ($l=3.6$ Å, $k=0$ Å, $\mu^+=0.105$ cm^2/V·s), which shows again the precision of E_{bind} in π-π stack according to the CT properties.

This correct prediction of the hopping mobilities is explained with the fact that experimentally obtained structure is very close to the structure (the shifts over *k* and *l*) obtained from the calculation of the binding energies. Moreover, this is the reason why dimers with the deepest minimum in E_{bind} value ($l=1.6$, $k=0$ Å) predicted correct μ^+, which coincide with the experiment as it was already mentioned.

It is interesting that in a polymer of *Th-DPP-Th* with one additional *Th* unit and branched side chains the mobilities are one order of magnitude lower than for the small molecule ($\mu^-=0.01$ and $\mu^+=0.04$ cm^2/V·s, for polymer [271] and $\mu^+=0.3$ cm^2/V·s, for small molecule [272], respectively).

Here the mobility of this polymer (only μ^+) is predicted by one of the points (l=1.6 Å, k=0 Å, μ^+=0.04 cm^2/V·s) obtained from E_{bind} for *Th-DPP-Th* small molecule. The lower mobility of the polymer can be explained with not planar backbones in the polymeric material or by the addition of a second *Th* flank per monomer unit.

It can be concluded that the CT properties (mainly *V* values) in isolated stacks depend on the π-orbital overlapping, which is stronger for parallel oriented or high symmetric molecules. The X_{atom} has influence in anti-parallel orientation where shorter $d_{\pi\text{-}\pi}$ between dimers (from E_{bind}) are obtained as well as reduced e^- density overlap, which leads to lower experimentally measured mobility. The difference between the molecules in the corresponding orientations can be explained with slightly difference in the geometry (orbital overlapping).

4.5. Charge Transport in Molecular Crystals

More investigations of the CT properties are performed of the experimentally resolved crystal structure of *Th-BTZ-Th* small molecules [263] where the unit cell is replicated three times in all directions in order to create a larger super cell and further it is simulated with MD within NVT (t =10 ns) ensemble with PBC (Fig. 28, p. 77).

All the possible nearest dimers (shown as pathways in Fig. 28, p. 77) are represented as hopping direction of a charge in the unit cell. Dimers are extracted every 100000 frame in order to reproduce average values (each value is averaged over 100 frames) for the electronic couplings (*V*) throughout the whole simulation at two different temperatures: *T*=298 K (Table 13, p. 77) and *T*=430 K (Table 14, p 78). After the extraction of each pair of dimers a DFT procedure is applied in order to obtain the electronic energies.

At *T*=298 K the average and standard deviations of *V* values are at the same order of magnitude for all the dimer stacks (pathways), which suggests that this molecule could exhibit two times higher or two time lower CT properties than the average values. The maximum obtained values for *V* correspond to path1 and path5, which are cofacial arrangement, so it can be concluded that cofacial CT will be preferable in molecular crystal as compared to herringbone CT (Fig. 5, p. 18). The average *V* values are in the range of 45÷88 meV.

The distance between the molecules (d_h - center-to-center) has small deviation from the equilibrium position in all the dimer stacks and the molecules only oscillate around their equilibrium positions during the MD simulation.

If the charge rate constant (K_{CT}) are compared the dominant CT (the highest K_{CT}) will be ascribed to path1 and path5 because they have the largest *V* values and the smallest contribution to the CT will be realized by path3 and path4, which correspond to the lowest *V* values.

If the hopping mobilities are compared μ^- is one order of magnitude larger than μ^+, which again proves the fact e^- mobility is preferable. The only exception is path5 where both electron and hole mobilities are on the same order of magnitude and also path5 has the maximum values for both e^- and h^+ mobilities.

All the other pathways have the same values (two and more times lower values than path5).

The superiority of path5 comes from the fact the hopping mobilities depend strongly on the distance between the molecules according to eq. 3 (p. 23), which is valid only for one dimension (like in stack of polymers) and in 3D molecular crystal it is difficult to be determined the distance between two molecules - the center-to-center distance only maximize the mobilities. At the same time, as it is shown in recent publications [290], this approximation remains reliable and allows comparing the CT properties in cofacial stacks using the center-to-center distance. All the pathways overestimate the mobilities according to the experiment and there is (at least) one order of magnitude difference between computed and measured hopping mobilities: μ^+=0.038 [263] and μ^+=0.335 cm^2/V·s (the lowest value of path1), for experiment and theory, respectively.
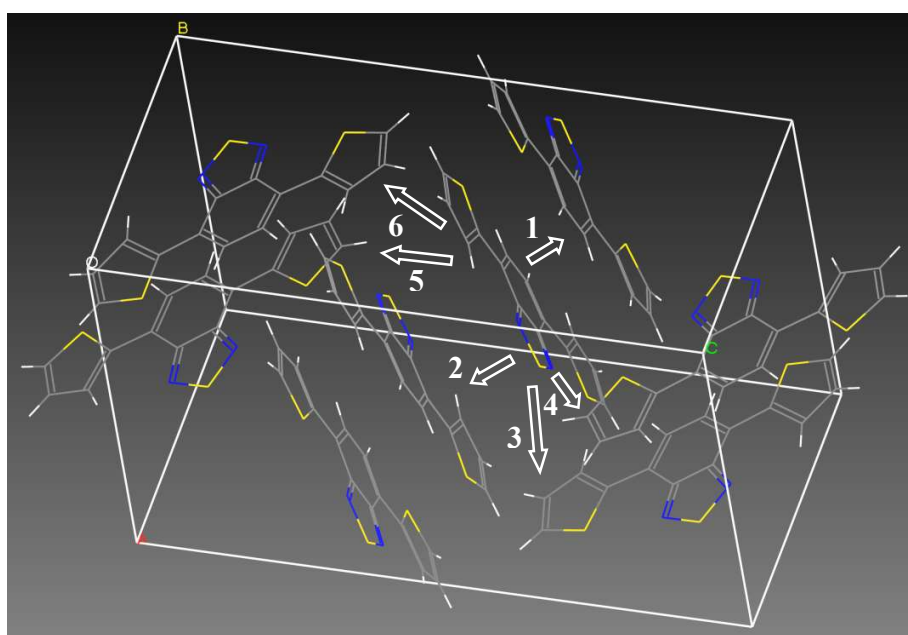

Figure 28. Unit cell of *cis-trans* conformer of *Th-BTZ-Th* molecule (anti-parallel orientation) [263] with parameters: α=β=γ=90°, a=12.81 Å, b=9.99 Å and c=20.31 Å. All the possible pathways (extracted dimers) for charge transport are shown with arrows.

T = 298 K	Path 1	Path 2	Path 3	Path 4	Path 5	Path 6
$<d_h>$ [Å]	4.78 ± 0.26	8.08 ± 0.31	8.72 ± 0.30	9.67 ± 0.33	10.52 ± 0.31	10.59 ± 0.32
$<V^{ET}>$ [eV]	0.888 ± 0.509	0.623 ± 0.313	0.499 ± 0.411	0.457 ± 0.330	0.770 ± 0.519	0.573 ± 0.4089
$<V^{HT}>$ [eV]	0.718 ± 0.489	0.510 ± 0.349	0.570 ± 0.428	0.458 ± 0.349	0.836 ± 0.555	0.558 ± 0.393
K^-_{CT} [1·10^{13}/s]	2.899 ± 0.952	1.427 ± 0.361	0.914 ± 0.621	0.766 ± 0.399	2.176 ± 0.991	1.207 ± 0.614
K^+_{CT} [1·10^{13}/s]	0.753 ± 0.349	0.378 ± 0.178	0.475 ± 0.267	0.306 ± 0.177	1.020 ± 0.449	0.455 ± 0.226
μ^- [cm^2/V·s]	1.288 ± 0.423	1.814 ± 0.458	1.352 ± 0.920	1.395 ± 0.727	4.686 ± 2.134	2.636 ± 1.341
μ^+ [cm^2/V·s]	0.335 ± 0.155	0.483 ± 0.226	0.703 ± 0.396	0.558 ± 0.324	2.197 ± 0.968	0.994 ± 0.493
μ^-/μ^+	3.850	3.757	1.925	2.499	2.133	2.653

Table 13. Summary of the CT properties of *Th-BTZ-Th* crystal cell [263] at *T*=298 K obtained from MD (B3LYP/6-31G*, ε=0). The pathways are shown in Figure 28.

This deviation can be explained with the difficulty to measure the distance between the molecules in 3D space, which is not a problem in case of polymers when the backbones are stacked or additionally, presence of defects can influence on the experimental crystal structure and later to the hopping mobilities.

It should be also kept in mind that the standard deviations of the mobilities are one order of magnitude or double time reduced as compared to the average values (which is valid also in the case for higher temperature) and this can lead to large deviations in devices.

At 430 K (Table 14) the minimum values of V are slightly increased up to 55 meV and the dominant pathways become number 1 and number 6 and only in path6 the V^{HT} is above 1 eV (1.106 eV). Thus with increasing the temperature V values are increased and the carrier mobilities will be also increased. Indeed, all the hopping mobilities (as well as the standard deviations) are higher as compared to T=298 K. This proves the fact that at higher temperature the organic semiconductors exhibit higher mobilities. Moreover, all the pathways shows the same order of magnitude mobilities for both e^- and h^+ carriers, which means besides the improved mobilities at higher temperature the molecule possess balanced charge carriers (the ratio is $\mu^-/\mu^+ \leq 1.67$), which proves the effectiveness of the annealing procedures.

At this stage it can be concluded that the approach of calculating the dependence of V on molecular shifts in dimer structure (Fig. 25, p. 69) should be considered as an approximation as it gives only the range of values, which are accessible. In case of the estimation of E_{bind} (Fig. 22, p. 63) this scan of the potential surface is in the same range of shifts over the axes but further it can be used to reproduce accurate values for the hopping mobilities (as well as for the mutual orientation of the molecules in the crystal structure) in the certain points, which are equal to minimum energy (usually the global and/or the secondary minima).

T = 430 K	Path 1	Path 2	Path 3	Path 4	Path 5	Path 6
$<d_h>$ [Å]	5.03 ± 0.32	8.99 ± 0.43	7.93 ± 0.35	9.54 ± 0.36	10.51 ± 0.35	10.45 ± 0.33
$<V^{ET}>$ [eV]	0.833 ± 0.447	0.554 ± 0.381	0.649 ± 0.420	0.594 ± 0.440	0.687 ± 0.523	0.807 ± 0.522
$<V^{HT}>$ [eV]	0.969 ± 0.491	0.604 ± 0.449	0.829 ± 0.543	0.665 ± 0.528	0.811 ± 0.580	1.106 ± 0.622
K^-_{CT} [1·10^{13}/s]	4.238 ± 1.218	1.876 ± 0.884	2.568 ± 1.076	2.151 ± 1.183	2.880 ± 1.672	3.974 ± 1.662
K^+_{CT} [1·10^{13}/s]	2.889 ± 0.741	1.122 ± 0.620	2.118 ± 0.908	1.361 ± 0.857	2.027 ± 1.037	3.766 ± 1.192
μ^- [cm^2/V·s]	1.447 ± 0.416	2.0451 ± 0.964	2.178 ± 0.912	2.641 ± 1.453	4.288 ± 2.489	5.852 ± 2.447
μ^+ [cm^2/V·s]	0.986 ± 0.253	1.223 ± 0.676	1.796 ± 0.771	1.671 ± 1.052	3.018 ± 1.544	5.547 ± 1.756
μ^-/μ^+	1.467	1.672	1.213	1.581	1.421	1.055

Table 14. Summary of the CT properties of *Th-BTZ-Th* crystal cell [263] at *T*=430 K obtained from MD (B3LYP/6-31G*, ε=0). The pathways are shown in Figure 28 (p. 77).

One disadvantage of the E_{bind} scan is that is more expensive than the scan of V values. The second disadvantage is that it does not give average values like MD simulations. Third disadvantage is that the points, which reproduce correct values of the CT properties are usually not the global minima of E_{bind} (for anti-parallel orientation or non-symmetric molecules) and finally it is not suitable for herringbone orientation since 3D scan is required.

5. Di-Block Monomers

In this chapter results for attached monomer units (n=1) are shown obtained by DFT calculations. Additionally, n-mers (n≥2) are also studied for comparison with experimental data.

5.1.   Geometric, Electronic and Optical Properties

Monomers are constructed from the most stable *trans-trans* conformers of small *BTZ* and *DPP* compounds and further the geometries are optimized using DFT (Fig. 29). A conformational search is not performed since it is expected that these will be the most stable structures.
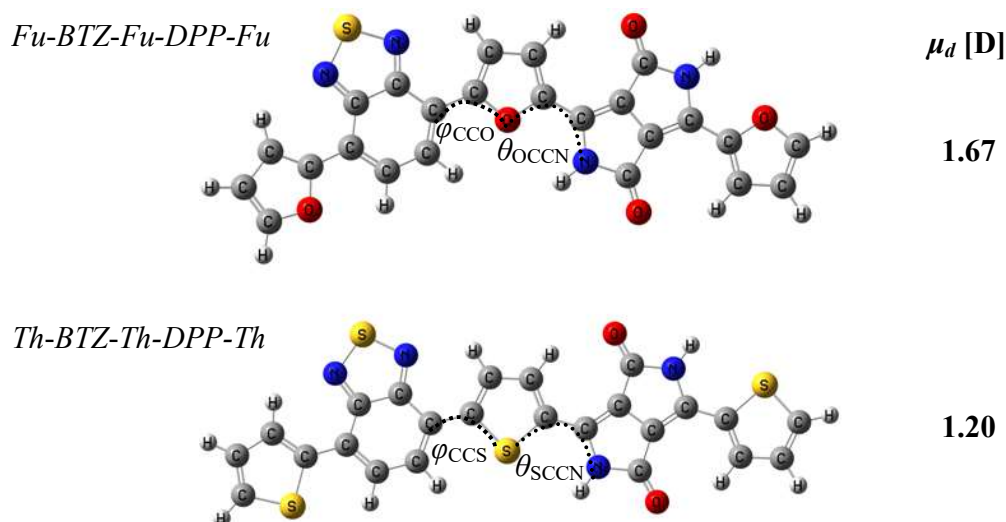

Figure 29. Optimized geometries of monomers: *Fu-BTZ-Fu-DPP-Fu* (top) and *Th-BTZ-Th-DPP-Th* (bottom). The dipole moments (in D) are also shown (B3LYP/6-31G*, $\varepsilon=0$).

The monomer units remain planar and the torsion angles are equal to 0.0° ($\theta_{OCCN}=\theta_{SCCN}=0.0°$) independently of the X_{atom} in the flanks. If the hydrogen atoms of N-H groups in *DPP* core are substituted with methyl groups the molecules still remain planar and there is no change in the torsion angles. Optimized geometries with M06-2X/cc-pVTZ show only slight distortion of 0.7 and 1.4°, for *Fu* and *Th* based monomer units, respectively, where *Th* monomer has two time larger torsion angle. This leads to the assumption that the charge transport will be favourable for more planar structures of the monomer units. Besides, that the monomers have a dipole moment in contrast with their corresponding *trans-trans* small molecules (Fig. 12, p. 45 and Fig. 13, p. 46). μ_d of the *Fu* based monomer is higher, which explains the better solubility of the molecules having this flank.

Additionally, due to difference in the angles between the core and the flank (φ_{CCX}), *Fu* monomer shows an arc-like geometry and *Th* based one is more like a straight line ($\varphi_{CCO} < \varphi_{CCS,}$) 117° and 121° for *Fu* and *Th* molecules, respectively, which is affected later to the super cells of the copolymers where *Fu* based copolymers have shorter "b" lattice vector along the backbones. This is more pronounced when pentamers (n=5) are optimized (Fig. 33, p. 83).

The frontier orbitals shapes and energies of the monomer units are shown in Figure 30 and Table 15, respectively. If the electron density of the frontier orbitals of the monomers are compared with their constitutive small molecules (Fig. 19, p. 58), there are only minor differences in the monomers where the LUMO orbitals in the *DPP* core are slightly bared from electron density and in thiadiazole part of *BTZ* is also observed small difference of the HOMO orbitals. Generally, the orbital shapes are not changed and attaching of D_--A_+ small molecules into joint monomers does not lead to any changes in the electron density distribution as compared to their isolated small component compounds.
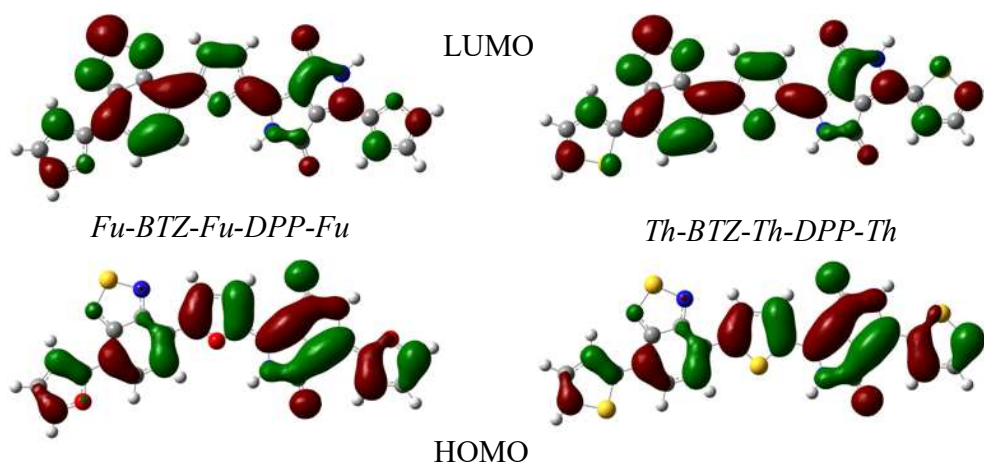

LUMO

Fu-BTZ-Fu-DPP-Fu   *Th-BTZ-Th-DPP-Th*

HOMO

Figure 30. Frontier orbitals (LUMO top and HOMO bottom) of the monomer units (B3LYP/6-31G*, ε=0). Here the lobes of MOs are represented by the isodensity surfaces with a contour of ±0.02 a.u. with positive (green) and negative (red) phases of the wave function. MOs show similar and complete delocalization.

B3LYP/6-31G*, ε=0	*Fu-BTZ-Fu-DPP-Fu*	*Th-BTZ-Th-DPP-Th*
HOMO [eV]	-4.89	-5.01
LUMO [eV]	-2.90	-3.02
E_g [eV]	1.99	1.99
E_g [Exp., eV] - polymer	1.26[228]	1.20[227]/ 1.20/ 1.48[230]

Table 15. Summary of the orbital energies of the monomers. E_g are shown as well. The experimental results correspond to polymers with branched (-C_2H_3-(C_8H_{17})-$C_{10}H_{21}$) side chains.

If one compares the energies of the frontier orbitals of the monomers with the values for the isolated small molecules (Table 6, p. 57), generally the HOMO energies of the monomers are larger and LUMO are smaller, which leads to smaller E_g.

Combing *BTZ* and *DPP* units into monomers reduces E_g values with more than 0.5 eV because of increased conjugation of the systems, and both monomers show the same E_g values (1.99 eV) independently of the X_{atom} in the flanks. According to the experiments E_g values of the small molecules (Table 6, p. 57) are two times larger than their corresponding polymers (Table 15, p. 80): 2.10÷2.30 eV, and 1.20÷1.26 eV, for small molecules and polymers, respectively. This difference can be explained by a huge increase of the conjugation length in the polymers. The theoretical prediction of E_g values (1.99 eV) does not agree with experimentally measured of 1.26 eV [228] for *Fu* polymer, and 1.20 eV [227] and 1.20/1.48 eV [230] for *Th* polymers, and here the theory deviates more from the experiment than in the case of small compounds. Since the theory is performed only for monomers (n=1) a large derivation is obtained and better results could be reproduced if n-mers (n≥2) are studied, which is shown later.

For instance, *DPP* molecules (linked either with *Fu* or *Th* flanks) in monomers have E_g values of 2.14 and 2.16 eV (for *Fu* and *Th*, respectively) and in polymers they have E_g values of 1.61 eV and 1.50 eV (for *Fu* and *Th*, respectively), which shows a reduction of $E_g \sim 0.5$ eV estimated in experiment [270] when polymers are formed from monomers (increasing n).

It can be concluded that in monomer units E_g values remain unaffected from the heteroatom in the *Fl* in both theoretical and experimental investigations.

In Figure 29 and Table 16 are shown the UV-VIS spectra and absorption wavelengths, respectively, for the monomers.
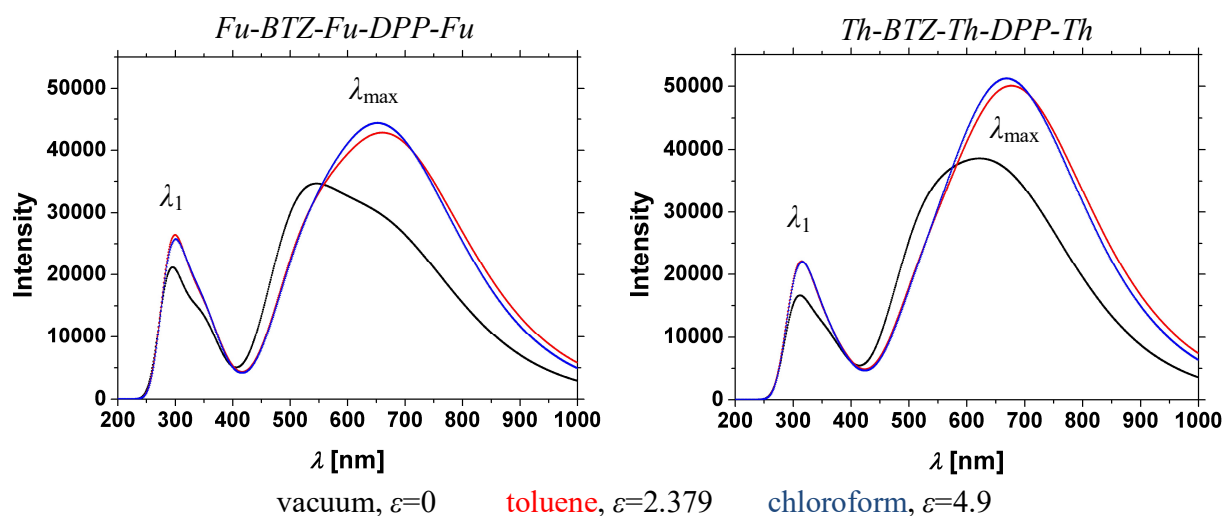

vacuum, ε=0   toluene, ε=2.379   chloroform, ε=4.9

Figure 31. UV-VIS spectra of the monomers obtained from TD-DFT/B3LYP/6-31G*.

TD-DFT	vacuum ε=0, toluene ε=2.379, chloroform ε=4.9		Exp.
	λ_{max} [nm]	λ_1 [nm]	λ_{max}/λ_1 [nm]
Fu-BTZ-Fu-DPP-Fu	523, 694, 683	286, 289, 291	880/-[228]
Th-BTZ-Th-DPP-Th	678, 696, 686	307, 324, 324	895/-[227]

Table 16. Summary of the wavelengths of UV-VIS spectra of the monomer units shown in Figure 31 (TD-DFT/B3LYP/6-31G*).

If the UV-VIS spectra of the small compounds (Fig. 20, p. 59) are compared with monomer units it can be seen that the spectra of D_--A_+ small molecules are broadened and the result spectra of the monomers have wider bands. First of all, λ_1 and λ_2 from small units are already merged together in one single band independently on the X_{atom} and these bands are slightly less intensive in the monomers as compared to small molecules. Second, λ_{max} is much wider and more intensive and moreover, it is red shifted wih 200 nm in the monomers than in small molecules, whereas the second band (λ_1) remains unaffected. This shows an effective way how can be increased the absorbance range of conjugated systems by attaching D_--A_+ small molecules with different maximum of the absorbance bands.

According to the experiment λ_{max} are positioned with 200 nm difference as compared to the theoretical investigation: 880 and 895 nm according to the experiment (*Fu* [228] and *Th* [227] based polymers, respectively), and 683 and 686 nm according to the theory (*Fu* and *Th* monomers, respectively). This deviation could be explained by the fact that experimental measurements corresponds to polymers (conjugated systems) and the theory is estimated only for monomers, which was also ascribed to the deviation of the band gaps estimated from the orbital energies. One proof of this is that when the small molecules are attached to monomer units λ_{max} is shifted with 200 nm according to the theory.

There is only a slight difference in the intensity between the spectra of *Fu* and *Th* containing monomers and at this level the effect of the X_{atom} also disappears.

In order to reproduce better experimental results n-mers (up to pentamers, n=5) are optimized only in *trans-trans* conformations and the results of the frontier orbitals and the band gaps are shown in Figure 32 and Table 17 (p. 83), respectively. A linear extrapolation method is utilized in order to obtain the orbital energies for infinity number of monomers (n=∞) where the energies are plotted as a function the inverse monomer length (n^{-1}) and the values corresponding to n=∞ are obtained from the intercept of the linear functions.
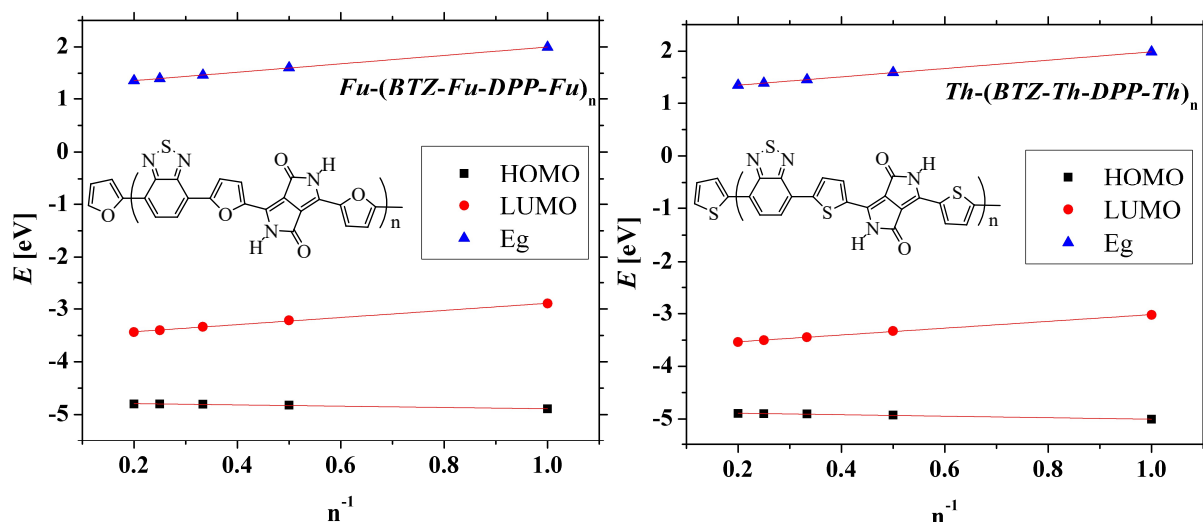

Figure 32. Linear extrapolation of the orbital energies and the band gaps (in eV) as a function of the inverse monomer length (n^{-1}) for *Fu* (left) and *Th* (right) based molecules (B3LYP/6-31G*, ε=0).

	Fu-BTZ-Fu-DPP-Fu (X=O)						Th-BTZ-Th-DPP-Th (X=S)					
n	1	2	3	4	5	∞	1	2	3	4	5	∞
HOMO [eV]	-4.89	-4.82	-4.80	-4.80	-4.80	-4.77	-5.01	-4.93	-4.91	-4.90	-4.90	-4.86
LUMO [eV]	-2.90	-3.21	-3.34	-3.40	-3.40	-3.57	-3.02	-3.33	-3.45	-3.50	-3.54	-3.66
E_g [eV]	1.99	1.61	1.47	1.40	1.36	1.20	1.99	1.60	1.46	1.39	1.36	1.20

Table 17. Summary of the orbital energies and E_g (in eV) of the monomer units as a function of the monomer length (n) - B3LYP/6-31G*, $\varepsilon=0$
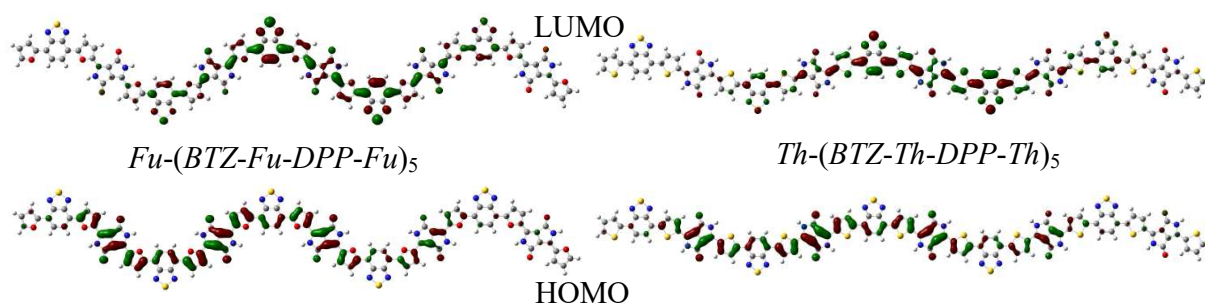

Figure 33. Frontier orbitals (LUMO top and HOMO bottom) of the pentamers (n=5) - B3LYP/6-31G*, $\varepsilon=0$. Here the lobes of MOs are represented by the isodensity surfaces with a contour of ±0.02 a.u. with positive (green) and negative (red) phases of the wave function. MOs show similar and complete delocalization.

The extrapolation method predicts for both polymers E_g value of 1.20 eV independently of the flank, which coincides perfectly with the experimental values for *Fu* based polymer of 1.26 eV [228] and for *Th* based one of 1.20 eV [227, 230], respectively.

Additionally, the shapes of the frontier orbital are shown in Figure 33 where again can be seen complete delocalization of the electron density but only along three-four (n=3÷4) units. Moreover, the curvature of the backbone is very well pronounced of the pentamers where *Fu* based polymer has a zigzag backbone shape, whereas *Th* based one has very straight backbone due to difference of the valence angle φ_{CCX} between flank and A_+ units (Fig. 29, p. 79), which was mentioned. This zigzag behaviour of the *Fu* based pentamer suggests that its polymer could possess more disorder crystal structure due to side chains repulsion, which is observed within MD results and it is demonstrated in the next chapter.

TD-DFT	vacuum $\varepsilon=0$, toluene $\varepsilon=2.379$, chloroform $\varepsilon=4.9$				
	λ_{max} [nm]		λ_1 [nm]		
n	2	5	2	5	
Fu-(BTZ-Fu-DPP-Fu)ₙ	860, 893, 878	1089, 1092, 1073	561, 557, 554	-	
Fu-(BTZ-Fu-DPP-Fu)ₙ	861, 896, 882	1089, 1094, 1076	549, 550, 546	-	

Table 18. Summary of the wavelengths of UV-VIS spectra of D_-A_+ dimers (n=2) and pentamers (n=5) - TD-DFT/B3LYP/6-31G*.

The absorption bands are also estimated for n-mers and the results for dimers (n=2) agree very well with the experiments where 878 and 882 nm for λ_{max} are calculated in chloroform, and

880 and 895 nm are measured for *Fu* [228] and *Th* [227] based polymers, respectively. Interesting, pentamers (n=5) overestimate the absorptions bands with values above 1000 nm as well as the second band (λ_1) disappears for both polymers. All the wavelengths are summarized in Table 18 (p. 83).

5.2.   Binding Energies

Binding energies of isolated stacks of dimers are investigated in cases of parallel and anti-parallel orientations where one of the molecules is shifted in all the spatial directions similar to the case of small molecules described in the previous chapter. First, the dependence of E_{bind} of the distance between the molecules (*d*) is considered in order to obtain the equilibrium distances between the monomers (Figure 34).
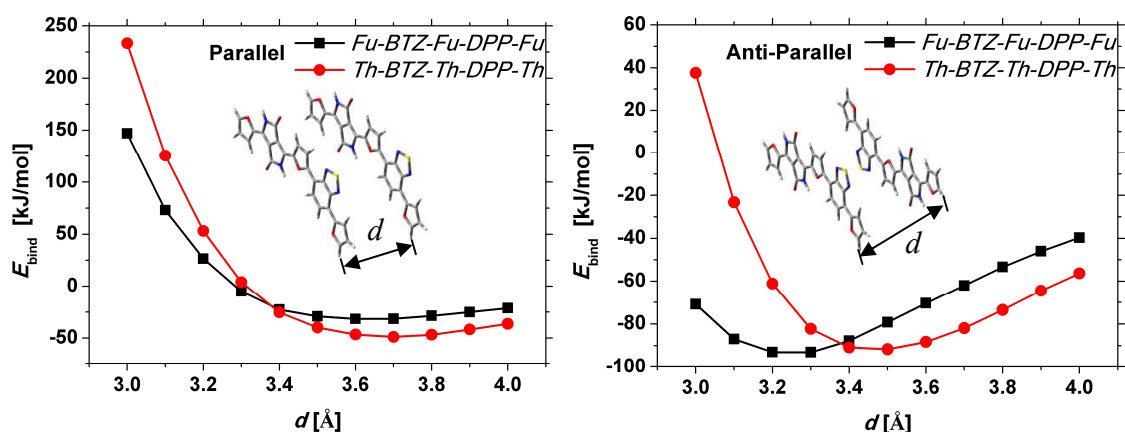

Figure 34. Binding energies (in kJ/mol) of the monomers in segregated stacks as a function of distance between them (*d*) in case of parallel (left) and anti-parallel (right) orientation - M06-2X/cc-pVTZ, ε=0.

If the graphic (Fig. 34) for monomers is compared with the analogous graphic obtained for small molecules (Fig. 21, p. 62) the same behaviour and the same conclusions are present for monomer units. Again E_{bind} for parallel orientation is much higher (two times) than the case of anti-parallel orientation since there are strong orbital interaction in parallel orientation and it could be expected again that these monomers (or polymers) will adopt anti-parallel orientation (and/or shifted stacks). In anti-parallel orientation all the distances are accessible (except of a very close distance in case of *Th* monomer), whereas in parallel orientation at closer distances E_{bind} become with positive values like in the case of small constitutive compounds.

All the distances for monomer units coincide with the distances obtained from small molecules: for parallel oriented monomer units *d*=3.6 and 3.7Å, for *Fu* and *Th* monomers, respectively, and for small parallel oriented *BTZ* molecules (both *Fu* and *Th*) *d*=3.7 Å, and for *DPP* *d*=3.6 and 3.7 Å, for *Fu* and *Th*, respectively. The exception of *Fu-DPP-Fu* stack (*d*=3.6 Å) is observed again in the case of *Fu-BTZ-Fu-DPP-Fu* stack (*d*=3.6 Å).

In anti-parallel orientation the monomers have the same dependence on the X_{atom}, d=3.3 and 3.5 Å, for Fu and Th monomers, respectively, as compared to small BTZ anti-parallel oriented molecules. Thus, it is expected again that Fu containing monomer (or polymer) will be at closer distance than Th one. Additionally, in the case of parallel oriented molecules shallow curves are again obtained where the equilibrium distances are not well defined similar to the small parallel oriented molecules.

It can be concluded that monomers (or polymers) constructed from D_--A_+ component units will have the same equilibrium distances like their small consisting units and the dependence of the X_{atom} in the flank is valid only in anti-parallel (unsymmetrical) orientation.

If stacks which are not fully segregated (shifted starting position), with an initial shift of one of the molecules, are considered similar E_{bind} dependencies and equilibrium distances are obtained: when BTZ is faced to DPP in parallel stack (shift over l) the obtained E_{bind} dependence reproduce the values of equilibrium distances equal to anti-parallel orientation case, d=3.2 and 3.5 Å, for Fu and Th monomers, respectively); if DPP is faced to DPP in anti-parallel orientation (shift over l where DPP molecules will be exactly above each other because of symmetry reasons) equilibrium distances of parallel and anti-parallel orientations are obtained, d=3.5 and 3.8 Å, for Fu and Th monomers, respectively; finally if BTZ molecule is faced to the other BTZ in anti-parallel orientation (shift over l where benzene rings overlap) the equilibrium distances take values as anti-parallel orientation, d=3.3 and 3.5 Å, for Fu and Th monomers, respectively.

It can be concluded that if the stack of molecules is shifted, the equilibrium distance between them (d) will be slightly (negligibly) different and this distance can be assumed as a constant corresponding to parallel or anti-parallel cases, respectively.

Experimentally π-π distance of 4.2÷4.66 Å for Fu based polymer [228], and 3.73 [227] and 3.65 Å [230] for Th based polymer are obtained. It can be seen that there is a perfect agreement for Th based polymer (the theory predicts 3.5 and 3.7 Å in anti-parallel and parallel orientation, respectively) according to two experiments. For Fu based polymer there is a large deviation (3.3 and 3.5 Å in anti-parallel and parallel orientation, respectively, according to the theory), which can be attributed to the experimentally unfavourable broad peak of measurement [228], which suggests that the sample is not completely homogeneous and contain defects, which will be shown in the next chapter within MD results where closer $d_{\pi\text{-}\pi}$ value to the experiment is obtained from the concentration profile of branched side chains. Nevertheless, the equilibrium d values obtained from the E_{bind} are utilized later.

2D charts (Fig. 35, p. 86) of E_{bind} are computed for molecule stacks when one of the molecules in a stack is shifted over both horizontal and vertical axes (k and l) with constant d obtained from the equilibrium distances of d dependence (Fig. 34, p. 84).

In the case of parallel orientation both molecules have the same coordinates of the minimum points at k=-0.2 Å, l=3.4 Å in the global minimum of E_{bind} (orange points) and k=0.0 Å, l=1.4 Å (with very small deviation: $k(Fu)$=0.2 Å) in the second minimum of E_{bind} (red points), and these points differ with up to 3 kJ/mol (ΔE_{bind}=3 kJ/mol) for each flank. The points of the second minimum correspond to structures where the ring fragments of the molecules are half size shifted thus there is a minimum π-π repulsion (avoiding of e^- density overlap).

The global minimum points represent interactions between the A_+ units (*BTZ* or *DPP*) with the flanks where again the dimer stacks have reduced repulsive orbital interactions. This shows again that the molecular stacks do not prefer parallel orientated (segregated case) and they tend always to be shifted (or anti-parallel oriented). Since E_{bind}(parallel)>E_{bind}(anti-parallel) in anti-parallel orientation π-π (repulsive) interactions are much smaller than in parallel orientation, which was also observed for small molecules.

In anti-parallel orientation the compounds have different behaviour depending on the X_{atom} in the *Fl* since the symmetry is broken and E_{bind} is very sensitive to small molecular shift (and the monomers differ slightly in the valence angle φ_{CCX} - Fig. 29, p. 79). First, three minima can be seen for *Fu* containing monomer unit and only two for *Th* containing one, and the coordinates of the points do not coincide unlike parallel orientation (due to broken symmetry).
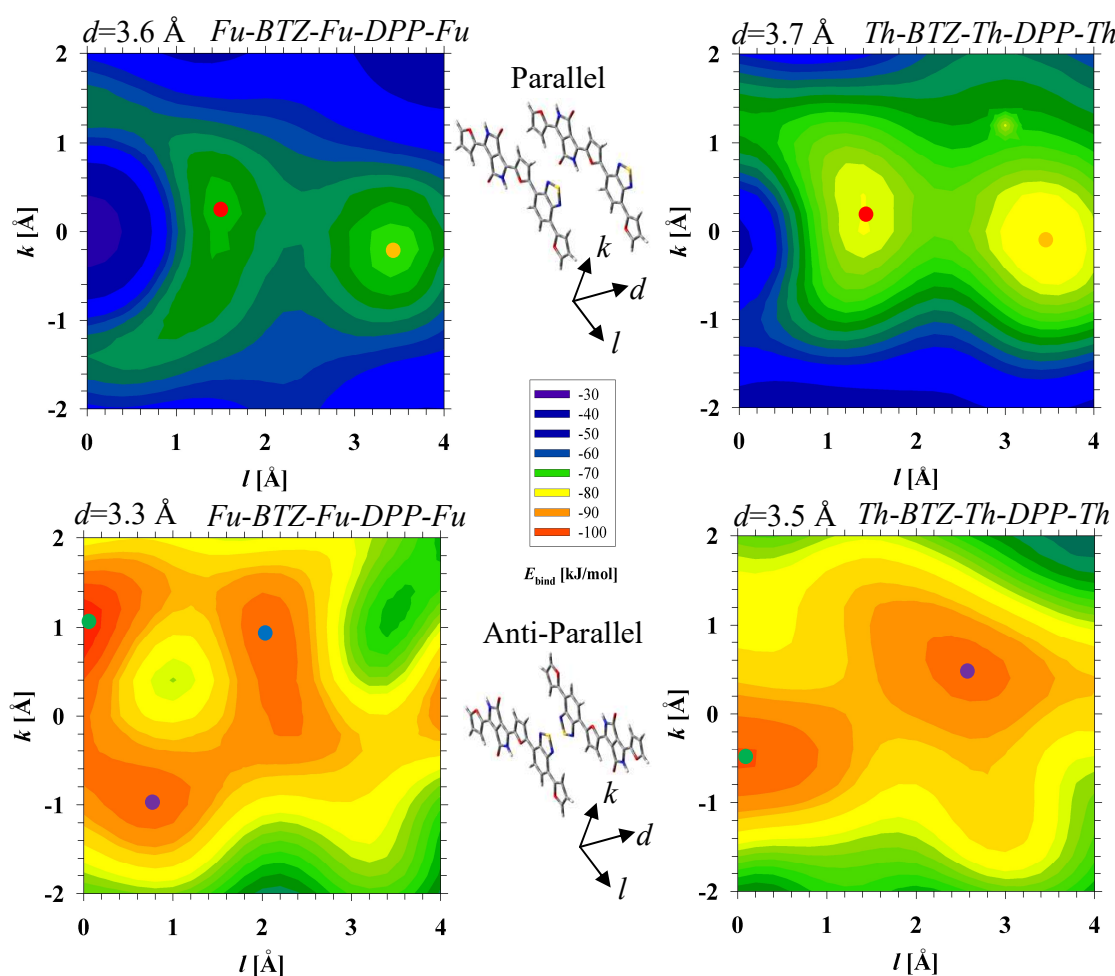

Figure 35. Binding energies (in kJ/mol) of the monomer units with *Fu* (left) or *Th* (right) flanks in parallel (top) and anti-parallel (bottom) orientation in slipped cofacial stacks as a function of both transverse and longitudinal (*k* and *l*) shifts. The distances between molecules (*d*) are taken from Fig. 34 (p. 84). The configurations with minimum energies are marked with points (M06-2X/cc-pVTZ, ε=0).

The global minimum in anti-parallel orientation of E_{bind} (green points) corresponds to k=1.0 Å, l=0.0 Å and k=-0.4 Å, l=0.0 Å, for *Fu* and *Th* monomers, respectively, and their coordinates coincide only in *l* shift. The second minimum (purple points) corresponds to k=-1.0 Å, l=0.8 Å and k=0.4 Å, l=2.6 Å, for *Fu* and *Th* monomers, respectively. And finally, the third minimum available only for *Fu* containing monomer (blue point) at k=1.0 Å, l=2.0 Å. Actually, the third point of *Fu* monomer is close to the second point of *Th* monomer with respect to the coordinates.

All of these points in anti-parallel orientation correspond to geometrical positions where the ring fragments of the molecules are not fully overlapping, which leads to reduced repulsive interactions similar to the parallel orientation. Additionally, most of the points represent a superposition of *BTZ* above *DPP* unit, which leads to favourable interactions, whereas the rest points are slightly shifted. Moreover, the *Fl* are also stacked in the global minima. The second minimum points show slightly shifted stacks in order to increase the attractive interactions. This is additionally confirmed by MD simulations described in the next chapter where in the most of the cases *BTZ* faces *DPP* as well as the flanks are forming columns if the samples are homogeneous and the structures are not distorted. The global minimum points from anti-parallel dimes where *BTZ* perfectly coincides with *DPP* and the flanks are overlapping are shown in Figure 51 (p. 106).

The coordinates of minimum points in anti-parallel orientation do not coincide because there is a slight difference in the size and the shape of the flanks, which was already mentioned.

The minimum points for each monomer in anti-parallel orientation differ with 7 and 3 kJ/mol, for *Fu* and *Th* monomer, respectively, whereas in parallel orientation both *Fu* and *Th* containing monomers have the same 3 kJ/mol energy difference between the minimum points of E_{bind}. The second and the third minimum of *Fu* anti-parallel monomer differ with less than 1 kJ/mol.

Generally, *Th* monomer has lower E_{bind} as compared to *Fu* one in parallel orientation, whereas in anti-parallel orientation this dependence is inverse and *Fu* monomer has lower E_{bind}. In anti-parallel orientation the energy difference between *Fu* and *Th* minimum points in E_{bind} is much less (ΔE_{bind}=1÷7 kJ/mol) and in the case of second minimum this difference is less than 1 kJ/mol. In parallel orientation this energy difference between *Fu* and *Th* monomers is higher (ΔE_{bind}=10÷17 kJ/mol).

It could be expected that all the minimum points either in parallel or anti-parallel can be presented in polymers (backbone shifts) because they have only minor difference in the E_{bind} and they can be realized due to thermal fluctuations. All the minimum points of the monomers (as well as k=l=0) are summarized in Table 20 (p. 88).

If 2D E_{bind} approximation of the monomers (Fig 35, p. 86) is compared with 1D E_{bind} of small molecules (Fig. 22, p. 63), it is clear that they have similar behaviour. One minimum in parallel orientated small compounds is observed as a function of the shift along *k* axis and two minima as a function of *l* shift, which is in agreement with two minima which have been seen in the 2D representation of the monomers. In anti-parallel orientation of small (*BTZ*) molecules three minima are observed as a function of *k* shift and two minima as a function of *l* shift, which

again correspond to three minima for *Fu* containing monomer and two minima for *Th* monomer where for *Th* monomer one peak disappears in the 2D graphic. It seems that the behaviour of E_{bind} depends on the shape of frontier orbitals (bonding/anti/bonding pattern) of the molecules.

It can be concluded that in crystal structure the molecules will prefer anti-parallel orientation (or shifted stacks) due to increased attractive interactions observed in E_{bind}, which may explain a reduction of the charge carrier mobilities described in the next section.

5.3.   Charge Transport Properties

Before discussing the calculated hopping mobilities, first the reorganization energies will be explained (Table 19).

	Fu-BTZ-Fu-DPP-Fu	*Th-BTZ-Th-DPP-Th*
λ_i^- [eV]	0.177	0.180
λ_i^+ [eV]	0.259	0.266

Table 19. Inner reorganization energies of the monomer units (B3LYP/6-31G*, $\varepsilon=0$).

	Coordinates: *Fu/Th* [Å]	μ [cm^2/V·s]	-BTZ- -DPP- *Fu*	*Th*	E_{bind} [kJ/mol] *Fu/Th*
Parallel	$k=l=0$	μ^-	12.630	10.628	-31.69/-48.87
		μ^+	3.701	2.722	
	$k=0.2, l=1.4$ / $k=0.0, l=1.4$	μ^-	0.929	0.729	-67.07/-78.33
		μ^+	0.085	0.012	
	$k=-0.2, l=3.4$ / $k=-0.2, l=3.4$	μ^-	0.001	0.542	-69.27/-81.94
		μ^+	0.043	0.059	
	Average	$<\mu^->$	0.470	0.636	-
	Average	$<\mu^+>$	0.064	0.036	
Anti-Parallel	$k=l=0$	μ^-	0.359	5.700	-93.06/-91.69
		μ^+	0.149	0.628	
	$k=1.0, l=2.0$ / $k=-, l=-$	μ^-	0.683	-	-94.70/-
		μ^+	0.152	-	
	$k=-1.0, l=0.8$ / $k=0.4, l=2.6$	μ^-	0.844	0.199	-94.99/-93.64
		μ^+	0.264	0.289	
	$k=1.0, l=0.0$ / $k=-0.4, l=0.0$	μ^-	0.016	5.143	-103.07/-96.21
		μ^+	0.087	0.822	
	Average	$<\mu^->$	0.514	2.671	-
	Average	$<\mu^+>$	0.168	0.556	
Exp.	$k=-, l=-$	μ^-	0.56[a]	0.40[b], 0.58[c], 0.57[d]	-
	$k=-, l=-$	μ^+	0.20[a]	0.35[b], 0.53[c], 0.33[d]	

Table 20. Summary and average values of the electron (μ^-) and hole (μ^+) mobilities (in cm^2/V·s) of the monomer units (with *Fu* or *Th* flanks) for non-shifted stacks ($k=l=0$) and in the minimum points of E_{bind} (Fig. 35, p. 86) - B3LYP/6-31G*, $\varepsilon=0$. [a][228], [b][227], [c][229], [d][230].

Both monomer units have similar value of λ_i independently of the X_{atom} (0.01 eV difference) in the *Fl* similar to the small constitutive compounds. The monomer units have much lower reorganization energy for negative charged state than for the positive charged one, which proves again that these molecules do not favour the h^+ hopping.

If the monomers are substituted with methyl groups in the *DPP* core the reorganization energies are slightly affected: for *Fu* based monomer 0.171 and 0.260 eV, for λ_i^- and λ_i^+, respectively, and for *Th* based monomer 0.183 and 0.269 eV, for λ_i^- and λ_i^+, respectively.

If λ_i of monomer units (Table 19, p. 88) are compared with the values of the small molecules (Table 8 and Table 9, p. 65) it can be seen that monomer units have intermediate for λ_i^- values and the lowest λ_i^+ than the small compounds as it was already mentioned. Thereby, if proper combination of donor and acceptors is chosen the reorganization energies for positive and negative charged states can be modified (equalized).

Finally, the hopping mobilities of the monomer units are calculated at the minimum points of E_{bind} (Fig. 35, p. 86) and for non-shifted stacks ($k=l=0$) for comparison, and the results are summarized in Table 20 (p. 88). Again in parallel orientation the monomer units have higher hopping mobilities than anti-parallel orientation if non-shifted position are compared, similar to the case of the small molecules. This proves the fact that higher charge carrier mobilities can be obtained if there is a strong orbital interaction (for example in symmetric or asymmetric molecules, which do not have explicit anti-parallel orientation like *DPP* derivatives). For instance, increasing the symmetry of *DPP* base polymer (in this case increasing of the number of *Th* units) an increase of the hole mobility is observed experimentally [291].

In parallel orientation both *Fu* and *Th* based monomers have mobilities of the same order of magnitude for non-shifted stacks and in the second minimum, whereas at the global minimum, they differ only in the μ^- values. The electron mobilities are always one order of magnitude higher than the h^+ mobilities in all cases due to difference in the reorganization energies for the corresponding charge states. Thereby, again the symmetry leads to equalization of the CT properties independently of the heteroatom in the flanks. Another reason for these similar values could be that they have the same k, l coordinates in the minima of potential surface (E_{bind}).

According to the experimentally obtained mobilities only the values in the second minimum (parallel case) as well as the average value calculated from the minima points ($<\mu^->$) agree and only for μ^-. The points of non-shifted stacks predict much higher values, whereas in the points of E_{bind} the mobilities are much less (without afore mentioned point for μ^- of the second minimum or the average value) with exception of the global minimum and the average value ($<\mu^->$) of *Th* containing monomer where the values for μ^- coincide very well with the experiment. However, these points which agree with the experiment (or the average values) cover only the e^- mobilities and h^+ mobilities are not described well.

In anti-parallel orientation *Th* based monomers dominate in some of the cases over *Fu* based ones according to the CT properties. This can be explained with the higher V values of anti-parallel oriented *Th-BTZ-Th* dimer in the case of d dependence (Fig. 23, p. 66) where the electronic couplings of *Th-BTZ-Th* are much higher than *Fu* based molecules especially for the hole coupling (V^{HT}), probably due to an overestimation of the sulphur atom.

In anti-parallel orientation non-shifted stacks of dimers already predict good values with respect to the experimentally obtained mobilities with one exception of μ^- for *Th* based monomer. In the second minimum (and the third one only for *Fu*) these charge carrier mobilities from theory coincide perfectly with experiment: according to the theory μ^-=0.844 and 0.199 cm^2/V·s, for *Fu* and *Th* based monomers, respectively, and for μ^+=0.264 and 0.289 cm^2/V·s, for *Fu* and *Th* monomers, respectively, and according to the experiment values with the same order of magnitude are measured: μ^-=0.56 and μ^+=0.20 cm^2/V·s, for *Fu* [228] based polymer, and for *Th* based polymer μ^-=0.40÷0.58 and μ^+=0.33÷0.53 cm^2/V·s [227, 229, 230]. Second minimum of E_{bind} gives accurate values as compared to the experiment similar to the case of anti-parallel small *BTZ* molecules. The global minimum points again do not reproduce good hopping mobilities as compared with experiment (only in the case of *Th*, μ^+ coincides). The effect of the X_{atom} disappears in second minimum point (and almost in non-shifted stacks) for monomers. Additionally, the average values calculated from the minimum points ($<\mu^{-/+}>$) coincide well with the experimentally obtained mobilities (for *Fu* $<\mu^->$=0.514 and $<\mu^+>$=0.168 cm^2/V·s, and for *Th* $<\mu^->$=2.671 and $<\mu^+>$=0.556 cm^2/V·s) where only for *Th* $<\mu^->$ overestimates the experimental quantity, which can be explained with the overestimation of the S atom in the electronic couplings from Figure 23 (p. 66) in anti-parallel orientation, which was already mentioned.

Interesting, a selenophene derivative of the same polymer (X_{atom}=Se) reproduce hopping mobilities of the same order of magnitude (0.84 and 0.46 cm^2/V·s for electron and hole hoppings, respectively) [230]. It seems that the effect of the X_{atom} is negligible since these polymers possess nearly the same mobilities, which is confirmed also from the experiments. Additionally, all the electronic couplings are summarized in Table 21.

	Coordinates:	V^{ET}/V^{HT} [eV]	
	Fu/*Th* [Å]	*Fu-BTZ-Fu-DPP-Fu*	*Th-BTZ-Th-DPP-Th*
	k=l=0	0.265/0.236	0.242/0.204
	k=0.2, l=1.4	0.072/0.036	-
Parallel	k=0.0, l=1.4	-	0.063/0.013
	k=-0.2, l=3.4	0.003/0.025	-
	k=-0.2, l=3.4	-	0.055/0.030
	k=l=0	0.049/0.052	0.187/0.103
	k=1.0, l=2.0	0.067/0.052	-
	k=-, l=-	-	-
Anti-Parallel	k=-1.0, l=0.8	0.075/0.069	-
	k=0.4, l=2.6	-	0.035/0.070
	k=1.0, l=0.0	0.010/0.039	-
	k=-0.4, l=0.0	-	0.178/0.119

Table 21. Summary of the electron (V^{ET}) and hole (V^{HT}) couplings (in eV) of the monomer units (with *Fu* or *Th* flanks) for non-shifted stacks (k=l=0) and in the minimum points of E_{bind} (Fig. 35, p. 86). For definition see Table 20 (p. 88) - B3LYP/6-31G*, ε=0.

Thus it can be concluded that polymers will occupy orientations with lower energy (anti-parallel orientation and/or shifted stacks) and all the molecular shifts could be expected due to non-equilibrium methods for device fabrication (for instance, spin-coating) as well as they differ only in few kJ/mol in E_{bind}.

Moreover, dimers with minimum E_{bind} give a reliable charge transport properties as compared to the experiment (usually not from the global minimum in anti-parallel orientation) without knowledge of the crystal structure.

A second conclusion can be made that if molecules are placed one above and if the repulsive interactions are somehow reduced, this will lead to a system with the best charge transport performance since the highest attractive energy of E_{bind} (fully segregated parallel oriented monomers) reproduce the maximum hopping mobilities (maximum strong orbital interactions) and all the other points with lower E_{bind} have reduced CT properties (reduced e^- density overlap).

6. Block Copolymers

This chapter describes primary polymers based on the monomer units discussed in the previous chapter using combined MD and DFT approach.

6.1. Side Chain Engineering

Even though this chapter is named block copolymers, first the side chains are attached to the small *DPP* molecule linked with either *Fu* or *Th* as flanking units with two types of side chains: linear or branched. Two general possible orientations can adopt the side chains in isolated *DPP* molecule: when they are at the same plane of *DPP* molecule (Z_{con} conformer) and when they are at different planes of it (E_{con} conformer) - Figure 36.
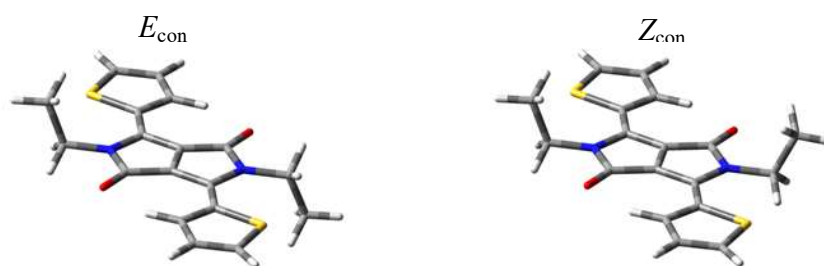

Figure 36. General side chain conformations in isolated *DPP* molecule when the side chains are at different planes (E_{con} conformer, left) and when the side chains are at the same plane (Z_{con} conformer, right) with respect to *DPP* molecule. Here the side chains are shown only with ethyl (-C_2H_5) groups.

Branched and linear side chains are attached stepwise where the number of the carbon atoms is increased by two and later geometry optimization is applied. In Table 22 and 23 (p. 93) the results are summarized for linear and branched side chains, respectively, depending on the heteroatom in the flank (X_{atom}=O for *Fu* and X_{atom}=S for *Th*) and depending of the conformer (E_{con} or Z_{con}).

For linear side chains it is seen that there is no change in the electronic properties ("E_g") when the length of the side chain is increased and the "band gap" remains constant for both *DPP* derivatives independently of the conformer (E_{con} or Z_{con}). It is worth noting that E_{con} conformers for both *Fu* and *Th* flanks do not have dipole moment (close to zero), whereas the molecules with Z_{con} side chain conformation have dipole moments and for *Th* molecules μ_d is larger than (almost two times) *Fu* ones. Moreover, the dipole moment is increasing with increasing of the chain length of the Z_{con} conformers, which is better pronounced for *Th* compounds.

R:	-DPP-	Fu (X_{atom}=O)		Th (X_{atom}=S)	
	Conformer:	E_{con}	Z_{con}	E_{con}	Z_{con}
-C$_2$H$_5$	E_g [eV]	2.50	2.50	2.45	2.45
	μ_d [D]	0.0005	0.1736	0.0001	0.2542
	ΔE [kJ/mol]	-0.007		0.100	
-C$_4$H$_9$	E_g [eV]	2.50	2.50	2.45	2.45
	μ_d [D]	0.0007	0.3084	0.0002	0.4300
	ΔE [kJ/mol]	0.006		-0.181	
-C$_6$H$_{13}$	E_g [eV]	2.50	2.50	2.45	2.45
	μ_d [D]	0.0001	0.3788	0.0001	0.4911
	ΔE [kJ/mol]	-0.139		0.159	
-C$_8$H$_{17}$	E_g [eV]	2.50	2.50	2.45	2.45
	μ_d [D]	0.0000	0.3457	0.0002	0.5038
	ΔE [kJ/mol]	0.109		0.083	
-C$_{10}$H$_{21}$	E_g [eV]	2.50	2.50	2.45	2.45
	μ_d [D]	0.0362	0.3447	0.0876	0.5186
	ΔE [kJ/mol]	0.335		0.185	
-C$_{10}$H$_{21}$	E_g [eV]	2.50	2.50	2.45	2.45
	μ_d [D]	0.0277	0.3486	0.0763	0.5250
	ΔE [kJ/mol]	0.455		0.261	

Table 22. Summary of the properties of *DPP* molecules linked with *Fu* (X_{atom}=O) or with *Th* (X_{atom}=S) flank as a function of the length of linear side chains (R). ΔE is taken as the difference between E_{con} and Z_{con} conformers ($\Delta E=E_{con}-Z_{con}$) - B3LYP/6-31G*, ε=0.

R:	-DPP-	Fu (X_{atom}=O)		Th (X_{atom}=S)	
	Conformer:	E_{con}	Z_{con}	E_{con}	Z_{con}
-C$_2$H$_3$-2(C$_2$H$_5$)	E_g [eV]	2.50	2.50	2.45	2.46
	μ_d [D]	0.0007	0.1140	0.0004	0.1249
	ΔE [kJ/mol]	0.019		0.451	
-C$_2$H$_3$-2(C$_4$H$_9$)	E_g [eV]	2.50	-	2.45	-
	μ_d [D]	0.0000	-	0.0000	-
	ΔE [kJ/mol]	-		-	
-C$_2$H$_3$-2(C$_6$H$_{12}$)	E_g [eV]	2.50	-	2.45	-
	μ_d [D]	0.0000	-	0.0003	-
	ΔE [kJ/mol]	-		-	

Table 23. Summary of the properties of *DPP* molecules linked with *Fu* (X_{atom}=O) or with *Th* (X_{atom}=S) flank as a function of the length of branched side chains (R). ΔE is taken as the difference between E_{con} and Z_{con} conformers ($\Delta E=E_{con}-Z_{con}$) - B3LYP/6-31G*, ε=0.

Also it is noticeable that the energy difference (ΔE) is slightly increased with increasing the length of the side chain where this ΔE is larger for *Fu* molecules than *Th* ones but this energy difference is still less than 1 kJ/mol, which means that both conformers could be expected for realization in the crystal structures.

If the solvent interactions are taken into account (PCM model), "E_g" values remain unaffected and the dipole moments are slightly increased. According to the energy difference of E_{con} and Z_{con} conformers for *Fu* compounds it remains the same, whereas for *Th* molecules is increased but this ΔE is still less than 1 kJ/mol. If the energy of the different solvents is compared (toluene and chloroform) $\Delta E_{toluene}(E_{vacuum}-E_{toluene})$ is much less (7 kJ/mol) than $\Delta E_{chloroform}(E_{vacuum}-E_{chloroform})$ (20 kJ/mol) with three times difference and this difference is not affected with increasing the side chain length or with conformer orientation (E_{con} or Z_{con}). This leads to the fact that chloroform solvent is more favourable for synthesis as compared to toluene.

In the case of branched side chains one can make the same conclusions. The "E_g" values are not affected and Z_{con} conformers have larger dipole moments than E_{con} conformers. Branched side chains with Z_{con} conformation are difficult to converge and they are not optimized as well as E_{con} conformers with longer side chains. If the solvent interactions are taken into account again $\Delta E_{toluene}$ is much less than $\Delta E_{chloroform}$ similar to linear side chains (7 versus 20 kJ/mol, for toluene and chloroform, respectively).

Branched side chains $-C_2H_3-(C_8H_{17})-C_{10}H_{21}$ are chosen for MD simulations of polymers because they are employed in experiments [227, 228] and only E_{con} conformers are taken into account for the starting configurations. Linear (*LN*) side chains ($-C_{12}H_{25}$) with E_{con} conformation are additionally simulated for comparison.

6.2.   MD Results

In order to reproduce a polymeric material one backbone is constructed from six monomers (n=6) and four backbones are stacked one above and further this is replicated four times in the direction of the side chains (16 backbones in a super cell) simulated with PBC in all directions. Since the periodicity is along the backbone bonds the polymer chain (n) goes to infinity. In polymers anti-parallel orientation is not allowed if it is assumed that the termination unit of the polymer is *BTZ* with opposite orientation (Figure 37).
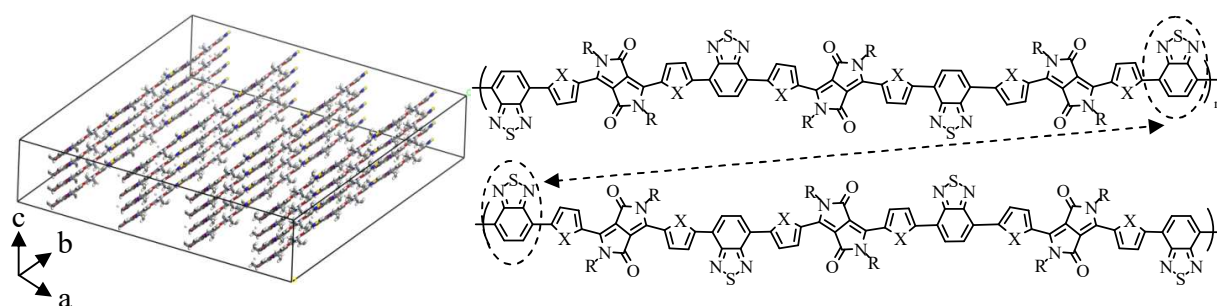

Figure 37. Super cell (left, the side chains are omitted for clarity) and schematic orientation (right) of the simulated polymers. If "parallel" oriented (top) polymer is attached to "anti-parallel" oriented one (bottom) the same polymer will be reproduced (elongated) - shown with an arrow (X=O or S). The lattice vectors are also shown.

Even though of the symmetry of the polymers the "anti-parallel" orientation of the monomers (shown in Fig. 35, p. 86) could be realized locally if the backbones are shifted enough.

Two starting positions of the backbones (side chains) are taken into account for polymer simulations: when the backbones are not shifted (*NS*, non-interdigitating side chains) and when the backbones are initially shifted (by 9 Å where *BTZ* coincides with *DPP - SH*, interdigitating side chains) shown in Figure 6 (p. 19) named here *NS* and *SH*, respectively. For starting configurations only stretched side chains (with E_{con} conformations) with extended box sizes are taken into account where the steric repulsion are minimized for all polymers. All the periodic boxes are orthorhombic ($\alpha=\beta=\gamma=90°$) due to limitation of the LAMMPS software.

First, the torsion angles between the units are measured throughout a productive run trajectory shown in Figure 38.
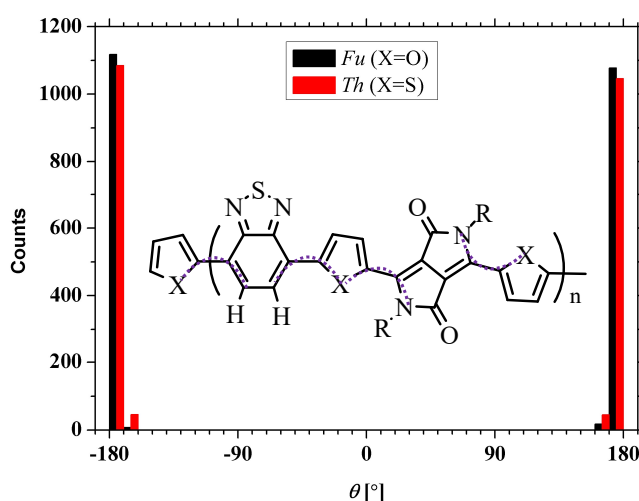

Figure 38. Torsion angle distribution of the marked angles between the units of the polymers (n=6) obtained from MD simulation with *Fu* (X=O) and *Th* (X=S) flanks (FF=PCFF). The torsion angles are measured of one whole backbone (23 torsions for each polymer).

According to Figure 38 the backbones remain planar during the MD simulations and the torsion angles are in the range of $\pm164\div180°$ and PCFF shows good planarity of the backbones of these polymers for both *Fl*.

First, MD results for furan (*Fu*) based polymers with linear (*LN*) side chains are discussed where two configurations of the side chains are taken into account: *NS* or *SH* side chains shown in Figure 39 (p. 96). During the whole simulations the backbones remain planar as the initial positions (*t*=0 ns) of the polymers independently of the configuration of the side chains (*NS* or *SH*). It can be concluded that linear side chains do not influence of the planarity since the backbones are perfectly stacked. This is additionally proved by the arrangement of the units in the bulk shown in Figure 40 (p. 96) where *DPP* is placed above *BTZ* and the flanks form columns in the box. Similar situation is observed in experiment [292]. Moreover, the global minimum of 2D E_{bind} scan shows perfected superposition of *DPP* and *BTZ* for both *Fu* and *Th* stack of dimers and the *Fl* also overlap (Fig. 51, p. 106).
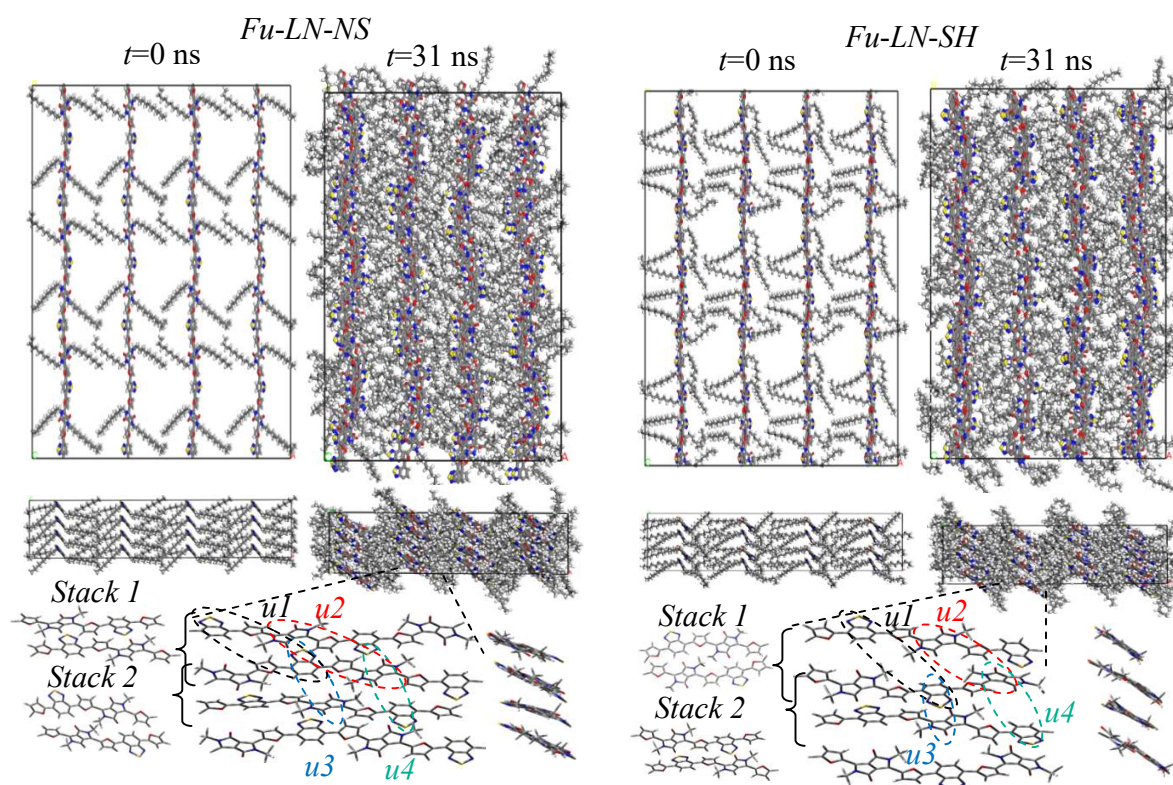
Figure 39. Crystal cells of the *Fu* based polymers with linear (*LN*) side chains when the chains are *NS* (left) and *SH* (right) shown with two perspectives (top and side views) for the initial (*t*=0 ns) and final (*t*=31 ns) frames of MD simulations. At the bottom panel are shown pieces of the polymers where center-to-center (d_h) distances of the units (*u1*, *u2*, *u3* and *u4* - Figure 41, p. 97) are measured and the stacks (*Stack 1* and *Stack 2*), which are extracted in order to evaluate the hopping mobilities (Table 29, p. 110). The crystal cell parameters are shown in Table 24 (p. 97).
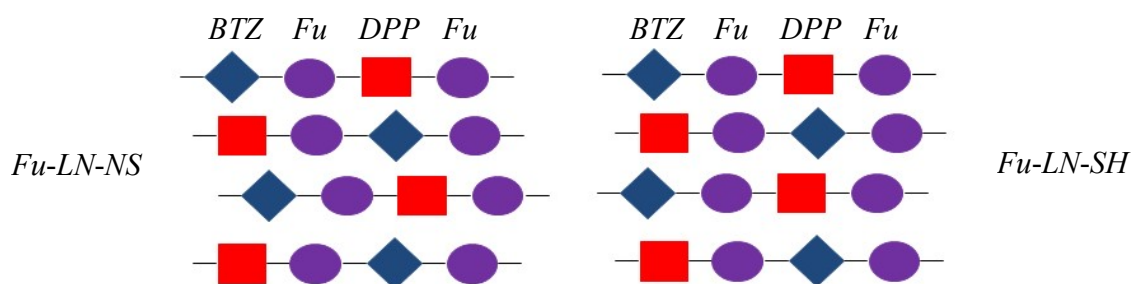

Figure 40. Schematic representation of the arrangement of the units in the bulk of the *Fu* based polymer with linear (*LN*) side chains shown in Figure 39 with two initial configurations: *NS* (left) and *SH* (right) side chains. The corresponding units are: *BTZ* (rhomb), *DPP* (rectangle) and *Fu* (oval).
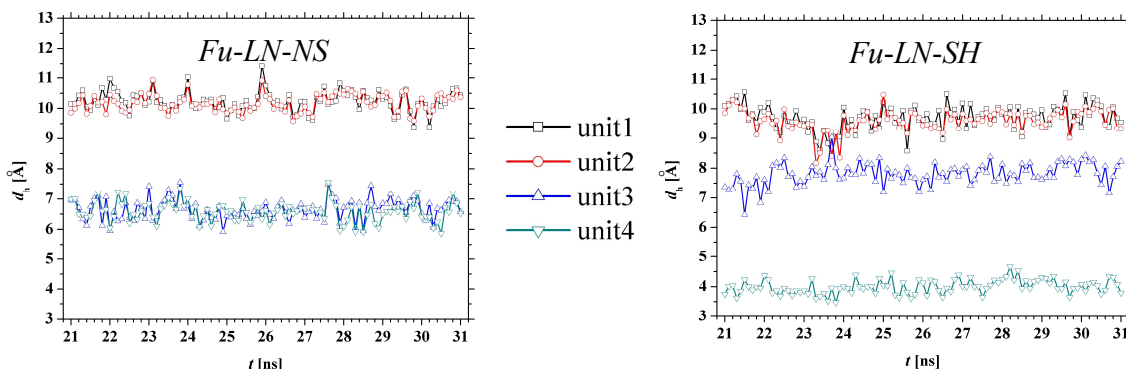
Figure 41. Time evolution of the center-to-center (d_h) distances (in Å) of the units taken from Figure 39 (p. 96) with *NS* (left) and *SH* (right) linear (*LN*) side chains. The corresponding units are: unit1 - *BTZ-BTZ* (squares), unit2 - *DPP-DPP* (circles), unit3 - *BTZ-DPP* (triangles up) and unit4 - *DPP-BTZ* (triangles down).

According to Figure 41 the units only oscillate around their equilibrium positions and they do not drift during the productive run of the MD simulations. Moreover, unit1 and unit2 are at the same d_h distances independently on the configurations of the side chains (*NS* or *SH*), whereas unit3 and unit4 are different, which suggests that there is a slight slip of the backbones after annealing procedure depending on the configuration of the side chains.

The crystal cell parameters and the calculated properties of the *Fu* based polymers with linear (*LN*) side chains are shown in Table 24. The π-π ($d_{\pi\text{-}\pi}$) and lamella (d_{lamella}) distances are measured locally: $d_{\pi\text{-}\pi}$ as a distance from a point (taken as a center of mass of a local ring, for example *Fu*) to a plane (taken as three points defined from one core, for instance *BTZ* molecule) and it is measured several times averaged along the MD productive runs; d_{lamella} distances are calculated from a point (atom in the vicinity of the side chains) to another point (another atom from the opposite backbone on the back side across the side chains - which is equal to side chains plus backbone distance) and it is measured again several times averaged along the MD productive runs. The angle between the measuring points of $d_{\pi\text{-}\pi}$ and d_{lamella} is chosen to be close to 90°. The most planar regions of the samples are chosen for analysis of the polymers.

	Theory:	
	Fu-LN-NS	*Fu-LN-SH*
$d_{\pi\text{-}\pi}$ [Å]	3.78±0.13	3.80±0.12
d_{lamella} [Å]	15.55±0.31	16.20±0.29
ρ [g/cm^3]	1.06	1.05
a [Å]	64.79	62.33
b [Å]	91.55	91.59
c [Å]	18.60	19.54

Table 24. Crystal cell parameters of *Fu* based polymers with linear (*LN*) side chains depending of the initial configurations (*NS* or *SH*). π-π and lamella distances as well as the densities are also shown.

Both side chains configurations show very similar results for the $d_{\pi\text{-}\pi}$ and d_{lamella} where *SH* side chains have slightly higher values. Moreover, both polymers have very close lattice vectors and the same density close to unity, which is acceptable for polymers. It can be concluded that initial configuration of the *LN* side chains are not important for the structural parameters.

When *Fu* based polymers are decorated with branched (*BR*) side chains (Fig. 42) there is significant impact into the backbones from the chains. The branched side chains penetrate between the backbones, which is more pronounced for *SH* configuration and it was not observed in the case of the linear (*LN*) side chains. This explains why *BR* side chains are much more favourable in experiments as compared to linear ones since the *BR* side chains can penetrate between the backbones and this leads to increased solubility. Even though the backbone planarity is distorted, experimentally this can be overcome, for instance, with vapour annealing, which was mentioned in the introduction.

Unlike linear side chains, the position of the units is distorted after the MD simulation in case of *SH* branched chains due to the side chain penetration (shown with red in Fig. 42) but the
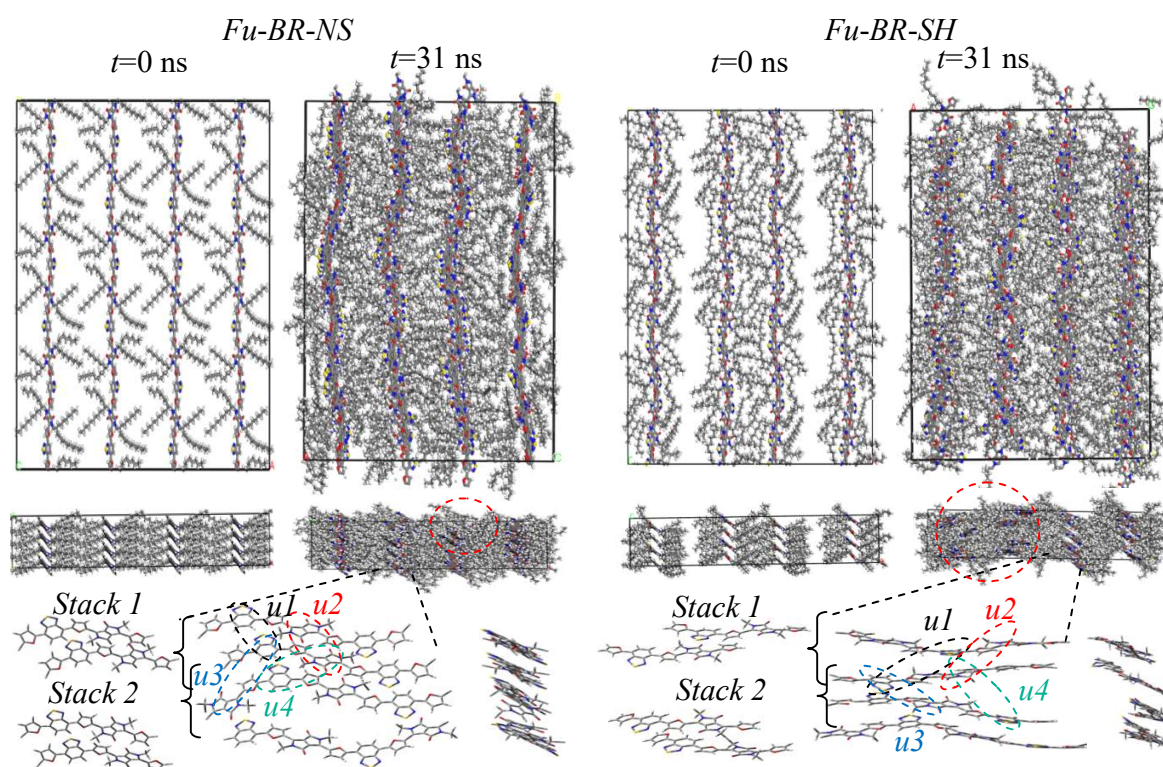

Figure 42. Crystal cells of the *Fu* based polymers with branched (*BR*) side chains when the chains are *NS* (left) and *SH* (right) shown with two perspectives (top and side views) for the initial (*t*=0 ns) and final (*t*=31 ns) frames of MD simulations. At the bottom panel are shown pieces of the polymers where center-to-center (d_{h}) distances of the units (*u1*, *u2*, *u3* and *u4* - Figure 44, p. 99) are measured and the stacks (*Stack 1* and *Stack 2*), which are extracted in order to evaluate the hopping mobilities (Table 31, p. 112). The crystal cell parameters are shown in Table 25 (p. 100). Side chain penetration is also shown.
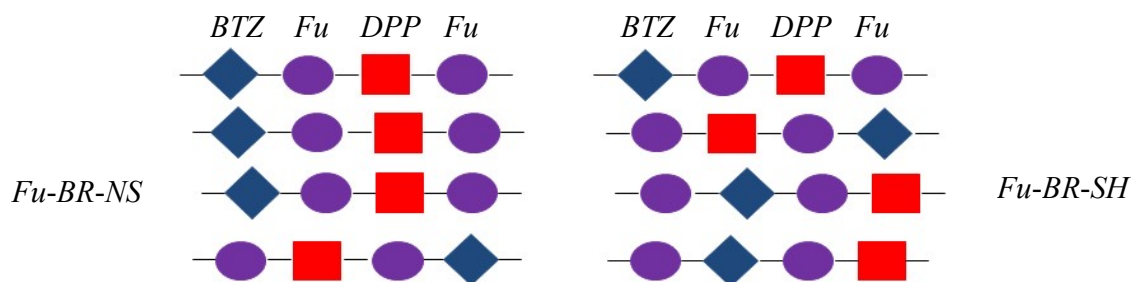
Figure 43. Schematic representation of the arrangement of the units in the bulk of the *Fu* based polymer with branched (*BR*) side chains shown in Figure 42 (p. 98) with two initial configurations: *NS* (left) and *SH* (right) side chains. The corresponding units are: *BTZ* (rhomb), *DPP* (rectangle) and *Fu* (oval).

flanks (*Fu*) remain approximately in one column (Fig. 43). Although the distortion there are some faced *DPP-BTZ* stacks. Additionally, *NS* chain remain approximately at the initial configurations (*t*=0) since the bulkier *BR* chains prevent shifting of the backbones during the MD simulations.

It can be concluded that this mixed units stacking mode will be favourable in block polymers and the dominant interactions will be between the building blocks (*DPP* and *BTZ*) and the *Fl* will form columns if the samples are crystalline and homogeneous (obtained from *LN* chains), and there are no present defects.
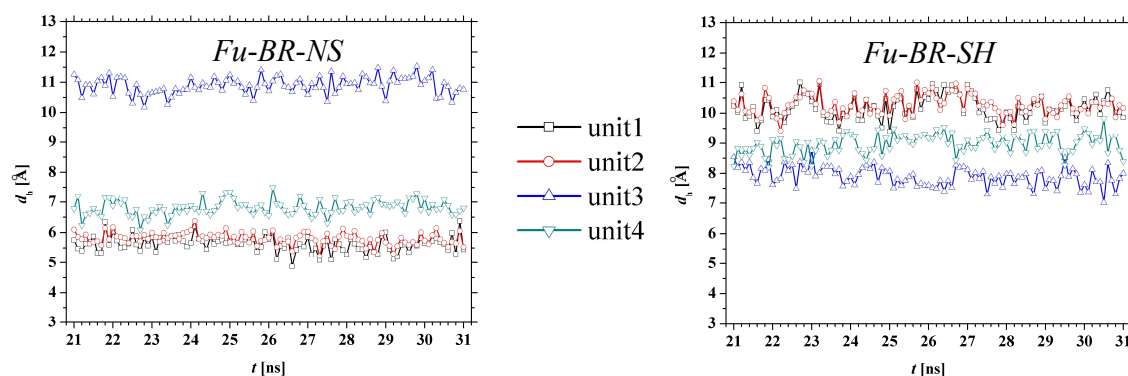

Figure 44. Time evolution of the center-to-center (d_h) distances (in Å) of the units taken from Figure 42 (p. 98) with *NS* (left) and *SH* (right) branched (*BR*) side chains. The corresponding units are: unit1 - *BTZ-BTZ* (squares), unit2 - *DPP-DPP* (circles), unit3 - *BTZ-DPP* (triangles up) and unit4 - *DPP-BTZ* (triangles down).

Unit-to-unit distances (Fig. 44) oscillate around the their equilibrium positions and they do not shift during the productive MD run (like with *LN* chains). Also it can be seen that center-to-center distances at longer distance for *SH* chains since the backbones are distorted from the bulkier chains and the backbones are slipped. This backbone distortion is more pronounced for *SH* backbones since they are initially shifted and *BR* chains prevent sliding of the backbones.

According to the crystal cell parameters (Table 25, p. 100) both configurations (*NS* and *SH*) have very similar properties and the density is again close to unity (like *LN* chains).

	Theory:		Experiment[228]:
	Fu-BR-NS	*Fu-BR-SH*	-
$d_{\pi\text{-}\pi}$ [Å]	3.47±0.13	3.56±0.09	4.2÷4.66
d_{lamella} [Å]	17.92±0.29	17.43±0.28	16.78
ρ [g/cm³]	0.99	0.97	-
a [Å]	77.07	80.69	-
b [Å]	89.79	91.68	-
c [Å]	22.34	21.31	-

Table 25. Crystal cell parameters of *Fu* based polymers with branched (*BR*) side chains depending of the initial configurations (*NS* or *SH*). π-π and lamella distances as well as the densities are also shown.

Comparing with experiment, d_{lamella} is very well predicted with an average value ca. 17.43 and 17.92 Å for *SH* and *NS* chains, respectively, and 16.78 Å according to the experiment [228]. Nevertheless, this small deviation of 1 Å can be ascribed to the fact that orthorhombic cells are simulated. There is a significant difference in the predicted and the experimental $d_{\pi\text{-}\pi}$ with 0.7 Å (3.5 and 4.2 Å in theory and experiment, respectively) and this large deviation could be due to difficulties in experimental measurement where the peak, which determines $d_{\pi\text{-}\pi}$ is too broad [228], which suggests an inhomogeneous sample or high presence of defects, which was pointed out in the E_{bind} section of monomers. Moreover, DFT confirms the measured distance from MD (3.3 and 3.6 Å in anti-parallel and parallel dimers, respectively, Fig. 34, p. 84). Additionally, later is shown that the concentration profile estimates $d_{\pi\text{-}\pi}$ very well with respect to the experiment (Figure 52, p. 107).

If the crystal cell parameters of *LN* and *BR* side chains of *Fu* based polymers are compared (Table 24, p. 97 and Table 25) the main difference is in the "a" lattice vector, which is with approximately 20 Å larger for *BR* side chains. The reason is that at this direction are placed the side chains and *BR* ones are much bulkier than *LN* chains. It can be concluded that polymer with *BR* side chains will lead to bigger crystal cell. d_{lamella} for *LN* chains are up to 2 Å shorter than *BR* chains, which could be explained with the bigger size of the latter chains. There is 0.2 Å difference in the $d_{\pi\text{-}\pi}$ of *BR* chains as compared to *LN* ones, which leads to the fact that *BR* chains induce stronger steric repulsion, which leads to shorter distance between the backbones. It is noticeable that $d_{\pi\text{-}\pi}$ from MD coincides with the π-π distances obtained from E_{bind} (Fig. 34, p. 84) where linear side chains correspond to parallel oriented dimers (ca. 3.8 and 3.6 Å, from MD and E_{bind}, respectively) and branched chains correspond to anti-parallel oriented dimers (ca. 3.5 and 3.3 Å, from MD and E_{bind}, respectively).

It can be concluded that polymers with *LN* and *BR* side chains will be stacked locally at distance close to parallel and anti-parallel orientation due to reduced and increased steric interactions, respectively.

The same procedure is done for *Th* based polymers and the MD results for *LN* side chains are shown in Figure 45 (p. 101). Similar to the *Fu* case, *Th* based polymers have only slight difference between the starting and final frames of MD simulations where in *SH* configuration the

backbones are slightly slipped but they are still planar. It can be concluded again that *LN* side chains have only minor influence into the backbones.
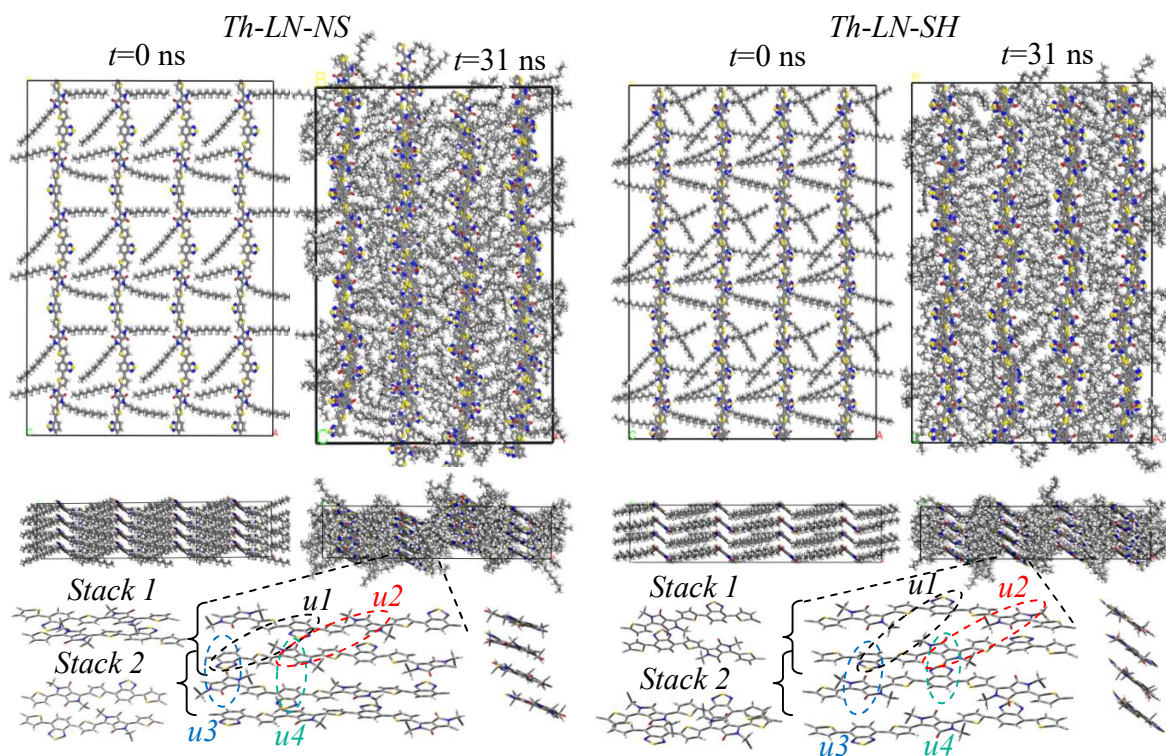

Figure 45. Crystal cells of the *Th* based polymers with linear (*LN*) side chains when the chains are *NS* (left) and *SH* (right) shown with two perspectives (top and side views) for the initial (*t*=0 ns) and final (*t*=31 ns) frames of MD simulations. At the bottom panel are shown pieces of the polymers where center-to-center (d_h) distances of the units (*u1*, *u2*, *u3* and *u4* - Figure 47, p. 102) are measured and the stacks (*Stack 1* and *Stack 2*), which are extracted in order to evaluate the hopping mobilities (Table 30, p. 110). The crystal cell parameters are shown in Table 26 (p. 102).
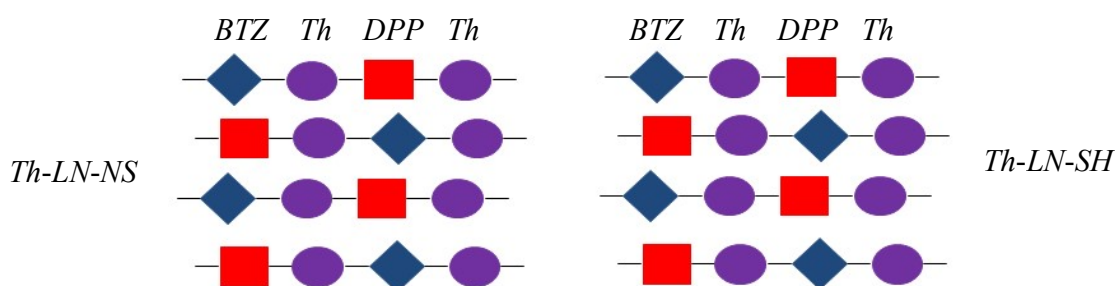

Figure 46. Schematic representation of the arrangement of the units in the bulk of the *Th* based polymer with linear (*LN*) side chains shown in Figure 45 with two initial configurations: *NS* (left) and *SH* (right) side chains. The corresponding units are: *BTZ* (rhomb), *DPP* (rectangle) and *Th* (oval).
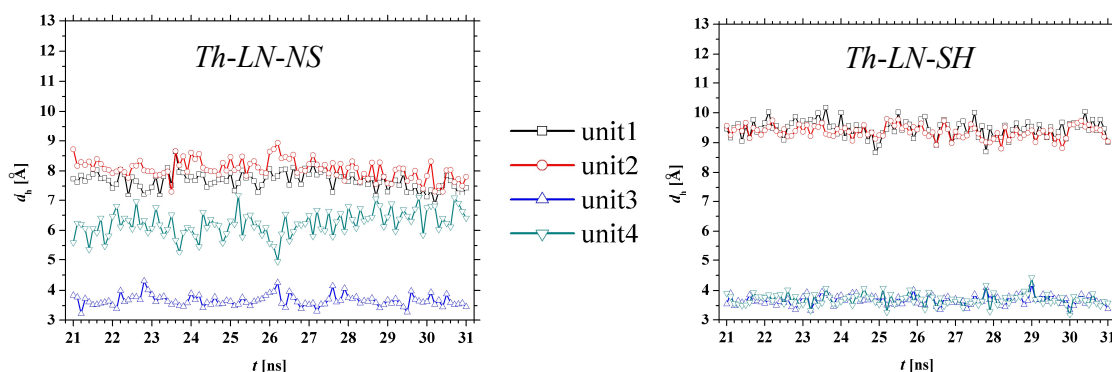
Figure 47. Time evolution of the center-to-center (d_h) distances (in Å) of the units taken from Figure 45 (p. 101) with *NS* (left) and *SH* (right) linear (*LN*) side chains. The corresponding units are: unit1 - *BTZ-BTZ* (squares), unit2 - *DPP-DPP* (circles), unit3 - *BTZ-DPP* (triangles up) and unit4 - *DPP-BTZ* (triangles down).

Also, side chain penetration between the backbones is not observed in the case of *LN* chains (like *Fu* based polymers with *LN* chains), which suggests that the samples would be more homogeneous if the same polymers are synthesized with linear chains.

The arrangement of the units shown in Figure 46 (p. 101) demonstrates again that *DPP-BTZ* interactions are favourable in the polymers independently of the starting configuration of the side chains (*NS* or *SH*) as well as *Th* flanks form columns. If the unit positions between *Fu* and *Th* based polymers with linear side chains are compared (Fig. 40, p. 96 and Fig. 46, p. 101) it is seen that there is no difference and the arrangement is the same independently on the heteroatom, which is additionally confirmed by E_{bind} for both *Fu* and *Th* monomer stacks (Fig. 51, p. 106).

Unit-to-unit distances (Fig. 47) show that the backbones of the polymers oscillate only around their equilibrium positions. It is interesting that the backbones of *NS* chains oscillate at larger amplitude since they are more even as compare to *NS* chains (Fig. 45 bottom panel, p. 101).

Comparing the crystal cell parameters of the two configurations (Table 26) of *Th* based polymers with *LN* chains there is only one main difference in the "a" lattice vector, which the direction of the side chains.

	Theory:	
	Th-LN-NS	*Th-LN-SH*
$d_{\pi\text{-}\pi}$ [Å]	3.65±0.10	3.66±0.10
$d_{lamella}$ [Å]	20.87±0.43	16.08±0.25
ρ [g/cm^3]	1.10	1.10
a [Å]	70.81	63.16
b [Å]	97.40	97.00
c [Å]	16.18	18.13

Table 26. Crystal cell parameters of *Th* based polymers with linear (*LN*) side chains depending of the initial configurations (*NS* or *SH*). π-π and lamella distances as well as the densities are also shown.

For *NS* configuration "a" is with 7 Å larger than *SH*, which could be explained with the afore mentioned increased tilting of the backbones (more even backbone). Also, this is affected to the d_{lamella}, which is with ca. 5 Å larger for *NS* chains than *SH* ones (Fig. 45 bottom panel, p. 101).

It can be concluded that the difference between the *NS* and *SH* configurations of the side chains are due to slightly change in the backbone tilt angle, which influences of the "a" lattice vector and d_{lamella}.

If the crystal cells of *Fu* and *Th* based polymers with *LN* chains are compared (Table 24, p. 97 and Table 26, p. 102) the main difference in only in "b" lattice vector (along the backbone) where for *Th* based polymer is larger due to difference in the size of the five-membered rings (zigzag versus straight line), which was already pointed out when n-mers were investigated in the previous chapter (Fig. 29, p. 79 and Fig. 33, p. 83). The effect of the zigzag curvature of *Fu* based polymer is also pronounced for *NS* chains where the d_{lamella} is with 3 Å shorter for *Fu* polymer than *Th* one . Moreover, there is a small difference in "a" lattice vector (with 7 Å) only for *NS* case where for *Fu* based polymer is bigger. It can be concluded that the effect of the X_{atom} is only due to different shape of the flanks, which leads to slightly difference in the structure parameters.
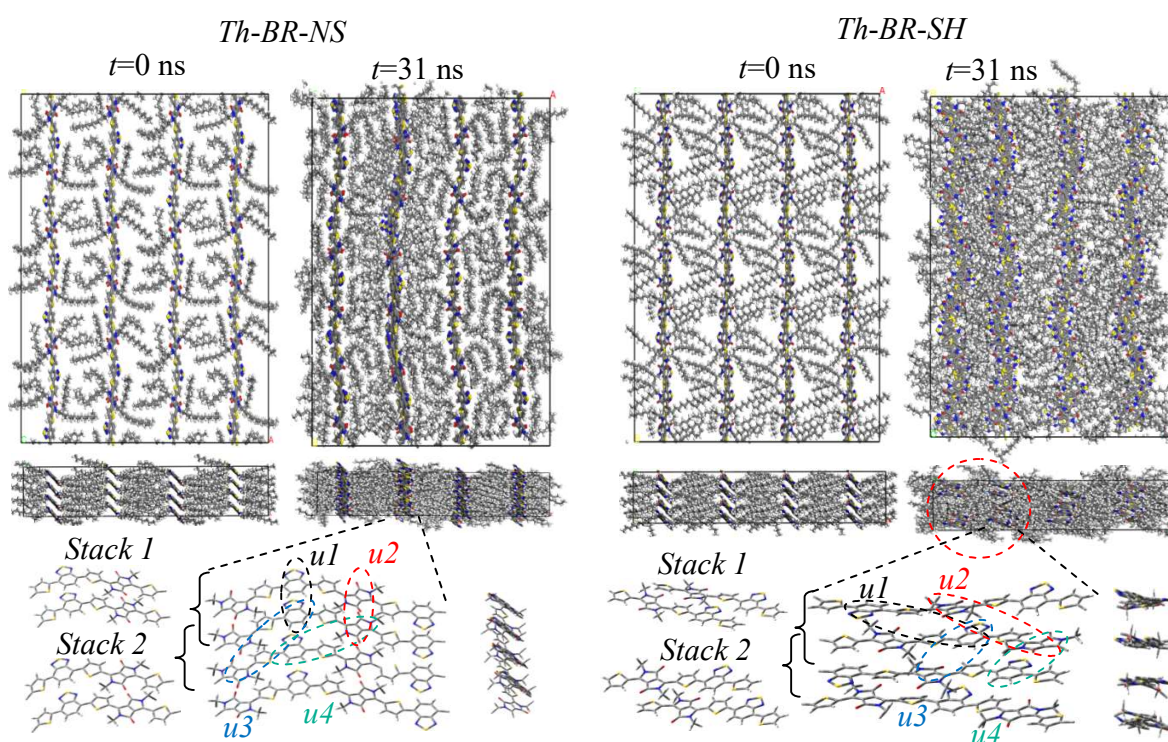
Figure 48. Crystal cells of the *Th* based polymers with branched (*BR*) side chains when the chains are *NS* (left) and *SH* (right) shown with two perspectives (top and side views) for the initial (*t*=0 ns) and final (*t*=31 ns) frames of MD simulations. At the bottom panel are shown pieces of the polymers where center-to-center (d_{h}) distances of the units (*u1*, *u2*, *u3* and *u4* - Figure 50, p. 104) are measured and the stacks (*Stack 1* and *Stack 2*), which are extracted in order to evaluate the hopping mobilities (Table 32, p. 112). The crystal cell parameters are shown in Table 27 (p. 105). Side chain penetration is also shown.

Finally, *Th* based polymer is investigated with *BR* side chains shown in Figure 48 (p. 103). It can be seen that *BR* side chains penetrate between the backbones only in the case of *NS* side chains and for *NS* configuration this is not observed. The reason is that in *SH* configuration due to side chain steric interactions a wave like behaviour of the backbones is obtained and this compensates the penetration effect between the backbones. Additionally, the backbones are not in one plane in *NS* configuration unlike *SH* case, which is observable in the side view panel. This wave like behaviour of the backbones is also observed in *Fu* analogue polymer but here this effect is much better pronounced.

Moreover, if the unit positions in the bulk are analyzed, in *NS* configuration they remain nearly undistorted as compared to the initial position (*t*=0) of the polymer and several *DPP-BTZ* interactions are observable only in *SH* configuration since the bulkier side chains prevent backbone sliding (like in case of *Fu* based polymer with *BR* chains). Nevertheless, *Th* flanks remain as columns in the polymer independently of the configuration of the side chains (similar to *Fu* based polymer with *BR* chains).
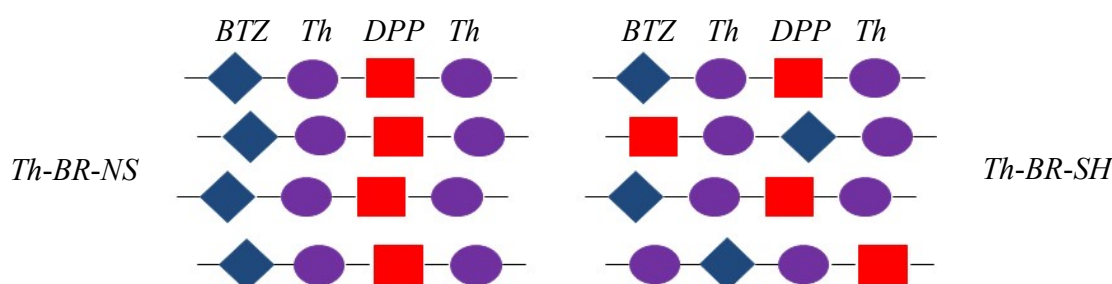
Figure 49. Schematic representation of the arrangement of the units in the bulk of the *Th* based polymer with branched (*BR*) side chains shown in Figure 48 (p. 103) with two initial configurations: *NS* (left) and *SH* (right) side chains. The corresponding units are: *BTZ* (rhomb), *DPP* (rectangle) and *Th* (oval).
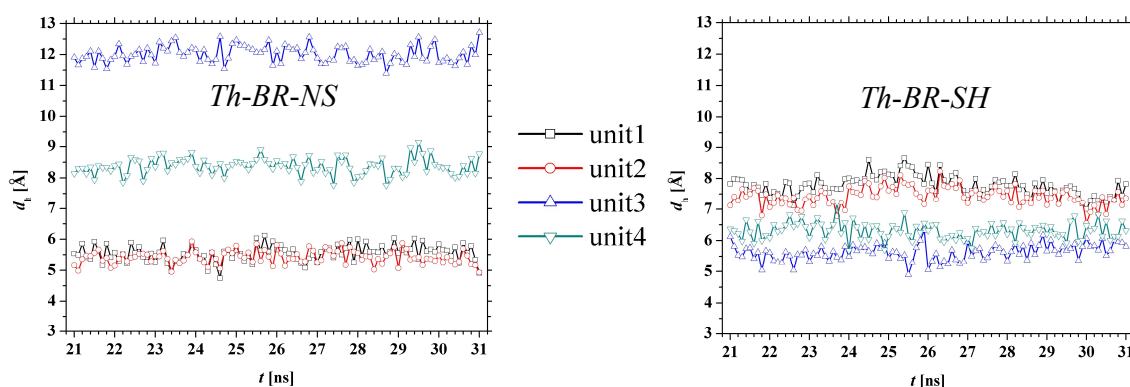
Figure 50. Time evolution of the center-to-center (d_h) distances (in Å) of the units taken from Figure 48 (p. 103) with *NS* (left) and *SH* (right) branched (*BR*) side chains. The corresponding units are: unit1 - *BTZ-BTZ* (squares), unit2 - *DPP-DPP* (circles), unit3 - *BTZ-DPP* (triangles up) and unit4 - *DPP-BTZ* (triangles down).

Even though *NS* of *Th* polymer with *BR* chains has wave like character of the backbone, the unit-to-unit distances again oscillate around they equilibrium positions like *SH* configuration shown in Figure 50 (p. 104) but they have different values since they are slipped or distorted. Similar results for the unit-to-unit distances are obtained for *Fu* based polymers with *BR* chains (Fig. 44, p. 99) with respect to their values.

Considering the crystal cell parameters of *Th* based *BR* polymer (Table 27) there are only minor difference between *NS* and *SH* configurations. They have the same density of 1 g/cm^3 and very close $d_{\pi\text{-}\pi}$ and $d_{lamella}$ although *NS* chains have wave like character.

Comparing with experiment, *Th* based polymer with *BR* chains, $d_{\pi\text{-}\pi}$ is very well predicted from the theory with 3.5 and 3.6 Å for *NS* and *SH* chains, respectively, and 3.73 Å [227], 3.65 Å [230] according to the experiments. Moreover, $d_{lamella}$ is also well predicted with 19.8 and 20.1 Å for *NS* and *SH* chains, respectively, and 21.5 Å in experiment [227] and the small deviation of 1 Å can be explained with the restriction of orthorhombic (α=β=γ=90°) super cells. Additionally, DFT showed also closer $d_{\pi\text{-}\pi}$ of 3.5 and 3.7 Å (Fig. 34, p. 84) in the corresponding orientations.

If the crystal cell parameters of the *LN* and *BR* chains of *Th* based polymers are compared (Table 26, p. 102 and Table 27) the main difference is in the "a" lattice vector and $d_{lamella}$ due to different size of the side chains, which is also true for *Fu* based polymers. It makes impression that $d_{lemella}$ of *NS LN* chains is equal to *NS* for *BR* chains, which can be explained with the fact that *Th* based polymer with *NS LN* chains have more even backbones. Moreover, the obtained $d_{\pi\text{-}\pi}$ from MD coincide with these ones obtained from E_{bind} scan in the corresponding orientation (Fig. 34, p. 84) where for *LN* chains coincide with parallel oriented dimers (ca. 3.65 and 3.7 Å from MD and DFT, respectively) and for *BR* chains coincide with anti-parallel dimers (ca. 3.5÷3.6 and 3.5 Å from MD and DFT, respectively), which was also found for the *Fu* based polymers.

If unit arrangement of the *LN* and *BR Th* based is compared (Fig. 46, p. 101 and Fig. 49, p. 104), *LN* chains reproduce perfect stacking between *DPP* and *BTZ* cores and the flanks are forming columns, whereas for *BR* chains the units remain near their initial position since *BR* chains hinder the sliding of the backbone during the simulations but the flanks still form columns and *DPP-BTZ* interactions can be found only locally. All this results were valid also for the *Fu* based polymers.

	Theory:		Experiment:
	Th-BR-NS	*Th-BR-SH*	-
$d_{\pi\text{-}\pi}$ [Å]	3.49±0.13	3.60±0.10	3.73[227], 3.65[230]
$d_{lamella}$ [Å]	19.76±0.40	20.09±0.23	21.5
ρ [g/cm^3]	1.02	1.03	-
a [Å]	76.75	78.75	-
b [Å]	94.88	97.20	-
c [Å]	21.40	20.13	-

Table 27. Crystal cell parameters of *Th* based polymers with branched (*BR*) side chains depending of the initial configurations (*NS* or *SH*). π-π and lamella distances as well as the densities are also shown.

If the crystal cell parameters of the *Fu* and *Th* based *BR* polymers are compared (Table 25, p. 100 and Table 27, p. 105) the differences are in the $d_{lemella}$ and in the "b" lattice vectors where for *Fu* based polymer are shorter (with 3÷5 Å) than *Th* based one, which can be explained with the zigzag curvature of *Fu* based polymer which originates from the minor difference in the size of the five membered flank as aforementioned for *LN* chains (Fig. 33, p. 83). The other parameters are very close and they are independently of the side chains and the heteroatom.

Generally, the polymers with *LN* side chains have only minor difference is the crystal cell parameters (Table 24, p. 97 and Table 26, p. 102), which is additionally proved by the same unit arrangement (Fig. 40, p. 96 and Fig. 46, p. 101) as well as the unit-to-unit distances are very close (Fig. 41 , p. 97 and Fig. 47, p. 102). Moreover, *DPP* is always stack above *BTZ* and the flanks are forming columns (which is additionally confirmed by DFT) independently on the starting configuration of the side chains and the backbones remain always planar. This suggests that the structural parameters and the unit arrangement in the bulk are independent of the X_{atom} in the flank if the samples are homogeneous and crystalline (obtained from *LN* side chains according to the theory) and they do not contain defects.

Polymers with *BR* side chains again showed close crystal structure parameters (Table 25, p. 100 and Table 27, p. 105) but they have different unit arrangements (Fig. 43, p. 99 and Fig. 49, p. 104) and unit-to-unit distances (Fig. 44, p. 99 and Fig. 50, p. 104) since the *BR* chains prevent sliding of the backbones during the simulations and the backbone are usually distorted. However, the flanks are still arranged in columns. Moreover, polymers with *BR* chains reproduced structures close to their initial configuration (*t*=0 ns) of the side chains: *NS* or *SH* chains where the former ones showed nearly unaffected crystal cell without any backbone shift and the later ones demonstrated only locally *BTZ-DPP* interactions due to distortion of the backbone. The *BR* side chain can penetrate between the backbones especially in the case of *SH* backbones, which was not observed for *LN* chains. It seems that more inhomogeneous samples are obtained with *BR*

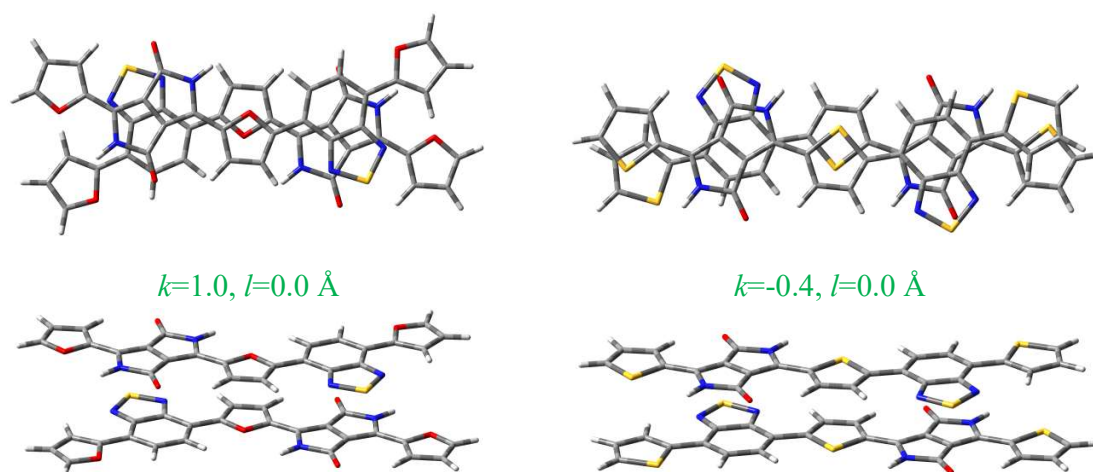*k*=1.0, *l*=0.0 Å   *k*=-0.4, *l*=0.0 Å

Figure 51. Dimer configurations of the global minimum points obtained from 2D E_{bind} approximation (Fig. 33, p. 85) where perfect superposition of *BTZ* and *DPP* is represented as well as the flanks are also overlapping.

side chains according to the theory where the annealing procedure does not cover completely the experimental conditions. However, the most of the available experimental characteristics are predicted very well from the most planar regions of the MD simulations with *BR* chains.

The main difference between *LN* and *BR* side chains is due to the bulkier size of the later ones, which hinder the backbone shifts, lead to greater "a" lattice parameter along the chain direction, grater $d_{lamella}$, shorter $d_{\pi-\pi}$, and distortion of the backbone.

The main difference of *Fu* and *Th* polymers is due to the small difference in the size of the five membered flank. *Fu* polymers show always shorter "b" lattice vector along the backbone, shorter $d_{lamella}$ due to zigzag behaviour of the backbones as compared to *Th* based polymers.

Interesting, the $d_{\pi-\pi}$ obtained from MD of *LN* side chains coincides with the distances of parallel oriented stack of dimers from DFT and the $d_{\pi-\pi}$ obtained from *BR* chains coincide with the distances of anti-parallel oriented dimers as it was pointed out.

Figure 52. Concentration profiles (the concentration of N, S, O and C atoms belonging to the backbone of polymers in a given layer) along "a" lattice vector of the simulation boxes for *Fu* based (a and b) and *Th* based (c and d) copolymers with *NS* (hatched left) and *SH* (hatched right) side chains. The reported values are relative to a random distribution.

The available structural parameters from experiments ($d_{\pi-\pi}$ and $d_{lamella}$) are in very good agreement in the most of the cases independently of the type of the side chains (*LN* or *BR*) or the initial configurations (*NS* or *SH*) with few exceptions from the simulated (within MD) guess crystal structures.

It seems that polymers prefer to be stacked in chains if they are crystalline and the samples are homogeneous (without presence of defects).

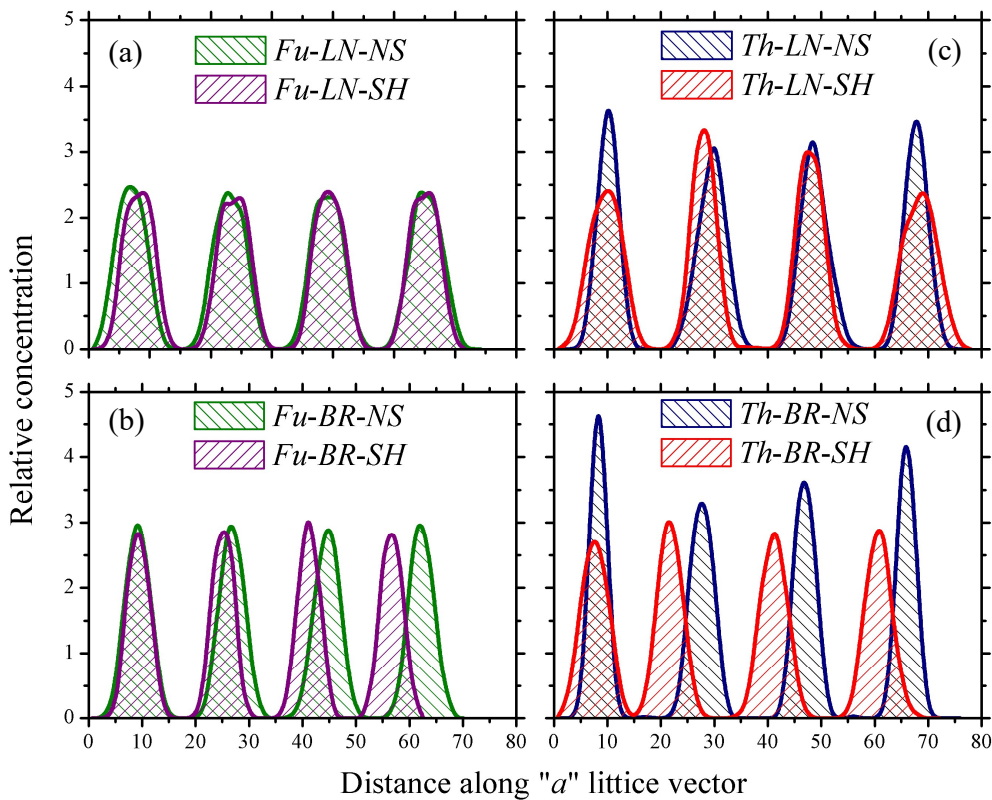Additionally, concentration profiles are calculated where the relative concentration of N, S, O and C atoms belonging to the backbone of a polymer in a given layer along "a" lattice vector is estimated from the last snapshot of the MD simulations. $d_{\pi\text{-}\pi}$ are measured as a interval between the peaks across the conjugated stacks ("c" lattice vector) and $d_{lamella}$ are obtained from the maxima between the peaks (Fig. 52, p. 107) and the results are summarized in Table 28.

From Table 28 it can be seen that $d_{\pi\text{-}\pi}$ ranges from 3.78 to 4.37 Å for all the simulated polymers. All these values are higher as compared to the locally obtained parameters (the tables corresponding for each polymer, 3.47÷3.80 Å) since the measurements of the later one are estimated from the most planar region of the samples. Interesting, the $d_{\pi\text{-}\pi}$ for *LN NS* and *BR SH* chains obtained locally coincides with the concentration profiles independently on the polymers: according to the local parameters *Fu-LN-NS* (Table 24, p. 97) has 3.78 and 3.87 Å in compliance with the concentration profile (Table 28); $d_{\pi\text{-}\pi}$ for *Fu-BR-SH* is 3.56 and 3.78 Å calculated locally (Table 25, p. 100) and the concentration profile, respectively. Similarly for *Th* based polymer are obtained 3.65 and 3.78 Å with *LN-NS* side chains according to the local analysis (Table 26, p. 102) and the concentration profile, respectively, as well as for *BR-NS* chains are calculated 3.60 Å in compliance of the local measurement (Table 27, p. 105) and 3.76 Å according to the concentration profile.

Polymer	Chain	Configuration	$d_{\pi\text{-}\pi}$ [Å]	$d_{lamella}$ [Å]	Exp. $d_{\pi\text{-}\pi}$/ $d_{lamella}$ [Å]
Fu	*LN*	NS	3.87±0.46	15.99±0.54	-
		SH	4.17±0.80	15.93±0.29	-
	BR	NS	4.37±0.49	17.71±0.54	4.2÷4.66[228]/ 16.78[228]
		SH	3.78±0.57	18.21±0.97	
Th	*LN*	NS	3.78±0.24	19.26±0.57	-
		SH	3.95±0.18	19.59±0.41	-
	BR	NS	4.02±0.51	19.26±0.41	3.73[227], 3.65[230]/ 21.5[227]
		SH	3.76±0.42	17.79±2.70	

Table 28. Summary of the $d_{\pi\text{-}\pi}$ and $d_{lamella}$ (in Å) of *Fu* and *Th* based polymers with *LN* and *BR* side chains depending on their initial configuration (*NS* or *SH*) obtained from the concentration profile analysis (Fig. 52, p. 107).

The other $d_{\pi\text{-}\pi}$ deviate with up to 1 Å due to side chains penetration between the backbones (for *BR* chains) or due to tilting of the backbones (for *LN* chains). It makes impression that $d_{\pi\text{-}\pi}$ of *BR-NS* chains of the concentration profile (4.37 Å) of *Fu* based polymer is very well predicted as compared to the experiment (4.2÷4.66 Å [228]), which confirms that the experimental sample could contain defects since MD showed distortion of the backbones. Moreover, the π-π distance of *Th-BR-SH* polymer is in agreement with the experiments where 3.76 Å is calculated, and 3.73 [227] and 3.65 Å [230] are measured. On the other side, the other configuration of *Th* with *BR* chains (*NS*) overestimates this experiment slightly with ca. 0.3 Å (4.02 Å calculated).

However, for the calculation of the charge carrier mobilities are utilized $d_{\pi\text{-}\pi}$ obtained measured locally since the dimers are extracted locally (from the most planar region of the samples). Moreover, hopping mobilities calculated with the $d_{\pi\text{-}\pi}$ obtained from the concentration profiles (Table 28, p. 108) showed only slightly higher values due to slightly higher distances.

According to the lamella distances, the results of the local investigation coincide very well with the concentration profile where the former ones range in 15.55÷17.92 Å for *Fu* based polymers and 19.76÷20.87 Å for *Th* based polymers (with one exception of 16.08 Å for *Th-LN-SH*), and the later ones shows 15.93÷18.21 Å and 19.26÷19.59 Å, for *Fu* and *Th* based polymers, respectively (with one exception for *Th-BR-SH* of 17.79 Å). Moreover, all the values of d_{lamella} are in agreement with the experiments (Table 28, p. 108).

Interesting, the standard deviations from the concentration profiles are much larger (at least 2-3 times) than the standard deviations of the locally measured parametrs.

It can be concluded that $d_{\pi\text{-}\pi}$ and d_{lamella} will remain unaffected if the crystal structures of the polymers are crystalline and homogeneous (no defects) and the side chains do not influence on the morphology.

6.3. Charge Transport Properties

The CT properties are calculated from extracted dimers from the corresponding polymers (Fig. 39, 42, 45 and 48, p. 96, 98, 101 and 103, respectively) from every 100000 frame of the MD productive runs (each value is averaged over 100 frames). For each polymer two stacks of dimers are extracted (*Stack 1* and *Stack 2*) from the middle of the periodic box as well as from the middle of the backbones and they belong to the most planar regions of the samples. Since four backbones are stacked one above, one stack is chosen close to the "top" (or "bottom") of the periodic box and the other one corresponds to the middle part. After dimers extraction, later the dimers are saturated and the side chains are substituted with methyl groups and further single point DFT calculations (B3LYP/6-31G*, $\varepsilon=0$) are performed in order to obtain the electronic energies.

First, the results of *Fu* based polymer with *LN* side chains (Table 29, p. 110) are shown. The electronic couplings (*V*) in all cases have average values in range of 0.038÷0.087 eV and the standard deviations are of the same order of magnitude with two times lower values (0.028÷0.037 eV). Similar situation was observed with the CT properties of the crystal structure of *Th-BTZ-Th* small molecule where the values are slightly higher (Table 13, p. 77 and Table 14, p. 78). Charge transport is allowed only along the π-π direction in polymers (only cofacial stacks) since only stacked polymers are simulated (and intrachain CT is not taken into account), which simplifies the procedure unlike *Th-BTZ-Th* crystal structure. The charge rate constants of *NS* case of *Stack 1* slightly dominates over *Stack 2*, which is the opposite for *SH* case but these values are of the same order of magnitude and the average quantities of the hopping mobilities are very close (μ^-=0.4 and 0.3, μ^+=0.2 and 0.3 cm^2/V·s, for *NS* and *SH* configurations, respectively). It is worth noting that the standard deviations of the mobilities is also from the same order of magnitude (usually two times lower) and the predicted values for *LN* side chains correspond perfectly with

	Fu-LN-NS:		
	Stack 1:	Stack 2:	Average:
$<V^{ET}>$ [eV]	0.049±0.030	0.042±0.029	0.046±0.030
$<V^{HT}>$ [eV]	0.066±0.028	0.049±0.027	0.058±0.028
K^{-}_{CT} [$1\cdot10^{13}\cdot$s^{-1}]	1.667±0.623	1.217±0.578	1.433±0.606
K^{+}_{CT} [$1\cdot10^{13}\cdot$s^{-1}]	1.144±0.203	0.639±0.187	0.873±0.212
μ^{-} [cm^2/V·s]	0.463±0.173	0.338±0.161	0.398±0.169
μ^{+} [cm^2/V·s]	0.318±0.056	0.178±0.052	0.243±0.059
μ^{-}/μ^{+}	1.458	1.904	1.641
	Fu-LN-SH:		
	Stack 1:	Stack 2:	Average:
$<V^{ET}>$ [eV]	0.038±0.028	0.046±0.028	0.042±0.028
$<V^{HT}>$ [eV]	0.043±0.031	0.087±0.029	0.065±0.037
K^{-}_{CT} [$1\cdot10^{13}\cdot$s^{-1}]	0.985±0.546	1.488±0.527	1.205±0.545
K^{+}_{CT} [$1\cdot10^{13}\cdot$s^{-1}]	0.488±0.248	2.001±0.220	1.116±0.361
μ^{-} [cm^2/V·s]	0.277±0.153	0.407±0.148	0.339±0.153
μ^{+} [cm^2/V·s]	0.137±0.070	0.562±0.062	0.314±0.102
μ^{-}/μ^{+}	2.020	0.724	1.080

Table 29. Charge transport properties of *Fu* based polymer with linear (*LN*) side chains depending of the initial configurations (*NS* or *SH*) obtained from MD simulations. The stacks of dimers are taken from Figure 39 (p. 96) - B3LYP/6-31G*, ε=0.

	Th-LN-NS:		
	Stack 1:	Stack 2:	Average:
$<V^{ET}>$ [eV]	0.058±0.028	0.065±0.034	0.052±0.028
$<V^{HT}>$ [eV]	0.059±0.033	0.071±0.027	0.057±0.030
K^{-}_{CT} [$1\cdot10^{13}\cdot$s^{-1}]	2.267±0.517	2.783±0.776	1.771±0.504
K^{+}_{CT} [$1\cdot10^{13}\cdot$s^{-1}]	0.830±0.252	1.196±0.178	0.765±0.217
μ^{-} [cm^2/V·s]	0.588±0.134	0.722±0.201	0.459±0.131
μ^{+} [cm^2/V·s]	0.215±0.065	0.310±0.046	0.198±0.056
μ^{-}/μ^{+}	2.729	2.328	2.315
	Th-LN-SH:		
	Stack 1:	Stack 2:	Average:
$<V^{ET}>$ [eV]	0.050±0.029	0.065±0.034	0.057±0.029
$<V^{HT}>$ [eV]	0.066±0.034	0.071±0.027	0.065±0.035
K^{-}_{CT} [$1\cdot10^{13}\cdot$s^{-1}]	1.638±0.541	2.784±0.776	2.144±0.571
K^{+}_{CT} [$1\cdot10^{13}\cdot$s^{-1}]	1.014±0.276	1.196±0.178	0.990±0.247
μ^{-} [cm^2/V·s]	0.428±0.141	0.728±0.203	0.561±0.149
μ^{+} [cm^2/V·s]	0.265±0.072	0.313±0.046	0.259±0.065
μ^{-}/μ^{+}	1.614	2.328	2.167

Table 30. Charge transport properties of *Th* based polymer with linear (*LN*) side chains depending of the initial configurations (*NS* or *SH*) obtained from MD simulations. The stacks of dimers are taken from Figure 45 (p. 101) - B3LYP/6-31G*, ε=0.

the experimental measurements for *BR* side chains (μ^-=0.56 and μ^+=0.20 cm^2/V·s [228]).

The results of *Th* based polymer with *LN* side chains (Table 30, p. 110) are very similar to the results obtained for *Fu* analogue. The conductive properties are approximately of the same range as well as the standard deviations like in the case for *Fu* polymer with *LN* chains. In *Th* polymer *Stack 2* has slightly higher CT properties than *Stack 1* for both configurations but again these values are of the same order of magnitude and the average values for all the other quantities (charge rate constants and hopping mobilities) are also from the same order of magnitude like *Fu* based polymer. Moreover, the theoretical obtained values for hopping mobilities (μ^-=0.5 and 0.6, μ^+=0.2 and 0.3 cm^2/V·s, for *NS* and *SH* configurations, respectively) again very well agree with the experimentally obtained ones with *BR* side chains (μ^-=0.40÷0.58 and μ^+=0.33÷0.53 cm^2/V·s [227, 229, 230]).

It can be concluded that there is no difference between these two polymers with linear side chains according to their charge transport properties. The combined MD/QM approach predicts very well the CT properties as compared to the experimental data (even though the experiments correspond to *BR* chains). Additionally, the values of the CT properties are averaged unlike, for instance, the values obtained from dimers with minimum E_{bind} (single values).

The same procedure is done for *BR* side chains. First, the results for *Fu* based polymer (Table 31, p. 112) are described. The *V* values are at the slightly higher range 0.056÷0.083 eV than the *LN* chains and there is only one exception for *Stack 2* of *NS* configuration for V^{ET} where this value is 0.106 eV. The higher values of the electron transfer lead to one order higher μ^- than the experiment and this is the only one exception, which deviates from the experiment. This exception can be explained with stacks at the shorter π-π distance obtained for this case of 3.47 Å (Table 25, p. 100) and with the distortion of the backbones due to bulkier size of the *BR* side chains. Additionally, the larger values of the electronic couplings lead to bigger standard deviations, which are again two times smaller than the average values. Moreover, the μ^- are higher than the μ^+ as well as this is observed also in experiment (μ^-=0.56>μ^+=0.20 cm^2/V·s [228]). Nevertheless, these values are of the same order of magnitude and the polymer remains ambipolar. Again the theory predicts very well the hopping mobilities (μ^-=1.4 and 0.9, μ^+=0.3 and 0.3 cm^2/V·s, for *NS* and *SH* configurations, respectively) with the only one exception, which was mentioned above.

If the CT properties of *Fu* based polymers with *LN* and *BR* side chains are compared (Table 29, p. 110 and Table 31, p. 112, respectively), it can be seen that *BR* chains reproduce only slightly higher mobilities only for μ^- (maybe due to distortion of the backbone caused by the bulkier chains) as compared to *LN* chains and it can be concluded that generally the mobilities are independent of the side chains (with one exception). Additionally, there is a difference in the ratio of the mobilities (μ^-/ μ^+) where for *LN* chains is closer to unity than *BR* chains but the mobilities are still from the same order of magnitude and the difference is only in the higher μ^- of *BR* chains.

Finally, the charge transport properties of *Th* based polymer with *BR* chains are investigated (Table 32, p. 112). Similar to the case with *LN* chains, the electronic couplings are in the range of 0.063÷0.079 eV for *BR* chains where for *LN* ones the range is slightly lower of 0.050÷0.071 eV (Table 30, p. 110) but these values are again from the same order of magnitude.

	Fu-BR-NS:			Experiment[228]:
	Stack 1:	Stack 2:	Average:	
$<V^{ET}>$ [eV]	0.082±0.043	0.106±0.045	0.094±0.045	-
$<V^{HT}>$ [eV]	0.083±0.025	0.058±0.033	0.071±0.032	-
K^{-}_{CT} [$1·10^{13}·s^{-1}$]	4.676±1.265	7.657±1.373	6.075±1.404	-
K^{+}_{CT} [$1·10^{13}·s^{-1}$]	1.815±0.639	0.874±0.286	1.302±0.266	-
μ^{-} [$cm^2/V·s$]	1.100±0.298	1.802±0.323	1.429±0.330	0.56
μ^{+} [$cm^2/V·s$]	0.427±0.039	0.206±0.067	0.306±0.063	0.20
μ^{-}/μ^{+}	2.576	8.758	4.665	2.80
	Fu-BR-SH:			
	Stack 1:	Stack 2:	Average:	
$<V^{ET}>$ [eV]	0.078±0.049	0.065±0.034	0.071±0.043	-
$<V^{HT}>$ [eV]	0.056±0.038	0.071±0.027	0.064±0.034	-
K^{-}_{CT} [$1·10^{13}·s^{-1}$]	4.208±1.669	2.879±0.802	3.512±1.261	-
K^{+}_{CT} [$1·10^{13}·s^{-1}$]	0.813±0.370	1.326±0.197	1.054±0.298	-
μ^{-} [$cm^2/V·s$]	1.038±0.412	0.710±0.198	0.867±0.311	0.56
μ^{+} [$cm^2/V·s$]	0.201±0.091	0.327±0.049	0.260±0.074	0.20
μ^{-}/μ^{+}	5.172	2.171	3.332	2.80

Table 31. Charge transport properties of *Fu* based polymer with branched (*BR*) side chains depending of the initial configurations (*NS* or *SH*) obtained from MD simulations. The stacks of dimers are taken from Figure 42 (p. 98) - B3LYP/6-31G*, ε=0

	Th-BR-NS:			Experiment:
	Stack 1:	Stack 2:	Average:	
$<V^{ET}>$ [eV]	0.067±0.031	0.065±0.034	0.068±0.030	-
$<V^{HT}>$ [eV]	0.079±0.033	0.071±0.027	0.076±0.034	-
K^{-}_{CT} [$1·10^{13}·s^{-1}$]	2.994±0.628	2.783±0.776	3.087±0.610	-
K^{+}_{CT} [$1·10^{13}·s^{-1}$]	1.453±0.251	1.196±0.178	1.367±0.273	-
μ^{-} [$cm^2/V·s$]	0.712±0.149	0.662±0.184	0.734±0.145	0.40[a], 0.58[b], 0.57[c]
μ^{+} [$cm^2/V·s$]	0.346±0.060	0.284±0.042	0.325±0.065	0.35[a], 0.53[b], 0.33[c]
μ^{-}/μ^{+}	2.060	2.328	2.259	1.14[a], 1.09[b], 1.73[c]
	Th-BR-SH:			
	Stack 1:	Stack 2:	Average:	
$<V^{ET}>$ [eV]	0.063±0.033	0.065±0.034	0.064±0.034	-
$<V^{HT}>$ [eV]	0.072±0.035	0.071±0.027	0.078±0.037	-
K^{-}_{CT} [$1·10^{13}·s^{-1}$]	2.648±0.710	2.783±0.776	2.726±0.748	-
K^{+}_{CT} [$1·10^{13}·s^{-1}$]	1.212±0.294	1.196±0.178	1.436±0.322	-
μ^{-} [$cm^2/V·s$]	0.671±0.180	0.705±0.196	0.690±0.189	0.40[a], 0.58[b], 0.57[c]
μ^{+} [$cm^2/V·s$]	0.307±0.074	0.303±0.045	0.364±0.082	0.35[a], 0.53[b], 0.33[c]
μ^{-}/μ^{+}	2.185	2.328	1.898	1.14[a], 1.09[b], 1.73[c]

Table 32. Charge transport properties of *Th* based polymer with branched (*BR*) side chains depending of the initial configurations (*NS* or *SH*) obtained from MD simulations. The stacks of dimers are taken from Figure 48 (p. 103) - B3LYP/6-31G*, ε=0. [a][227], [b][229], [c][230].

The CT properties of *Th* polymer with *BR* chains for *NS* and *SH* configurations including not only the *V* values but also the charge rate constants and the charge carrier mobilities are very close. Comparing the predicted and experimentally obtained hopping mobilities again it can be seen a perfect agreement of the theory and experiment: theoretically μ^-=0.7 and 0.7, μ^+=0.3 and 0.4 cm^2/V·s, for *NS* and *SH* configurations, respectively, and experimentally μ^-=0.40÷0.58 and μ^+=0.33÷0.53 cm^2/V·s [227, 229, 230], which again proves the precision of the combined MD/QM approach for the calculation of the CT properties.

Comparing *Th* based polymer with *LN* and *BR* chains (Table 30, p. 110 and Table 32, p. 112) all the hopping mobilities are of the same order of magnitude, the exact values are very close as aforementioned as well as the electron mobilities are slightly higher than the h^+ mobilities independently on the configurations of the side chains.

It can be conclude that the side chains do not influence the CT properties in polymers if the side chains do not affect the morphology and the polymers remain crystalline and homogeneous.

If *Fu* and *Th* polymers with *BR* side chains are compared (Table 31 and Table 32, p. 112) again the differences are only minor and the CT properties are unaffected of the X$_{atom}$ in the flank (with one exception of μ^- for *Fu* with *NS* and in the limit of *SH* chains), which might be due to the symmetry of the polymers.

Generally, all the simulated polymers with MD/QM approach exhibit charge carrier mobilities of the same order of magnitude independently of the type of the side chains (*LN* and *BR*), the side chain configurations (*NS* or *SH*) or the heteroatom in the flank (oxygen or sulphur, in *Fu* and *Th* flanks, respectively) with one exception of *Fu* for μ^-, however, these are average values. In all the cases the polymers were crystalline and it seems that the crystallinity is the main factor for high and balanced hopping mobilities.

A second reason why these polymers remain with unaffected CT properties is that they do not have anti-parallel orientation, which it was pointed out (Fig. 37, p. 94) similar to the case of small molecules (for instance *DPP*) where the effect of the X$_{atom}$ disappeared.

7. Conclusion and Outlook

Semiconducting molecules were investigated systematically starting from small constitutive D_-A_+ compounds, through monomers up to block copolymers using different methods regarding the number of the atoms in the systems. Geometric, electronic and charge transport properties were calculated and compared on every stage of the investigation. The charge transport properties were estimated with four different ways: scanning the potential surface with electronic coupling, scanning the potential surface with binding energies (E_{bind}) and later the minimum points were utilized, calculating the charge transport (CT) properties of experimentally resolved crystal structure for all the possible dimers, which correspond to pathways and finally using combined MD/QM approach of simulations of polymeric materials extracting pairs of dimers.

The most expensive method for calculation of the charge transport properties was the combined MD/QM dimer extraction approach of polymers, which allows calculating of average values from assumed (guess) crystal structure. Since the investigated polymers were modelled as crystalline the mobilities were very well predicted with respect to the experimental measurements. Next cheaper method utilizing dimers with minimum energy in E_{bind} (for monomers and small molecules) provided correct values of the hopping mobilities from the global minimum points (and/or the second minimum) without knowledge of the crystal structure. The last method utilizes known crystal structure where the charge transport properties were evaluated for each stack of dimers (pathway), which usually overestimates the charge carrier mobilities due to incorrect definition of the distance between the molecules.

Effect of the heteroatom (X_{atom}) in the five-membered rings (flanks) was investigated and it was shown that the X_{atom} affects primary the conformational properties of isolated molecules, the torsion potential barriers and rigidity (Kuhn's length) with different type of H-bonding and increased electrostatic interactions. The X_{atom} has a minor effect to the electronic and optical properties but has a great impact on the curvature of the polymeric backbones due to slightly difference in the geometry. In dimers it was demonstrated that the effect of heteroatom appears only in the case of non-symmetric (anti-parallel oriented) molecules. In such anti-parallel orientation the heteroatom influences primary to the E_{bind} (different equilibrium distances (d) between the molecules) and further to the electronic couplings (V) due to reduced overlap of electron density (reduced strong orbital interactions) and later affects the CT properties where the hopping mobilities were always smaller as compared to parallel orientation. Parallel oriented (or symmetric) molecules have no effect of the X_{atom} with respect to the CT properties due to similar pattern and overlap of the frontier orbitals and they possess better charge carrier mobilities due to better π-orbital interactions.

Block copolymers were investigated with Periodic Boundary Conditions with two types of side chains (linear and branched, *LN* and *BR*, respectively) and additionally, with two different

starting positions: shifted (*SH*) and non-shifted side chains (*NS*), with or without initial shift of the backbones, respectively. It was demonstrated that there is only minor difference in the crystal cell parameters between linear and branched side chains (primary in "b" lattice vector along the chains and lamella distance due to difference in the size of the five membered rings). Different starting configurations (*SH* or *NS*) of the side chains showed different unit-to-unit distances where *SH* chains represented structures close to the starting configurations only in case of *BR* side chains. Lamella and π-π distances were measured in polymer systems where the they were predicted very well from local measurement of the samples as well as the concentration profile showed similar values if there is no distortion of the crystal structures (homogeneous samples). The effect of the heteroatom substitution disappeared due to symmetry reasons of the polymer units with respect to the charge transport properties and the most of the structural parameters.

The stacking modes of the constitutive units were investigated in the polymers and it was demonstrated that the flanks are forming columns and the different acceptor units are facing each other if the samples are crystalline and homogeneous (obtained from *LN* side chains) later confirmed by DFT dimers from the minimum points of E_{bind}.. The charge transport properties were obtained by the mean of combined MD/QM approach throughout the trajectories. The hopping mobilities were in very good agreement with the experimental available data due to crystallinity of the simulated polymers.

- o It was found that the most stable conformers of small molecules prefer maximum H-bonding and reduced electrostatic interactions.
- o It was observed that the heteroatom does not influence on the reorganization energies.
- o In all cases the molecules have higher reorganization energies for positive charged state as compared to negative ones ($\lambda_i^- < \lambda_i^+$) due to reduced conjugation length of positive charged molecules, which led to the fact that electron mobility is more favourable as compared to hole mobility in the most of the cases.
- o Dimers with minimum E_{bind} give accurate coordinates of the molecular shifts (as well as π-π distances), which coincide with experimentally obtained crystal structures for small molecules, which is applicable only for cofacial orientation.
- o Anti-parallel orientation is preferable than parallel one due to increased attraction in E_{bind} and reduced repulsive (π-orbital) interactions in dimers.
- o Dimers at closer (π-π) distance exhibit stronger electronic couplings, which led to better charge transport properties.
- o Equilibrium (π-π) distances (obtained from E_{bind}) were found for anti-parallel oriented dimers. For parallel oriented dimers there were no clear minimum points and molecules had only weak attraction. Additionally, such weak attractive dimers could behave like disordered structures where the distances between dimers can vary due to thermal fluctuations and they are not able to form stable crystals. This is confirmed by the fact that the crystal structure of *DPP* based molecules are not resolved without side chains.
- o The minimum distance (*d*) from E_{bind} of small dimer molecules coincided with the same distances for monomers.

o Parallel oriented dimers have larger minimum (π-π) distances as compared to anti-parallel oriented dimers due to stronger π orbital interactions.

o In anti-parallel orientation the equilibrium (π-π) distance depends on the heteroatom substitution where for oxygen was shorter as compared to sulphur atom due to difference in their radii.

o Parallel oriented dimers (or high symmetric molecules) had the same dependencies of electronic coupling due to similar delocalized distributions of the frontier orbitals.

o Parallel oriented dimers or high symmetric molecules led to higher and balanced electronic coupling due to increased e^- density overlap (increased strong orbital interactions) and further to high charge carrier mobilities than anti-parallel oriented dimers.

o Parallel oriented dimers prefer to be shifted in order to compensate the weak interactions obtained from the shallow curves of E_{bind}.

o Parallel oriented dimers, which are not shifted (exactly face-to-face) led to higher electronic couplings and further better charge carrier mobilities due to strong orbital interactions.

o It was demonstrated that in anti-parallel oriented dimers (*BTZ* molecules) the *V* values can be enhanced if the molecules are placed at special positions, which usually led to unbalanced e^- and h^+ mobilities.

o In the crystal structure of *Th-BTZ-Th* cofacial charge transport is favourable as compared to herringbone one. At higher temperature, the mobilities were increased as well as they become balanced ($\mu^- \approx \mu^+$).

o Attaching the small molecules led to improvement of the electronic properties (UV-VIS spectra) as well as it can be used in order to manipulate the reorganization energies (λ_i).

o Stacks of dimers prefer to be shifted and/or anti-parallel oriented in order to compensate the strong repulsive orbital interactions since they form of configurations, which exhibit stronger attractive forces obtained from the minimum points of E_{bind} (which led to reduced CT properties) especially for the case of monomer units.

o It was demonstrated that *LN* and *BR* chains differ primary in the "a" lattice vector along the side chains since the later ones are bulkier. Moreover, Additionally, *BR* side chains demonstrated longer lamella distances and slightly shorter π-π distances than *LN* chains, which is related to stronger steric interactions according to the local measurements. All the other crystal cell parameters were approximately the same.

o It was shown that *LN* chains reproduce much planar backbones as compared to *BR* side chains.

o Branched side chains hindered the sliding of the backbones during the simulations and these polymers remained close to their starting configurations.

o Branched side chains showed penetration between the backbones (which explains the increased solubility of them as compared to linear side chains).

o Polymers with linear side chains exhibited π-π distances like parallel oriented stack of monomers and branched side chains exhibit π-π distances like anti-parallel oriented stack of monomers according to the local measurements and E_{bind}, respectively.

o *Fu* based polymers have shorter lamella distance and "b" lattice vectors as compared to *Th* based polymers due to difference of the curvature of the backbones (the size of the five membered ring) where former one has zigzag shape, whereas later one has more straight backbone.

o The charge carrier mobilities obtained from the samples with BR chains were slightly higher as compared to the case with LN chains. However, most of them were from the same order of magnitude where it was observed only one exception (for μ^- of *Fu-BR-NS* and in the limit of *SH* chains), which deviated also from the experiment. Generally, the side chains do not influence directly on the charge transport properties if the samples remain homogeneous and there are no present defects (and the morphology is not affected).

o Usually the A_+ and D_- building moieties were independently situated one above in polymers (as well as in monomers with minimum energies from E_{bind}) when the polymers are perfectly crystalline but the charge transport properties remained from the same order of magnitude in the most of the cases.

o Flanking units (furan or thiophene) usually were forming columns in the crystal structures in the polymers.

o The effect of the heteroatom in copolymers was vanished due to symmetry reasons and favourable interactions between the units as well as due to crystallinity of the samples and as a result the charge transport properties remained unaffected in the most of the cases.

Final conclusion can be made that if stack of conjugated molecules is placed exactly one above (for instance, parallel orientation or symmetric molecules) and as much as shorter π-π distance between them thus will lead to the best charge performance device independently on the type of the molecules. At this situation will be realized maximum strong orbital interactions (due to maximum π-orbitals overlap) where usually the molecules form unstable stacks and they prefer to be shifted and/or at longer π-π distance.

Further investigations can be done for the same polymers if the side chains are replaced to *BTZ* part of the molecules and/or to be added additional side chains to this part. Moreover, it will be interesting if the mechanical properties of these polymers are estimated.

In order to clarify better the charge transport in isolated stacks of molecules it can be investigated symmetric or asymmetric molecules, which do not have explicit anti-parallel orientation. Additionally, an heteroatom can be added in the backbone, for example, substitution of hydrogen atom with fluorine one leading to a supplemental non-covalent interaction (X···F).

References:

[1] E. E. Havinga, W. Hoeve & H. Wynberg, Alternate Donor-Acceptor Small-Band-Gap Semiconducting Polymers; Polysquaraines and Polycroconaines, *Synth. Met.*, 1993, 55, 299-306.

[2] J. Li, Y. Zhao, H. S. Tan, Y. Guo, C.-A. Di, G. Yu, Y. Liu, Ming Lin, S. H. Lim, Y. Zhou, H. Su & B. S. Ong, A Stable Solution-Processed Polymer Semiconductor with Record High-Mobility for Printed Transistors, *Sci. Rep.*, 2012, 2 (754), 1-9.

[3] H. Bronstein, Z. Chen, R. S. Ashraf, W. Zhang, J. Du, J. R. Durrant, P. S. Tuladhar, K. Song, S. E. Watkins, Y. Geerts, M. M. Wienk, R. A. J. Janssen, T. Anthopoulos, H. Sirringhaus, M. Heeney & I. McCulloch, Thieno[3,2-b]thiophene-Diketopyrrolopyrrole-Containing Polymers for High-Performance Organic Field-Effect Transistors and Organic Photovoltaic Devices, *J. Am. Chem. Soc.*, 2011, 133, 3272-3275.

[4] T. L. Nelson, T. M. Young, J. Liu, S. P. Mishra, J. A. Belot, C. L. Balliet, A. E. Javier, T. Kowalewski & R. D. McCullough, Transistor Paint: High Mobilities in Small Bandgap Polymer Semiconductor Based on the Strong Acceptor, Diketopyrrolopyrrole and Strong Donor, Dithienopyrrole, *Adv. Mater.*, 2010, 22, 4617-4621.

[5] H. Yan, Z. Chen, Y. Zheng, C. Newman, J. R. Quinn, F. Dötz, M. Kastler & A. Facchetti, A High-Mobility Electron-Transporting Polymer for Printed Transistors, *Nature*, 2009, 8, 952-958.

[6] H. Xu, J. Li, B. H. K. Leung, C. C. Y. Poon, B. S. Ong, Y. Zhang & N. Zhao, A High-Sensitivity Near-Infrared Phototransistor Based on an Organic Bulk Heterojunction, *Nanoscale*, 2013, 5, 11850-11855.

[7] J. Kirkpatrick, C. B. Nielsen, W. Zhang, H. Bronstein, R. S. Ashraf, M. Heeney & I. McCulloch, A Systematic Approach to the Design Optimization of Light-Absorbing Indenofluorene Polymers for Organic Photovoltaics, *Adv. Energy Mater.*, 2012, 2, 260-265.

[8] Y. Li, S. P. Singh & P. Sonar, A High Mobility p-Type DPP-Thieno[3,2-b]thiophene Copolymer for Organic Thin-Film Transistors, *Adv. Mater.*, 2010, 22, 4862-4866.

[9] P. M. Beaujuge, S. Ellinger & J. R. Reynolds, The Donor-Acceptor Approach Allows a Back-to-Transmissive Switching Polymeric Electrochrome, *Nat. Mater.*, 2008, 7, 795-799.

[10] H. Xu, J. Li, J. Mai, T. Xiao, X. Lu & N. Zhao, Influence of Donor-Acceptor Arrangement on Charge Transport in Conjugated Copolymers, *J. Phys. Chem. C*, 2014, 118, 5600-5605.

[11] H. Li, F. Li, X. Wang, C. Gu, P. Wang & H. Fu, Diketopyrrolopyrrole-Thiophene-Benzothiadiazole Random Copolymers: An Effective Strategy to Adjust Thin-Film Crystallinity for Transistor and Photovoltaic Properties, *Macromolecules*, 2013, 46, 9211-9219.

[12] J. Li, K.-H. Ong, P. Sonar, S.-L. Lim, G.-M. Ng, H.-K. Wong, H.-S. Tan & Z.-K. Chen, Design and Modification of Three-Component Randomly Incorporated Copolymers for High Performance Organic Photovoltaic Applications, *Polym. Chem.*, 2013, 4, 804-811.

[13] J. Li, K.-H. Ong, P. Sonar, S.-L. Lim, G.-M. Ng, H.-K. Wong, H.-S. Tan & Z.-K. Chen, A Random Copolymer Based on Dithienothiophene and Diketopyrrolopyrrole Units for High Performance Organic Solar Cells, *Chem. Commun.*, 2011, 47, 9480-9482.

[14] M. Brinkmann, E. Gonthier, S. Bogen, K. Tremel, S. Ludwigs, M. Hufnagel & M. Sommer, Stacking in Highly Oriented Films of Naphthalene Diimide Bithiophene Copolymers, *ACS Nano*, 2012, 6, 10319-10326.

[15] C. L. Donley, J. Zaumseil, J. W. Andreasen, M. M. Nielsen, H. Sirringhaus, R. H. Friend & J.-S. Kim, Effects of Packing Structure on the Optoelectronic and Charge Transport Properties in Poly(9,9-di-n-octylfluorene-alt-benzothiadiazole), *J. Am. Chem. Soc.*, 2005, 127, 12890-12899.

References

[16] H. Sirringhaus, M. Bird, T. Richards & N. Zhao, Charge Transport Physics of Conjugated Polymer Field-Effect Transistors, *Adv. Mater.*, 2010, 22, 3893-3898.

[17] K. Y. Seah, J. Li, K.-H. Ong, H.-S. Tan, S.-L. Lim, H.-K. Wong & Z.-K. Chen, An Alternating Copolymer Based on Dithienothiophene and Diketopyrrolopyrrole Units for Thin-Film Transistors and Organic Solar Cells, *Polym. Chem.*, 2013, 4, 260-263.

[18] J. D. Yuen, R. Kumar, D. Zakhidov, J. Seifert, B. Lim, A. J. Heeger & F. Wudl, Ambipolarity in Benzobisthiadiazole-Based Donor-Acceptor Conjugated Polymers, *Adv. Mater.*, 2011, 23, 3780-3785.

[19] J. S. Ha, K. H. Kim & D. H. Choi, 2,5-Bis(2-octyldodecyl)pyrrolo[3,4-c]pyrrole-1,4-(2H,5H)-dione-Based Donor-Acceptor Alternating Copolymer Bearing 5,5'-Di(thiophen-2-yl)-2,2'-biselenophene Exhibiting 1.5 $cm^2 \cdot V^{-1} s^{-1}$ Hole Mobility in Thin-Film Transistors, *J. Am. Chem. Soc.*, 2011, 133, 10364-10367.

[20] H. N. Tsao, D. M. Cho, I. Park, M. R. Hansen, A. Mavrinskiy, D. Y. Yoon, R. Graf, W. Pisula, H. W. Spiess & K. Müllen, Ultrahigh Mobility in Polymer Field-Effect Transistors by Design, *J. Am. Chem. Soc.*, 2011, 133, 2605-2612.

[21] J. Rivnay, M. F. Toney, Y. Zheng, I. V. Kauvar, Z. Chen, V. Wagner, A. Facchetti & A. Salleo, Unconventional Face-On Texture and Exceptional In-Plane Order of a High Mobility n-Type Polymer, *Adv. Mater.*, 2010, 22, 4359-4363.

[22] J. Mei, D. H. Kim, A. L. Ayzner, M. F. Toney & Z. Bao, Siloxane-Terminated Solubilizing Side Chains: Bringing Conjugated Polymer Backbones Closer and Boosting Hole Mobilities in Thin-Films Transistors, *J. Am. Chem. Soc.*, 2011, 133, 20130-20133.

[23] H. Yan, Z. Chen, Y. Zheng, C. Newman, J. R. Quinn, F. Dötz, M. Kastler & A. Facchetii, A High-Mobility Electron-Transporting Polymer for Printed Transistors, Nature, 2009, 457, 679-686.

[24] J. Rivnay, L. H. Jimison, J. E. Northrup, M. F. Toney, R. Noriega, S. Lu, T. J. Marks, A. Facchetti and A. Salleo, Large Modulation of Carrier Transport by Grain-Boundary Molecular Packing and Microstructure in Organic Thin Films, *Nat. Mater.*, 2009, 8, 952-958.

[25] I. McCulloch, M. Heeney, C. Bailey, K. Genevicius, I. MacDonald, M. Shkunov, D. Sparrowe, S. Tierney, R. Wagner, W. Zhang, M. L. Chabinyc, R. J. Kline, M. D. McGehee & M. F. Toney, Liquid-Crystalline Semiconducting Polymers with High Charge-Carrier Mobility, *Nat. Mater.*, 2006, 5, 328-333.

[26] Y. Liu, J. Zhao, Z. Li, C. Mu, W. Ma, H. Hu, K. Jiang, H. Lin, H. Ade & H. Ya, Aggregation and Morphology Control Enables Multiple Cases of High-Efficiency Polymer Solar Cells, *Nat. Commun.*, 2014, 5, 5293-5301.

[27] V. Vohra, K. Kawashima, T. Kakara, T. Koganezawa, I. Osaka, K. Takimiya & H. Murata, Following the Nanostructural Molecular Orientation Guidelines for Sulfur Versus Thiophene Units in Small Molecule Photovoltaic Cells, *Nat. Photonics*, 2015, 9, 403–409.

[28] X. Guo, N. Zhou, S. J. Lou, J. Smith, D. B. Tice, J. W. Hennek, R. P. Ortiz, J. T. L. Navarrete, S. Li, J. Strzalka, L. X. Chen, R. P. H. Chang, A. Facchetti & T. J. Marks, Polymer Solar Cells with Enhanced Fill Factors, *Nat. Photonics*, 2013, 7, 825-833.

[29] M. Saito, I. Osaka, Y. Suzuki, K. Takimiya, T. Okabe, S. Ikeda & T. Asano, Highly Efficient and Stable Solar Cells Based on Thiazolothiazole and Naphthobisthiadiazole Copolymers, *Sci. Rep.*, 2015, 5, 14202 (1-9).

[30] W. Yue, R. S. Ashraf, C. B. Nielsen, E. Collado-Fregoso, M. R. Niazi, S. A. Yousaf, M. Kirkus, H.-Y. Chen, A. Amassian, J. R. Durrant & I. McCulloch, A Thieno[3,2-b][1]benzothiophene Isoindigo Building Block for Additive- and Annealing-Free High-Performance Polymer Solar Cells, *Adv, Mater.*, 2015, 27, 4702-4707.

[31] J. W. Jo, J. W. Jung, E. H. Jung, H. Ahn, T. J. Shin & W. H. Jo, Fluorination on Both D and A Unit in D-A Type Conjugated Copolymer Based on Difluorobithiophene and Benzothiadiazole for High Efficient Polymer Solar Cells, *Energy Environ. Sci.*, 2015, 8, 2427-2434.

[32] J.-H. Kim, J. B. Park, I. H. Jung, A. C. Grimsdale, S. C. Yoon, H. Yang & D.-H. Hwang, Well-controlled Thieno[3,4-c]pyrrole-4,6-(5H)-dione Based Conjugated Polymers for High Performance Organic Photovoltaic Cells with the Power Conversion Efficiency Exceeding 9%, *Energy Environ. Sci.*, 2015, 8, 2352-2356.

[33] T. L. Nguyen, H. Choi, S.-J. Ko, M. A. Uddin, B. Walker, S. Yum, J.-E. Joeng, M. H. Yun, T. J. Shin, S. Hwang, J. Y. Kim & H. Y. Woo, Semi-Crystalline Photovoltaic Polymers with Efficiency Exceeding 9% in a ~300 nm Thick Conventional Single-Cell Device, *Energy Environ. Sci.*, 2014, 7, 3040-3051.

[34] A. J. Heeger, 25th Anniversary Article: Bulk Heterojunction Solar Cells: Understanding the Mechanism of Operation, *Adv. Mater.*, 2014, 26, 10-28.

[35] Y. Huang, E. J. Kramer, A. J. Heeger & G. C. Bazan, Bulk Heterojunction Solar Cells: Morphology and Performance Relationships, *Chem. Rev.*, 2014, 114, 7006-7043.

[36] X. Guo, S. R. Puniredd, M. Baumgarten, W. Pisula & K. Müllen, Benzotrithiophene-Based Donor-Acceptor Copolymers with Distinct Supramolecular Organizations, *J. Am. Chem. Soc.*, 2012, 134, 8404-8407.

[37] Y.-J. Cheng, S.-H. Yang & C.-S. Hsu, Synthesis of Conjugated Polymers for Organic Solar Cell Applications, *Chem. Rev.*, 2009, 109, 5868-5923.

[38] C.-Y. Chang, Y.-J. Cheng, S.-H. Hung, J.-S. Wu, W.-S. Kao, C.-H. Lee & C.-S. Hsu, Combination of Molecular, Morphological, and Interfacial Engineering to Achieve Highly Efficient and Stable Plastic Solar Cells, *Adv. Mater.*, 2012, 24, 549-553.

[39] J.-S. Wu, Y.-J. Cheng, T.-Y. Lin, C.-Y. Chang, P.-I. Shih & C.-S. Hsu, Dithienocarbazole-Based Ladder-Type Heptacyclic Arenes with Silicon, Carbon, and Nitrogen Bridges: Synthesis, Molecular Properties, Field-Effect Transistors, and Photovoltaic Applications, *Adv. Funct. Mater.*, 2012, 22, 1711-1722.

[40] J. Jacob, S. Sax, T. Piok, E. J. W. List, A. C. Grimsdale & K. Müllen, Ladder-Type Pentaphenylenes and Their Polymers: Efficient Blue-Light Emitters and Electron-Accepting Materials via a Common Intermediate, *J. Am. Chem. Soc.*, 2004, 126, 6987-6995.

[41] A. K. Mishra, M. Graf, F. Grasse, J. Jacob, E. J. W. List & K. Müllen, Blue-Emitting Carbon- and Nitrogen-Bridged Poly(ladder-type tetraphenylene)s, *Chem. Mater.*, 2006, 18, 2879-2885.

[42] H. Saitoh, K. Saito, Y. Yamamura, H. Matsuyama, K. Kikuchi & I. Ikemoto, X-ray Study on Structural Phase Transitions of 4,4''-diflouro-p-terphenyl and 4,4'''-difluoro-p-quaterphenyl, *Solid State Commun.*, 1994, 91, 89-92.

[43] H. Chen, Y. Guo, G. Yu, Y. Zhao, J. Zhang, D. Gao, H. Liu & Y. Liu, Highly π-Extended Copolymers with Diketopyrrolopyrrole Moieties for High-Performance Field-Effect Transistors, *Adv. Mater.*, 2012, 24, 4618-4622.

[44] Z. Chen, M. J. Lee, R. S. Ashraf, Y. Gu, S. Albert-Seifried, M. M. Nielsen, B. Schroeder, T. D. Anthopoulos, M. Heeney, I. McCulloch & H. Sirringhaus, High-Performance Ambipolar Diketopyrrolopyrrole-thieno[3,2-b]thiophene Copolymer Field-Effect Transistors with Balanced Hole and Electron Mobilities, *Adv. Mater.*, 2012, 24, 647-652.

[45] P. A. Vah Hal, E. C. P. Smits, T. C. T. Geuns, H. B. Akkerman, B. C. De Brito, S. Perissinotto, G. Lanzani, A. J. Kronemeijer, V. Geskin, J. Cornil, P. W. M. Blom, B. De Boer & D. M. De Leeuw, Upscaling, Integration and Electrical Characterization of Molecular Junctions, *Nat. Nanotechnol.*, 2008, 3, 749-754.

[46] A. J. Kronemeijer, E. Gili, M. Shahid, J. Rivnay, A. Salleo, M. Heeney & H. Sirringhaus, A Selenophene-Based Low-Bandgap Donor-Acceptor Polymer Leading to Fast Ambipolar Logic, *Adv. Mater.*, 2012, 24, 1558-1565.

[47] G. Lu, J. Blakesley, S. Himmelberger, P. Pingel, J. Frisch, I. Lieberwirth, I. Salzmann, M. Oehzelt, R. D. Pietro, A. Salleo, N. Koch & D. Neher, Moderate Doping Leads to High Performance of Semiconductor/Insulator Polymer Blend Transistors, *Nat. Commun.*, 2013, 4, No. 1588 (1-8).

[48] X. Zhang, H. Bronstein, A. J. Kronemeijer, J. Smith, Y. Kim, R. J. Kline, L. J. Richter, T. D. Anthopoulos, H. Sirringshaus, K. Song, M. Heeney, W. Zhang, I. McCulloch & D. M. DeLongchamp, Molecular Origin of High Field-Effect Mobility in an Indacenodithiophene-benzothiadiazole Copolymer, *Nat. Commun.*, 2013, 4, No. 2238 (1-9).

[49] A. W. Chow, S. P. Bitler, P. E. Penwell, D. J. Osborne & J. F. Wolfe, Synthesis and Solution Properties of Extended Chain Poly(2,6-benzothiazole) and Poly(2,5-benzoxazole), *Macromolecules*, 1989, 22, 3514-3520.

[50] L. Yu & Z. Bao, Conjugated Polymers Exhibiting Liquid Crystallinity, *Adv. Mater.*, 1994, 6, 156-159.

[51] S. Inoue, H. Minemawari, J. Tsutsumi, M. Chikamatsu, T. Yamada, S. Horiuchi, M. Tanaka, R. Kumai, M. Yoneya & T. Hasegawa, Effects of Subsituted Alkyl Chain Length on Solution-Processable Layered Organic Semiconductor Crystals, *Chem. Mater.*, 2015, 27, 3809-3812.

[52] Kuzmany & J. Kürti, The Physical Meaning of the Conjugation Length in Polymers, *Synth. Met.*, 1987, 21, 95-102.

[53] R. H. Baughman & L. W. Shacklette, Conductivity as a Function of Conjugation Length: Theory and Experiment for Conducting Polymer Complexes, *Phys. Rev. B*, 1989, 39, 5872-5886.

[54] M. Koppe, M. Scharber, C. Brabec, W. Duffy, M. Heeney & I. McCulloch, Polyterthiophenes as Donors for Polymer Solar Cells, *Adv. Funct. Mater.*, 2007, 17, 1371-1376.

[55] R. J. Kline, D. M. DeLongchamp, D. A. Fischer, E. K. Lin, L. J. Richter, M. L. Chabinyc, M. F. Toney, M. Heeney & I. McCulloch, Critical Role of Side-Chain Attachment Density on the Order and Device Performance of Polythiophenes, *Macromolecules*, 2007, 40, 7960-7965.

[56] S. K. Lee, S. Cho, M. Tong, J. H. Seo & A. J. Heeger, Effects of Substituted Side-Chain Position on Donor-Acceptor Conjugated Copolymers, *J. Polym. Sci.*, *Part A: Polym. Chem.*, 2011, 49, 1821-1829.

[57] Q. Shi, H. Fan, Y. Liu, J. Chen, Z. Shuai, W. Hu, Y. Li & X. Zhan, Thiazolothiazole-Containing Polythiophenes with Low HOMO Level and High Hole Mobility for Polymer Solar Cells, *J. Polym. Sci.*, *Part A: Polym. Chem.*, 2011, 49, 4875-4885.

[58] B. McCulloch, V. Ho, M. Hoarfrost, C. Stanley, C. Do, W. T. Heller & R. A. Segalman, Polymer Chain Shape of Poly(3-alkylthiophenes) in Solution Using Small-Angle Neutron Scattering, *Macromolecules*, 2013, 46, 1899-1907.

[59] S. Kishino, Y. Ueno, K. Ochiai, M. Rikukawa, K. Sanui, T. Kobayashi, H. Kunugita & K. Ema, Estimate of the Effective Conjugation Length of Polythiophene from its $|\chi^{(3)} (\omega;\omega,\omega,-\omega)|$ Spectrum at Excitonic Resonance, *Phys. Rev. B*, 1998, 58, 430-433.

[60] T. Kobayashi, J. Hamazaki, H. Kunugita & K. Ema, Distribution of the effective Conjugation Length of Polythiophene Determined by its Absorption and $\chi^{(3)}$ Spectra, *J. Nonlinear Optic. Phys. Mat.*, 2000, 9, 55-61.

[61] F. Etzold, I. A. Howard, N. Forler, D. M. Cho, M. Meister, H. Mangold, J. Shu, M. R. Hansen, K. Müllen & F. Laquai, The Effect of Solvent Additives on Morphology and Excited-State Dynamics in PCPDTBT:PCBM Photovoltaic Blends, *J. Am. Chem. Soc.*, 2012, 134, 10569-10583.

[62] F. S. U. Fischer, D. Trefz, J. Back, N. Kayunkid, B. Tornow, S. Albrecht, K. G. Yager, G. Singh, A. Karim, D. Neher, M. Brinkmann & S. Ludwigs, Highly Crystalline Films of PCPDTBT with Branched Side Chains by Solvent Vapor Crystallization: Influence on Opto-Electronic Properties, *Adv. Mater.*, 2015, 27, 1223-1228.

[63] C. Wang, Y. Qin, Y. Sun, Y.-S. Guan, W. Xu & D. Zhu, Thiophene-Diketopyrrolopyrrole-Based Quinidal Small Molecules as Solution Processable and Air-Stable Organic Semiconductors: Tuning of the Length and Branching Position of Alkyl Side Chain toward High-Performanc n-Channel Organic Field-Effect Transistor, *ACS Appl. Mater. Interfaces*, 2015, 7, 15978-15987.

[64] S. Chen, B. Sun, W. Hong, H. Aziz, Y. Meng & Y. Li, Influence of Side Chain Length and Bifurcation Point on the Crystalline Structure and Charge Transport of Diketopyrrolopyrrole-Quaterthiophene Copolymers (PDQTs), *J. Mater. Chem. C*, 2014, 2, 2183-2190.

[65] J. S. Lee, S. K. Son, S. Song, H. Kim, D. R. Lee, K. Kim, M. J. Ko, D. H. Choi, B. Kim & J. H. Cho, Importance of Solubilizing Group and Backbone Planarity in Low Band Gap Polymers for High Performance Ambipolar Field-Effect Transistors, *Chem. Mater.*, 2012, 24, 1316-1323.

[66] B. Fu, J. Baltazar, A. R. Sankar, P.-H. Chu, S. Zhang, D. M. Collard & E. Reichmains, Enhancing Field-Effect Mobility of Conjugated Polymers Through Rational Design of Branched Side Chains, *Adv. Funct. Mater.*, 2014, 24, 3734-3744.

[67] J.-H. Dou, Y.-Q. Zheng, T. Lei, S.-D. Zhang, Z. Wang, W.-B. Zhang, J.-Y. Wang & J. Pei, Systematic Investigation of Side-Chain Branching Position Effect on Electron Carrier Mobility in Conjugated Polymers, *Adv. Funct. Mater.*, 2014, 24, 6270-6278.

[68] T. Lei, J.-H. Dou & J. Pei, Influence of Alkyl Chain Branching Positions on the Hole Mobilities of Polymer Thin-Film Transistors, *Adv. Mater.*, 2012, 24, 6457-6461.

[69] J. Li, X. Qiao, Y. Xiong, H. Li & D. Zhu, Five-Ring Fused Tetracyanothienoquinoids as High-Performance and Solution-Processable n-Channel Organic Semiconductors: Effect of the Branching Position of Alkyl Chains, *Chem. Mater.*, 2014, 26, 5782-5788.

[70] F. Zhang, Y. Hu, T. Schuettfort, C. Di, X. Gao, C. R. McNeill, L. Thomsen, S. C. B. Mannsfeld, W. Yuan, H. Sirringhaus & D. Zhu, Critical Role of Alkyl Chain Branching of Organic Semiconductors in Enabling Solution-Processed N-Channel Organic Rhin-Film Transistors with Mobility of up to 3.50 cm^{2}V^{-1}s^{-1}, *J. Am. Chem. Soc.*, 2013, 135, 2338-2349.

[71] H. B. Akkerman, S. C. B. Mannsfeld, A. P. Kaushik, E. Verploegen, L. Burnier, A. P. Zoombelt, J. D. Aaathoff, S. Hong, S. Atahan-Evrenk, X. Liu, A. Aspuru-Guzik, M. F. Toney, P. Clancy & Z. Bao, Effects of Odd-Even Side Chain Length of Alkyl-Substituted Diphenylbithiophenes on First Monolayer Thin Film Packing Structure, *J. Am. Chem. Soc.*, 2013, 135, 11006-11014

[72] J. Y. Back, H. Yu, I. Song, I. Kang, H. Ahn, T. J. Shin, S.-K. Kwon, J. H. Oh & Y.-H. Kim, Investigation of Structure-Property Relationships in Diketopyrrolopyrrole (DPP)-Based Polymer Semiconductors via Side Chain Engineering, *Chem. Mater.*, 2015, 27, 1732-1739.

[73] J. Liu, Y. Zhang, H. Phan, A. Sharenko, P. Moonsin, B. Walker, V. Promarak & T.-Q. Nguyen, Effects of Stereoisomerism on the Crystallization Behavior and Optoelectrical Properties of Conjugated Molecules, *Adv. Mater.*, 2013, 25, 3645-3650.

[74] L. Yang, H. Zhou & W. You, Quantitatively Analyzing the Influence of Side Chains on Photovoltaic Properties of Polymer-Fullerene Solar Cells, *J. Phys. Chem. C*, 2010, 114, 16793-16800.

[75] Q. Shi, H. Fan, Y. Liu, J. Chen, L. Ma, W. Hu, Z. Shuai, Y. Li & X. Zhan, Side Chain Engineering of Copolymers based on Bithiazole and Benzodithiophene for Enhanced Photovoltaic Performance, *Macromolecules*, 2011, 44, 4230-4240.

[76] G. Tu, S. Massip, P. M. Oberhumer, X. He, R. H. Friend, N. C. Greenham & W. T. S. Huck, Synthesis and Characterization of Low Bandgap Conjugated Donor-Acceptor Polymers for Polymer: PCBM Solar Cells, *J. Mater. Chem.*, 2010, 20, 9231-9238.

[77] Z.-G. Zhang, J. Min, S. Zhang, J. Zhang, M. Zhang & Y. Li, Alkyl Chain Engineering on a Dithieno[3,2-b:2',3'-d]silole-alt-dithienylthiazole[5,4-d]thiazole Copolymer toward High Performance Bulk Heterojunction Solar Cells, *Chem. Commun.*, 2011, 47, 9474-9476.

[78] K. H. Kim, D. S. Chung, C. E. Park & D. H. Choi, π-Conjugated Main Chain Polymers Containing Bis(bithiophenyl dithienothiophene)-based Repeating Group and their Application to Polymer Solar Cells, *Mol. Cryst. Liq. Cryst.*, 2011, 538, 187-192.

[79] L. Biniek, S. Fall, C. L. Chochos, D. V. Anokhin, D. A. Ivanov, N. Lecler, P. Lévêque & T. Heiser, Impact of the Alkyl Side Chains on the Optoeletronic Properties of Series of Photovoltaic Low-Band-Gap Copolymers, *Macromolecules*, 2010, 43, 9779-9786.

[80] H. Zhou, L. Yang, S. Xiao, S. Liu & W. You, Donor-Acceptor Polymers Incorporating Alkylated Dithienylbenzothiadiazole for Bulk Heterojunction Solar Cells: Pronounced Effect of Positioning Alkyl Chains, *Macromolecules*, 2010, 43, 811-820.

[81] M. Brinkmann, Structure and Morphology Control in Thin Films of Regioregular Poly(3-hexylthiophene, *J. Polym. Sci. Polym. Phys.*, 2011, 49, 1218-1233.

[82] K. Tremel & S. Ludwigs, Morphology of P3HT in Thin Films in Relation to Optical and Electrical Properties, *Adv. Polym. Sci.*, 2014, 265, 39-82.

[83] F. Pop, W. Lewis & D. B. Amabilino, Solid State Supramolecular Structure of Diketopyrrolopyrrole Chromophores: Correlating Stacking Geometry with Visible Light Absorption, *CrystEngComm.,* 2016, 18, 8933-8943.

[84] C. L. Gettinger, A. J. Heeger, J. M. Drake & D. J. Pine, A Photoluminescence Study of Poly(phenylene vinylene) Derivatives: The Effect of Intrinsic Persistence length, *J. Chem. Phys.*, 1994, 101, 1673-1678.

[85] G. Xue, X. Zhao, G. Qu, T. Xu, A. Gumyusenge, Z. Zhang, Y. Zhao, Y. Diao, H. Li & J. Mei, Symmetry Breaking in Side Chains Leading to Mixed Orientations and Improved Charge transport in Isoindigo-alt-Bithiophene Based Polymer Thin Films, *Appl. Mater. Interfaces*, 2017, 9, 25426-25433.

[86] A. S. Özen, C. Atilgan & G. Sonmez, Noncovalent Intramolecular Interactions in the Monomers and Oligomers of the Acceptor and Donor Type of Low Band Gap Conducting Polymers, *J. Phys. Chem. C*, 2007, 111, 16362-16371.

[87] D. G. Patel, F. Feng, Y. Ohnishi, K. A. Abboud, S. Hirata, K. S. Schanze & J. R. Reynolds, It Takes More Than an Imine: The Role of the Central Atom on the Electron-Accepting Ability of Benzotriazole and Benzothiadiazole, *J. Am. Chem. Soc.*, 2012, 134, 2599-2612.

[88] J. Huang & M. Kertesz, Electronic Structures and Charge Transport Properties of the Organic Semiconductor Bis[1,2,5]thiadiazole-p-quinobis(1,3-dithiole), BTQBT, and its Derivatives, *J. Phys. Chem. B*, 2005, 109, 12891-12898.

[89] N. E. Jackson, B. M. Savoie, K. L. Kohlsedt, M. O. de la Cruz, G. C. Schatz, L. X. Chen & M. A. Ratner, Controlling Conformations of Conjugated Polymers and Small Molecules: The Role of Nonbonding Interactions, *J. Am. Chem. Soc.*, 2013, 135, 10475-10483.

[90] J. E. Coughlin, A. Zhugayevych, R. C. Bakus, T. S. v. d. Poll, G. C. Welch, S. J. Teat, G. C. Bazan & S. Tretiak, A Combined Experimental and Theoretical Study of Conformational Preferences of Molecular Semiconductors, *J. Phys. Chem. C*, 2014, 118, 15610-15623.

[91] Y. Wang, H. Masunaga, T. Hikima, H. Matsumoto, T. Mori & T. Michinobu, New Semiconducting Polymers based on Benzobisthiadiazole Analogues: Tuning of Charge Polarity in Thin Film Transistors via Heteroatom Substitution, *Macromolecules*, 2015, 48, 4012-4023.

[92] J.-F. Jheng, Y.-Y. Lai, J.-S. Wu, Y.-H. Chao, C.-L. Wang & C.-S. Hsu, Influences of the Non-Covalent Interaction Strength on Reaching High Solid-State Order and Device Performance of a Low Bandgap Polymer with Axisymmetrical Structural Units, *Adv. Mater.*, 2013, 25, 2445-2451.

[93] H. Zhou, L. Yang, A. C. Stuart, S. C. Price, S. Liu & W. You, Development of Fluorinated Benzothiadiazole as a Structural Unit for a Polymer Solar Cell of 7 % Efficiency, *Angew. Chem. Int. Ed.*, 2011, 50, 2995-2998.

[94] C. B. Nielsen, A. J. P. White & I. McCulloch, Effect of Fluorination of 2,1,3-Benzothiadiazole, *J. Org. Chem.*, 2015, 80, 5045-5048.

[95] A. Casey, Y. Han, Z. Fei, A. J. P. White, T. D. Anthopoulos & M. Heeney, Cyano Substituted Bezothiadiazole: A Novel Acceptor Inducing n-Type Behaviour in Conjugated Polymers, *J. Mater. Chem. C*, 2015, 3, 265-275.

[96] F. S. U. Fischer, N. Kayunkid, D. Trefz, S. Ludwigs & M. Brinkmann, Structural Models of Poly(cyclopentadithiophene-alt-benzothiadiazole) with Branched Side Chains: Impact of a Single Fluorine Atom on the Crystal Structure and Polymorphism of a Conjugated Polymer, *Macromolecules*, 2015, 48, 3974-3982.

[97] M. B. Nielsen, M. Schreiber, Y. G. Beak, P. Seiler, S. Lecomte, C. Boudon, R. R. Tykwinski, J.-P. Gisselbrecht, V. Gramlich, P. J. Skinner, C. Bosshard, P. Günter, M. Gross & F. Diedrich, Highly Functionalized Dimeric Tetraethynylethenes and Expanded Radialenes: Strong Evidence for Macrocyclic Cross-Conjugation, *Chem. Eur. J.*, 2001, 7, 3263-3280.

[98] Y. Zhao, R. McDonald & R. R. Tykwinski, Study of Cross-Conjugated iso-Polytriacetylenes and Related Oligoenynes, *J. Org. Chem.*, 2002, 67, 2805-2812.

[99] P. Sonar, J. Chang, Z. Shi, E. Gann, J. Li, J. Wu & C. R. McNeill, Hole Mobility of 3.56 $cm^2V^{-1}s^{-1}$ Accomplished Using More Extended Dithienothiophene with Furan Flanked Diketopyrrolopyrrole Polymer, *J. Mater. Chem. C*, 2015, 3, 9299-9305.

[100] G. Kim, S.-J. Kangm, G. K. Dutta, Y.-K. Han, T. J. Shin, Y.-Y. Noh & C. Yang, A Thienoisoindigo-Naphthalene Polymer with Ultrahigh Mobility of 14.4 cm^2/V·s That Substantially Exceeds Benchmark Values for Amorphous Silicon Semiconductors, *J. Am. Chem. Soc.*, 2014, 136, 9477-9483.

[101] S. M. Ryno, C. Risko & J.-L. Brédas, Noncovalent Interactions and Impact of Charge Penetration Effects in Linear Oligoacene Dimers and Single Crystals, *Chem. Mater.*, 2016, 28, 3990-4000.

[102] C. Sutton, C. Risko & J.-L. Brédas, Non-Covalent Intermolecular Interactions in Organic Electronic Materials: Implications for the Molecular Packing vs. Electronic Properties of Acenes, *Chem. Mater.*, 2016, 28, 3-16.

[103] J. N. Scott & J. M. Vanderkooi, A New Hydrogen Bond Angle/Distance Potential Energy Surface of the Quantum Water Dimer, *Water*, 2010, 2, 14-28.

[104] B. Nepal & S. Scheiner, Angular Dependence of Hydrogen Bond Energy in Neutral and Charged Systems Containing CH and NH Proton Donors, *Chem. Phys. Lett.*, 2015, 630, 6-11.

[105] B. Wang, W. Jiang, X. Dai, Y. Gao, Z. Wang and R.-Q. Zhang, Molecular Orbital Analysis of the Hydrogen Bonded Water Dimer, *Sci. Rep.*, 2015, 6, 22099 (1-7).

[106] C. Fu, P. Beldon & D. F. Perepichka, H-Bonding Control of Supramolecular Ordering of Diketopyrrolopyrroles, *Chem. Mater.*, 2017, 29, 2979-2987.

[107] I. Kang, T. K. An, J. Hong, H.-J. Yun, R. Kim, D. S. Chungm, C. E. Park, Y.-H. Kim & S.-K. Kwon, Effect of Selenophene in a DPP Copolymer Incorporating a Vinyl Group for High-Performance Organic Field-Effect Transistors, *Adv. Mater.*, 2013, 25, 524-528.

References

[108] I. Kang, H.-J. Yun, D. S. Chung, S.-K. Kwon & Y.-H. Kim, Record High Hole Mobility in Polymer Semiconductors via Side-Chain Engineering, *J. Am. Chem. Soc.*, 2013, 135, 14896-14899.

[109] H.-J. Yun, H. H. Choi, S.-K. Kwon, Y.-H. Kim & K. Cho, Polarity Engineering of Conjugated Polymers by Variatoin of Chemical Linkages Connecting Conjugated Backbones, *ACS Appl. Mater. Interfaces*, 2015, 7, 5898-5906.

[110] J. Kim, A.-R. Han, J. Hing, G. Kim, J. Lee, T. J. Shin, J. H. Oh & C. Yang, Ambipolar Semiconducting Polymers with π-spacer Linked Bis-benzothiadiazole Blocks as Strong Accepting Units, *Chem. Mater.*, 2014, 26, 4933-4942.

[111] J. Mei, N. C. Heston, S. V. Vasilyeva & J. R. Reynolds, A Facile Approach to Defect-Free Vinylene-Linked Benzothiadiazole-thiophene Low-Bandgap Conjugated Polymers for Organic Electronics, *Macromolecules*, 2009, 42, 1482-1487.

[112] P. M. Beaujuge, H. N. Tsao, M. R. Hansen, C. M. Amb, C. Risko, J. Subbiah, K. R. Choudhury, A. Mavrinskiy, W. Pisula, J.-L. Brédas, F. So, K. Müllen & R. Reynolds, Synthetic Principles Directing Charge Transport in Low-Band-Gap Dithienosilole-Benzothiadiazole Copolymers, *J. Am. Chem. Soc.*, 2012, 134, 8944-8957

[113] M. Morana, M. Wegscheider, A. Bonanni, N. Kopidakis, S. Shaheen, M. Scharber, Z. Zhu, D. Waller, R. Gaudiana & C. Brabec, Bipolar Charge Transport in PCPDTBT-PCBM Bulk-Heterojunctions for Photovoltaic Applications, *Adv. Funct. Mater.*, 2008, 18, 1757-1766

[114] P. Schilinsky, U. Asawapiron, U. Scherf, M. Biele & C. J. Brabec, Influence of the Molecular Weight of Poly(3-hexylthiophene) on the Performance of Bulk Heterojunction Solar Cells, *Chem. Mater.*, 2005, 17, 2175-2180.

[115] W. Ma, J. Y. Kim, K. Lee & A. J. Heeger, Effect of the Molecular Weight of Poly(3-hexylthiophene) on the Morphology and Performance of Polymer Bulk Heterojunction Solar Cells, *Macromol. Rapid Commun.*, 2007, 28, 1776-1780.

[116] A. M. Ballantyne, L. Chen, J. Dane, T. Hammant, F. M. Braun, M. Heeney, W. Duffy, I. McCulloch, D. D. C. Bradley & J. Nelson, The Effect of Poly(3-hexylthiophene) Molecular Weight on Charge Transport and the Performance of Polymer: Fullerene Solar Cells, *Adv. Funct. Mater.*, 2008, 18, 2373-2380.

[117] W. L. Leong, G. C. Welch, L. G. Kaake, C. J. Takacs, Y. Sun, G. C. Bazan & A. J. Heeger, Role of Trace Impurities in the Photovoltaic Performance of Solution Processed Small-Molecule Bulk Hererojunction Solar Cells, *Chem. Sci.*, 2012, 3, 2103-2109.

[118] K. T. Nielsen, K. Bechgaard & F. C. Krebs, Removal of Palladium Nanoparticles from Polymer Materials, *Macromolecules*, 2005, 38, 658-659.

[119] Y. Kim, S. Cook, J. Kirkpatrick, J. Nelson, J. R. Durrant, D. D. C. Bradley, M. Giles, M. Heeney, R. Hamilton & I. McCulloch, Effect of the End Group of Regioregular Poly(3-hexylthiophene) Polymers on the Performance of Polymer/Fullerene Solar Cells, *J. Phys. Chem. C*, 2007, 111, 8137-8141.

[120] J. K. Park, J. Jo, J. H. Seo, J. S. Moon, Y. D. Park, K. Lee, A. J. Heeger & G. C. Bazan, End-Capping Effect of a Narrow Bandgap Conjugated Polymer on Bulk Heterojunction Solar Cells, *Adv. Mater.*, 2011, 23, 2430-2435.

[121] J. S. Kim, Y. Lee, J. H. Lee, J. H. Park, J. K. Kim & K. Cho, High-Efficiency Organic Solar Cells based on End-Functional-Group-Modified Poly(3-hexylthiophene), *Adv. Mater.*, 2010, 22, 1355-1360.

[122] I. Osaka & R. D. McCullough, Advances in Molecular Design and Synthesis of Regioregular Polythiophenes, *Acc. Chem. Res.*, 2008, 41, 1202-1214.

[123] H. Sirringhaus, P. J. Brown, R. H. Friend, M. M. Nielsen, K. Bechgaard, B. M. W. Langeveld-Voss, A. J. H. Spiering, R. A. J. Janssen, E. W. Meijer, P. Herwig & D. M. de Leeuw, Two-Dimensional Charge Transport in Self-Organized, High-Mobility Conjugated Polymers, *Nature*, 1999, 401, 685-688.

[124] Y. Kim, S. Cook, S. M. Tuladhar, S. A. Choulis, J. Nelson, J. R. Durrant, D. D. C. Bradley, M. Giles, I. McCulloch, C.-S. Ha & M. Ree, A Strong Regioregularity Effect in Self-Organizing Conjugated Polymer Films and High-Efficiency Polythiophene: Fullerene Solar Cells, *Nat. Mater.*, 2006, 5, 197-203.

[125] R. Steyrleuthner, M. Schubert, I. Howard, B. Klaumünzer, K. Schilling, Z. Chen, P. Saalfrank, F. Laquai, A. Facchetti & D. Neher, Aggregation in a High-Mobility n-Type Low-Bandgap Copolymer with Implications on Semicrystalline Morphology, *J. Am. Chem. Soc.*, 2012, 134, 18303-18317.

[126] R. Steyrleuthner, R. D. Pietro, B. A. Collins, F. Polzer, S. Himmelberger, M. Schubert, Z. Chen, S. Zhang, A. Salleo, H. Ade, A. Facchetti & D. Neher, The Role of Regioregularity, Crystallinity, and Chain Orientation on Electron Transport in a High-Mobility n-Type Copolymer, *J. Am. Chem. Soc.*, 2014, 136, 4245-4256.

[127] F. Zhang, K. G. Jespersen, C. Björström, M. Svensson, M. R. Andersson, V. Sundström, K. Magnusson, E. Moons, A. Zartsev & O. Inganäs, Influence of Solvent Mixing on the Morphology and Peformance of Solar Cells Based on Polyfluorene Copolymer/Fullerene Blends, *Adv. Funct. Mater.*, 2006, 16, 667-674.

[128] E. J. W. Crossland, K. Tremel, F. Fischer, K. Rahimi, G. Reiter, U. Steiner & S. Ludwigs, Anisotropic Charge Transport in Spherulitic Poly(3-hexylthiophene) Films, *Adv. Mater.*, 2012, 24, 839-844.

[129] E. J. W. Crossland, K. Rahimi, G. Reiter, U. Steiner & S. Ludwigs, Systematic Control of Nucleation Density in Poly(3-Hexylthiophene) Thin Films, *Adv. Funct. Mater.*, 2011, 21, 518-524.

[130] M. J. Lee, D. Gupta, N. Zhao, M. Heeney, I. McCulloch & H. Sirringhaus, Anisotropy of Charge Transport in a Uniaxially Aligned and Chained-Extended, High-Mobility, Conjugated Polymer Semiconductor, *Adv. Funct. Mater.*, 2011, 21, 932-940.

[131] D. M. DeLongchamp, R. J. Kline, Y. Jung, D. S. Germack, E. K. Lin, A. J. Moad, L. J. Richter, M. F. Toney, M. Heeney & I. McCulloch, Controlling the Orientation of Terraced Nanoscale "Ribbons" of a Poly(thiophene) Semiconductor, *ACS Nano*, 2009, 3, 780-787.

[132] C. Müller, M. Aghamohammadi, S. Himmelberger, P. Sonar, M. Garriga, A. Salleo & M. Campoy-Quiles, One-Step Macroscopic Alignment of Conjugated Polymer Systems by Epitaxial Crystallization during Spin-Coating, *Adv. Funct. Mater.* 2013, 23, 2368-2377.

[133] M. Brinkmann & J.-C. Wittmann, Orientation of Regioregular Poly(3-hexylthiophene) by Directional Solidification: A Simple Method to Reveal the Semicrystalline Structure of a Conjugated Polymer, *Adv. Mater.*, 2006, 18, 860-863.

[134] M. Brinkmann, N. Charoenthai, R. Traiphol, P. Piyakulawat, J. Wlosnewski & U. Asawapirom, Structure and Morphology in Highly Oriented Films of Poly(9,9-bis(n-octyl)fluoreme-2,7-diyl) and Poly(9,9-bis(2-ethylhexyl)fluorene-2,7-diyl) Grown on Friction Transferred Poly(tetrafluoroethylene), *Macromolecules*, 2009, 42, 8298-8306.

[135] N. Kayunkid, S. Uttiya & M. Brinkmann, Structural Model of Regioregular Poly(3-hexylthiophene) Obtained by Electron Diffraction Analysis, *Macromolecules*, 2010, 43, 4961-4967.

[136] L. Hartmann, K. Tremel, S. Uttiya, E. Crossland, S. Ludwigs, N. Kayunkid, C. Vergnat & M. Brinkmann, 2D Versus 3D Crystalline Order in Thin Films of Regioregular Poly(3-

hexylthiophene) Oriented by Mechanical Rubbing and Epitaxy, *Adv. Funct. Mater.*, 2011, 21, 4047-4057.

[137] L. Biniek, N. Leclerc, T. Heiser, R. Bechara & M. Brinkmann, Large Scale Alignment and Charge Transport Anisotropy of PBTTT Films Oriented by High Temperature Rubbing, *Macromolecules*, 2013, 46, 4014-4023.

[138] L. Biniek, S. Pouget, D. Djurado, E. Gonthier, K. Tremel, N. Kayunkid, E. Zaborova, N. Crespo-Monteiro, O. Boyron, N. Leclerc, S. Ludwigs & M. Brinkmann, High-Temperature Rubbing: A Versatile Method to Align π-Conjugated Polymers without Alignment Substrate, *Macromolecules*, 2014, 47, 3871-3879.

[139] K. Tremel, F. S. U. Fischer, N. Kayunkid, R. D. Pietro, R. Tkachov, A. Kiriy, D. Neher, S. Ludwigs & M. Brinkmann, Charge Transport Anisotropy in Highly Oriented Thin Films of the Acceptor Polymer P(NDI2OD-T2), *Adv. Energy Mater.*, 2014, 4, 1301659 (1-13).

[140] M. Brinkmann, L. Hartmann, L. Biniek, K. Tremel & N. Kayunkid, Orienting Semi-Conducting π-Conjugated Polymers, *Macromol. Rapid Commun.*, 2014, 35 (1), 9-26.

[141] J. T. Rogers, K. Schmidt, M. F. Toney, E. J. Kramer & G. C. Bazan, Structural Order in Bulk Heterojunction Films Prepared with Solvent Additives, *Adv. Mater.*, 2011, 23, 2284-2288.

[142] T. Agostinelli, T. A. M. Ferenczi, E. Pires, S. Foster, A. Maurano, C. Müller, A. Ballantyne, M. Hampton, S. Lilliu, M. Campoy-Quiles, H. Azimi, M. Morana, D. D. C. Bradley, J. Durrant, J. E. Macdonald, N. Stingelin & J. Nelson, The Role of Alkane Dithiols in Controlling Polymer Crystallization in Small Band Gap Polymer:fullerene Solar Cells, *J. Polym. Sci., Part B: Polym. Phys.*, 2011, 49, 717-724.

[143] Y. Gu, C. Wang & T. P. Russell, Multi-Length-Scale Morphologies in PCPDTBT/PCBM Bulk-Heterojunction Solar Cells, *Adv. Energy Mater.*, 2012, 2, 683-690.

[144] J. Peet, N. S. Cho, S. K. Lee & G. C. Bazan, Transition from Solution to the Solid State in Polymer Solar Cells Cast from Mixed Solvents, *Macromolecules*, 2008, 41, 8655-8659.

[145] J. Peet, J. Y. Kim, N. E. Coates, W. L. Ma, D. Moses, A. J. Heeger & G. C. Bazan, Efficiency Enhancement in Low-Bandgap Polymer Solar Cells by Processing with Alkane Dithiols, *Nat. Mater.*, 2007, 6, 497-500.

[146] T.-Y. Chu, S. Alem, S.-W. Tsang, S.-C. Tse, S. Wakim, J. Lu, G. Dennier, D. Waller, R. Gaudiana & Y. Tao, Morphology Control in Polycarbazole Based Bulk Heterojuction Solar Cells and Its Impact on Device Performance, *Appl. Phys. Lett.*, 2011, 98, 253301 (1-3).

[147] R. Steim, F. R. Kogler & C. J. Brabec, Interface Materials for Organic Solar Cells, *J. Mater. Chem.*, 2010, 20, 2499-2512.

[148] J. Veres, S. D. Ogier, S. W. Leeming, D. C. Cupertino & S. M. Khaffaf, Low-k Insulators as the Choice of Dielectrics in Organic Field-Effect Transistors, *Adv. Funct. Mater.*, 2003, 13, 199-204.

[149] S. Wang, A. Kiersnowski, W. Pisula & K. Müllen, Microstructure Evolution and Device Performance in Solution-Processed Polymeric Field-Effect Transistors: The Key Role of the First Monolayer, *J. Am. Chem. Soc.*, 2012, 134, 4015-4018.

[150] S. O'Dwyer, H. Xie, J. Corish & D. A. Morton-Blake, An Atomistic Simulation of the Effect of Pressure on Conductive Polymers, *J. Phys.: Condens. Matter*, 2001, 13, 2395-2410.

[151] Z. Rang, M. I. Nathan, P. P. Ruden, V. Podzorov, M. E. Gershenson, C. R. Newman & C. D. Frisbie, Hydrostatic Pressure Dependence of Charge Carrier Transport in Single-Crystal Rubrene Devices, *Appl. Phys. Lett.*, 2005, 86, 123501 (1-3).

[152] R. C. Coffin, J. Peet, J. Rogers & G. C. Bazan, Streamlined Microwave-Assisted Preparation of Narrow-Bandgap Conjugated Polymers for High-Performance Bulk Heterojunction Solar Cells, *Nature Chem.*, 2009, 1, 657-661.

[153] K. Okamoto & C. K. Luscombe, Controlled Polymerizations for the Synthesis of Semiconducting Conjugated Polymers, *Polym. Chem.*, 2011, 2, 2424-2434.

[154] B. Carsten, F. He, H. J. Son, T. Xu & L. Yu, Stille Polycondensation for Synthesis of Functional Materials, *Chem. Rev.*, 2011, 111, 1493-1528.

[155] P. Berrouard, A. Najari, A. Pron, D. Gendron, P.-O. Morin, J.-R. Pouliot, J. Veilleux & M. Leclerc, Synthesis of 5-Alkyl[3,4-c]thienopyrrole-4,6-dione-Based Polymers by Direct Heteroarylation, *Angew. Chem. Int. Ed.*, 2012, 51, 2068-2071.

[156] R. J. Kline, M. D. McGehee, E. N. Kadnikova, J. Liu & J. M. J. Fréchet, Controlling the Field-Effect Mobility of Regioregular Polythiophene by Changing the Molecular Weight, *Adv. Mater.*, 2003, 15, 1519-1522.

[157] Y.-H. Tian & M. Kertes, Ladder-Type Polyenazine Based on Intramolecular S···N Interactions: A Theoretical Study of a Small-Bandgap Polymer, *Macromolecules*, 2009, 42, 6123-6127.

[158] H. Kayi, A Computational Study on 4,7-di(furan-2-yl)benzo[c][1,2,5] Thiadiaole Monomer and its Oligomers, *J. Mol. Model*, 2014, 20, 2269-2275.

[159] N.-A. Sánchez-Bojorge, L.-M. Rodríguez-Valdez, I. García-Cruz & N. Flores-Holguín, Unexpected Electron Acceptor Behavior of the 1,3,4-thiadiazole Oligomer, a DFT Study, *Comp. and Theor. Chem.*, 2015, 1068, 109-116.

[160] C. S. Ra, S. Yim & G. Park, DFT Studies of Band Gaps of the Fused Thiophene Oligomers, *Bull. Korean Chem. Soc.*, 2008, 29, 891-892.

[161] G. García, M. Moral, A. Garzon, G. Garcia, J. M. Granadino-Roldan, A. Navarro & M. Fernández-Gómez, Poly(arylenethynyl-thienoacenes) as Candidates for Organic Semiconducting Materials. A DFT Insight, *Org. Electron.*, 2012, 13, 3244-3253.

[162] Y. Li & J. B. Lagowski, Charge Carrier Mobility in Conjugated Organic Polymers-Simulation of an Electron Mobility in a Carbazole-Benzothiadiazole Based Polymer, *Proc. SPIE 8007 Photonics North*, 2011, 80071Z (1-10).

[163] P. Li, Y. Cui, C. Song & H. Zhang, Electronic and Charge Transport Properties of Dimers of Dithienothiophenes: Effect of Structural Symmetry and Linking Mode, *RSC Adv.*, 2015, 5, 50212-50222.

[164] A. N. Sokolov, S. Atahan-Evrenk, R. Mondal, H. B. Akkerman, R. S. Sánchez-Carrera, S. Granados-Focil, J. Schrier, S. C. B. Mannsfeld, A. P. Zoombelt, Z. Bao & A. Aspuru-Guzik, From Computational Discovery to Experimental Characterization of a High Hole Mobility Organic Crystal, *Nat. Commun.*, 2011, 2, 437-445.

[165] J. Calvo-Castro, M. Warzecha, I. D. H. Oswald, A. R. Kennedy, G. Morris, A. J. McLean & C. J. McHugh, Intermolecular Interactions and Energetics in the Crystalline π-π Stacks and Associated Model Dimer Systems of Asymmetric Halogenated Diketopyrrolopyrroles, *Cryst. Growth Des.*, 2016, 16, 1531-1542.

[166] J. Vura-Weis, M. A. Ratner & M. R. Wasielewski, Geometry and Electronic Coupling in Perylenediimide Stacks: Mapping Structure-Charge Transport Relationships, *J. Am. Chem. Soc.*, 2010, 132, 1738-1739.

[167] S. M. Ryno, C. Risko & J.-L. Brédas, Noncovalent Interactions and Impact of Charge Penetration Effects in Linear Oligoacene Dimers and Single Crystals, *Chem. Mater.*, 2016. 28, 3390-4000.

[168] E.-G. Kim & J.-L. Brédas, Electronic Evolution of Poly(3,4-ethylenedioxythiophene) (PEDOT): From the Isolated Chain to the Pristine and Heavily Doped Crystals, *J. Am. Chem. Soc.*, 2008, 130, 16880-16889.

[169] G. Zhang, Y. Pei & J. Ma, Packing Structure and Packing Effects on Excitation Energies of Amorphous Phase Oligothiophenes, *J. Phys. Chem. B*, 2004, 108, 6988-6995.

[170] M. Moral, A. Garzon, G. Garcia, J. M. Granadino-Roldan & M. Fernández-Gómez, DFT Study of the Ambipolar Character of Polymers Based on S-Tetrazine and Aryl Rings, *J. Phys. Chem. C*, 2015, 119, 4588-4599.

[171] G. Zhang, J. Ma & J. Wen, Interchain Impact on Electronic Structures of Heterocyclic Oligomers and Polymers Containing Group 14, 15, an 16 Heteroatoms: Quantum Chemical Calculations in Combination with Molecular Dynamics Simulations, *J. Phys. Chem. B*, 2007, 111, 11670-11679.

[172] M. J. Eslamibidgoli & J. B. Lagowski, The Effect of Side-Chain Length on the Solid-State Structure and Optoelectronic Properties of Fluorene-alt-Benzothiadiazole Based Conjugated Polymers - A DFT Study, *J. Phys. Chem. A*, 2012, 116, 10597-10606.

[173] Z. Ma, H. Geng, D. Wang & Z. Shuai, Influence of Alkyl Side-Chain Length on the Carrier Mobilities in Organic Semiconductors: Herringbone vs. pi-pi Stacking, *J. Mater. Chem. C*, 2016, 4, 4546-4555.

[174] S. B. Darling, Isolating the Effect of Torsional Defects on Mobility and Band Gap in Conjugated Polymers, *J. Phys. Chem. B*, 2008, 112, 8891-8895.

[175] T. J. Prosa & M. J. Winokur, Evidence of a Novel Side Chain Structure in Regioregular Poly(3-alkylthiophenes), *Macromolecules*, 1996, 29, 3654-3656.

[176] L. Gontrani, F. Ramondo & R. Caminiti, Furan and Thiophene in Liquid Phase: An X-ray and Molecular Dynamics Study, *Chem. Phys. Lett.*, 2006, 422, 256-261.

[177] O. A. Guskova, E. Mena-Osteritz, E. Schillinger, P. G. Khalatur, P. Bäuerle & A. R. Khokhlov, Self-Assembled Monolayers of β-Alkylated Oligothiophenes on Graphite Substrate: Molecular Dynamics Simulation, *J. Phys. Chem. C*, 2007, 111, 7165-7174.

[178] Y. Olivier, D. Niedzialek, V. Lemaur, W. Risula, K. Müllen, U. Koldemir, J. R. Reynolds, R. Lazzaroni, J. Cornil & D. Beljonne, 25th Anniversary Article: High-Mobility Hole and Electron Transport Conjugated Polymers: How Structure Defines Function, *Adv. Mater.*, 2014, 26, 2119-2136.

[179] L.-L. Chua, J. Zaumseil, J.-F. Chang, E. C.-W. Ou, P. K.-H. Ho, H. Sirringhaus & R. H. Friend, General Observation of n-Typee Field-Effect Behaviour in Organic Semiconductors, *Nature*, 2005, 434, 194-199.

[180] Z. Wang, R. L. J. Qiu, C. H. Lee, Z. Zhang & X. P. A. Gao, Ambipolar Surface Conduction in Ternary Topological Insulator $Bi_2(Te_{1-x}Se_x)_3$ Nanoribbons, *ACS Nano*, 2013, 7, 2126-2131.

[181] H. Steinberg, D. R. Gardner, Y. S. Lee & P. Jarillo-Herrero, Surface State Transport and Ambipolar Electric Field Effect in Bi_2Se_3 Nanodevices, *Nano Lett.*, 2010, 10, 5032-5036.

[182] M. Ahles, R. Schmechel & H. von Seggern, Complementary Inverter Based on Interface Doped Pentacene, *Appl. Phys. Lett.*, 87, 2005, 113505 (1-3).

[183] B. Crone, A. Dodabalapur, Y.-Y. Lin, R. W. Filas, Z. Bao, A. LaDuca, R. Sarpeshkar, H. E. Katz & W. Li, Large-Scale Complementary Integrated Circuits Based on Organic Transistors, *Nature*, 2000, 403, 521-523.

[184] G. H. Gelinck, H. E. A. Huitema, E. van Veenendaal, E. Cantatore, L. Schrijnemakers, J. B. P. H. van der Putten, T. C. T. Geuns, M. Beenhakkers, J. B. Giesbers, B.-H. Huisman, E. J. Meijer, E. M. Benito, F. J. Touwslager, A. W. Marsman, B. J. E. van Rens & D. M. de Leeuw, Flexible Active-Matrix Displays and Shift Register Based on Solution-Processed Organic Transistors, *Nat. Mater.*, 2004, 3, 106-110.

[185] T. D. Anthopoulos, D. M. de Leeuw, E. Cantatore, S. Setayeesh & E. J. Meijer, Organic Complementary-Like Inverters Employing Methanofullerene-Based Ambipolar Field-Effect Transistors, *Appl. Phys. Lett.*, 2004, 85, 4205-4207.

[186] J. Zaumseil & H. Sirringhaus, Electron and Ambipolar Transport in Organic Field-Effect Transistors, *Chem. Rev.*, 2007, 107, 1296-1323.

[187] T. D. Anthopoulos, C. Tanase, S. Setayesh, E. J. Meijer, J. C. Hummelen, P. W. M. Blom & D. M. De Leeuw, Ambipolar Organic Field-Effect Transistors Based on a Solution-Processed Methanofullerene, *Adv. Mater.*, 2004, 16, 2174-2179.

[188] J. S. Swensen, C. Soci & A. J. Heeger, Light Emission from an Ambipolar Semiconducting Polymer Field-Effect Transistor, *Appl. Phys. Lett.*, 2005, 87, 253511 (1-3).

[189] A. Dodabalapur, H. E. Katz, L. Torsi & R. C. Haddon, Organic Heterostructure Field-Effect Transistors, *Science*, 1995, 269, 1560-1562.

[190] E. J. Meijer, D. M. de Leeuw, S. Setayesh, E. van Veenendaal, B.-H. Huisman, P. W. M. Blom, J. C. Hummelen, U. Scherf & T. M. Klapwijk, Solution-Processed Ambipolar Organic Field-Effect Transistors and Inverters, *Nat. Mater.*, 2003, 2, 678-682.

[191] R. Capelli, S. Toffanin, G. Generali, H. Usta, A. Facchetii & M. Muccini, Organic Light-Emitting Transistors with an Efficiency that Outperforms the Equivalent Light-Emitting Diodes, *Nat. Mater.*, 2010, 9, 496-503.

[192] C. Gu, W. Hu, J. Yao & H. Fu, Naphthalenediimide-Benzothiadiazole Copolymer Semiconductors: Rational Molecular Design for Air-Stable Ambipolar Charge Transport, *Chem. Mater.*, 2013, 25, 2178-2183.

[193] D. Wang, L. Tang, M. Long & Z. Shuai, Anisotropic Thermal Transport in Organic Molecular Crystals from Nonequilibrium Molecular Dynamics Simulations, *J. Phys. Chem. C*, 2011, 115, 5940-5946.

[194] J. Chen, D. Wang & Z. Shuai, First Principles Predictions of Thermoelectric Figure of Merit for Organic Materials: Deformation Potential Approximation, *J. Chem. Theory Comput.*, 2012, 8, 3338-3347.

[195] A. Nangia, Conformational Polymorphism in Organic Crystals, *Acc. Chem. Res.*, 2008, 41, 595-604.

[196] P. A. Heiney, J. E. Fischer, A. R. McGhie, W. J. Romanow, A. M. Denenstein, J. P. McCauley & A. B. Smith, Oreintational Ordering Transition in Solid C_{60}, *Phys. Rev. Lett.*, 1991, 66, 2911–2914.

[197] J. Skabara, J.-B. Arlin & Y. H. Geerts, Close Encounters of the 3D Kind - Exploiting High Dimensionality in Molecular Semiconductors, *Adv. Mater.*, 2013, 25, 1948-1954.

[198] F. Oton, R. Pfattner, E. Pavlica, Y. Olivier, E. Moreno, J. Puigdollers, G. Bratina, J. Cornil, X. Fontrodona, M. Mas-Torrent, J. Veciana & R. Rovira, Electron-Withdrawing Substituted Tetrathiafulvalenes as Ambipolar Simiconductors, *Chem. Mater.*, 2011, 23, 851-861.

[199] N. Karl, K.-H. Kraft, J. Marktanner, M. Münch, F. Schatz, R. Stehle & H.-M. Uhde, Fast Electronic Transport in Organic Molecular Solids, *J. Vac. Sci. Technol.*, 1999, A17, 2318-2328.

[200] V. Podzorov, E. Menard, A. Borissov, V. Kiryukhin, J. A. Rogers & M. E. Gershenson, Intrinsic Charge Transport on the Surface of Organic Semiconductors, *Phys. Rev. Lett.*, 2004, 93, 086602 (1-4).

[201] T. Okamoto, C. Mitsui, M. Yamagishi, K. Nakahara, J. Soeda, Y. Hirose, K. Miwa, H. Sato, A. Yamano, T. Matsushita, T. Uemura & J. Takeya, V-Shaped Organic Semiconductors With Solution Processability, High Mobility and High Thermal Durability, *Adv. Mater.*, 2013, 25, 6392-6397.

[202] Y. Chen, B. Lee, H. T. Yi, S. S. Lee, M. M. Payne, S. Pola, C.-H. Kuo, Y.-L. Loo, J. E. Anthony, Y. T. Tao & V. Podzorov, Dynamic Character of Charge Transport Parameters in Disordered Organic Semiconductor Field-Effect Transistors, *Phys. Chem. Chem. Phys.*, 2012, 14, 14142-14151.

[203] G. Schweicher, Y. Olivier, V. Lemaur & Y. H. Geerts, What Currently Limits Charge Carrier Mobility in Crystals of Molecular Semiconductors, *Isr. J. Chem.*, 2013, 53, 1-27.

[204] J. G. Labram, Y.-H. Lin & T. D. Anthopoulos, Exploring Two-Dimensional Transport Phenomena in Metal Oxide Heterointerfaces for Next-Generation, High-Performance, Thin-Film Transistor Technologies, *Small*, 2015, 11, 5472-5482.

[205] Y. Tsutsui, G. Schweicher, B. Chattopadhyay, T. Sakurai, J.-B. Arlin, C. Ruzié, A. Aliev, A. Ciesielski, S. Colella, A. R. Kennedy, V. Lemaur, Y. Olivier, R. Hadji, L. Sanguinet, F. Castet, S. Osella, D. Dudenko, D. Beljonne, J. Cornil, P. Samori, S. Seki & Y. H. Geerts, Unraveling Unprecedented Charge Carrier Mobility through Structure Property Relationship of Four Isomers of Didodecy[1]benzothieno[3,2-b][1]benzothiophene, *Adv. Mater.*, 2016, 28, 7106-7114.

[206] J.-L. Brédas, D. Belijonne, V. Coropceanu & J. Cornil, Charge-Transfer and Energy-Transfer Processes in π-Conjugated Oligomers and Polymers: A Molecular Picture, *Chem. Rev.*, 2004, 104, 4971-5004.

[207] L. Wang, G. Nan, X. Yang, Q. Peng, Q. Li & Z. Shuai, Computational Methods for Design of Organic Materials with High Charge Mobility, *Chem. Soc. Rev.*, 2010, 39, 423-434.

[208] Z. G. Shuai, L. J. Wang & Q. K. Li, Evaluation of Charge Mobility in Organic Materials: From Localized to Delocalized Descriptions at a First-Principles Level, *Adv. Mater.*, 2011, 23, 1145-1153.

[209] T. Sakanoue & H. Sirringhaus, Band-Like Temperature Dependence of Mobility in a Solution-Processed Organic Semiconductor, *Nat. Mater.*, 2010, 9, 736-740.

[210] R. A. Marcus & N. Sutin, Electron Transfers in Chemistry and Biology, *Biochimica et Biophysica Acta*, 1985, 811, 265-322.

[211] R. A. Marcus, Electron Transfer Reactions in Chemistry. Theory and Experiment, *Rev. mod. Phys.,* 1993, 65, 599-610..

[212] V. Umansky, M. Heiblum, Y. Levinson, J. Smet, J. Nübler & M. Dolev, MBE Growth of Ultra-Low Disorder 2DEG with Mobility Exceeding $35{\times}10^6$ cm^2/V·s, *J. Cryst. Growth*, 2009, 311, 1658-1661.

[213] V. Coropceanu, J. Cornil, D. A. S. Filho, Y. Olivier, R. Silbey & J.-L. Brédas, Charge Transport in Organic Semiconductors, *Chem. Rev.*, 2007, 107, 926-952.

[214] M. V. Basilevsky, I. V. Rostov & M. D. Newton, A Frequency-Resolved Cavity Model (FRCM) for Treating Equilibrium and Non-Equilibrium Solvation Energies, *Chem. Phys.*, 1998, 232, 189-199.

[215] M. D. Newton, M. V. Basilevsky & I. V. Rostov, Chem. Phys., A Frequency-Resolved Cavity Model (FRCM) for Treating Equilibrium and Non-Equilibrium Solvation Energies: 2: Evaluation of Solvent Reorganization Energies, *Chem. Phys.*, 1998, 232, 201-210.

[216] V. Vaissier, P. Barnes, J. Kirkpatrick & J. Nelson, Influence of Polar Medium on the Reorganization Energy of Charge Transfer Between Dyes in a Dye Sensitized film, *Phys. Chem. Chem. Phys.*, 2013, 15, 4804-4814.

[217] J.-L. Brédas, J. P. Calbert, D. A. da Silva & J. Cornil, Organic Semiconductors: A Theoretical Characterization of the Basic Parameters Governing Charge Transport, *Proc. Natl. Acad. Sci. U.S.A.*, 2002, 99, 5804-5809.

[218] C.-P. Hsu, The Electronic Couplings in Electronic Transfer and Excitation Energy Transfer, *Acc. Chem. Res.*, 2009, 42, 509-518.

[219] M. D. Newton, Quantum Chemical Probes of Electron-Transfer Kinetics: The Nature of Donor-Acceptor Interactions, *Chem. Rev.*, 1991, 91, 767-792.

[220] J. Du, M. C. Biewer & M. C. Stefan, Benzothiadiazole Building Units in Solution-Processable Small Molecules for Organic Photovoltaics, *J. Mater. Chem. A*, 2016, 4, 15771-15787.

[221] A. V. Akkuratov & P. A. Troshin, Conjugated Polymers with Benzothiadiazole, Benzoxadiazole, and Benzotriazole Moieties as Promising Semiconductor Materials, *Polym. Sci. Ser. B*, 2014, 56, 414-442.

[222] Y.-L. Chen, W.-S. Kao, C.-E. Tsai, Y.-Y. Lai, Y.-J. Cheng & C.-S. Hsu, A New Ladder-Type Benzodi(cyclopentadithiophene)-Based Donor-Acceptor Polymer and a Modified Hole-Collecting PEDOT:PSS Layer to Achieve Tandem Solar Cells with an Open-Circuit Voltage of 1.62 V, *Chem. Commun.*, 2013, 49, 7702-7704.

[223] A. Efrem, K. Wang, T. Jia & M. Wang, Direct Arylation Polymerization toward a Narrow Bandgap Donor-Acceptor Conjugated Polymer of Alternating 5,6-difluoro-2,1,3-benzothiadiazole and Alkyl-Quarternarythiophene: From Synthesis, Optoelectronic Properties to Devices, *J. Polym. Sci. Part A: Polym. Chem.*, 2017, 55, 1869-1879.

[224] M. Gruber, S.-H. Jung, S. Schott, D. Venkateshvaran, A. J. Kronemeijer, J. W. Andreasen, C. R. McNeill, W. W. H. Wong, M. Shahid, M. Heeney, J.-K. Lee & H. Sirringhaus, Enabling High-Mobility, Ambipolar Charge-Transport in a DPP-benzotriazole Copolymer by Side-Chain Engineering, *Chem. Sci.*, 2015, 6, 6949-6960.

[225] S. M. Lee, H. R. Lee, A.-R. Han, J. Lee, J. H. Oh & C. Tang, High-Performance Furan-Containing Conjugated Polymer for Environmentally Benign Processing, *ACS Appl. Mater. Interfaces*, 2017, 9, 15652-15661.

[226] H. Chen, Y. Guo, Z. Mao, D. Gao & G. Yu, High-Performance Field-Effect Transistors based on Furan-Containing Diketopyrrolopyrrole Copolymer under a Mild Annealing Temperature, *J. Polym. Sci. Part A: Polym. Chem.*, 2014, 52, 1970-1977.

[227] P. Sonar, S. P. Singh, Y. Li, M. S. Soh & A. Dodabalapur, A Low-Bandgap Diketopyrrolopyrrole-Benzothiadiazole-Based Copolymer for High-Mobility Ambipolar Organic Thin-Film Transistors, *Adv. Mater.*, 2010, 22, 5409-5413.

[228] P. Sonar, T. R. B. Foong, S. P. Singh, Y. Li & A. Dodabalapur, A Furan-Containing Conjugated Polymer for High Mobility Ambipolar Organic Thin Film Transistors, *Chem. Commun.*, 2012, 48, 8383-8385.

[229] T.-J. Ha, P. Sonar, S. P. Singh & A. Dodabalapur, Characteristics of High-Performance Ambipolar Organic Field-Effect Transistors Based on a Diketopyrrolopyrroleb-benzothiadiazole Copolymer, *IEEE Trans. Electron Devices*, 2012, 59, 1494-1500

[230] A. J. Kronemeijer, E. Gili, M. Shahid, J. Rivnay, A. Salleo, M. Heeney & H. Sirringhaus, A Selephone-Based Low-Bandgap Donor-Acceptor Polymer Leading to Fast Ambipolar Logic, *Adv. Mater.*, 2012, 24, 1558-1565.

[231] S. Cho, J. Lee, M. Tong, J. Seo & C. Yang, Poly(diketo-pyrrolopyrrole-benzothiadiazole) with Ambipolarity Approaching 100% Equivalency, *Adv. Funct. Mat.*, 2011, 21, 1910-1916.

[232] S. Zhang, Y. Guo, H. Fan, Y. Liu, H.-Y. Chen, G. Yang, X. Zhan, Y. Liu, Y. Li & Y. Yang, Low Bandgap π-Conjugated Copolymers Based on Fused Thiophenes and Benzothiadiazole: Synthesis and Structure-Property Relation Study, *J. Polym. Sci. Part A: Polym. Chem.*, 2009, 47, 5498–5508.

[233] H. Mori, H. Nonobe & Y. Nishihara, Highly Crystalline, Low Band-Gap Semiconducting Polymers Based on Phenanthrodithiophene-benzothiadiazole for Solar Cells and Transistors, *Polym. Chem.*, 2016, 7, 1549-1558.

[234] M. Svensson, F. L. Zhang, S. C. Veenstra, W. J. H. Verhees, J. C. Hummelen, J. M. Kroon, O. Inganas & M. R. Andersson, High-Performance Polymer Solar Cells of an Alternating Polyfluorene Copolymer and a Fullerene Derivative, *Adv. Mater.*, 2003, 15, 988-991.

[235] S. Günes, H. Neugebauer & N. S. Sariciftci, Conjugated Polymer-Based Organic Solar Cells, *Chem. Rev.*, 2007, 107, 1324-1338.

[236] D. Fichou, Structural Order in Conjugated Oligothiophenes and its Implications on Opto-Electronic Devices, *J. Mater. Chem.*, 2000, 10, 571-588.

[237] J. E. Northrup, Atomic and Electronic Structure of Polymer Organic Semiconductors: P3HT, PQT, and PBTTT, *Phys. Rev. B*, 2007, 76, 245202 (1-6).

[238] G. R. Hutchison, M. A. Ratner & T. J. Marks, Intermolecular Charge Transfer between Heterocyclic Oligomers. Effects of Heteroatom and Molecular Packing on Hopping Transport in Organic Semiconductors, *J. Am. Chem. Soc.*, 2005, 127, 16866-16881.

[239] K. Takimiya, Y. Kunugi, Y. Konda, N. Niihara & T. Otsubo, 2,6-Diphenylbenzo[1,2-b:4,5-b']dichalcogenophenes: A New Class of High-Performance Semiconductors for Organic Field-Effect Transistors, *J. Am. Chem. Soc.*, 2004, 126, 5084-5085.

[240] J. B. Binder & R. T. Raines, Simple Chemical Transformation of Lignocellulosic Biomass Into Furans for Fuels and Chemicals, *J. Am. Chem. Soc.*, 2009, 131, 1979-1985.

[241] A. Gandini, Polymers from Renewable Resources: A Challenge for the Future of Macromolecular Materials, *Macromolecules*, 2008, 41, 9491-9504.

[242] P. Sonar, J. Chang, J. H. Kim, K.-H. Ong, E. Gann, S. Manzhos, J. Wu & C. R. McNeill, High-Mobility Ambipolar Organic Thin-Film Transistor Processed From a Nonchlorinated Solvent, *ACS Appl. Mater. Interfaces*, 2016, 8, 24325-24330.

[243] O. Gidron & M. Bendikov, α-Oligofurans: An Emerging Class of Conjugated Oligomers for Organic Electronics, *Angew. Chem. Int. Ed.*, 2014, 53, 2546-2555.

[244] S. Sharma & M. Bendikov, α-Oligofurans: A Computational Study, *Chem. Eur. J.*, 2013, 19, 13127-13139.

[245] M. S. Chen, O. P. Lee, J. R. Niskala, A. T. Yiu, C. J. Tassone, K. Schmidt, P. M. Beaujuge, S. S. Onishi, M. F. Toney, A. Zettl & J. M. J. Fréchet, Enhanced Solid-State Order and Field-Effect Hole Mobility through Control of Nanoscale Polymer Aggregation, *J. Am. Chem. Soc.*, 2013, 135, 19229-19236.,

[246] O. Gidron, Y. Diskin-Posner & M. Brndikov, α-Oligofurans, *J. Am. Chem. Soc.*, 2010, 132, 2148-2150.

[247] Y. Miyata, T. Nishinaga & K. Komatsu, Synthesis and Structural, Electronic, and Optical Properties of Oligo(thienylfuran)s in Comparison with Oligothiophenes and Oligofurans, *J. Org. Chem.*, 2005, 70, 1147-1153.

[248] O. Gidron, A. Dadvand, E. W.-H. Sun, I. Chung, L. J. W. Shimon, M. Bendikov & D. F. Perepichka, Oligofuran-Containing Molecules for Organic Electronics, *J. Mater. Chem. C*, 2013, 1, 4358-4367.

[249] M. Montejo, A. Navarro, G. J. Kearley, J. Vázquez & J. J. López-González, Intermolecular Charge Transfer and Hydrogen Bonding in Solid Furan, *J. Am. Chem. Soc.*, 2004, 126, 15087-15095.

[250] C. L. Chochos, A. Avgeropoulos & E. Lidorikis, Theoretical Study of Phenyl-Substituted Indacenodithiophene Copolymers for High Performance Organic Photovoltaics, *J. Chem. Phys.*, 2013, 138, 064901 (1-6).

[251] W. Zhang, E. D. Gomez & S. T. Milner, Predicting Chain Dimensions of Semiflexible Polymers from Dihedral Potentials, *Macromolecules*, 2014, 47, 6453-6461.

[252] Y. Li, L.-Y. Zou & A.-M. Ren, Charge Transport and Fluorescence Properties of a Series of Red-Emitting Materials Based on Benzothiadiazole and Silafluorene, *Acta Phys.-Chim. Sin.*, 2014, 30, 855-865.

[253] C. Lee, W. Yang & R. G. Parr, Development of the Colle-Salvetti Correlation-Energy Formula into a Functional of the Electron Density, *Phys. Rev. B*, 1988, 37, 785-789.

[254] G. García, J. M. Granido-Roldán, A. Garzón, M. Moral, T. Peña-Ruiz, A. Navarro, M. P. Fernández-Liencres & M. Fernández-Gómez, Theoretical Study of bis(phenylethynyl)thienoacenes as Precursors of Molecular Wires for Molecular Electronics, *J. Phys. Chem. C.*, 2010, 114, 12325-12334.

[255] Y. C. Hung, J. C. Jiang, C. Y. Chao, W. F. Su & S. T. Lin, Theoretical Study on the Correlation between Band Gap, Bandwidth and Oscillator Strength in Fluorene-Based Donor-Acceptor Conjugated Copolymers, *J. Phys. Chem. B*, 2009, 113, 8268-8277.

[256] B. C. Lin, C. P. Cheng & Z. P. M. Lao, Reorganization Energies in the Transports of Holes and Electrons in Organic Amines in Organic Electroluminescence Studied by Density Functional Theory, *J. Chem. Phys. A.*, 2003, 107, 5241-5251.

[257] Y. Zhao & D. G. Truhlar, The M06 Suite of Density Functionals for Main Group Thermochemistry, Thermochemical Kinetics, Noncovalent Interactions, Excited States, and Transition Elements: Two New Functionals and Systematic Testing of Four M06-Class Functionals and 12 other Functionals, *Theor. Chem. Account*, 2006, 120, 215–241.

[258] B. H. Besler, K. M. Merz & P. A. Kollman, Atomic Charges Derived from Semiempirical Methods, *J. Comput. Chem.*, 1990, 11, 431-439.

[259] J. Tomasi, B. Mennucci & R. Cammi, Quantum Mechanical Continuum Solvation Models, *Chem. Rev.*, 2005, 105, 2999-3094.

[260] M. İçli-Özkut, H. İpek, B. Karabay, A. Cihaner & A. M. Önal, Furan and Benzochalcogenodiazole Based Multichromic Polymers via a Donor–Acceptor Approach, *Polym. Chem.*, 2013, 4, 2457-2463.

[261] P. Sonar, S. P. Singh, P. Leclère, M. Surin, R. Lazzaroni, T. T. Lin, A. Dobalapur & A. Sellinger, Synthesis, Characterization and Comparative Study of Thiophene-benzothiadiazole Based Donor-Acceptor-Donor (D-A-D) Materials, *J. Mater. Chem.*, 2009, 19, 3228-3237.

[262] A. A. Y. Guilbert, J. M. Frost, T. Agostinelli, E. Pires, S. Lilliu, J. E. Macdonald & J. Nelson, Influence of Bridging Atom and Side Chains on the Structure and Crystallinity of Cyclopentadithiophene-Benzothiadiazole Polymers, *Chem. Mater.*, 2014, 26, 1226-1233.

[263] P. B. Pati, S. P. Senanayak, K. S. Narayan & S. S. Zade, Solution Processable Benzooxadiazole and Benzothiadiazole Based D-A-D Molecules with Chalcogenophene: Field Effect Transistor Study and Structure Property Relationship, *ACS Appl. Mater. Interfaces*, 2013, 5, 12460-12468.

[264] J. Dhar, K. Swathi, D. P. Karothu, K. S. Narayan & S. Patil, Modulation of Electronic and Self-Assembly Properties of a Donor–Acceptor–Donor-Based Molecular Materials via Atomistic Approach, *ACS Appl. Mater. Interfaces*, 2015, 7, 670-681.

[265] S. Tortorella, M. M. Talamo, A. Cardone, M. Pastore & F. De Angelis, Benchmarking DFT and Semi-Empirical Methods for a Reliable and Cost-Efficient Computational Screening of Benzofulvene Derivatives as Donor Materials for Small-Molecule Organic Solar Cells, *J. Phys.: Condens. Matter*, 2016, 28, 074005 (1-11)

[266] J. Pina, J. S. de Melo, D. Breusov & U. Scherf, Donor-Acceptor-Donor Thienyl/Nethienyl-Benzothiadiazole/Quinoxaline Model Oligomers: Experimental and Theoretical Studies, *Phys. Chem. Chem. Phys.*, 2013, 15, 15204-15213.

[267] I. T. Lima, C. Risko, A. G. Aziz, D. A. da Silva Filho & J.-L. Brédas, Interplay of Alternative Conjugated Pathways and Steric Interactions on the Electronic and Optical Properties of Donor-Acceptor Conjugated Polymers, *J. Mater. Chem. C*, 2014, 2, 8873-8879.

[268] R. Grisorio, L. De Marco, R. Giannuzzi, G. Gigli & G. P. Suranna, Molecular Engineering of Largely π-Extended Metal-Free Sensitizers Containing Benzothiadiazole Units: Approaching 10% Efficiency Dye-Sensitized Solar Cells Using Iodine-Based Electrolytes, *Dyes Pigments*, 2016, 131, 282-292.

[269] C. Fu, F. Bélanger-Gariépy & D. F. Perepichka, Supramolecular Ordering of Difuryldiketopyrrolopyrrole: the Effect of Akyl Chains and Inter-Ring Twisting, *CrysEngComm*, 2016, 18, 4285-4289.

[270] S. P. Ponnappa, S. Arumugam, H. J. Spratt, S. Manzhos, A. P. O'Mullane, G. A. Ayoko & P. Sonar, A Comparative Study of Electrochemical, Optical Properties and Electropolymerization behavior of Thiophene- and Furan-Substituted Diketopyrrolopyrrole, *J. Mater. Res.*, 2017, 32, 810-821.

[271] J. C. Bijleveld, B. P. Karsten, S. G. J. Mathijssen, M. M. Wienk, D. M. de Leeuw & R. A. Janssen, Small Band Gap Copolymers Based on Furan and Diketopyrrolopyrrole for Field-Effect Transistors and Photovoltaic Cells, *J. Mater. Chem.*, 2011, 21, 1600-1606.

[272] J. Dhar, D. P. Karothu & S. Patil, Herringbone to Cofacial Solid State Packing via H-Bonding in Diketopyrrolopyrrole (DPP) Based Molecular Crystals: Influence on Charge Transport, *Chem. Commun.*, 2015, 51, 97-100.

[273] M. A. Naik, N. Venkatramaiah, C. Kanimozhi & S. Patil, Influence of Side-Chain on Structural Order and Photophysical Properties in Thiophene Based Diketopyrrolopyrroles: A Systematic Study, *J. Phys. Chem. C*, 2012, 116, 26128-26137.

[274] C. M. Mauck, P. E. Hartnett, E. A. Margulies, L. Ma, C. E. Miller, G. C. Schatz, T. J. Marks & M. R. Wasielewski, Singlet Fission via an Excimer-Like Intermediate in 3,6-Bis(thiophene-2-yl)diketopyrrolopyrrole Derivatives, *J. Am. Chem. Soc.*, 2016, 138, 11749-11761.

[275] H.Y. Woo, M.A. Uddin & S. Hwang, Density Functional Theoretical and Time-Dependent Density Functional Study of Thiophene-benzothiadiazole-Based Polymers, *Bull. Korean Chem. Soc.*, 2015, 36, 427-430.

[276] M. A. Uddin, T. H. Lee, S. Xu, S. Y. Park, T. Kim, S. Song, T. L. Nguyen, S.-J. Ko, S. Hwang, J. Y. Kim & H. Y. Woo, Interplay of Intramolecular Noncovalent Coulomb Interactions for Semicrystalline Photovoltaic Polymers, *Chem. Mater.*, 2015, 27, 5997-6007.

[277] G. Conboy, H. J. Spencer, E. Angioni, A. L. Kanibolotsky, N. J. Findlay, S. J. Coles, C. Wilson, M. B. Pitak, C. Risko, V. Coropceanu, J.-L. Brédas & P. J. Skabara, To Bend or not to Bend – are Heteroatom Interactions within Conjugated Molecules Effective in Dictating Conformation and Planarity, *Mater. Horiz.*, 2016, 3, 333-339.

[278] I. A. Nyrkova, A. N. Semenov, J.-F. Joanny & A. R. Khokhlov, Highly Anisotropic Rigidity of "Ribbon-Like" Polymers: I. Chain Conformation in Dilute Solutions, *J. Phys. II France*, 1996, 6, 1411-1428.

[279] A. Adejoro, B. T. Ogunyemi & B. Semire, Theoretical Study on the Structural and Electronic Properties of New Materials Based on Benzothiodiazole and Pyrrole Derivative, *Der Pharma Chemica*, 2012, 4, 2214-2221.

[280] R. Acharya, S. Cekli, C. J. Zeman, IV, R. M. Altamimi & K. S. Schanze, Effect of Selenium Substitution on Intersystem Crossing in π-Conjugated Donor–Acceptor–Donor Chromophores: The LUMO Matters the most, *J. Phys. Chem. Lett.*, 2016, 7, 693-697.

[281] K. J. Thorley & C. Risko, On the Impact of Isomer Structure and Packing Disorder in Thienoacene Organic Semiconductors, *J. Mater. Chem. C*, 2016, 4, 4040-4048.

[282] R. Jin & K. Wang, Rational Design of Diketopyrrolopyrrole-Based Small Molecules as Donating Materials for Organic Solar Cells, *Int. J. Mol. Sci.*, 2015, 16, 20326-20343.

[283] B. Lüssem, C.-M. Keum, D. Kasemann, B. Naab, Z. Bao & K. Leo, Doped Organic Transistors, *Chem. Rev.*, 2016, 116, 13714-13751.

[284] M. Kang, J.-S. Yeo, W.-T. Park, N.-K. Kim, D.-H. Lim, H. Hwang, K.-J. Baeg, Y.-Y. Noh & D.-Y. Kim, Favorable Molecular Orientation Enhancement in Semiconducting Polymer Assisted by Conjugated Organic Small Molecules, *Adv. Funct. Mater.*, 2016, 26, 8527-8536.

[285] R. Frisenda, V. A. E. C. Janssen, F. C. Grozema, H. S. J. van der Zant & N. Renaud, Mechanically Controlled Quantum Interference in Individual π-Stacked Dimers, *Nat. Chem.*, 2016, 8, 1099-1104.

[286] D. Niedzialek, V. Lemaur, D. Dudenko, J. Shu, M. R. Hansen, J. W. Andreasen, W. Pisula, K. Müllen, J. Cornil & D. Beljonne, Probing the Relation Between Charge Transport and Supramolecular Organization Down to Ångtröm Resolution in a Benzothiadiazole-Cyclopentadithiophene Copolymer, *Adv. Mater.*, 2013, 25, 1939-1947.

[287] M. Qiu, D. Zhu, L. Yan, N. Wang, L. Han, X. Bao, Z. Du, Y. Niu & R. Yang, Strategy to Manipulate Molecular Orientation and Charge Mobility in D-A Type Conjugated Polymer through Rational Fluorination for Improvements of Photovoltaic Performances, *J. Phys. Chem. C*, 2016, 120, 22757-22765.

[288] N. Banerji, E. Gagnon, P.-Y. Morgantini, S. Valouch, A. R. Mohebbi, J.-H. Seo, M. Leclerc, & A. J. Heeger, Breaking Down the Problem: Optical Transitions, Electronic Structure, and Photoconductivity in Conjugated Polymer PCDTBT and in its Separate Building Blocks, *J. Phys. Chem. C*, 2012, 116, 11456-11469.

[289] K. Ong, S. Lim, H. Tan, H. Wong, J. Li, Z. Ma, L. C. H. Moh, S. Lim, J. C. de Mello & Z.-K. Chen, A Versatile Low Bandgap Polymer for Air-Stable, High-Mobility Field-Effect Transistors and Efficient Polymer Solar Cells, *Adv. Mater.*, 2011, 23, 1409-1413.

[290] Y. Park, K. S. Park, B. Jun, Y.-E. K. Lee, S. U. Lee & M. M. Sung, Quantitative Correlation between Carrier Mobility and Intermolecular Center-to-Center Distance in Organic Single Crystals, *Chem. Mater.*, 2017, 29, 4072-4079.

[291] Q. Liu, A. Surendran, K. Feron, S. Manzhos, X. Jiao, C. R. McNeill, S. E. Bottle, J. Bell, W. L. Leong & P. Sonar, Diketopyrrolopyrrole Based Organic Semiconductors with Different Numbers of Thiophene Units: Symmetry Tuning Effect on Electronic Devices, *New J. Chem.*, 2018, 42, 4017-4028.

[292] S. R. Chaudhari, J. M. Griffin, K. Broch, A. Lesage, V. Lemaur, D. Dudenko, Y. Olivier, H. Sirringhaus, L. Emsley & C. O. Grey, Donor-Acceptor Stacking Arrangements in Bulk and Thin-Film High-Mobility Conjugated Polymers Characterized using Molecular Modelling and MAS and Surface-Enhanced Solid-State NMR Spectroscopy, *Chem. Sci.*, 2017, 8, 3126-3136.

Versicherung

Hiermit versichere ich, dass die vorliegende Arbeit ohne unzulässige Hilfe Dritter und ohne Benutzung anderer als der angegeben Hilfsmittel angefertigt habe; die aus fremden Quellen direkt oder indirekt übernommenen Gedanken sind als solche kenntlich gemacht. Die Arbeit wurde bisher weder im Inland noch im Ausland in gleicher oder ähnlicher Form einer anderen Prüfungsbehörde vorgelegt.

Die vorliegende Dissertation wurde in dem Zeitraum von Oktober 2015 bis Dezember 2018 am Leibniz-Institut für Polymerforschung Dresden e.V. unter wissenchaftlicher Betreuung von Herrn Prof. Dr. Gotthard Seifert, Herrn Prof. Dr. Jens-Uwe Sommer und Frau Dr. Olga Guskova angefertigt.

Frühere Promotionsvefahren fanden nicht statt.

Ich erkenne die Promotionsordnung des Bereichs Fakultät Mathematik und Naturwissenschaften der Technischen Universität Dresden vom 23.02.2011 in zuletzt geänderter Fassung vom 15.06.2011 und 18.06.2014 in vollem Umfang an.

Deyan Raychev   Dresden, den 20. März 2019